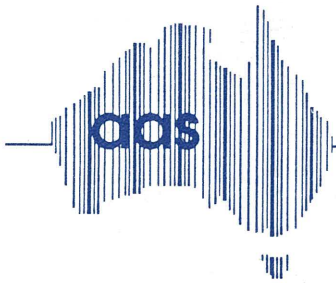

Australian Acoustical Society A.C.N. 000 712 658

ANNUAL CONFERENCE 1993

9 - 10 November
Glenelg, South Australia

PROGRESS IN ACOUSTICS, NOISE & VIBRATION CONTROL

Proceedings

Australian Acoustical Society

A.C.N. 000 712 658

Aims

The Australian Acoustical Society has as its aim the promotion and advancement of the science and practice of acoustics in all its branches and the exchange of ideas in relation thereto.

Activities

The principal activities of the Society are the technical meetings held by each State Division, the Annual Conferences which are held by the State Divisions in rotation, and the publication of a journal.

In each state, a number of technical meetings are held each year according to the availability of speakers and places of interest.

These meetings normally consist of a lecture given by an invited guest speaker on some subject related to acoustics. Other technical meetings consist of workshops, a visit to a factory, laboratory, auditorium or some other place of interest to the members of the Society.

The Society's journal *'Acoustics Australia'* is published thrice yearly and includes technical articles and general information regarding the Society and acoustics.

For information regarding membership of the Australian Acoustical Society, please contact the general secretary at:

The Australian Acoustical Society
Science Centre Foundation
Private Bag 1
Darlinghurst NSW 2010

SUSTAINING MEMBERS

ABB FLAKT RICHARDSON PTY LTD
340 BALLARAT ROAD
BRAYBROOK VICTORIA 3019

ASSOCIATION OF AUSTRALIAN ACOUSTICAL CONSULTANTS
SCIENCE CENTRE FOUNDATION
PRIVATE BAG 1,
DARLINGHURST 2010

ASSOCIATION OF NOISE CONTROL ENGINEERING
P.O. BOX 484
MT. ELIZA 3930

AWA DISTRIBUTION
112-118 TAVALERA RD,
NORTH RYDE 2113

BARCLAY ENGINEERING
PO BOX 1153,
CANNING VALE 6155

BHP STEEL,
SHEET & COIL PRODUCTS DIVISION
PO BOX 77,
PORT KEMBLA 2505

BILSOM AUSTRALIA PTY LTD
19 TEPKO ROAD,
TERRY HILLS 2084

BORAL AUSTRALIAN GYPSUM
676 LORIMER ST,
PORT MELBOURNE 3207

BRUEL & KJAER AUSTRALIA PTY LTD
PO BOX 177, TERREY HILLS 2084

CHADWICK TECHNOLOGY
292 BURNS BAY RD,
LANE COVE 2066

CSR GYPROCK & BRADFORD INSULATION
LEVEL 5, 9 HELP STREET
CHATSWOOD 2067

ENVIRONMENTAL NOISE CONTROL P/L
50 RIVERSIDE ROAD
CHIPPING NORTON 2170

G P EMBELTON & CO PTY LTD
PO BOX 207
COBURG 3058

INC CORPORATION PTY LTD
22 CLEELAND ROAD
OAKLEIGH SOUTH 3167

JOYCE AUSTRALIA
5-9 BRIDGE ROAD,
MOOREBANK 2170

NAP SILENTFLO PTY LTD
58 BUCKLAND ST,
CLAYTON 3168

PEACE ENGINEERING PTY LTD
PO BOX 16,
REVESBY 2212

PYROTEK PTY LTD
147 MAGOWAR RD,
GIRRAWEEN 2145

REINFORCED EARTH PTY LTD
PO BOX 742,
GOSFORD 2250

ROCLA COMPOSITE PRODUCTS
SANDOWN RD,
SPRINGVALE 3171

SAFETY EQUPMENT AUSTRALIA PTY LTD
35/1-3 JUBLIEE AVE,
WARRIEWOOD 2102

STRAMIT INDUSTRIES LTD
219 DUNDAS STREET, PRESTON 3072

WARBURTON FRANKI
Division of Bell-IRH Industries Pty Ltd
1-5 CARTER STREET
LIDCOMBE 2141

WORKCOVER ACOUSTICS
132 LONDONDERRY RD
LONDONDERRY 2753

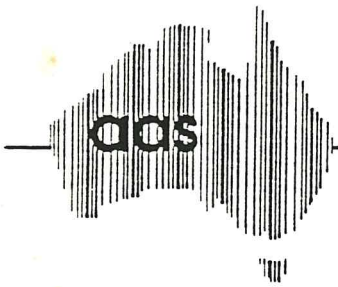

Australian Acoustical Society A.C.N. 000 712 658

ANNUAL CONFERENCE 1993

9 - 10 November
Glenelg, South Australia

PROGRESS IN ACOUSTICS, NOISE & VIBRATION CONTROL

Proceedings

Late Paper

IMPLICATIONS OF VARIABILITY IN CoRTN INTERPRETATIONS

By: David Wren
Vipac Engineers & Scientists Ltd

1.0 INTRODUCTION

The UK Department of Transport Welsh office method of Calculation of Road Traffic Noise (CoRTN) has been widely used to predict the impact of new roads and highways and is the prescribed method for predicting compliance with the current Vic Roads L_{10}(18 Hour) criterion of 63 dBA. In order to predict the noise impact of real-world carriageways and freeways, a number of interpretations must be given to various parameters and calculations within CoRTN. In this paper, we will discuss some of these interpretations and demonstrate the impact they have on the predicted L_{10}(18 Hour) sound pressure level.

2.0 BACKGROUND

Over the past number of years, State Regulatory Authorities charged with the implementation and upgrading of road networks have increasingly used and specified the CoRTN method to determine the effect on residencies of proposed changes to road systems including a change in traffic numbers, carriage way variations/construction or a combination of both.

The tendering process for major projects (which most times includes the design and construction of the noise abatement treatments as well as that of the road sections) often involves submitting a "Conforming Tender", which meets the (calculated) requirements as proposed by the State Regulatory Authority. These calculated requirements will include the position(s) of, as well as the height of the necessary noise barriers.

A "Conforming Tender" may also be jointly submitted with a "Non Conforming Tender". This "Non Conforming Tender" is based upon the tendering Private Sector Consortium's estimates and calculations. Often the location and height of noise abatement treatments such as noise barriers proposed in the "Conforming Tender" and the "Non Conforming Tender" are different, due to the reasons explained below.

3.0 DETERMINATION OF TRAFFIC NOISE USING CORTN

The CoRTN method of the calculation of traffic noise is primarily based upon the assumption that each source of noise (traffic flow) is a continual line source, with a 180° view of the road.

Given a traffic flow rate, percentage of heavy vehicles, traffic speed, gradient of road and road surface, the "Basic Noise Level" can be calculated.

This "Basic Noise Level" is then corrected for
- distance attenuation
- ground cover
- screening
- barriers
- θ, calculated from the angle subtended by the road
  ie $10\log(\theta/180)$
- Site layout

Calculation of distance attenuation and barrier attenuation are based upon the shortest slant distance from and the relative height of the receiver location to the "Effective Source Location". This "Effective Source Location" is defined to be the point on the source line of a perpendicular projection from the receiver position to the source line.(see Figure 1.)

If the road segment does not extend to a point where a perpendicular intersection can be drawn, then the source line is to be extended to a point where a perpendicular intersection can be drawn and any calculations are then made to this point.

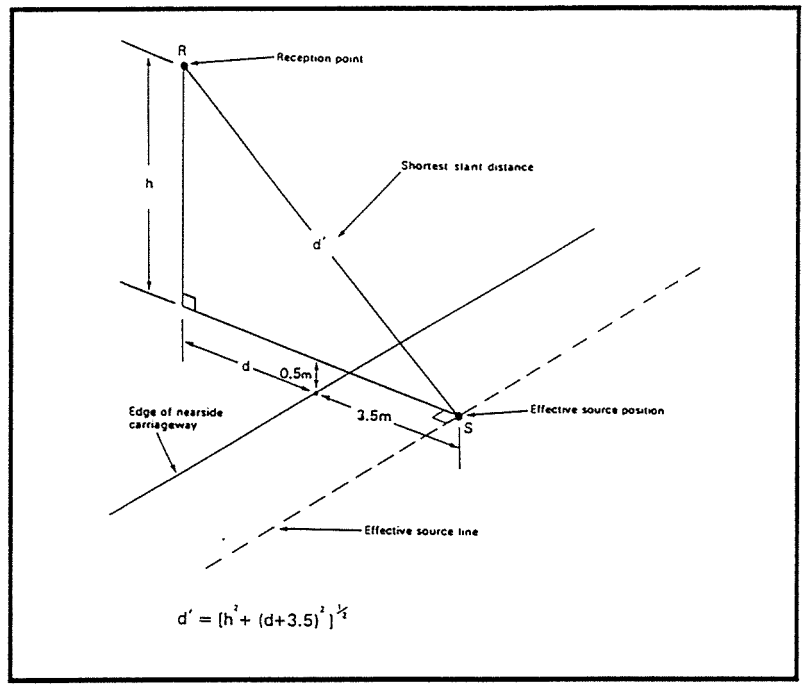

Figure 1

4.0 SOURCES OF VARIATIONS IN THE PREDICTION OF TRAFFIC NOISE LEVEL

It appears that the major variations in the calculated results of a CoRTN prediction occur in (i) the barrier path difference calculations and to a lesser degree in (ii) the distance attenuation calculations.

Both these factors are affected largely by the "Effective Source Position" location (as previously defined), both in terms of it's horizontal distance and it's relative height to the receiver position.

This is because three distinctively different receiver/sources arrangements can **all** have the same "Effective Source Position" location and thus the same perpendicular distance between the receiver and the "Effective Source Position" location. (See Figure 2)

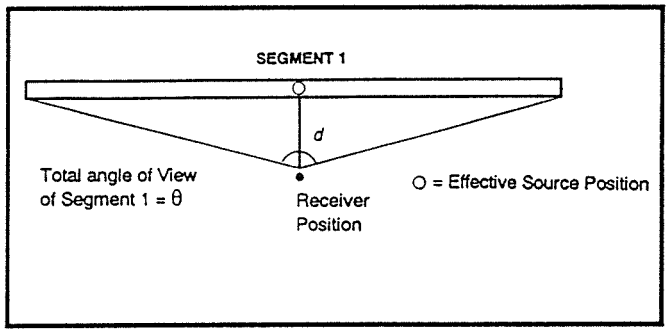

Figure 2a

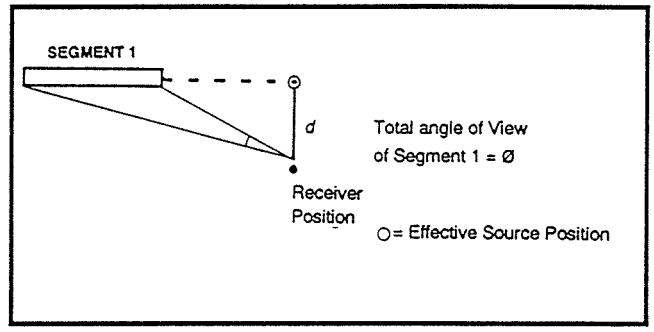

Figure 2b

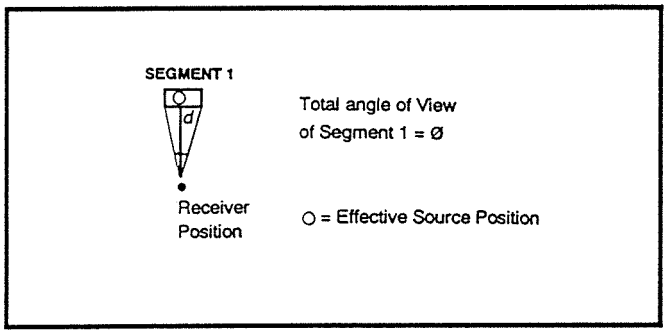

Figure 2c

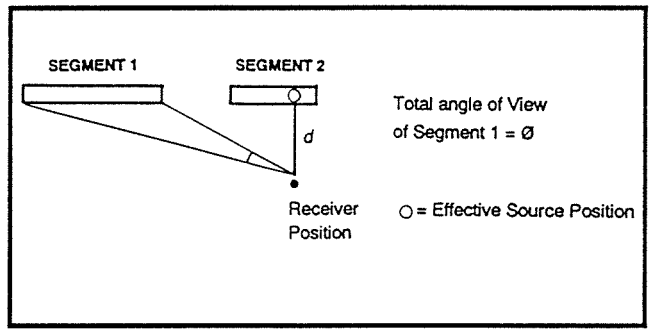

Figure 2d

4.1 Attenuation due to distance

CoRTN assumes the traffic flow (noise source) to be a "line source" and thus there is a 3dB increase in attenuation per doubling of distance.

For the four situations shown in Figures 2a, 2b, 2c & 2d , the predicted noise level, at the receiver is determined from the "Basic Noise Level" by correcting for the length of the road segment/source line via the "angle of view" ie by 10log(θ/180) for the configuration shown in Figure 2a and by 10log(ϕ /180) for the configuration shown in Figures 2b & 2c

CoRTN stipulates that the value *"d"* be used in the calculations to determine the distance attenuation, not the actual distance from the segment to the receiver point. Thus in Figures 2b & 2c the CoRTN calculated distance attenuations would be equal whereas in reality, the CoRTN calculated distance attenuation for Figure 2b, should be greater, in some cases considerably greater.

4.2 Attenuation due to Barriers

The CoRTN method for determining the attenuation correction due to barriers, is based upon the path difference δ, as shown in Figure 3.

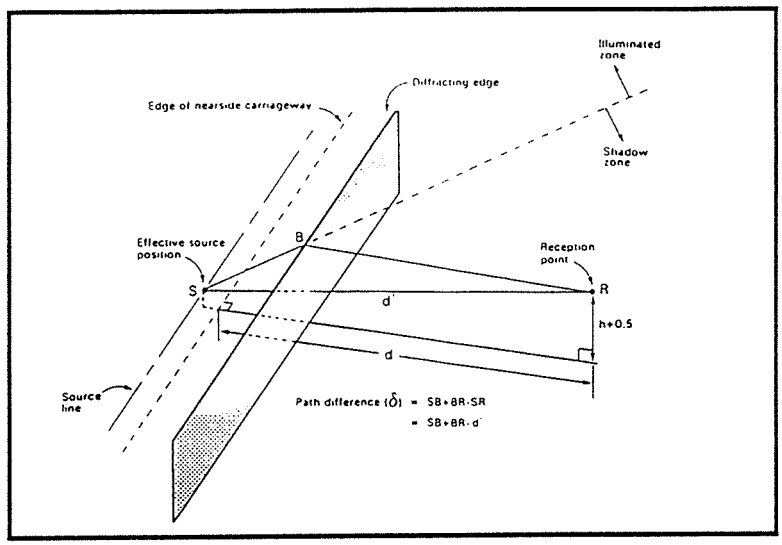

Figure 3

This path difference is calculated, as with the distance attenuation, using the horizontal perpendicular distance between the receiver point and the "Effective Source Position" location, **not** the actual distance from the receiver point to, say, a mid point in the particular line source.

The path difference is also calculated using the distance between the relative heights of the receiver point and the line source. While it is clear cut as to the height of the receiver point, the author has seen a number of interpretations used for the height of the line source.

These interpretations occur where there is a **difference** (or changing difference) in the relative level of the road segment under consideration to that of the relative level of the receiver point. The various interpretations of the height of the source line to be used in the path difference calculations can be summarised as follows:

Interpretation 1: For a road segment (of constant level) which actually contains the "Effective Source Position" location, the height of the source line to be used in the path difference calculations is the height of the "Effective Source Position" location – see Figures 2a & 2c

Interpretation 2: For a road segment (of varying level) which actually contains the "Effective Source Position" location, the height of the source line to be used in the path difference calculations is the height of the "Effective Source Position" location – see Figures 2a & 2c

Interpretation 3: For a road segment (of varying level) which actually contains the "Effective Source Position" location, the height of the source line to be used in the path difference calculations is the average height of the road segment – see Figures 2a & 2c

Interpretation 4: For a road segment (of constant level) which does not contain the "Effective Source Position" location, the height of the source line to be used in the path difference calculations is the height of the ***projected*** road segment at the "Effective Source Position" location (Essentially the actual height of the road segment)– see Figure 2b

Interpretation 5: For a road segment (α) (of constant level) which does not contain the "Effective Source Position" location, the height of the source line to be used in the path difference calculations is the height of the actual road segment (β) where the ***projection*** of road segment (α) intersects at the "Effective Source Position" location – see Figure 2d

Interpretation 6 : For a road segment (α) (of constant level) which does not contain the "Effective Source Position" location, the height of the source line to be used in the path difference calculations is the height of the actual land topography at the ***projection*** of road segment at the "Effective Source Position" location – see Figure 2b

4.3 The Model

To determine the degree of impact of the above factors, a simple model was chosen which simulated many of the situations and topography for freeways Vipac had recently been involved in.

The model consisted of a straight dual highway, with an "angle of view" of 172° to the receiver point. The receiver point was equidistant from each end of the road and approximately 40 metres (***d***) from the inside edge of the nearest carriageway. The road was divided into 3 segments of equal "angle of view", resulting in the outer segments being approximately 482 metres in length and the central segment being approximately 36 metres in length. (See Figure 4)

The gradient of the road segments (0°) and type of road surface was uniform through out the road segments. As only the **variations** in the **total level**, not the absolute levels, were of interest, the assumed traffic flow rate, road surface type, percentage of heavy vehicles, height of receiver (1.5m) and height of source above road (0.5m) were kept constant for all calculations.

The ground cover was taken as zero.

The barriers were assumed to be placed 3 metres from the outside edge of the nearest carriage way on the receiver side of the carriageway. The barriers were located parallel to and at the same level as that of the carriageways.

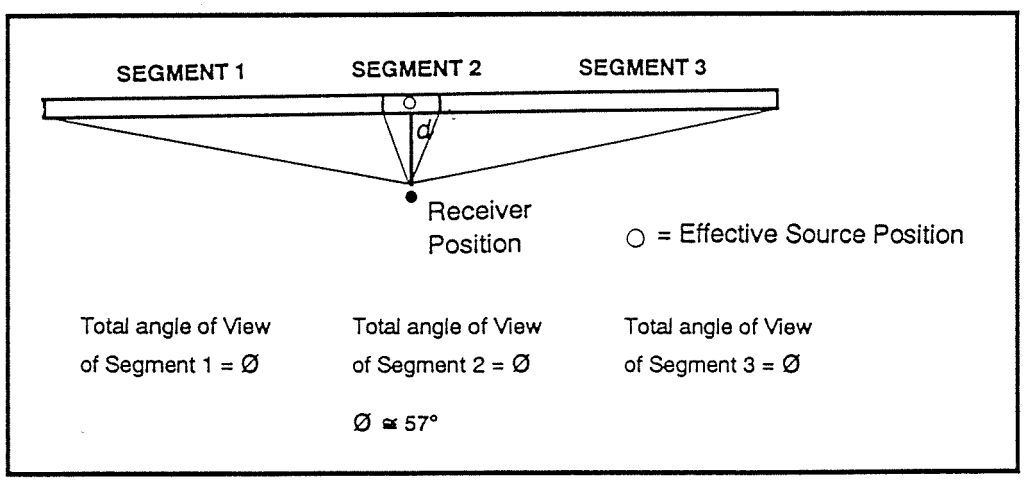

Figure 4

4.4 Parameters Varied

The variations considered were the horizontal distance between the receiver and source, the relative height between the receiver and source and the barrier height.

4.4.1 Relative height of source line to the receiver point.

The relative level of one outer segment was varied with respect to the receiver position/other two segments by between +4.0 to –4.0 metres. The barrier attenuation was then calculated. The barrier attenuation for the remaining two segments was based upon the relative levels of the segment and the "Effective Source Position" location. (As defined in interpretation 2 & 4)

All barrier calculations, for both the varied outer segment and the two remaining segments, were made using the horizontal distance *d* from the receiver point to the "Effective Source Position" location.

The size of the barrier height itself was varied from 0.5 – 4.0 metres.

The total Predicted Noise Level at the receiver point was then calculated for the entire section of road.

The above scenario was then repeated except that both outer segments were either raised or lowered with respect to the "Effective Source Position" location (Central Segment).

4.2.2 Variation in horizontal distance between receiver position and source line.

For this prediction, the height of the road segments was kept constant and equal to that of the ground level at the receiver position.

Two different horizontal distances were used to calculate the barrier path differences viz, the distance from the receiver position to the "Effective Source Position" location and the distance from the receiver position to the midpoint of the segments.

Barrier heights were varied as previously had been done. Also, as before, the effect of one outer segment and then two outer segments on the total Predicted Noise Level at the receiver point was then calculated for the entire section of road.

5.0 RESULTS

The results of the calculations are shown in Figures 5 – 7.

As Figures 5 – 7 show, the major variation in the total Predicted Noise Level occurs when the actual levels of the road segment are used as compared to the case when only the relative levels at the "Effective Source Position" location are used.

Variations of –3.0 dB to +1.0 dB occurred when one outer segment was assumed at it's actual relative height level, for various combinations of barrier height, while –3.5 dB to +2.0 dB variation occurred when both the outer segments were considered.

When the actual horizontal distance between the receiver point and the mid point of the segment, as compared to using the horizontal distance to the "Effective Source Position" location, a variation in

total Predicted Noise Level of –0.3 dB to +0.2 dB was observed if one outer segment was considered. If both outer segments were considered the variation was –0.5 dB to +0.7 dB.

6.0 DISCUSSION

The graphs in Figures 4 – 6 show some inconsistencies, however, these are likely to be due to the situation where the receiver point, top of the barrier for a particular segment and the source height on that segment all line up. The choice of a receiver point to be in the shadow or illumination zone of the barrier also effects the results.

In any case, the effect of the variations described above is certainly evident.

While certainly the model examined here is extremely simple, the effect of the variations on total Predicted Noise Level is very significant when the cost of barriers is considered in relation to meeting the current L_{10}(18 Hour) = 63 dBA criterion. A difference of only 0.2 dB to 0.5 dB can mean significantly increased requirement for barriers and thus the cost for noise mitigation.

When using CoRTN to predict the impact of new roads and highways to meet a compliance with the current L_{10}(18 Hour) criterion, care should be taken when determining the effect of various road segments and associated barriers.

7.0 CONCLUSION

Depending on the interpretation of the CoRTN methodology, variations in the total predicted noise level can occur which have a significant impact on the amount of noise barriers required and thus on the cost of noise mitigation for a given project. It is vital that standard interpretations be adopted.

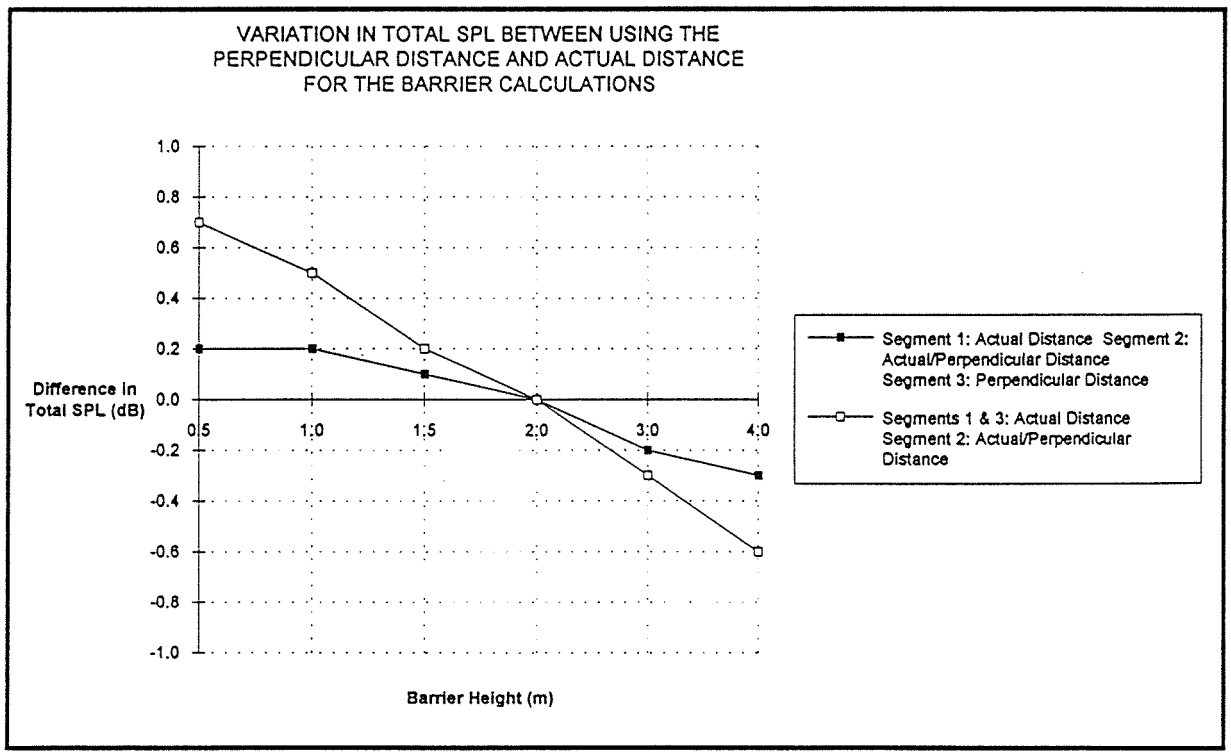

Figure 5

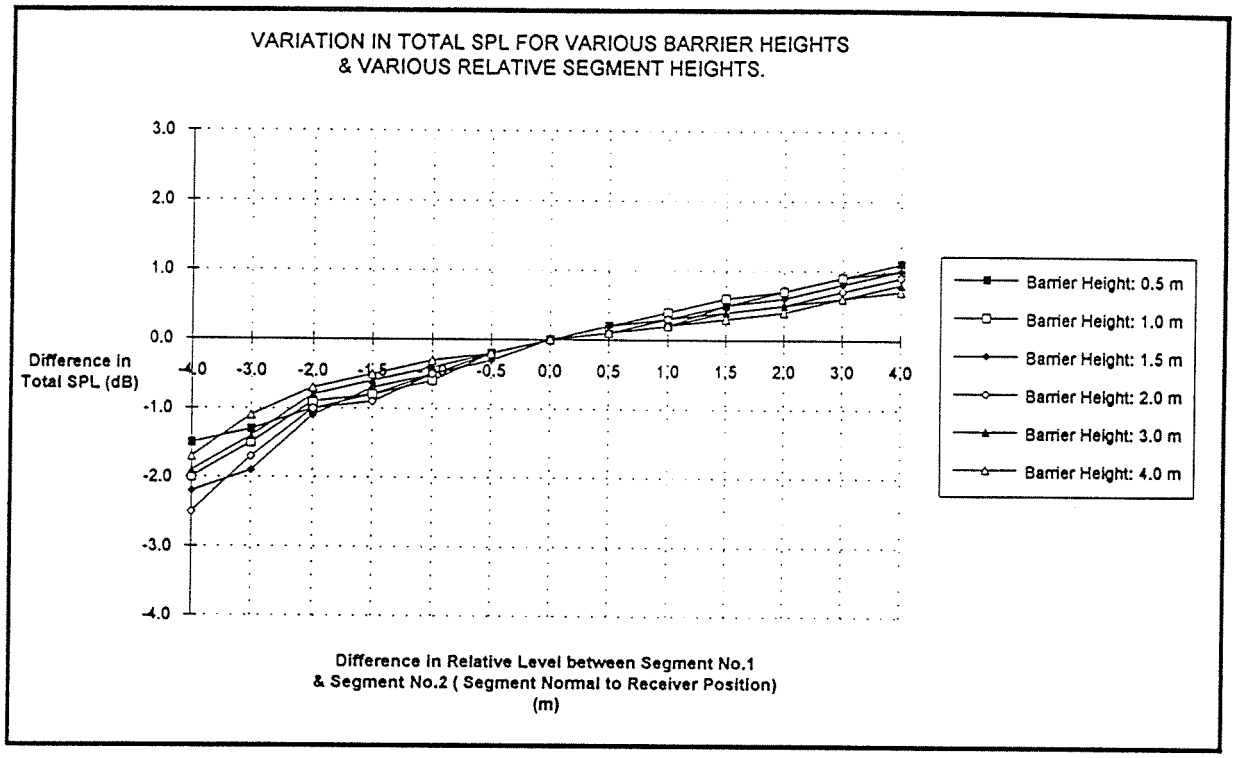

Figure 6

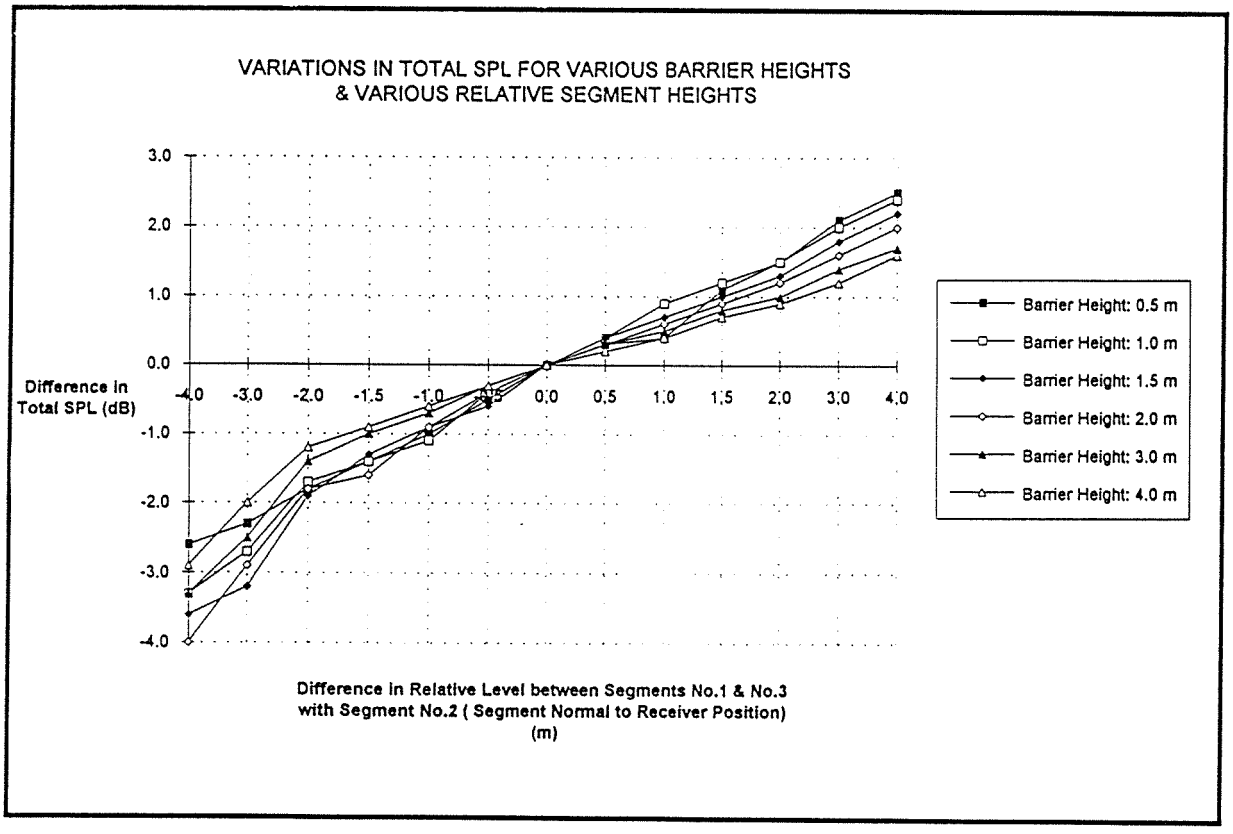

Figure 7

PETER HOLMES

PROGRESS IN ACOUSTICS, NOISE & VIBRATION CONTROL

Proceedings of the 1993 Annual Conference of the Australian Acoustical Society

A.C.N. 000 712 658

9 - 10 November 1993

VENUE:
RAMADA GRAND HOTEL
Glenelg, South Australia

CONFERENCE ORGANISING COMMITTEE:
Convenor: R.W. BOYCE
Committee:
S.A. DIVISION COMMITTEE OF THE AUSTRALIAN ACOUSTICAL SOCIETY

PUBLISHED BY:
S.A. DIVISION OF THE AUSTRALIAN ACOUSTICAL SOCIETY
C/o Dept. of Mechanical Engineering
University of Adelaide, South Australia 5005
November 1993

PRINTED BY:
MANNING PRINTERS PTY. LTD.
Melrose Park S.A. 5039

ISBN 0-909882-13-4

PROGRAMME 9-10TH NOVEMBER 1993

Australian Acoustical Society
Annual Conference 1993
Ramada Grand Hotel
Glenelg, South Australia

TUESDAY MORNING, 9th November 1993

8:00-9:30am **Registration**, 1st Floor Foyer

9:30-9:50am **Opening Address**, Colley Room
Mr Rob Thomas, Executive Director, Office of the EPA, South Australia

9:50-10:30am **Keynote Speaker**, Colley Room
Prof. Dr. Bernd Rohrmann, Lecturer, University of Melbourne, Adjunct Professor, University of Mannheim
"Psychological Perspectives on Regulating Noise Immissions"

10:30-11:00am Coffee Break

	STREAM I, Colley Room **Measurement and Control of Noise**	STREAM II, Hindmarsh Room **Acoustics in Solids**
11:00	A technique for measuring installed silencer attenuation performance, B.Martin	Sound attenuation, enhanced by forced resonance, of elastomer layers containing resonating air inserts, B.C.H. Wendlandt
11:30	Use of polyurethane dampers to reduce noise from a roll-former shear, H.M. Williamson and C.G. Speakman	Location of buried objects by an acoustic impulse technique, A.J. Rogers and C.G. Don
12:00	MS-DOS based systems for airport noise control, A.D. Wallis and R. Thorne	Attenuation and dispersion measurements in porous materials, D.E.P. Lawrence and C.G. Don

12:30-2:00pm Lunch

TUESDAY AFTERNOON, 9th November 1993

	STREAM I, Colley Room **Sound Propagation, Transmission and Attenuation**	STREAM II, Hindmarsh Room **Vibration Monitoring And Isolation**
2:00	The volume velocity method for determining the specific normal impedances of acoustical materials, K. Byrne	Surface excitation: surface mobility, J.Y. Zhao, H. Williamson and J. Baird

2:30	Sound power determination in the geometric near field of a source by pressure measurements alone, D.A. Bies and G.E. Bridges	Four pole parameter characterisation of isolator acoustic transmission performance, J. Dickens, C. Norwood and R. Juniper
3:00	Single and double pulse propagation in a turbulent atmosphere, I.D. McLeod, G.G. Swenson and C.G. Don	The use of the cepstrum to separate source and transmission path effects, R.B. Randall
3:30	Coffee Break	Coffee Break
4:00	Transmission of sound through apertures, K.A. Burgemeister and C.H. Hansen	
4:30	Sound propagation in ducts - modal scattering in rigid-walled ducts of arbitrary axial curvature, G.E. Bridges, D.A. Bies and C.H. Hansen	

5:15-5:45pm **Annual General Meeting of the Australian Acoustical Society**, Colley Room

7:00pm **Conference Dinner**, Grand Ballroom

WEDNESDAY MORNING, 10th November 1993

	STREAM I, Colley Room **Active Control of Noise and Vibration**	STREAM II, Hindmarsh Room **Noise Ratings And Management**
9:00	PVDF noise-control source in liquid-filled pipes, M. Podlesak and R.G. Juniper	Establishment of an outdoor learning environment for young deaf children in an acoustic climate dominated by road traffic noise, J. North and S.E. Samuels
9:30	Sensing vibration to control structural radiation, S.D. Snyder	Attitudes of residents, currently exposed to aircraft noise, to amelioration measures, M.A. Burgess and R.B. Zehner
10:00	Genetic algorithm adaptation of nonlinear filter structures, C.T. Wangl er and C.H. Hansen	Criteria for rail traffic noise, R.B. Bullen and S.E. Banks
10:30	Coffee Break	Coffee Break

11:00	Active control of aircraft interior noise with a view to application in light aircraft, M.T. Simpson and C.H. Hansen	Noise management in the workplace, W. Williams
11:30	Commercial application of active noise control in ducted systems, P.B. Swift	Public policy and the prevention of industrial deafness amongst Australian farmers, I. Eddington, D.Moore and P. Rooney
12:00		Low-frequency noise due to HVAC systems and its assessment, N. Broner

12:30-2:00pm Lunch

WEDNESDAY AFTERNOON, 10th November 1993

	STREAM I, Colley Room **Applications of Numerical Analysis**	STREAM II, Hindmarsh Room **General Papers Session**
2:00	Prediction of road barrier insertion loss by the boundary element method, Xiaojun Du and R.J. Alfredson	Monitoring of the support conditions of buried and sub-sea pipelines using a vibrating PIG, U.G. Kopke
2:30	Numerical acoustics-what are its applications?, J.C.S. Lai	

3:30-3:45pm **Presentation of President's Prize**; **Close of Conference**, Colley Room

TABLE OF CONTENTS

KEYNOTE SPEAKER

MEASUREMENT AND CONTROL OF NOISE

ACOUSTICS IN SOLIDS

SOUND PROPAGATION, TRANSMISSION AND ATTENUATION

VIBRATION MONITORING AND ISOLATION

ACTIVE CONTROL OF NOISE AND VIBRATION

NOISE RATINGS AND MANAGEMENT

APPLICATIONS OF NUMERICAL ANALYSIS

AUTHOR INDEX

Keynote Address:

Psychological Perspectives on Regulating Noise Immissions

Bernd Rohrmann (University of Melbourne, Dept. of Psychology)

(1) The problem: harmful noise effects

Environmental noise caused by road traffic, aircraft, railways, industrial facilities, construction work, leisure activities etc. has many adverse effects on human health and well-being. These physical, psychological and social impacts are significant for both the workplace and life in residential areas. Thus strict regulations are indispensable.

(2) Means of regulating the impacts of noise

Generally speaking, there are three ways in which noise impacts can be mitigated: changes at the source of emission (e.g., technical measures or restrictions of operation); changes at the point of immission (e.g., exposure limits or earplugs); and changes 'in between' (e.g., noise barriers or relocation). Usually regulations employ both technological and administrative approaches. Immission limits are the core of protective efforts in noise-exposed residential areas.

(3) Setting immision standards

If environmental immissions such as noise place human health and well-being at risk, it is the responsibility of the authorities to assess the scientific knowledge available in order to identify critical exposures and to initiate measures which protect the affected population, including emission or immission limits. Setting standards for noise protection requires dealing with five issues:

> The effects issue: What somatic/psychological/social impairments occur?
> The causality issue: Is the immission a primary cause of the observed effects?
> The relevancy issue: Which effects are to be evaluated as undesirable/unacceptable?
> The transformation issue: Which levels of exposure correspond to these critical effects?
> The regulation issue: Which technical and/or regulatory actions provide the desired protection?

As disturbance and annoyance are the most frequent effects of environmental noise, psychological findings turned out to be the crucial input into standard-setting efforts.

However, the utilization of scientific research for the purpose of respective risk assessment and political decision-making lead to a variety of problems. Cardinal difficulties are that the effects of environment stressors constitute a multicausal process: that data on somatic, psychological or social effects and evaluations of unacceptable impacts have to be converted into physical units; and that normative statements, not just empirical findings, are required.

(4) Effectiveness of noise regulations

Environmental standards should provide effective protection for people at risk; and it should be possible to verify their effectiveness. Actual immission limits for, e.g., traffic or industrial noise achieve that only moderately – mainly because the 'stimulus-response' (or dose-impact) relationship is embedded in a complex structure of effects. The less the physical and/or administrative/legal definition of a standard correlates with the medically or psychologically critical impact threshold, the larger will be the fraction of the affected population virtually left unprotected. Standards are defined (both on the stimulus and on the response side) on the basis of average conditions and are intended to generalize across specific situations and individual risk characteristics. Although this enhances their universal validity, at the same time it reduces their effectiveness in respect to individual cases, because the variability of responses is ignored. Only stricter limits can compensate for this. Another problem is the restriction to 'one-number' indices, as this might lead to an insufficient or even invalid characterization of noise impacts for particular exposure conditions.

(5) Outlook: Research & policy needs

Consequently, further approaches to defining and handling noise regulations for residential areas should be explored. Also, as setting environmental standards is virtually a normative process, the make-up of the decision-making body and its legitimation are of key importance. Finally, the effectiveness of immission limits has to be proved in terms of community response – therefore systematic social-scientific evaluation research is essential, both to check whether the desired protection of health and well-being is realized and to learn about possible improvements.

A TECHNIQUE FOR MEASURING INSTALLED SILENCER ATTENUATION PERFORMANCE

Byron Martin

VIPAC Engineers and Scientists, PO Box 439,
WOODVILLE SA 5011

INTRODUCTION

To quickly reduce tonal (blade pass) noise emissions from a large exhaust stack [1], an absorptive silencer was designed [2] and installed. This "quick-fix" would allow sufficient time for a reactive silencer to be designed, including model testing. The absorptive silencer was built and installed at a total cost of around $30,000. Immediately the complaints from the local and distant neighbourhoods about noise ceased, and the plant management cancelled the reactive design pending durability trials on the absorptive design. We predicted one to two years effective operation, and based on this "life" plant management considered it was more "cost effective" to regularly replace the absorptive in-fill, at about $12,000 a time, than to spend about $120,000 on a "permanent" silencer.

The location of the silencer and the details of its construction are shown in Figure 1. The presence of contaminates, dust and moisture, would eventually "clog" the absorptive material in the silencer. Therefore the acoustic attenuation was to be monitored to predict the degradation of the silencers acoustic performance. Trending the acoustic performance in this way would therefore allow sufficient lead time for maintenance to be programmed into the regular plant shut-downs.

Traditionally a far field monitoring station would be used to monitor the attenuation but several stations would be required to overcome the effects of the prevailing weather conditions. Also, the environmental (residential) background noise levels effect the accuracy of determining stack noise level increases and hence performance degradation. Measuring the attenuation in-duct overcomes these problems but in-duct noise measurements will be dominated by flow noise which will tend to mask the attenuation.

The aim of this work was to develop a reliable and repeatable

method for measuring the (tonal) acoustic attenuation of the silencer in-duct. The bandwidth of interest extended from 100 to 1000 Hz.

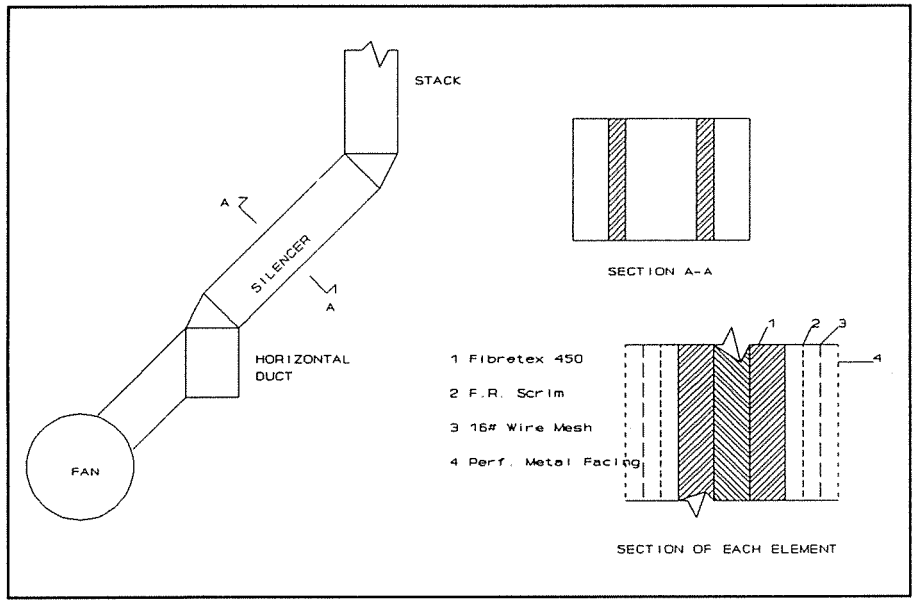

FIGURE 1
Schematic Layout of the Duct, Cross-Section of the Silencer and a view of the construction of each Element

The Time Synchronous Averaging technique detailed in this paper results from our attempts at minimising the convected noise field produced by the exhaust gas flow, in order to resolve the propagating tonal acoustic field responsible for the community annoyance.

MEASUREMENT TECHNIQUES

To minimise the effect of flow noise on the in-duct noise measurements, four microphone - probe combinations were trialled. These consisted of probes with two lengths; long - for SPL measurements in the centre of the duct and short for SPL measurements just off the wall on the duct, and two end styles; square and at 45°. Two microphones were used; a 1" B&K "reference" and 10mm RS "working" grade for possible permanent installation and low cost replacement because of the harsh environment inside the duct. Figure 2 shows these four microphone - probe configurations.

Both up and down-stream of the silencer the in-duct noise field would be measured in a grid pattern to determine if variances existed across the duct; using the long probes. Our aim being to determine if the noise field could be sampled near the duct wall at one place; using the short probes. Experience at similar installations by our engineers [3] had shown that a probe with a 45° end would minimise the effect of the flow noise.

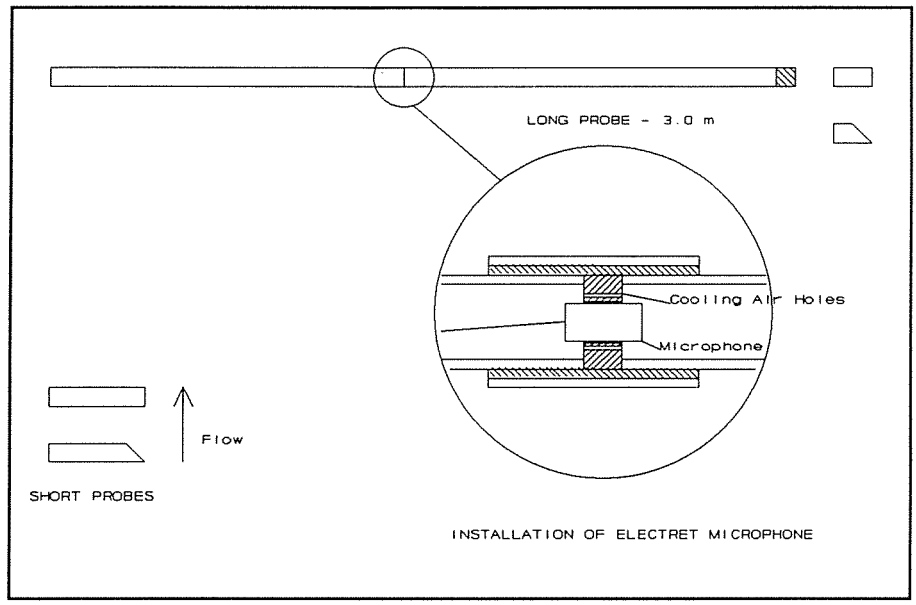

FIGURE 2

The four Microphone Probes used for this work, the Long Probe (3m) has two possible end pieces as well as provision for an Electret Microphone.

IN-DUCT NOISE FIELDS

Sound pressure levels were measured with both probe ends in a grid pattern in the sections of the duct down and up-stream of the silencer, see Figure 1. Typical narrow band spectra are presented in Figure 3, showing that the sound field up and down-stream were dominated by a tone at 31.5 Hz. This frequency corresponds to the long probe resonance, calculated with c = 395 m/s (@ 115°C) and a probe length of 3.0m. The blade-pass frequency is 180 Hz. Thus a probe would need to be much shorter than 0.5m, say 200mm. The "cooled" electret microphone was used in an attempt to "shorten" the probe length, but it melted. Unfortunately neither of the probe ends used with the long probe reduced the convected noise field sufficiently to reveal the fan blade pass or it's harmonics, as can be seen in Figure 3.

The sound pressure levels measured with the short probes showed no characteristic features *eg* blade pass tones. We knew however that a blade pass tone was audible away from the plant. Experience with the analysis of gear meshing vibrations suggested that the blade pass frequency and its harmonics should be fully synchronous with the fan rotation.

TIME SYNCHRONOUS AVERAGING

By synchronously averaging [4] the noise field within the duct with the fan run-speed, all the non-synchronous noise, *ie* flow noise, will

average to zero. The non-synchronous noise reduction is proportional to the square root of the number of averages. The synchronous part, in this case the blade pass and its harmonics, will remain and the convected noise field will be removed.

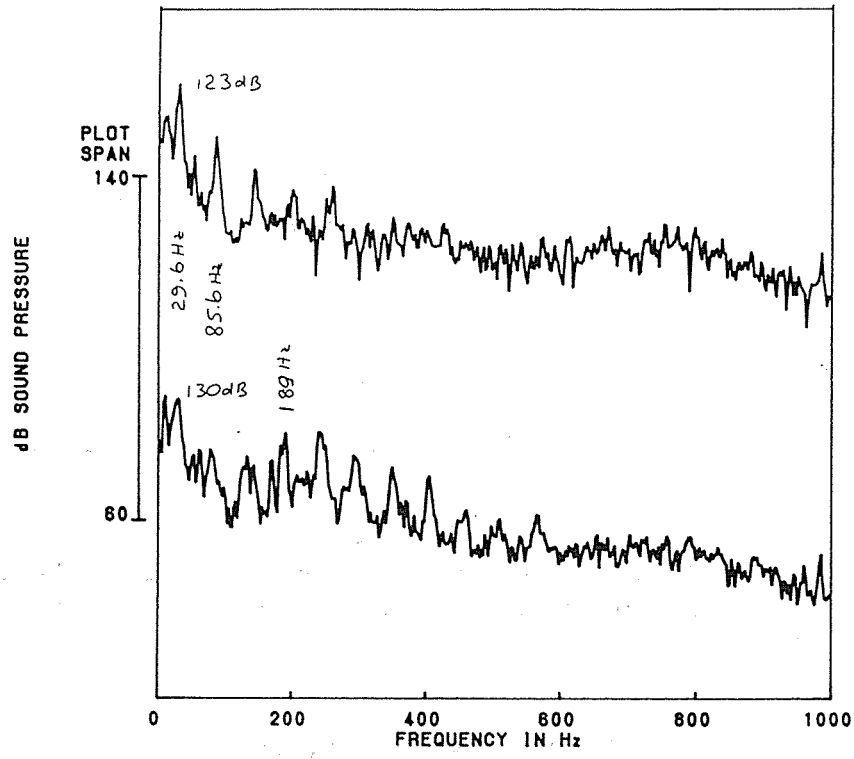

FIGURE 3
Typical sound pressure levels up and down-stream of the Silencer

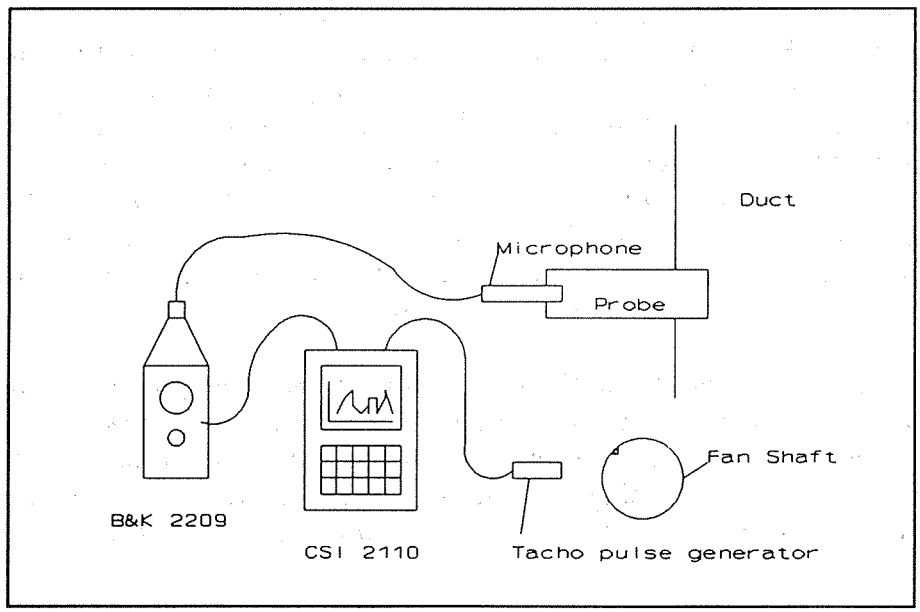

FIGURE 4
Equipment used for Time Synchronous Averaging

To achieve this improvement in signal-to-noise, the microphone probe (short with a square end) was inserted just inside the duct wall and a once-per-rev tacho pulse was taken off the fan shaft. The tacho pulse was then used to trigger the averaging mode in a spectral analyser. The equipment used was a B&K 2209 sound level meter and a CSI 2110 data collector and analyser, as shown in Figure 4. The resulting up and down-stream spectra shown in Figure 5, clearly show that TSA has reduced the non-synchronous flow noise by 20-30 dB and revealed the blade pass tones.

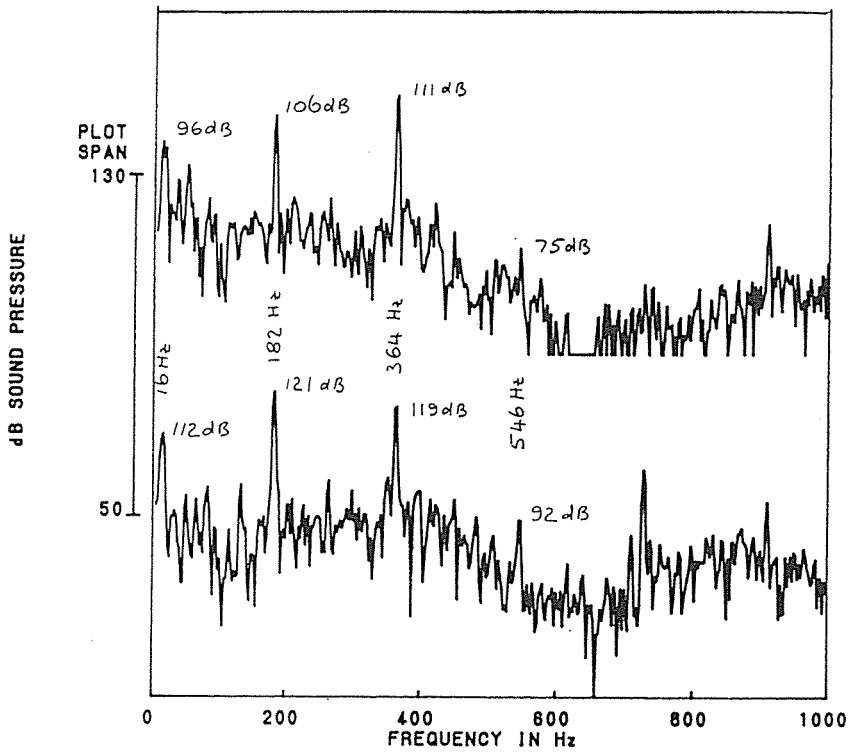

FIGURE 5
Up and Down-Stream Sound Pressure Level, after 100 Time Synchronous Averages, *cf* Figure 3

CONCLUSIONS

The technique of Time Synchronous Averaging an acoustic field inside a duct system with the fan rotations, allowed the removal of convected flow noise to reveal blade pass tones and their harmonics. These tones, measured both up and down-stream of a silencer, allowed the in-duct acoustic attenuation of the silencer to be readily calculated. Knowledge of this acoustic performance, in this case degradation, allowed sufficient time to warn the plant operators so that it could be rebuilt at a regular shut-down, well before any environmental noise complaints were made. Figure 6 shows how the gradual loss of attenuation occurred with time, until the fibreglass in-fill in the splitter elements was replaced after fifteen months operation.

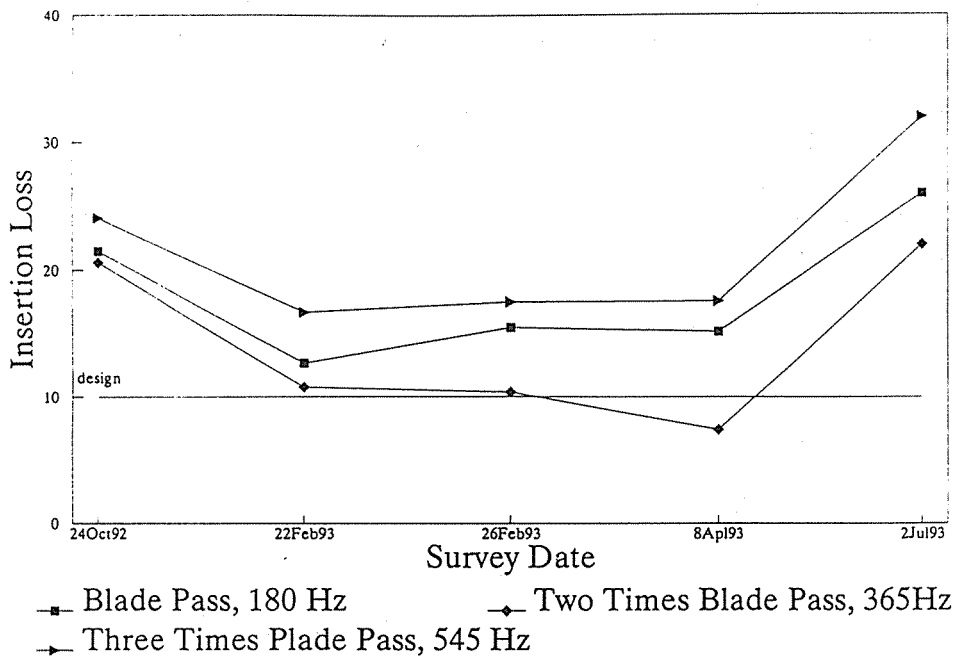

FIGURE 6

The acoustic performance degraded with time, until in May the silencer was rebuilt.

References

1 Martin B.T. and Rennison D.C. "Environmental Noise Control of a Large Cement Plant", Inter-Noise 92, Toronto 1992.

2 Bies D.A.and Hansen C.H. "Engineering Noise Control", Unwin and Hyman, London 1988.

3 Sparks D. "Investigation of Vibration of No.8 G.F. Boiler", a VIPAC report for APM Ltd. Morewell Vic.

4 Randall R. "Gearbox Vibration Analysis", Machine Condition Monitoring and Fault Diagnosis, Edited by C.H. Hansen, University of Adelaide, Vol 1, p308-331, June 1987.

USE OF POLYURETHANE DAMPERS TO REDUCE NOISE FROM A ROLL-FORMER SHEAR

H. M. Williamson, C. G. Speakman

Acoustics and Vibration Centre
University College, University of New South Wales
Australian Defence Force Academy
Canberra, ACT 2600

INTRODUCTION

Roll-formed products are made from rolls of sheet metal which are cold formed to the required shape by feeding a flat sheet through a series of profiled rollers. Production is normally a continuous process with the sheet passing from the rollers, through a shear and onto a run-out table. The sheet is cut to the required length using a flying shear which impacts the sheet at high speed. The lower shear blade is shaped to match the profile of the product whilst the upper blade has a small rake designed to improve cutting efficiency. Figure 1 shows a schematic diagram of a typical roll-forming operation using an 'airbag' shear (a shear powered by compressed air). Hydraulic shears are also common in roll-forming operations.

Roll-formed sheet metal products, which come in a variety of profiles, thicknesses and surface coatings are used extensively for roofing, walling and fencing of industrial and domestic buildings. Two common examples of roll-formed products are shown in figure 2. In order to reduce transport costs and to provide a rapid response to customers, a large number of roll forming production lines are distributed around urban and rural centres throughout the country.

High impulsive noise levels are produced by the cutting action and the resulting impact induced vibrations of the product and surrounding structure. The noise levels are of concern for both environmental and worker safety reasons. The operator works in close proximity to the shear removing and stacking sheets and is hence exposed to high noise levels during production. The operator requires frequent access to the shear to remove the finished product and to guide the sheet through the shear after roll changes. The need for access to the shear together with the high costs involved make the installation of noise enclosures an unattractive option unless significant noise reductions can be achieved.

Noise measurements were taken before and after the installation of noise enclosures around two roll-former shears (1). These measurements indicated that the performance of the enclosures was well below what would normally be expected. The enclosures were made to cover only the immediate area around the shear and because

the product extends well beyond the confines of the enclosure, openings were required for the inlet and outlet of the sheet. Analysis of the results suggested that noise radiated by structural vibrations (primarily from the product) were dominant after the installation of the enclosure. The effectiveness of noise enclosures placed around roll-former shears will therefore be severely limited unless some form of sheet damping is also installed.

An early investigation (2) indicated that a major source of noise in the shearing process was noise radiated from the sheet metal product. As a result of this investigation prototype sheet dampers were developed by Lysaght to test the effectiveness of sheet damping in reducing the noise from roll-former shears. The dampers were attached to a hydraulically actuated shear producing the Trimdek profile shown in Figure 2. These dampers consisted of polyurethane fingers which were attached to the shear carriage and clamped the sheet just prior to and after cutting. The resulting investigation (3) concluded that sheet damping was an effective an practical means of reducing impact noise from a roll-former shear. A reduction of 5.5 dB(A) was achieved under production conditions with upstream dampers in place and this was increased to 7.9 dB(A) with both upstream and downstream damping.

Larger dampers were constructed which conform to the profile of the product. The intention was to achieve a larger contact area than the dampers used in previous trials. This paper reports the results of tests conducted on these dampers and forms part of an ongoing investigation undertaken by the Acoustics and Vibration Centre and Lysaght Building Industries. The aim of this research is to find cost effective retrofit noise reduction techniques which can be applied to the large variety of roll-former machines currently in production.

EQUIPMENT AND TEST PROCEDURE

SHEAR

Tests were conducted on an 'air-bag' shear producing the Custom Orb profile. Figure 5 shows a schematic diagram of an 'air-bag' roll-former shear and the position of the sheet dampers. Figure 2 shows the common 'Custom-Orb' product. The shear is actuated by passing compressed air into air bags above the top blade carriage which is then forced downward. In normal operation the top blade makes contact with the sheet and the shear moves with it until the cutting stroke is complete. For this investigation, measurements were conducted with the roll-former static.

DAMPERS

Sheet dampers were constructed from a steel base plate coated with polyurethane which was moulded to the shape of the product profile as shown in figure 3. The dampers extend over the full width of the sheet and cover 200mm of sheet length. Two sets of dampers were manufactured using 40 and 60 durometer hardness polyurethane. The product was held firmly between the dampers by applying a clamping force between the upper damper and the lower blade carriage as shown in figure 4. The dampers were placed upstream of the shear as close as practicable to the cutting blades. No downstream dampers were used for these tests.

MEASURING EQUIPMENT

Simultaneous noise and vibration measurements were recorded using a micro-

computer based data acquisition system in conjunction with a Brüel and Kjær modular precision sound level meter type 2231 (SLM). The AC output from the SLM was connected to the data acquisition system and the noise from the cutting action was recorded simultaneously with the vibration measurements from two accelerometers. The first accelerometer attached to the upper blade carriage, was used to trigger the recording. The second accelerometer placed 400mm upstream of the shear blades recorded sheet vibrations. The SLM was placed 1.5m above the factory floor and 2m from the shear.

RESULTS AND DISCUSSION

The results shown in Table 1 are the noise levels achieved relative to the no sheet damping case, each value being the average result of four cuts. The digital data was processed using computer software to simulate the fast averaging response of the SLM. This allowed the noise signal to be separated into very short time periods and hence the L_{Aeq} and the L_{Amax} of the cutting pulse were calculated. The L_{Amax} was also read directly from the SLM and compared with the computer generated value in order to check the accuracy of the calculations. The calculated L_{Amax} values were within 0.1 dB of the SLM readings. The results show that the softer (40 durometer hardness) dampers were more effective in reducing sheet vibrations.

	L_{Aeq} of Cutting Pulse	L_{Amax} (fast response)
40 Durometer Dampers	- 3.8 dB(A)	- 4.0 dB(A)
60 Durometer Dampers	- 3.5 dB(A)	- 3.5 dB(A)

Table 1 - Noise levels relative to no sheet damping dB(A)

Figures 6 shows a typical example of the data obtained from the digital data acquisition system. The upper two traces of figure 6 show the acceleration recorded from an accelerometer placed 400mm upstream of the shear blades in the centre of the product. The accelerations recorded show that both the amplitude and duration of the sheet vibrations have been reduced by damping the product. The lower traces show the sound pressure resulting from the shear cutting. These results show the good correlation between the sound pressure and sheet vibration measurements as well as the reduction in noise levels achieved by damping the sheet. Further reductions in noise levels can be expected by adding dampers downstream of the shear.

As in previous investigations, sheet damping has proved an effective means of reducing the noise produced by roll-former shears. Only upstream damping was utilised in these tests. This is probably the reason why a smaller noise reduction was achieved in these tests compared to the finger damper case (2). Other factors influencing this result are;

- The large flat sections on the Trimdek profile may be more easily damped than the profiled sections on the Custom Orb product. It should be noted that the noise produced by shearing the Trimdek profile is up to 5 dB higher than that produced by shearing Custom Orb.
- The airbag shears have very rigid blade stops which were not present on the hydraulic shears used in previous tests. The noise produced by the blade striking these stops may have become increasingly dominant following the reduction in noise radiated by the product.

The noise reduction achieved by the polyurethane dampers has been encouraging and the dampers are currently being attached to the actuating mechanism of the shear in order to clamp the sheet just prior to cutting. Once the dampers are incorporated into the machine investigations will be carried out under production conditions in order to optimise the performance of the dampers and to find the most effective and durable damping material.

CONCLUSION

Noise radiated from the sheet is a major source of noise associated with shearing roll formed products. Damping sheet vibrations close to the blade has been shown to be an effective method of reducing this noise. The use of polyurethane dampers shaped to the profile of the product has shown promise and given further development significant noise reductions can be expected.

REFERENCES

1. "The effectiveness of roll-former noise enclosures", C.G. Speakman, J.C.S. Lai, Lysaght Building Industies, August 93
2. "A data acquisition system for the study of impact noise in machinery", M.J. Harrap, J.C.S Lai and H.M. Williamson, Inter-noise '91, pp 1097-1100.
3. "Some noise reduction measures applied to a sheet metal shear", M.J. Harrap, J.C.S Lai, H.M. Williamson and R.Brand, Inter-noise '92, Canada.

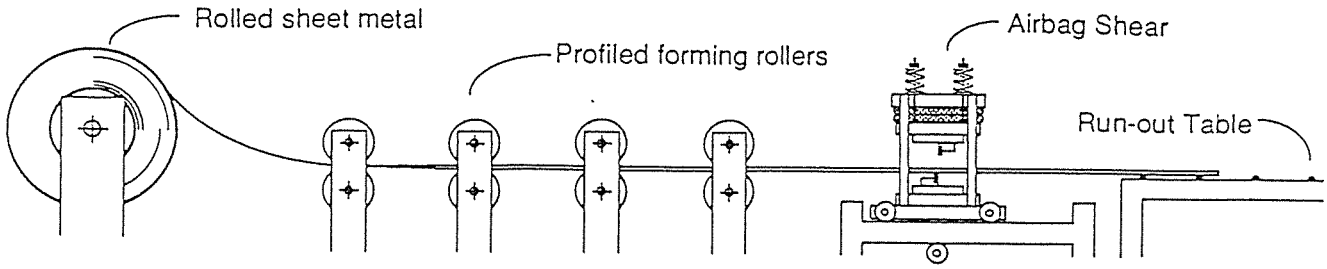

Figure 1 - Schematic diagram of a typical roll-former operation

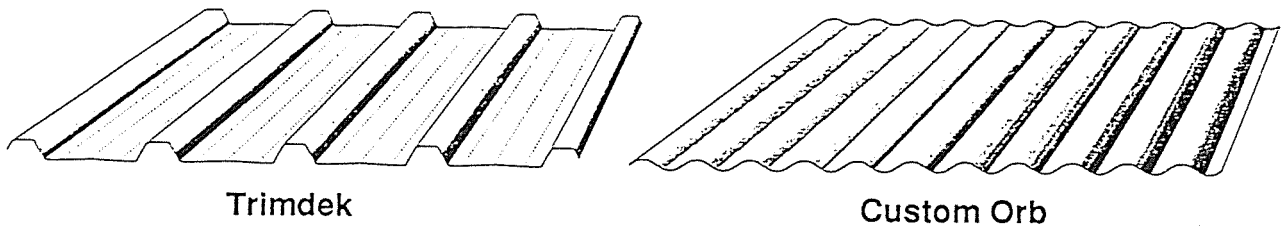

Figure 2 - Typical roll-formed products

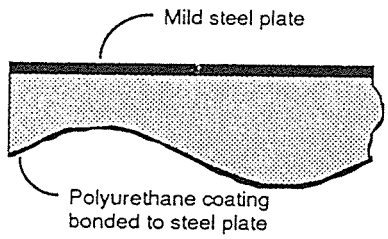

Figure 3 - Damper Construction

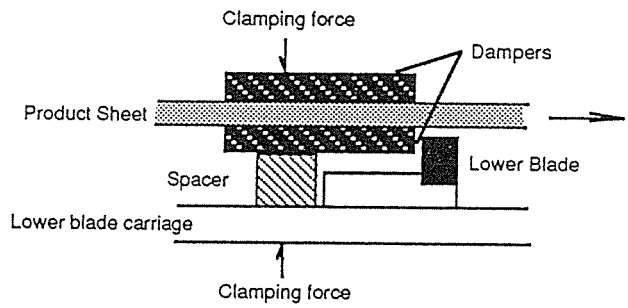

Figure 4 - Damper placement

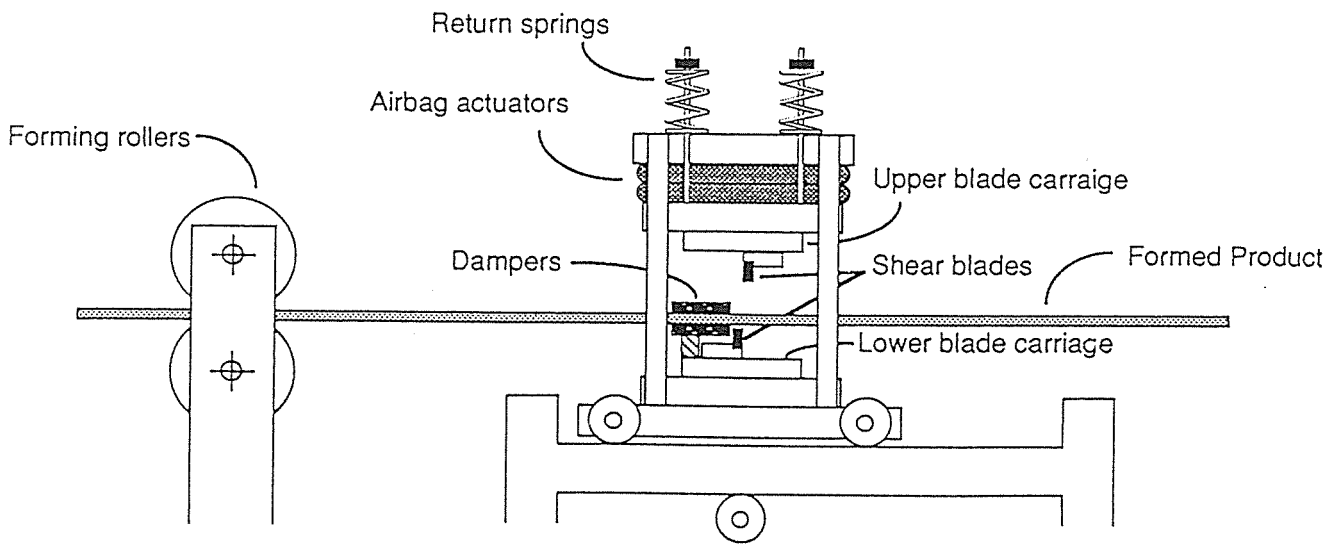

Figure 5 - Schematic diagram of an 'air-bag' shear

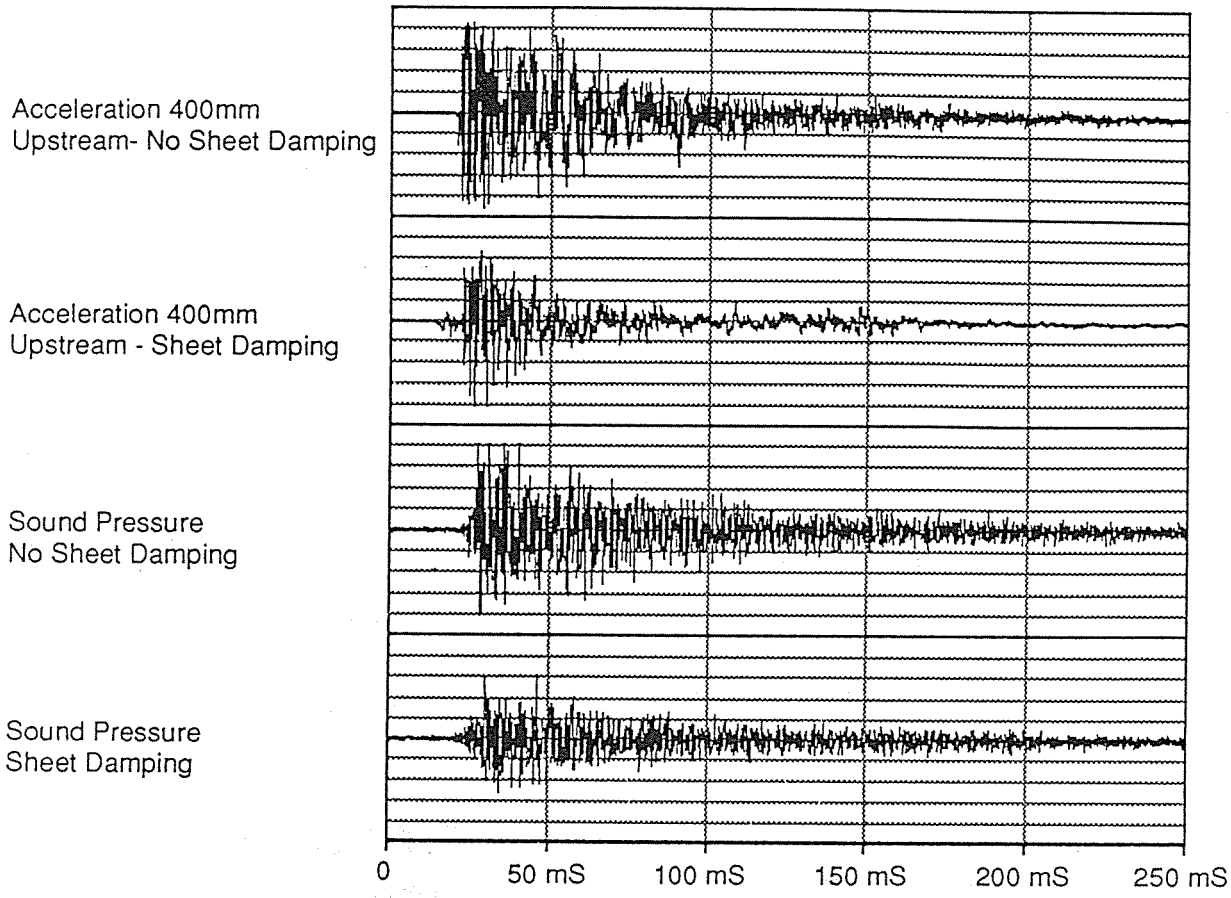

Figure 6 - Vibration and Sound Pressure versus Time

MS-DOS BASED SYSTEMS FOR AIRPORT NOISE CONTROL

A.D. Wallis MIOA (1), R. Thorne (2)

(1) Cirrus Research plc, Hunmanby, United Kingdom.
(2) Cirrus Research pty, Rotorua, New Zealand.

INTRODUCTION

In previous communications (*ref 1*), we have described the high technology noise monitors installed at Sydney, Brisbane and Melbourne airports. In this paper, we give a further report on the advances made in automatic aircraft recognition and subsequent measurement of aircraft noise. Some of these new ideas have been incorporated into noise monitoring systems fitted at Wellington, New Zealand as well as Warsaw, Poland and Miami, Florida, while the latest frequency measuring system is now fitted to a new system in Italy.

The installation at Sydney was fitted with what was then the most complex algorithm used in a commercial system. Figure 1 shows the basic elements. The use of guard times to identify reverse thrust were an essential addition, as at many airports such as Sydney, a simple algorithm would pick this noise up as a separate event and thus allow the event correlation to get out of step. At Sydney, a large, but slow UNIX system was adopted as the host because the complexity of the overall Noise and flight tracking system which militated against an MS-DOS application. Today, with the huge increase in computer speeds over the last few years, it now becomes practical to use MS-Windows to operate the whole system. This gives much faster operation and a huge saving for the user, with little, if any performance reduction; indeed today systems can run faster under DOS than UNIX.

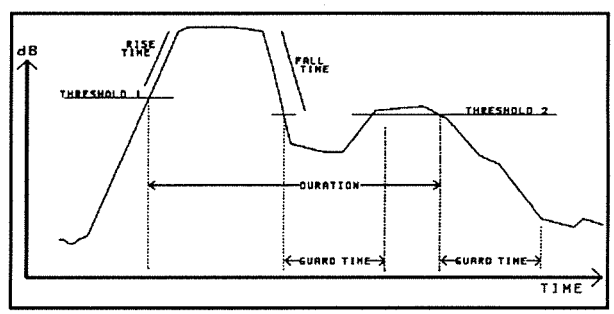

Figure 1: Original template

The main advance at Sydney was the very high standard of the actual noise monitors, which at the time took second place to the great publicity about the software used to read them and display the data. It is clear to anyone in the acoustic field that to have an accurate reliable system, the main requirement has to be a stable, accurate and reliable Noise Monitoring terminal, a fact usually forgotten by those who see the software as the main task. Since Sydney, the internal program in the terminals, normally called the firmware, has been modified out of all recognition to the original. However, the actual hardware has stood the test of time somewhat better and the physical modifications have been very minor, mainly in fact made to take advantage of new integrated devices, which can directly replace the original parts. The performance of the hardware was

demonstrated in 1993 by the formal approval of the Cirrus Research CRL 243 NMT by the most prestigious test house in the world.

USER COMMENTS

In any system such as an airport noise monitor, user comment and feedback is vital, as an instrument manufacturer cannot have as deep a knowledge of the practical problems as the end user. In the same way, users cannot have the deep knowledge of the field which enables them to specify accurately the latest technology. However, since Sydney, many users have realised the essential conceptual difference between the Cirrus acoustic approach and older 'dumb' terminals and have modified their demands as a result. In essence, the main difference is that Cirrus regard the NMT as a complex acoustic data computation unit, with significant 'intelligence', whereas older systems treated it simply as a 'microphone on a pole'.

To review some of the latest developments, it is useful to look at the differences these approaches create. In a traditional, software based system perhaps 16 monitors are all trying to communicate noise data to the host computer in real time. At the same time the host computer is trying to recognise each aircraft event, correlate these with flight or radar input data and simultaneously, carry out 'watchdog' and housekeeping functions. This multi-tasking concept initially determined the use of UNIX or some other complex operating system, not only for the complexity alone, but because of the greater perceived robustness of the UNIX operating system.

In the Cirrus concept, the operation is very different. Each monitor, or NMT, has complex recognition algorithms built in and thus it is only summary data that needs to be sent down to the host computer in real time. The workload reduction on the host computer is very significant, of the order of 30 times. For example, in the classic case, with 16 NMT's in use, 16 sets of raw data are arriving at the host every second, plus any alarms or other weather or environmental data in the system. Obviously, this itself is not an onerous task for the host, but if at the same time, it has to pass all these 16 sets of data through its recognition algorithms, the task can become outside the ability of even the fastest DOS machine.

Now, if the NMT itself sends only a summary of the aircraft data as ASCII data with all the recognition complete, all the host has to do is to store it in a database ready for subsequent correlation. In other words, not only is the power required at the host much reduced, it is in reality now just a graphic display for the 'intelligent' NMT's. A further advantage is that the NMT itself can use 62,5 mSec Short Leq data in its recognition process and thus get a much improved resolution. As it is impossible to pass data from 16 NMT's to the host at this speed, all other simpler devices are forced to use the 1 second Leq values in their recognition algorithm, with consequent lower performance.

THE ALGORITHMS

New since Sydney is the concept of adding rise and fall time filters to the basic algorithm. Fig 2 shows the general idea.

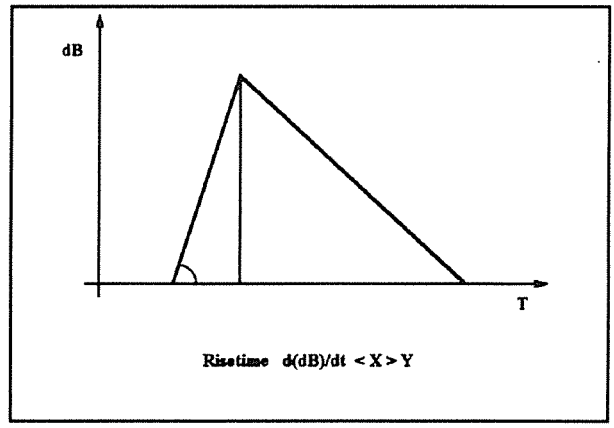

Figure 2: Risetime addition to algorithm

These filter out noises such as a road-breaker, a heavy vehicle moving very slowly and other obvious noises that can mimic the basic shape of an aircraft event. The improvement in the 'hit rate' is significant, almost halving the incorrectly identified events. In an ideal location, the current 'hit rate' is now of the order of 97%, but obviously, the figure depends very much on the particular location of the NMT. If there is a very good signal to noise ratio, the recognition can be as high as 99+%. If the background noise is very high and varying, the 'hit rate' can be very low indeed. The basic algorithms somewhat modified can be used for other types of noise event (ref 2).

Because the signal to noise ratio is of such prime importance, the NMT measures the background noise continuously, using several of the available parameters, but usually L_{99}, L_{92} and L_{85}. These three, taken together, can allow the recognition template to be altered to give a 'best fit' to the current noise climate. While certainly not foolproof, this gives a further improvement in the recognition process. The main problem of this algorithm modification, is that any Ln value is by its nature historical and does not reflect the noise situation at the event time. However, over the typical time scale of an aircraft event, say 100 seconds, the previous 300 second Ln values are very valuable in determining the threshold of an event.

Major further improvements to the recognition algorithm would seem to be difficult when the only data source is the 'A' weighted time history, but a few, such as the use of pattern recognition by neural networks, or learning algorithms, obviously have room for development. To get significantly better performance, more data is needed and thus, an FFT module has been added to the NMT. This takes a series of spectra several times per second and uses these spectra in many different ways to assist or modify the main algorithm. In addition, the FFT spectra can be converted to one third octave every half second and these data used to generate the EPNL. While it is quite wrong to attempt to use EPNL for the measurement of aircraft noise in service, many older or non technical users insist on having this data. The main use would seem to be to check that the original aircraft certification is correct, but as the flight path and measurement conditions are totally different for certification, this is usually a pointless exercise.

Current work in this area is centred on speeding up the FFT to have the data in about 7 milliseconds and using this data as input to a 'fuzzy logic' system to modify the recognition templates. Obviously, there are many FFT units today

which can generate an FFT in less time than 5 milliseconds, but for a successful noise monitor on a pole, the operating power is a critical parameter and it is the best speed/power combination that is desired over the 24 bands from 50Hz up to 10kHz. However, the minimum speed specification is set by the need to meet the technical requirements of appendix 16 of the ICAO protocol.

TRACK DATA INPUT

Conventional computer wisdom has been that to make a flight track and noise monitoring system, UNIX was the minimum system that was practical. However, today this view is being challenged. When the noise monitor itself does so much of the noise computing, the time left to run the vector algorithms of a flight track replay system is now adequate with current generation of 80486 based machines. As desktop computers will continue to get faster and faster, the 'UNIX only' view will clearly soon be out of date. Today, flight input data is part of the system described, but as we come from an acoustic background, we have concentrated on using this data for identification and not attempted to store actual flight tracks. The correlation of the flight track data is currently done using 'time band' algorithms, which grade the correlation into a series of probability bands and these are used to determine the actual flight data. The flight track data itself can come form manual input data or from flight informatoin systems, using UNIX or any other operating system, as it is an inconsequential task to read data from other operating systems.

CONCLUSION

In only four years since the Sydney system was developed, the performance of area noise monitoring systems has increased many times, making the system there seem almost 'old fashioned' in computing terms. As well MS-DOS systems have developed which have power far in advance of what was imaginged in 1990, making MS-DOS systems a practical reality.

Sydney was a milestone between the older 'mini' computer systems and the current high technology monitors and as such has a clear place in the history of airport monitors. However, current work in our laboratories seems to show that the next generation of monitoring systems will be at least as big an advance on those at Sydney, as Sydney was in 1990.

REFERENCES

Wallis & Krug. 'Sydney & Brisbane Noise terminals' Westprac, Brisbane 1991

Snell & Wallis 'Remote Blast Monitoring....analysis' Proc Internoise 1992

Sound attenuation, enhanced by forced resonance, of elastomer layers containing resonating air inserts

B.C.H. Wendlandt
Materials Research Laboratory
P.O Box 50, Ascot Vale 3032, Melbourne , Australia

Abstract

The acoustic response of perforated and air cavity filled viscous-plastic elastomer layers is described in terms of impedance and resonance behavior of the major acoustic structures commonly found in sound attenuating layers as applied to underwater structures. Normal reflection properties are predicted as a function of surface impedance variations due to potentially acoustically resonating features of the layer. Forced resonance of acoustic elements is shown to extend for practical application the effects of natural resonances. Such layers are important in quietening sound transmitting structures and reducing echoes from structures underwater.

INTRODUCTION

The acoustic properties of plastic-elastomer layers [1] used to quieten underwater structures commonly consist of one or several layers of elastomers of varying acoustic properties. The varying acoustic properties may be achieved by incorporating air filled cavities or material fillers. The layer structure aims to combine acoustic admittance to the layer system with increased absorption as the acoustic wave penetrates the system. The inserts or air filled cavities aim to combine a high degree of acoustic wave admittance with absorption of acoustic energy of the system by locally modifying material impedances and resonance conditions through geometric effects, such as resonances or Mindlin-Hermann-Poisson relaxation [2] or internal reflection, wave type transformation [3] or simple scattering [4] which absorb acoustic energy by direct absorption or secondary absorption of generated and scattered waves. This paper considers Alberich type anechoic layers [1] containing cylindrical cavities. The thickness of the coatings considered are very small compared to the wavelengths in water over the frequency range of interest which indicates that only dilatational waves are of importance and shear effects are introduced through the Mindlin-Hermann side-wise relaxation of material into cavities and material stretching above cavities. This assessment is supported by experimental estimates of the magnitude of the plane modulus of the coating which show agreement with the volume elasticity modulus [6] and indicate that dilatational wave effects dominate. This assessment is also supported by results of detailed simulation modelling [5] of such coatings.

These sound absorbing layers can be tuned to absorb acoustic emissions from machinery and may be very effective for internal quietening of underwater structures. The

tuning can be achieved through a combination of material and geometric features or through forced vibration of an acoustic element to make it appear at resonance [7].

Placement of such layers in pipes would be able to reduce sound, of wavelength greater than the twice the diameter of the pipe, propagating through fluid in the pipes, or air ducts. sound transmitted through and along walls of pipes , air ducts or other ship structures may also be attenuated by resonance absorption in such layers. Placement of such layers between sections of structure would also attenuate the transmission of sound through the structure. Attaching such layers to the outside of a ship's hull would act as an anechoic layer , decouple potential acoustic emissions and, if tuned to the frequency of the boundary layer, about $100Hz$ [8], should inhibit the onset of turbulence which should increase the speed of the vessel for a given propulsive force and also quieten turbulent flow noise. Thus anechoic and sound transmission and emission retarding layers are of great importance in underwater engineering.

Theory

The Alberich layers considered are shown in Fig. 1, and the discrete acoustic elements of these coatings are shown in Fig. 2. The two dominant acoustic active elements are the region above the cavity which responds to an acoustic excitation like a plug, constrained by the material around it, or as a plate when its thickness approaches that of the diameter of the cavity, and the cylindrical surrounds, see Fig. 2 . The changeover in acoustic response type may be assessed from numerical studies such as [5].

Average admittance

The acoustic impedance, Z , the ratio of the acoustic pressure to particle velocity in the material, of each element can be added analogously to electrical impedances of the equivalent electric circuit [1].

The acoustic reflection properties may be expressed in terms of an average surface admittance $g = Z_w/Z_c$, where Z_w and Z_c are the impedances of the material facing the coating and the surface impedance of the coating or layer respectively. The validity of the average admittance approach for a layer surface requires that the spatial extent of the non-uniformities of impedance are small with respect to the wavelength λ_w of the incident pressure wave, namely, $2\pi cos0\delta L/\lambda_w \ll 1$, where δL is the linear spatial extent of a typical non- uniformity of surface impedance Z_c and 0 is the angle of incidence; and that $|\delta Z_c/(Z_c + Z_w)| \ll 1$, [9], where δZ_c is the local variation in the impedance of the coating. The latter inequality is likely to be violated at high Q resonances, so the average admittance approach is more appropriate for low Q layers or Alberich style layers not at resonance. The low Q criteria are met for many practical coatings for acoustic frequencies below about $50kHz$ [1]. When these criteria are violated the Kirchhoff-Helmholtz or Greens function approach must be used to compute the near and far acoustic fields in front of the layer [10].

If the above limitations are fulfilled , the average surface admittance of a coating of type shown in Fig.1, backed by water on one side and steel plate on the other was first written by Oberst [1] as $g = g_e + \Sigma_i N_i g_i + g_s$ where g_e and g_s are the admittances due to the elastomer and steel backing plate respectively, N_i is the number of holes type $i/unitarea$ and g_i is the admittance of each hole type i, including rim and rim-plate interaction term. The impedance of any backing behind the steel plate is assumed to be small compared to that of steel.

Steel plate and elastomer region away from cavities

The admittance of steel plate is given by [1] $g_s = Z_w/(\imath\omega M_s + \hat{Z}_0)$ where ω is the angular frequency of the incident acoustic excitation, M_s is the mass per unit surface of the steel plate and $\hat{Z}_0$ is the specific resistance or impedance of the terminating medium on the other side of the steel plate. For air, $\hat{Z}_0$ can be taken to be zero. For water, $\hat{Z}_0$ will be equal to Z_w.

The admittance of the elastomer in the vibrating regions around the holes can be written to a good approximation as $g_e = \imath\omega t Z_w/(v_s^2\rho)$, where t is the thickness of the layer, v_s the longitudinal speed of sound in the elastomer and ρ is the density of the elastomer; and $v_s = \sqrt{M/\rho}$ where M is the plane-wave modulus [11].

Plates above cavities

The numerical studies of [3] of the acoustic response of elastomer above the cavity indicate that the manner of vibration depends on the ratio of the thickness of this layer to the diameter of the cavity. The plate may, to a first approximation [1],[6] be considered as an one dimensional mass-spring oscillator whose admittance is be approximated by $g_p = \imath\omega Z_w/(\omega_p^2 M_p\{1 - (\omega/\omega_p)^2 + \imath\eta_p\})$, where η_p is the sum of the thermal and viscous loss tangent and M_p is the effective mass of the plate. In this formulation the resonant frequency is that of an elastically constrained plug or of an unclamped plate of radius a when the thickness $d \ll 2a$. The effective radius a_{eff} of such a plate has been found experimentally [6] and numerical studies [5] to be approximately equal to the radius of the cavity if the layer above the cavity is thin to about $1.5times$ this radius when the layer becomes thicker. Results obtained from modelling an practical coating with $d = 2.5mm$ and $a = 5mm$, showed that $a_{eff} \approx 1.24 - 1.5a$, or between 1/4 and 1/2 of cavity separation for frequencies less than $100kHz$, which is in agreement with experimental work [6]. It is assumed here that the plate is free from static tensile stresses, an assumption which could break down if the plate were severely deformed by pressures acting externally to the coating [14]. Such an unloaded plate resonates, [1], at the fundamental frequency,

$f_0 = 0.47d\sqrt{\Re Y/(a_{eff}^4\rho(1-\nu^2))}$ for an unclamped plate ,where Y is Young's modulus, ρ is the density and ν is Poisson's ratio for the medium. Lamb [12] found that a plate with one side in contact with water and the other with air has its inertia increased and its characteristic frequencies lowered by the approximate factor $\sqrt{1 + 0.6689\rho_w a/(\rho d)}$ where ρ_w and ρ are the density of water and the plate respectively material.

When this correction is applied to a $5mm$ thick and $10mm$ diameter elastomer plate, the characteristic frequency of the plate is reduced to about $15kHz$ as observed by Oberst [1]. The effective mass M_{eff} of a plate of mass M_p loaded on both sides, is approximately given by $M_{eff} \approx M_p(1 + 0.6889\{\rho_w + \rho_b\}/\rho)$ where ρ_w and ρ_b are the densities of the material on either side of the plate. Hence the effective density of the plate would increase as $\rho_{eff} = M_{eff}/(\pi a_{eff}^2 d)$. The effect of water loading on the characteristic frequencies of plates has been verified experimentally[12].

Rim of cavity-plate/rim interaction and visco- elastic losses

The computer modelling indicates [3]that , as [1] assumed , at the lower practical frequencies of interest in underwater engineering, say below $30kHz$, that the inter-cavity spacing compresses like a short rod in line with the Mindlin-Hermann theory [2]and [1] approximated the fundamental frequency of this coating area by $f_r \approx v_\mu/4d$, where d is the height of the rim and v_μ is the speed of a shear wave in the coating material.

The most appropriate approximation for the admittance of the annulus appears to be found by early workers [1] and may be expressed as $g_r = \imath\omega Z_w/(\omega_r^2 M_r\{1-(\omega/\omega_r)^2+\imath\eta_r\})$, where $\omega_r = 2\pi f_r$ and is the angular resonant frequency of the rim. The variable M_r is the effective mass of the rim and includes the mass of the backing coating per area of the effective vibrator.

The rim or annulus and plate interact and the coupling admittance is defined by $g_{pr} = 2(S_p/S_r)\imath\omega Z_w(1+\imath\eta_p)/\{\omega_r^2 M_r(1-(\omega/\omega_p)^2+\imath\eta_p)(1-(\omega/\omega_r)^2+\imath\eta_r)\}$ where $S_p = \pi a^2$ and $Sr = \pi a_{eff}^2$ are the surface areas of the plate and rim or annulus respectively and it is assumed that $S_p < S_r$. Brendell found $S_p/S_r \approx 0.5$ a value which was also obtained for the coatings simulated [3].

The loss tangent for the vibrating elements may be expressed to a first approximation as [1] $\eta_i \approx \gamma tan\delta/(e\omega^2 M_i)$ where γ is the real part of Young's modulus for the plate and the real part of the shear modulus for the rim, as expected from the Mindlin-Hermann free surface relaxation theory; e is the effective volume of the acoustic element The variables $M_p and \mathrm{M}_r$ are effective masses and have dimensions $[M][L]^{-4}$.

Sound attenuation through forced resonance of acoustic elements

The sound attenuation properties of the Alberich style layers may be enhanced by actively moderating the acoustic impedances of the acoustic elements towards resonance conditions even if frequencies to be attenuated are far from the optimum condition.

Inspection of the impedance of the acoustic elements indicates that their effectiveness in absorption and reduction in echo can be increased if the effective mass of the element can be decreased. Now, to a first approximation, both the plate and the rim may be viewed as a mass spring oscillator of mass M and area S, whose resonance frequencies are described by the equivalent plate or Hermann-Mindlin effects described above. The motion of such systems are characterized by the second order differential equation of displacement x with respect to time t, $M_{p,r}(\partial^2 x/\partial t^2)+K(\partial x/\partial t)+Cx = Sp(t)$, where $p(t)$ is the external acoustic pressure. If an imposed force $Q(t)$ were used to excite the element according to $\delta M(\partial^2 x/\partial t^2)+\delta K(\partial x/\partial t)+\delta C x = Q(t)$, the total equilibrium of force on the acoustic element may be written as $(M-\delta M)(\partial^2 x/(\partial t^2)+(K-\delta K)(\partial x/\partial t)+(C-\delta C)x = Sp(t)$. Hence a forcing excitation is able to reduce the effective mass of the element by δM, the damping by δK and the spring constant of the element by δC. Complete elimination of effective mass and spring might would lead to optimum absorption and reflection properties for a given element [7]. However, stability requirements [7] require positive values of $(M-\delta M)$, $(K-\delta K)$ and $C-\delta C$. The total effectiveness of this forced acoustic impedance modification for a layer is obtained through the average admittance equation of summation of Huygen's wavelets in the near and far field.

If the criteria of displacement at natural resonance is chosen to determine the imposed force $Q(t)$ to drive the element to effective resonance at frequency ω, the effective mass of the element i, $M_i^{eff} = M_i\omega_i^2/\omega^2$, and $\delta M_i = M_i - M_i^{eff}$. Here it can be seen that if the resonance frequency is to be lowered, the effective mass increases and if the resonance frequency is to be raised the effective mass increases as might expected from first principles and also considering the formulation for f_s above. This adjustment of the effective mass does not consider the phase lag due to K and is hence an approximate resonance condition which whose accuracy increases with decreasing K. Under the adjusted mass criteria , based on displacement at natural resonance of the plate and rim, the admittance of the plate-rim oscillator may be written as $g_{plate+rim} = Z_w\{1/(\omega M_p^{eff}\eta_p^{eff}) + 1/(\omega M_r^{eff}\eta_r^{eff}) - \imath/[(1+\imath\eta_p)\omega M_r^{eff}\eta_p^{eff}\eta_r^{eff}]\}$, where

the increase in admittance due to resonance can be seen clearly.

Attenuation of reflection

The specular reflection coefficient R ,for a plane wave of a plane surface that interfaces with a semi-infinite fluid and that possesses a uniform surface admittance g is given [1] and [9] by $R = (1-g)/(1+g)$. The corresponding echo reduction T is normalized by comparison with the target strength of a perfectly reflecting sphere of $2m$ radius. In decibels, the attenuation is expressed as logarithm [9], $T = -20\log_{10}|R|$.

Minimisation of the reflection requires that the admittance of the layer be made unity as closely as possible over the desired frequency band. In general this requires that the resonant frequency of at least one of the elements of the inserts , usually the large cavities in the air-filled Alberich style coatings, must be in the mid-range of the frequencies to be absorbed. The small holes of the Alberich coatings resonate at higher frequencies which extends the bandwidth of the coatings and dissipate energy through adiabatic compression of the enclosed air, and shear losses in the elastomer. In addition, the small cavities modify the bulk compliance and hence the admittance of the elastomer.Inserts other than air permit coatings to be developed whose acoustic properties lie in the high attenuation regions shown in Fig. 3 to Fig. 5 [15].

Under conditions of strong, or high Q, resonance, the impedance varies greatly with spatial position on the surface of a layer, and the admittance averaging conditions are not satisfied, and R represents a local approximation to the reflection coefficient for a Huygen's wavelet only and Kirchhoff's integration must be used to find the far field reflection distribution[10].

Studies

The absorption properties of one ofa historical design of an Alberich style coating was examined using the above theory. A schematic sketch is shown in Figure 1. The coating was assumed to be $5mm$ thick and contain $2.5mm$ radius cavities, $1/cm^2$ and $2mm$ deep, and interspersed as shown with $1mm$ radius cavities also $2mm$ deep. Some of the absorption properties estimated by theory were compared with experiment at MRL but not by the author.The coating material was an elastomer representative of anechoic coatings. The shear modulus was assumed to be 1/3 that of the Young's modulus. Noting uncertainties in the material properties and experimental measurements, the overall agreement between theory and experiment was considered to be reasonable.

The attenuation, T, was evaluated for a number of acoustic excitation frequencies over the range of material properties typical of elastomers typical of elastomers used for anechoic coatings. the properties of such elastomers vary widely, with $10^7 Pa < Y_r < 10^{10} Pa$ and $0.03 < \tan\delta < 1.5$, and more than one elastomer will lead to a given target echo reduction capability of a coating for a given geometric configuration. Figure 4 indicates how the echo attenuation properties of a $5mm$ thick coating, containing 10^4 ($a = 2.5mm, l = 2mm$) cylindrical cavities per m^{-2} (one cavity $/cm^2$) and 4×10^4 ($a = 1mm, l = 2mm$) cylindrical cavity $/cm^2$, one cavity/ cm^2, varies with Y_r and $\tan\delta$. The layer response to $30kHz$ excitation is shown only.

The peaks in attenuation, indicated by the contours, correspond to the resonance absorption of the plate and rim vibrators and the interaction term. When the resonant frequency of one of the resonators , for instance the plate resonator, is set to almost zero, the two dominant peaks, Fig. 4, are replaced by one peak, Fig. 5, and the additional

peak arising from the interaction term disappears also. Attenuation close to that of the peaks would be expected when the plate and rim are forced to resonate at the incident frequency. Forced resonance provides a robust increase in attenuation, because even as resonance conditions are approached the admittance is increased and more radiation enters the oscillator. This is particularly so for low Q resonators. The strength of the interaction, between the plate and rim vibrators tends to force the peaks of attenuation apart, as is typical of coupled oscillators. The shift occurs along an approximate locus $Y_r \propto (S_p/S_r)/\tan\delta$. In addition, the magnitude of the local maximum in the lower left hand corner of the contour diagrams depends on the extent of coupling assumed in the model, see Figs. 3 and 4.

Discussion

The overall shift of the attenuation peaks with frequency is caused by the excitation of higher resonance harmonics of the elements. The inclusion of the resonance effects of the small cavities in the attenuation calculations indicates that small cavities introduce further maxima in the attenuation and spread the existing high attenuation regions Fig. 5.

In agreement with earlier authors, such as [1], [6], the modelling shows that the absorption properties of an anechoic layer are very much enhanced if resonance condition can be achieved over the frequency range where attenuation of an echo is to be achieved. Once resonances have been selected, maximum attenuation is achieved by maximizing the lossiness of the elastomer coating which is reflected in the distribution of the cavities or inserts, and the material properties of the coating.

Acoustic energy absorbing layers may be designed [16] to reduce the acoustic echo and also to dampen noise radiating from a hull underwater. For example if a piece of rotating machinery at a certain site produces sound of a specific frequency, cavities may be incorporated into this layer and designed or forced to resonate at this frequency and absorb much of the acoustic energy emitted by the machinery.

The average admittance approach can be significantly extended by using the Huygens principle embedded in the Kirchhoff, or Greens function, formulation [10] where each acoustic element is seen as a generator of a wavelet and all wavelets are added vectorially in the near or far field to provide the echo or sound radiated or the field in an enclosed volume, such as a pipe.

References

[1] Richardson J.: Technical Aspects of Sound. Vol. 2, Amsterdam:Elsevier 1957 .

[2] Skudrzyk E.:Simple and complex vibratory systems.London:The Pennsylvania State University Press 1968.

[3] Wendlandt B.C.H: Numerical simulation of acoustic response of discontinuous viscoelastic fluids. In: Sound and vibration damping with polymers (Corsaro, R., Sperling, R., eds.). American Chemical Society, Washington, 1990.

[4] Wendlandt B.C.H.:Modelling of non-linear dilatation response of fluids containing columns-plastic and shear relaxation considered. Acta Mechanica 94,73-83 (1992).

[5] Wendlandt B.C.H: Wave equation systems for dilatation and torsion for piece-wise continuous materials, Acta Mechanica, 88, 77-89 (1991).

[6] Brendell K. and Hinsch K.: Wasserschall- resonanzabsorber mit relaxationsverlusten in hochpolymeren. Acustica 21,4,189-198 (1969).

[7] Bschorr, O.: Integrierte mikrofon/lautsprechereinheit zur aktiven laermausloeschung, Fortschritte der Akustik - DAGA pp. 617 - 620, (1986).

[8] Marchaj C.A.:Sailing theory and practice, London:Adlard Coles 1971.

[9] Maidanik G. and Dickey J.: Designing a negligible specular reflection coefficient for a panel with a compliant layer. J. Acoust. Soc. Am. 90 (4), Pt. 1,2139- 2145,(1991).

[10] Jackson J.D.:Classical electrodynamics.New York:Wiley 1962.

[11] Payne A.R. and Scott J.R.: Engineering design with rubber. 166-190, Interscience, New York (1960).

[12] Wood A. B.:A text-book of sound. London:Bell 1930.

[13] Wendlandt B.C.H.: Propagation of dilatational waves in stratified media and their transformation into evanescent and torsional waves at interfaces. accepted for publication by Acta Mechanica, to be published Winter 1993.

[14] Dunham R.S., Wong F. and Castro J.C.:Collapse of various shaped cavities in a pressurized incompressible material. ANA-89-0081, NATECH Research Corp.,Naval Surface Weapons Center, White Oak, Maryland 1989.

[15] Scharnhorst K.P., Madigosky W.M. and Balizer E.: Scattering coefficients and the absorption edge of longitudinal coherent sound waves in selected inhomogeneous materials. Report NSWC TR 86-196, Silver Springs, 1985.

[16] Zimmerman S.:Submarine technology for the 21st century.Arlington:Pasha 1990.

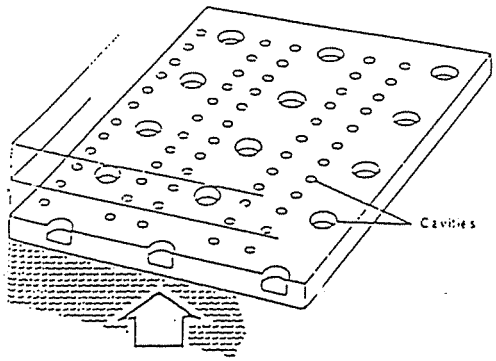

Figure 1: Section of a traditional Alberich style resonant anechoic layer. Dimensions shown are representative of early coatings.

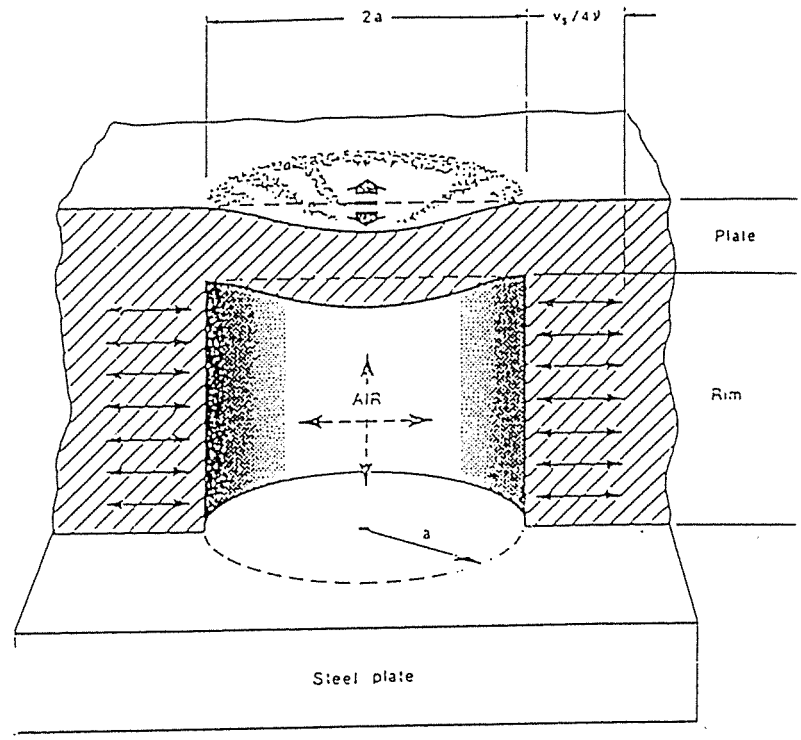

Figure 2: Resonant acoustic oscillators or elements around cavity approximated analytically. The diagram also displays the depression of the top plate under applied external pressure of around 1 atm. as measured by Oberst. The upper sidewalls were also observed to move inward slightly under pressure as also shown by Fig. 3.

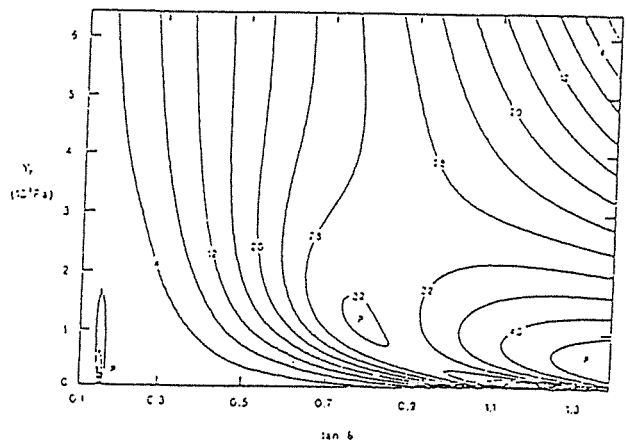

Figure 3: Acoustic echo attenuation of a coating containing $2.5mm$ and $0.1mm$ radius cavities shown in Fig.1, as function of the real part of Young's modulus and loss tangent of the elastomer. Excitation frequency is $30kHz$ and the broadening of the attenuation response of the coating due to the small cavities is evident. Plate, cavity and rim absorption mechanisms are considered in the calculations. Attenuation peaks are labelled P.

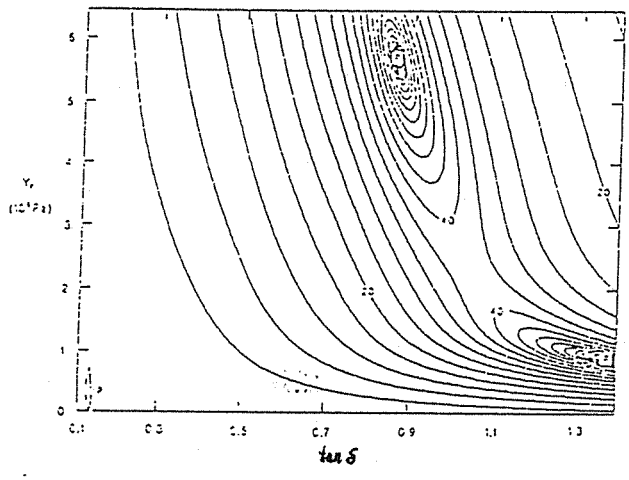

Figure 4 Acoustic echo attenuation of due to plate rim and rim- plate interaction of an elastomer layer, containing 2.5mm radius cylindrical cavities, one cavity per square centimeter, as a function of the real part of Young's modulus and loss tangent of elastomer. High regions of attenuation are labelled P. Approximate values of unmodified elastomers traditionally used in such coatings are shown shaded. Excitation frequency is 30kHz. Coupling factor, S_p/S_r, between plate and rim has been assumed to be 0.3

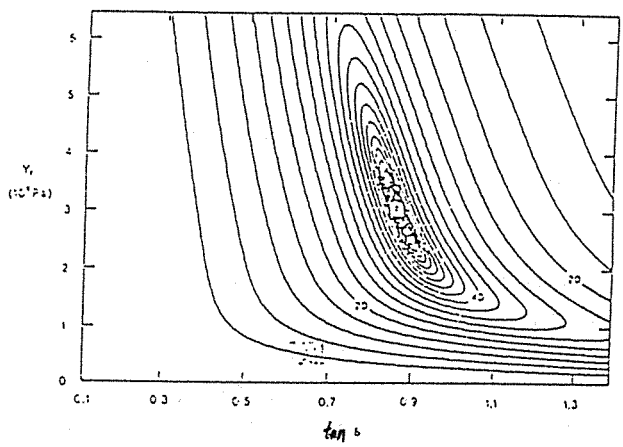

Figure 5 Acoustic echo attenuation due rim excitation of an elastomer layer, containing 2.5mm radius cylindrical cavities and one cavity per square centimeter,as a function of the real part of Young's modulus and loss tangent of elastomer. Approximate values of un-modified elastomers are shown shaded. The peak of attenuation due to rim excitation is labelled P.

LOCATION OF BURIED OBJECTS BY AN ACOUSTIC IMPULSE TECHNIQUE

A. J. Rogers and C. G. Don,
Department of Physics, Monash University, Clayton, Victoria.

Abstract

Often it is desirable to locate a shallowly buried object and deduce something of its shape and size, without digging up the ground in the process. If the object is metallic, then metal detectors are adequate, however, non-metallic objects are more difficult to locate. Since the acoustic impedance depends not only on the surface properties of a substance, but what lies within the region penetrated by the sound, an object under the surface will cause a change in impedance compared to a homogeneous sample.

Recently, a technique, utilizing two microphones equidistant from a stable impulse sound source, has been used to locate a plastic object buried under small pebbles. The method involves examining the differences between the two recorded signals, one of which contains a reflection from an object under the ground. The depth of the object can be deduced from the time delay of the reflected impulse from the buried object. Because its reflective surface is only at one depth, a flat, horizontal object gives a larger return signal than the same object when tilted. An irregular rock will give a more diffuse signal. With suitable signal processing it is possible to distinguish between unlike objects and to make an estimate of their shape, size and position.

Results are presented which distinguish between plastic strips, disks and rocks of varying sizes, buried in small pebbles between 4 cm and 15 cm deep. The advantages and limitations of the technique will be discussed.

INTRODUCTION

In our plastic oriented world, it would be useful to have a method for finding and identifying buried, non metallic objects. A technique for achieving this aim has recently been developed. It is based on the reflection of acoustic pulses from the ground surface and has applications in finding drainage pipes, archaeological artefacts and even plastic landmines.

The technique relies on sensing how the pulse waveform recorded above the ground surface is altered by the acoustic impedance produced by the object immersed in the ground matrix. Impedance is often determined at normal incidence[1] but it can also be calculated at any angle down to grazing incidence[2]. The normal incidence method determines the localised impedance of the area directly below the microphone, while using grazing incidence gives an averaged impedance over the whole region between the sound source and the microphone. To see the implications of these ideas, it is convenient to briefly examine the measurement of surface impedance.

IMPEDANCE OF PEBBLES

Measurements were undertaken over a large bed of approximately 1cm diameter pebbles, which permitted partial penetration of the sound as well as being a relatively homogeneous medium, allowing easy placement and retrieval of buried objects. The depth of the pebble bed was over 50cm, which meant that it could be treated as effectively an infinitely deep medium. Fig. 1(a) shows that over a pebble surface which has been smoothed as flat as possible, the normal and grazing incidence methods give complex impedance values which are relatively frequency independent out to 10kHz, although the real component tends to be higher for the grazing condition.

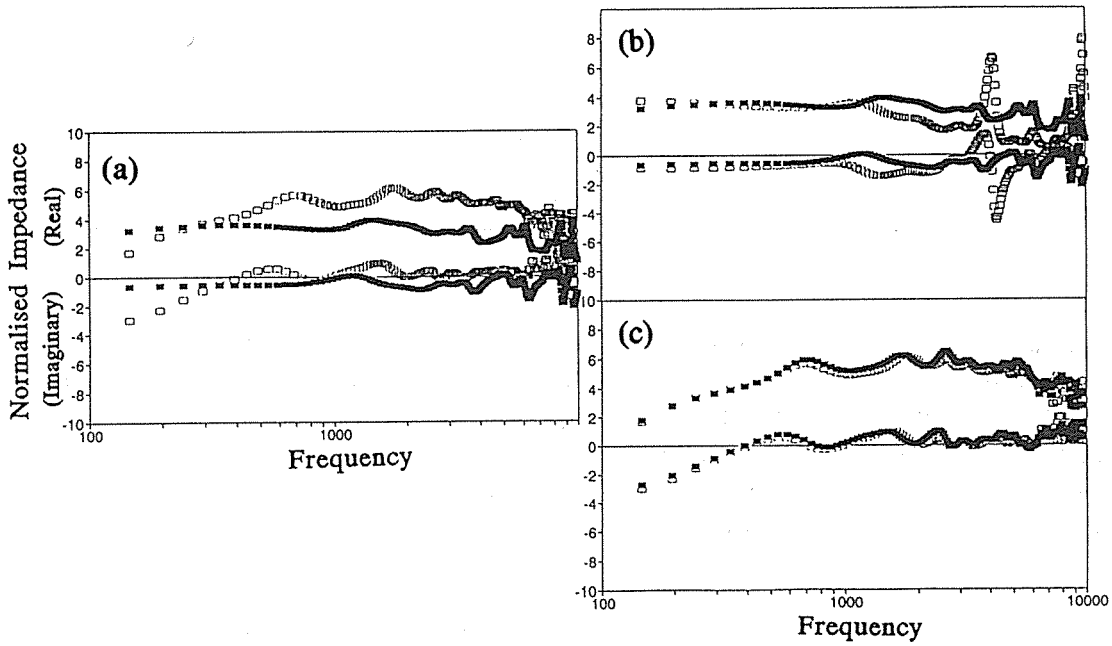

Fig. 1: The impedance of a pebble surface (a) when smoothed flat and using ■ normal, □ grazing incidence; (b) at normal incidence when ■ smooth, □ rough; (c) at grazing incidence when ■ smooth, □ rough.

If the surface is roughened, by producing, say, 4cm deep depressions, the effect on the normal impedance is very point dependent compared to the grazing result, as is apparent by comparison of figures 1(b) and (c). Thus, it would appear to be advantageous to use the grazing incidence technique as the results are virtually independent of the surface roughness. However, the inherent averaging over an area makes it impossible to locate a buried object precisely, making it necessary to use a near normal incidence geometry.

When a layer of pebbles is formed, by placing a large rigid sheet at a known depth below the top surface, broad "resonances" occur in the impedance due to interference between sound reflected from the top and bottom surface. As shown in Fig. (2), the two geometries result in resonances at different frequencies.

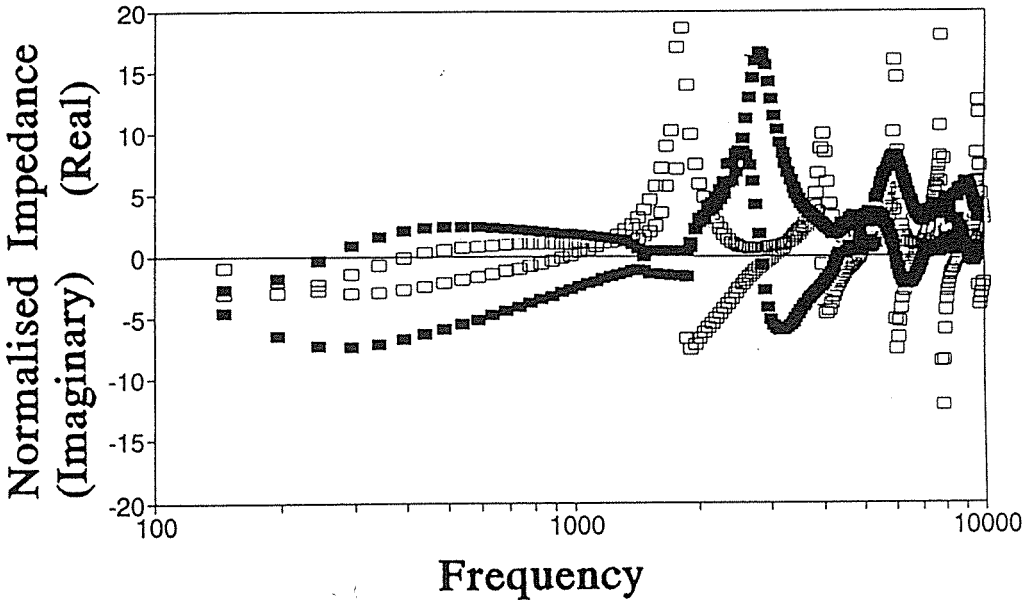

Fig. 2: The impedance of a 6cm deep layer of pebbles with a hard backing: ■ grazing, □ normal incidence.

A buried object creates a small layer just under the surface, which can be modelled as portion of a complete plane and so would be expected to produce similar but smaller magnitude resonances. The problem is, however, that irregularities in the impedance due to the surface roughness are of the same magnitude as the resonances caused by the layering. This can be seen by comparing Fig. 2 with Fig.1(b). Thus, it is not immediately possible to state the existence of an object by its layering effect alone.

In Fig. 3, resultant waveforms from a pulse reflected at normal incidence from two different regions of a roughened layered of pebbles are displayed. The first pressure maximum, A, is due to the reflection from the rough surface and is found to vary greatly from area to area. The second pressure maximum, B, is the result of reflection of the impulse from the bottom of the layer and is much more consistent, regardless of surface irregularities. It is this reflection which will contain the information about the buried object and so a technique is required which enhances this second reflection and removes, or minimises, the surface reflection.

DETECTION OF BURIED OBJECTS

The geometry adopted is shown in Fig. 4 where a microphone is located symmetrically on either side of a very reproducible acoustic pulse source created by a loud speaker acting down a long sound tube. Over a uniform surface, both microphones record the same direct and reflected pulse waveforms and the difference between the two signals is approximately zero. When an object lies under the surface near one of the microphones as shown in Fig. 5, it changes the impulse waveform of the sound reflected to this microphone and consequent the difference between the two microphones is no longer zero.

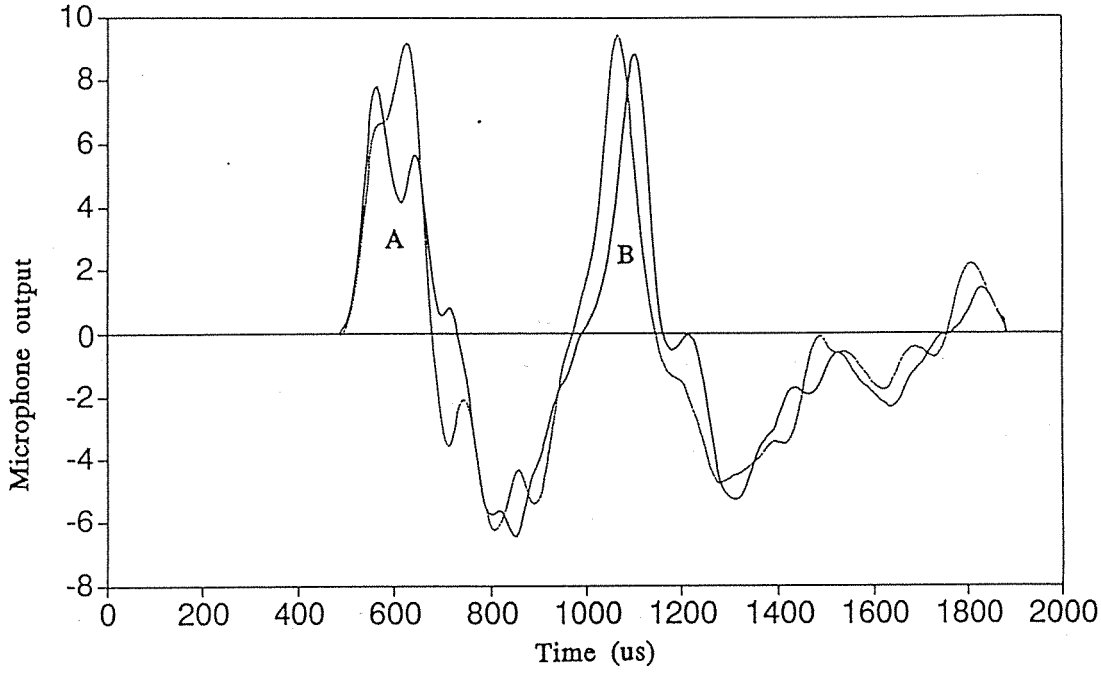

Fig. 3: Pulse waveforms obtained over two areas of a roughened layer of pebbles.

The impulse source consists of a JBL horn driver powered by an amplifier connected to a Data Precision 2020 polynomial waveform synthesizer. The signals are captured using two Brüel & Kjær 1/4 inch microphones and type 2218 sound level meters connected into a Data 6000 waveform analyser. At the present time the data are manipulated in the analyser but as more sophisticated processing is developed, it is expected that the data will be down loaded to a PC, in real time. The sensitivity of detection depends on the height of the microphone/source probe above the surface and the separation between the microphones. These factors are not independent, but if separation is too large the grazing condition is approached and spatial resolution is impaired. If the microphones are too close they both receive essential the same reflected signal and detecting the object becomes more difficult. The optimum separation is also linked to the probable width of the buried object. The

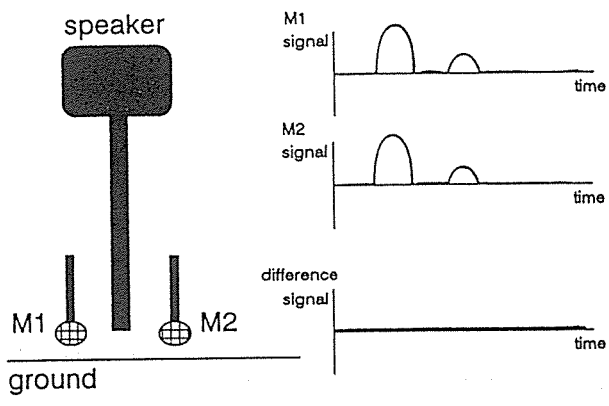

Fig. 4: Geometry of probe & waveforms over homogeneous ground.

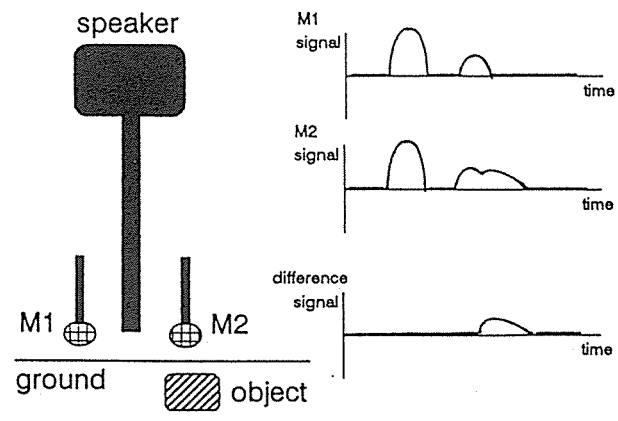

Fig. 5: Probe and waveforms over a buried object.

probe used in this study has a separation of 8cm and is supported 4cm above the ground.

In examining the idealized signals of Fig. 5, the characteristic reflection of the object can clearly be seen in both the individual and the subtracted signal. However, as discussed above, in actual measurements the reflection from an uneven surface is sufficiently variable that the signals do not cancel and may partially overlap with the pulse from the object. The wanted reflection is a function of the original pulse waveform, but the random surface noise remaining after subtraction is only weakly related. Use can be made of this fact by correlating[3] the known direct pulse shape, g(t), with the subtracted signal, s(t), to obtain a modified signal, x(t), where

$$x(t) = \frac{\sum_{n=0}^{\infty} g(t) * s(t+n)}{(g(t))^2} \qquad (1)$$

This process enhances the required reflection as the output, x(t), has a large magnitude whenever a portion of the subtracted signal has the same waveform as the direct pulse.

As an example of this technique, the signals obtained over a smoothed pebble surface, with a 21cm wide plastic strip buried 7cm deep, are shown in Fig. 6a. The reflection from the strip shows up as a small impulse at about 900μs (arrowed) in the signal from one of the microphones and is not present in the signal from the other microphone. Even over the relatively smooth surface of the pebbles, the difference signal, Fig.6(b), is dominated by the residue, arrising from the surface irregularities, preceding the required reflection. However, after correlating with a direct pulse there

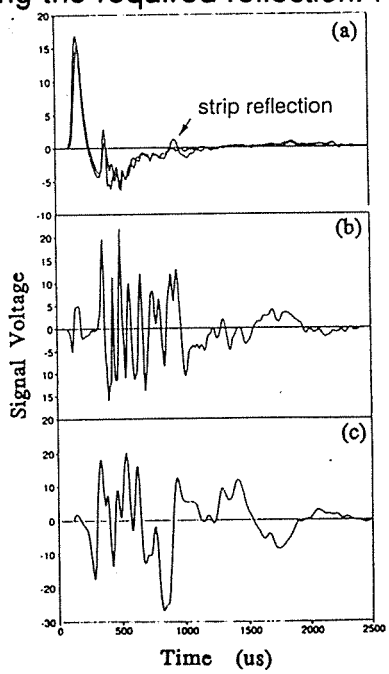

Fig. 6: Probe over buried strip: (a) Waveforms with one microphone showing reflection from strip, (b) Subtraction of waveforms, (c) Correlation of subtraction.

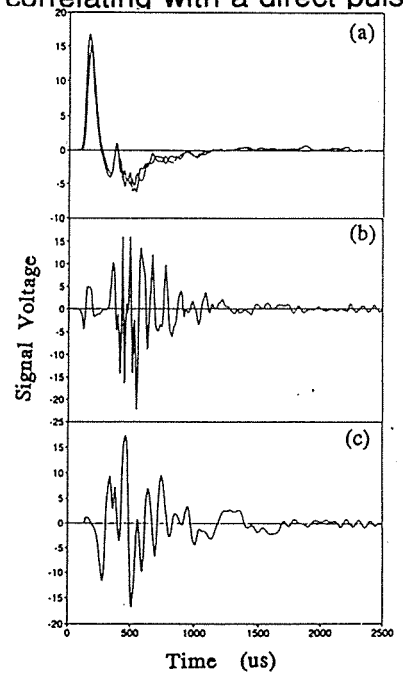

Fig. 7: Probe over smooth surface of homogeneous pebbles: (a) Waveforms with no strip, (b) Subtraction of waveforms, (c) Correlation of subtraction.

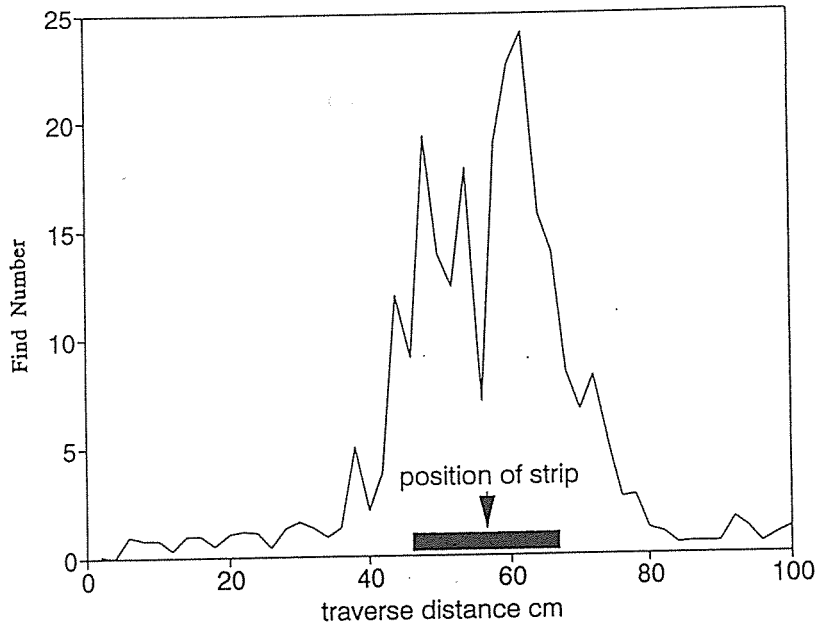

Fig. 8: The find number vs distance along pebble bed for a 21 cm wide strip, buried 7cm deep, showing the actual position of the strip.

is a significant enhancement of the reflection, Fig. 6(c). Compare these results with the signals in Fig. 7, where there was no buried strip. The final processed signal, Fig 7(c), contains the unavoidable remainder due to surface fluctuations. [Note that the vertical scales on Figs. 6 and 7 are arbitrary as they have been adjusted to display the signal variations.]

A rough surface increases the amount of noise in the correlated signal. As this occurs before the reflection from the object, it can be time isolated with a window which includes only the portion of the trace where an object reflection may occur. By summing the square of the instantaneous values of the correlated signal, such as Fig. 7(c), a single "find number" can be created for that probe position, which can then be used to locate the buried object. An example of the success of this technique is presented as Fig. 8, where the probe was progressively moved in 2cm steps across the buried strip. Note that there is a tendency for a minimum to occur in the find number when the probe is directly over the strip, as both microphones then record essentially the same signal.

The position of the time window can be adjusted to suit the depth being examined. For a deeply buried object, there will be a greater time delay before the appropriate reflection arrives at the microphone and so the appropriate time window will occur later. In the example of Fig.8, the window commenced 620μs along the correlated signal and was 320μs long. These values were determined experimentally by inspection of the signals but could be calculated theoretically if the acoustic properties of the matrix material are known.

As the strip is moved closer to the surface the strength of the reflection increases, however, it begins to overlap the surface noise, so the signal to noise ratio remains approximately the same. Although it is now almost impossible to distinguish the object reflected pulse in the microphone outputs, the correlated difference signal

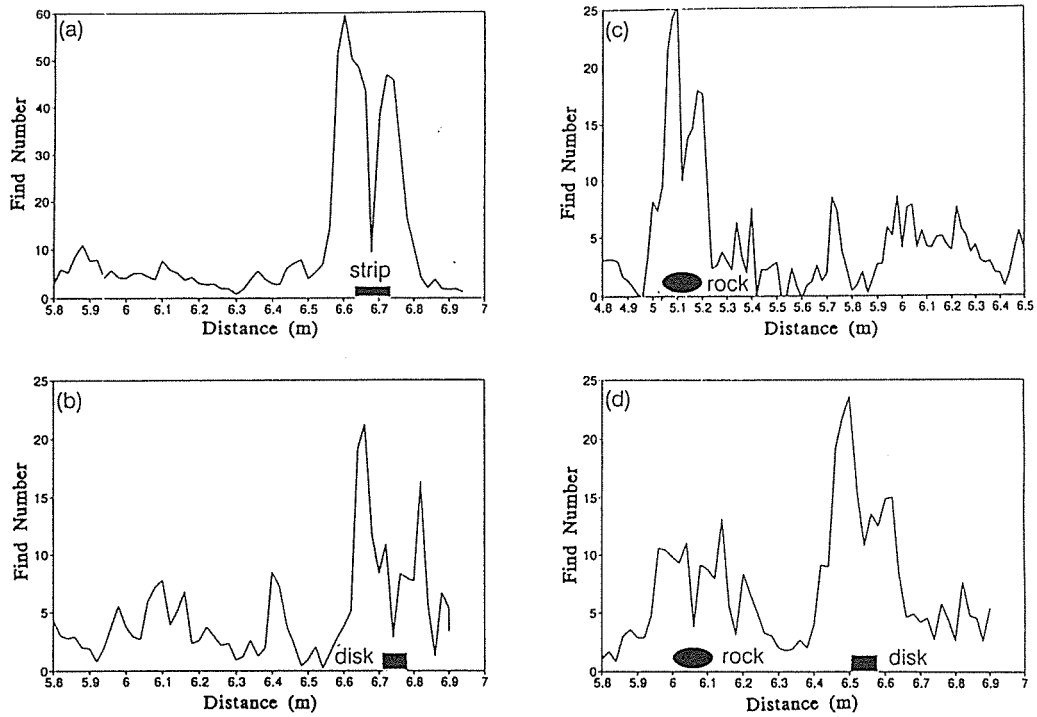

Fig. 9: The find number for (a) a 9 cm wide strip, (b) a 6 cm diameter disc, (c) a rock, (d) both the rock and the disk after additional processing.

indicates that a significant reflection occurs from the object. The technique can also be used to find smaller and more complex objects. It has successfully located a flat 9cm wide plastic strip, Fig. 9(a), while (b) and (c) show the location of a 6cm diameter plastic disc and a similar sized but irregularly shaped rock, all buried 5cm under pebbles. Further, Fig. 9(d) indicates that it is possible to distinguish between the rock and the disk when they are buried about 50cm apart under the pebbles.

More complex analysis, such as the use of multiple time windows, provides a way to establish the depth of the buried object. In fact, dual window processing was used in Fig. 9(d) to help differentiate between the objects as, after correlating, the irregular rock gave a signal in both windows while the flat disk signal occurred only in one window. A tilted object will also give rise to readings in more than one window. It is probable that different objects all have their own specific find number signature and thus further research may make the prediction of the size and shape of the object possible.

CONCLUSION

The system, as it stands at the moment, can easily detect objects as small as 6cm in diameter, buried as deep as 15cm in a pebble bed. A traverse is made in the direction set by the axis of the two microphones. If the object is midway between the microphones or large enough to extend beyond both microphones then the microphone signals become almost identical and a minimum in the find number may be recorded. This is because the system is essentially an edge detector, sensing a change of impedance. A number of traverses must be made to estimate both the length and width of the object, two more microphones positioned on an axis perpendicular to the direction of traverse would give information about the other dimension. This is the next stage in the development of the instrument.

The method is still to be tested over other matrix materials, although it is expected to work over dry soils and sands, where the sound will penetrate readily. It is unlikely to work on hard packed or water-soaked fields. With further development, the system could be preprogrammed for a particular matrix material so that the predicted pulse waveform for the reflection from a simple object buried in the matrix is calculated and then used in the correlation calculation to give an improved find signal.

REFERENCES

[1]C.G.Don and A.J.Cramond, "Soil Impedance Measurements by an Acoustic Pulse Technique," J. Acoust. Soc. Am. **77**, 1601-1609 (1985).

[2]A.J.Rogers, D.E.P.Lawrence, and C.G.Don, "Impulse Measurements of Acoustic Impedance using a Microphone on the Surface," Proc. A.A.S. Conference, Ballarat, 257-264 (1992).

[3]A.V.Oppenheim, A.S.Willsky and I.T.Young, *Signals and Systems* (Prentice Hall, 1983).

Attenuation and dispersion measurements in porous materials

D.E.P.Lawrence and C.G.Don
Department of Physics, Monash University, Clayton, Victoria, Australia.

INTRODUCTION

Noise control applications and outdoor sound propagation are areas that require characterisation of porous materials. In general, to calculate the surface impedance of a hard-backed or multi-layered porous material using the layered media equations of Brekhovskikh[1], requires a knowledge of the complex wavenumber in the material as well as its characteristic impedance. While both these quantities can be estimated from empirical equations[2] if the flow resistivity of the material is known, the latter equations have a limited validity. Alternatively, an approach which considers the pore structure, such as the rigid-frame model of Attenborough[3], may be used to generate the required wavenumbers and impedance. The more general approach of Allard *et al.*[4] is to calculate the layer impedance directly using a theory which specifies the properties of the solid frame as well as the pores. Predictions from these models will be compared with experimental data obtained using acoustic impulse techniques.

These techniques have been devised to measure both the impedance and wavenumber of foams and soils over the frequency range 200Hz to 10kHz. In addition, the layer impedance of various thicknesses of foam placed on a hard surface have been determined experimentally over the same frequency range. As the theoretical positions of resonances in the layer impedance are sensitive to the values of the acoustic parameters chosen, the system forms a rigorous check on both the validity of the measurements and the appropriateness of the theory.

THEORY

In this paper an $\exp(-i\omega t)$ time-dependence has been assumed, and the equations presented have been modified appropriately if the reference used the $\exp(i\omega t)$ form.

A number of parameters are used to characterise the pore structure. The porosity, h, of a substance with both solid and fluid constituents is the volume of fluid per unit volume of material. The flow resistivity, σ, is the resistance to a volume air flow of a unit area of material per unit thickness. The tortuosity, q, accounts for the effective increase in the inertia of the air when it is forced to travel a tortuous path through the pores. The shape factor, S, is intended to be characteristic of the size and geometry of the pores. Values of the shape factor have been calculated for exact pore geometries, but for a real material it is regarded as an adjustable parameter and is evaluated by fitting dispersion curves.

The empirical equations of Delany and Bazley[2], based solely on flow resistivity, were derived from extensive measurements on fibrous absorbents, for which tortuosity, shape factor and porosity are generally not significant factors. Attenborough's rigid-frame model[3] accounts for these variables, but inherently assumes that the propagation of sound in granular or fibrous materials depends entirely on the structure of the pores, and is independent of any property of the frame.

To calculate the impedance of a porous layer, of depth d, on an infinite-impedance backing, either the empirical equations or the rigid-frame model can be used to obtain

values of characteristic impedance, Z_c, and wavenumber, k. For normal incidence, the impedance of a hard-backed layer at a given frequency, can then be estimated by[1]

$$Z(d) = \frac{Z_c}{\tanh(-ikd)}. \tag{1}$$

The more general theory of Biot[5], which has been adapted to high porosity fibrous and foam materials by Allard *et al.*[4], takes into account the finite rigidity and density of the solid frame. For a partially or fully reticulated foam, Poisson's ratio is essentially zero, which, in conjunction with the assumption of high porosity, allows the elastic parameters, as given by Biot, to reduce to the Young's modulus, E, of the material[4].

Thermal and viscous effects within the pores are accounted for by a frequency-dependent complex fluid bulk modulus, K_f, and dynamic viscosity coefficient, b, which can be expressed as

$$K_f = \gamma p_0 \Big/ \left[1 + 2T(N_p^{1/2}\mu)(\gamma - 1)\Big/\left(N_p^{1/2}\mu\right)\right] \tag{2}$$

and

$$b = -\sigma h \mu^2 T(\mu) / [4(\mu - 2T(\mu))]. \tag{3}$$

Here, μ is a complex frequency-dependent parameter related to the thickness of the viscous boundary layer at the pore wall,

$$\mu = qS(i8\omega\rho_0 / h\sigma)^{1/2}, \tag{4}$$

ρ_0 is the density of air, γ is the ratio of specific heats of air, p_0 is atmospheric pressure, N_p is the Prandtl number, and $T(z)=J_1(z)/J_0(z)$ is the ratio of first and zeroth order Bessel functions for complex arguments.

Wavenumbers for each frequency are obtained by solving the following dispersion relation, with roots $\pm k_A$ and $\pm k_B$,

$$\begin{aligned} k^4(hK_fE) - k^2\left\{\omega^4\left[K_f\left(h\rho_0(1-h)^2 + h^2\rho_1 + \rho_a\right) + hE(h\rho_0 + \rho_a)\right] + i\omega b(K_f + hE)\right\} \\ + \omega^4\left[h\rho_a(h\rho_0 + \rho_1) + h^2\rho_0\rho_1\right] + i\omega^3 bh(h\rho_0 + \rho_1) = 0, \end{aligned} \tag{5}$$

where $\rho_a = (q^2h - 1)h\rho_0$ is the "additional mass" of the frame due to the fluid. Only the positive roots are taken, which correspond to two distinct compressional waves; the so-called waves of the first and second kind. Relative strain amplitudes, ϕ_A and ϕ_B, relate the disturbance of the fluid and frame, and are defined by,

$$\phi_{A,B} = \frac{k_{A,B}^2(1-h)K_f + \omega^2\rho_a + i\omega b}{-k_{A,B}^2 hK_f + \omega^2(h\rho_0 + \rho_a) + i\omega b} \tag{6}$$

when the appropriate k is used. These ratios decide whether the role of the air or the frame is dominant in the wave type under consideration. The wave to which the smaller ratio belongs, may be considered to be propagating mainly in the frame, the other to be propagating mainly in the air. For foams, the air wave is generally the faster of the two.

Four partial impedances $Z_1^{A,B}$, $Z_2^{A,B}$ can be distinguished, corresponding to the impedances of the fluid and frame to both types of wave. A plane-wave analysis using the boundary

conditions for an infinite impedance backing yields the normal incidence impedance of a layer of thickness d,

$$Z(d) = \frac{Z_1^A Z_2^B \phi_B - Z_1^B Z_2^A \phi_A}{\left[hZ_1^A - (1-h)Z_2^A \phi_A\right]\left[(1-h)+h\phi_B\right]\tanh(-ik_B d) - \left[hZ_1^B - (1-h)Z_2^B \phi_B\right]\left[(1-h)+h\phi_A\right]\tanh(-ik_A d)}. \quad (7)$$

Eqs.5 and 7 represent a more rigorous derivation than that of Allard *et al.*,[4] where the porosity, h, was assumed to be equal to one. Note that Eq.7 reduces to Eq.29 of Ref.4 when h=1 and the time dependence is exp(iωt). It can be shown, by considering a semi-infinite medium, that the characteristic impedance, Z_C, is given by Eq.7 when the layer thickness, d, tends to infinity, ie. when both tanh terms are equal to one, so $Z(\infty)=Z_C$. Indeed, Eq.7 is a more general form of Eq.1, and reduces to it when the motion in the frame and fluid become decoupled, for instance, if the density and rigidity of the frame are high, and only the wave of the second kind contributes to the acoustic impedance.

MEASUREMENT TECHNIQUES

The following measurements were taken with quarter inch Brüel & Kjær type 4135 microphones connected through a meter to an Analogic Data 6000 waveform analyser, which allowed the pulse to be digitised at 1μs intervals. Captured waveforms were stored on a disk, then later transferred to a PC for processing. The source was formed from a loud speaker acting down a 1m length of 2cm diameter tube, the speaker being controlled through an Analogic 2020 polynomial waveform synthesiser to produce a pulse of 0.5ms duration, which can be set to repeat at any interval. The pulse amplitude and waveform were extremely reproducible, no observable deviation in waveform occurring between pulses. The pulse amplitudes were found to closely follow the inverse square law for distances from a few centimetres to several metres from the tube exit.

(a) Surface impedance measurements

While an earlier impulse technique was adequate for measuring the impedance of extended areas, for example over grassland[6], an alternative approach was sought which could be used with samples about 1m square. Not unlike the method of Davis and Mulholland[7], the geometry adopted[8] is that shown in Fig.1(a). With the impulse source held between 0.9 and 1.3m above the impedance surface, the microphone was positioned directly below, at 5 to 10 cm from the top surface. At these distances, delayed reflections from the edge of the sample can be readily identified and eliminated from the waveform

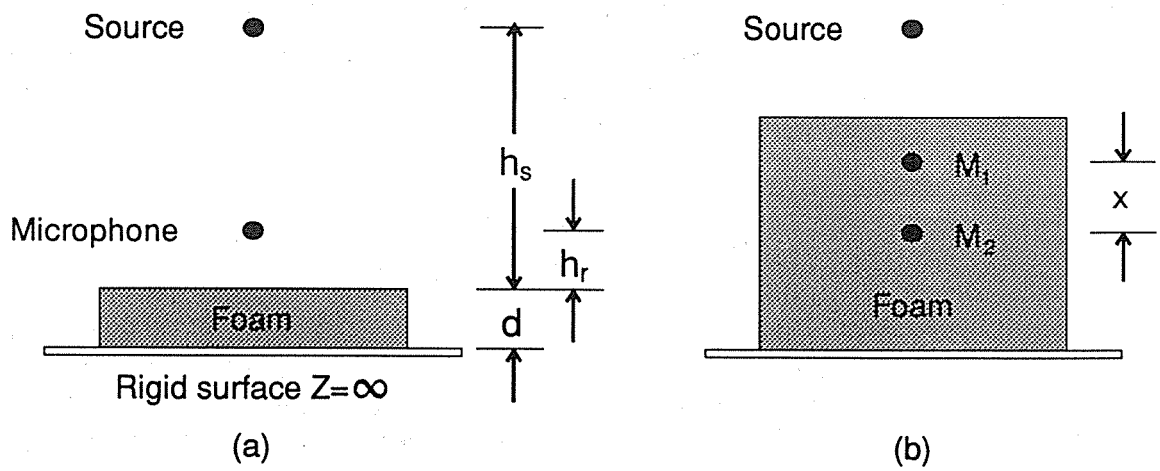

Fig.1. Measurement geometries for: (a) the surface impedance, and (b) the wavenumber in the material.

being analysed. Further, the microphone is sufficiently far from the surface that the leading edge of the direct pulse from the source is clearly identifiable, although its tail has merged with the reflected pulse. This permits an isolated direct pulse waveform, obtained in a separate measurement, to be precisely aligned in time and subtracted to give the desired reflected component. After making inverse-square law corrections, the reflected and direct waveforms are Fourier analysed and the plane wave reflection coefficient, R_p, at a particular frequency, is calculated from the ratio of the reflected to the direct component at that frequency. At each frequency, the normalised impedance of the surface is $Z = (1+R_p)/(1-R_p)\sin\varphi$, where φ is the complement of the angle of incidence and equal to 90^0 in the geometry of Fig.1(a).

If the thickness of the sample is such that any secondary reflections from the bottom of the sample, usually supported by an acoustically hard floor, are sufficiently delayed that they can be time isolated, then Z is the characteristic impedance of the sample. However, if this condition is not fulfilled, then Z is the impedance of a hard-backed layer and will be designated as Z(d) . One limitation of this method is that the thickness of the layer must be such that the bottom surface reflection has completely passed the microphone before any delayed signal arrives from the edges of the sample.

(b) Measurement of Wavenumber

To measure the wavenumber[9], two microphones were placed a distance x apart inside the material, as indicated in Fig.1(b), with the impulse source directly above but outside the material. For these measurements, the size of the block of material must be sufficiently large that no reflections from the edges interfere with the pulse coming directly from the source. In fact the samples were constructed from layers of foam, typically 5cm thick, with the microphones placed between the layers which were then pressed lightly together. If desired, microphone M_1 can be on the top surface.

For any frequency component of the pulse, the complex pressure amplitude at the more distant microphone, p, is related to that at the closer microphone, p_r, by

$$p = p_r \exp(ikx) \quad \text{or} \quad k = \ln(p/p_r)/ix, \tag{8}$$

where the complex wavenumber $k \equiv r\exp(i\theta)$. When processing the data, it is often necessary to increment θ by 2π, as θ is deduced via $\arctan[\mathrm{Im}(p/p_r)/\mathrm{Re}(p/p_r)]$. This is not a serious problem, as failure to do so results in a discontinuity in Re(k) as a function of frequency. Furthermore, Re(k) is related to the phase speed, and, because the group speed is easily determined from the delay between the arrival of the pulses at the two microphones, the correct value of θ can be deduced.

(c) Measurement of other foam properties

An estimate of the Young's modulus was obtained by measuring the speed, c_A, of a transient frame disturbance between two Brüel & Kjær type 4332 accelerometers placed in the foam. Since the wave of the first kind can be shown to be nearly non-dispersive, the speed obtained was assumed to be independent of frequency when calculating the corresponding Young's modulus.

These measurements gave information only about the magnitude of the Young's modulus, which is, in general, complex, ie. $E(1-i\eta)$, where η is termed the loss factor. For foams, the loss factor is commonly[4,10] in the order of 0.1, and this value is assumed for all calculations. The Young's modulus obtained should also be considered a static value, as the frequency content of the signals measured by the accelerometers was largely below 50Hz. The Young's modulus has been considered to be frequency independent, which is generally not the case[10].

50Hz. The Young's modulus has been considered to be frequency independent, which is generally not the case[10].

The flow resistivity of each sample was measured to ASTM-C522-80. The porosity was estimated by water displacement, which required the sample to be compressed in order to expel all air from the pores. This technique is only valid for completely open-celled foams, ie. those having no non-connected pore-space.

RESULTS

(a) High-porosity foams

Measurements using the above techniques were performed on three different plastic foams. Figs.2(a) and 2(b) show experimental results for the real and imaginary parts of normalised wavenumber, and the associated attenuation per unit length and phase speeds of a low flow resistivity foam, designated foam 1.

The tortuosity of foam 1 (q=1.04) was deduced by obtaining a high frequency fit with the normalised wavenumber, which theoretically approaches $k/k_0=q$ in the high frequency limit. The solid lines in Fig.2(a) are the values of k_B obtained from Eq.5, while those in Fig.2(b) are the corresponding attenuation and phase speed.

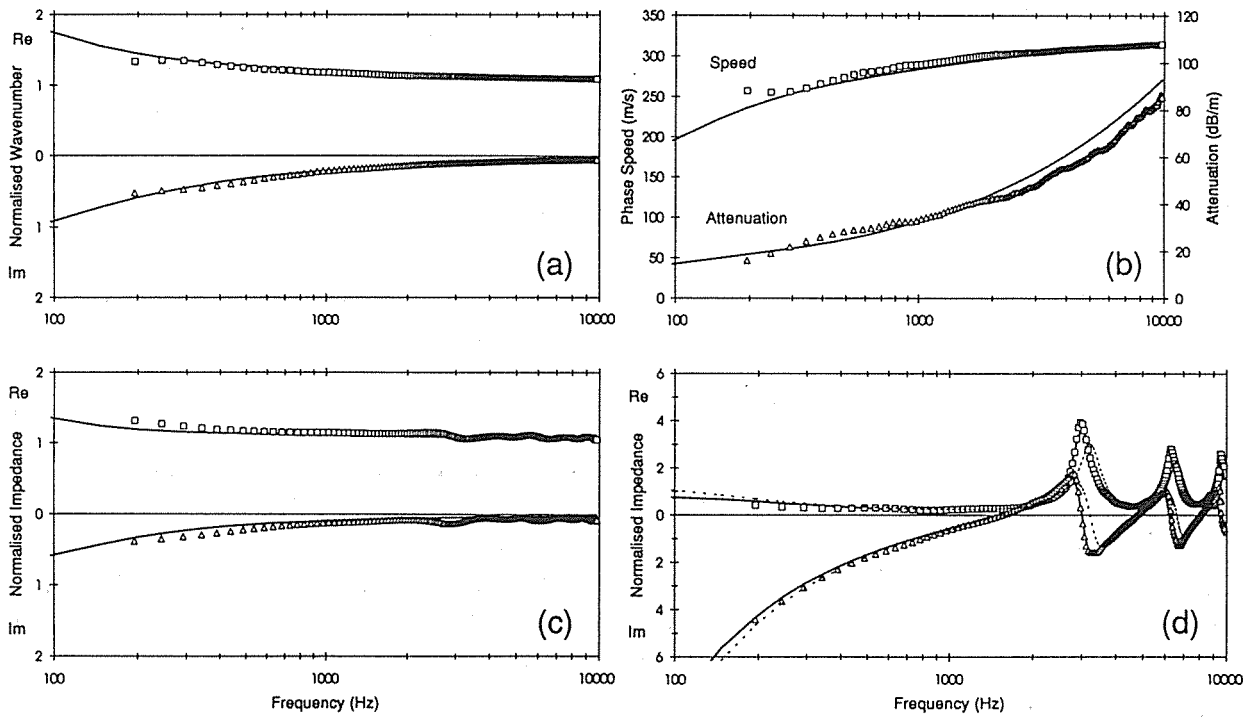

Fig.2. Experimental and theoretical results for foam 1; (a) wavenumber; (b) phase speed, attenuation; (c) characteristic impedance; (d) layer impedance.

Figs.2(c) and 2(d) show the measured normalised characteristic impedance and the normalised impedance of a 0.05m hard-backed layer of foam 1. The solid lines in Fig.2(d) are the predictions of Eq.7, and those in Fig.2(c) are the predictions of Eq.7 with the tanh terms equal to 1. The high frequency asymptote of the characteristic impedance has been shown to approach q/h. The measured characteristic impedance of foam 1 approaches 1.07, which is consistent with the measured porosity of 0.97 and the value of tortuosity estimated from the wavenumber results.

The shape factor for all samples was estimated by fitting the theoretical model to the low frquency results where the influence of the shape factor can be significant. The best fit of

As the values of q, h, and S are close to unity, the empirical equations of Ref.2 could be used to adequately fit the wavenumber and characteristic impedance results. However, the frequencies at which resonances occur in the layer impedance are sensitive to the real part of the wavenumber (related to the sound speed), which is dependent on the tortuosity. This sensitivity is apparent in Fig.2(d), where the dashed curve is the prediction of the empirical equations, where q is intrinsically equal to 1.0, compared with that from Eq.7 with q=1.04, both for a flow resistivity of 1790Nsm^{-4} .

The measured and deduced parameters for foam 1, as well as two other plastic foams used commercially as noise control materials, are shown in Table 1.

Measured quantities						Deduced values			
Foam	d (m)	σ (Nsm^{-4})	ρ_1 (kgm^{-3})	c_A (ms^{-1})	h	h	q	S	E (Nm^{-2})
1	0.050	1790	17	30	0.97	0.97	1.04	1.0	0.2x10^5
2	0.025	13100	34	46	0.95	0.95	1.4	1.0	0.7x10^5
3	0.050	25100	34	55	0.95	0.90	2.0	1.5	1.0x10^5

Table 1. Values used in the theoretical model.

Figs.3(a), (b), and (c) show the wavenumber, attenuation, phase speed, and characteristic impedance results for foam 2, while Fig.3(d) shows the impedance of a 0.025m hard-backed layer. As well as an increased density and flow resistivity, the tortuosity of foam 2 was significantly higher than foam 1, due to the more closed nature of the cells.

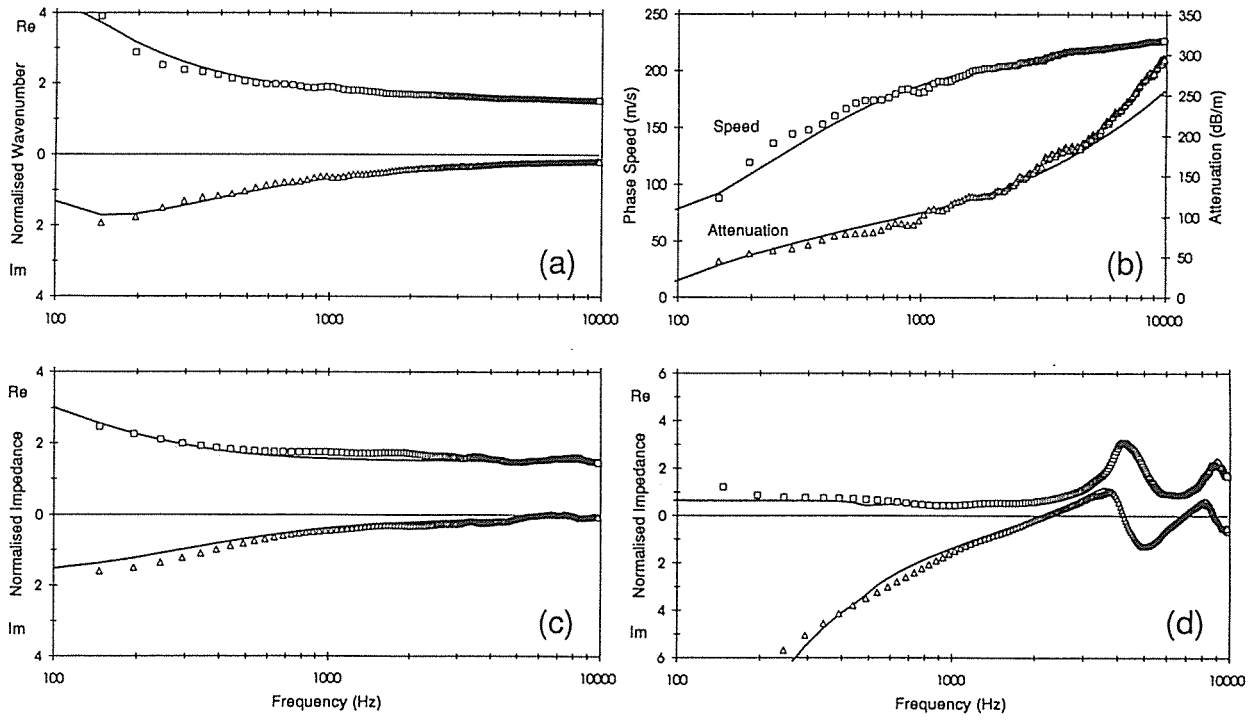

Fig.3. Experimental and theoretical results for foam 2; (a) wavenumber; (b) phase speed, attenuation; (c) characteristic impedance; (d) layer impedance.

Figs.4(a) to (d) show the results for foam 3, where the layer was 0.05m thick. This foam has a higher flow resistivity and tortuosity than foam 2. Unfortunately, the homogeneity of the foam was not good, and discontinuities between layers have caused fluctuations in the characteristic impedance and wavenumber data.

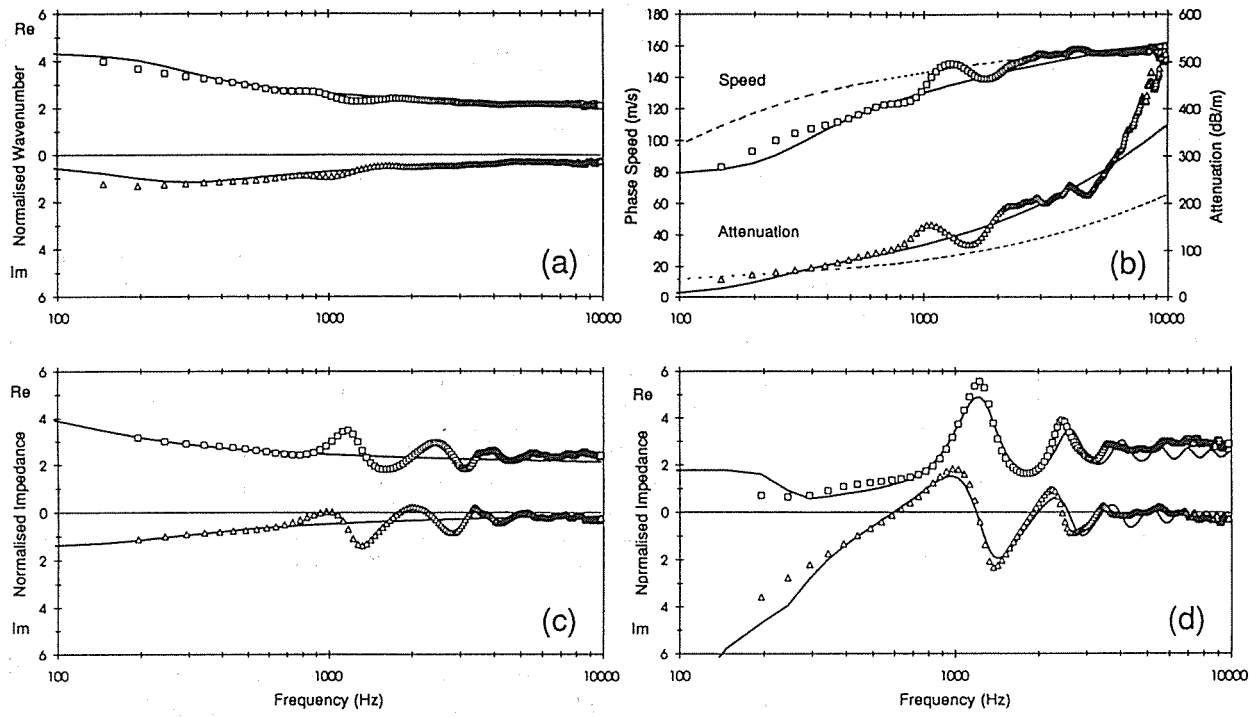

Fig.4. Experimental and theoretical results for foam 3; (a) wavenumber; (b) phase speed, attenuation; (c) characteristic impedance; (d) layer impedance.

Again, the shape factor was deduced by obtaining a best fit of the theory with the measurements and was found to be significantly higher than either foam 1 or foam 2.

For both foams 1 and 2 there is no evidence that the elasticity of the frame affects the acoustic behaviour, and so the rigid-frame model of Attenborough adequately fits the measurements. For foam 3, the theoretical curves from Eq.5 agree well with the measured wavenumber, although the corresponding result from the Attenborough model [dashed curves in Fig.4(b)] indicates that the rigid frame approximation is not valid.

Experimentally, the resonances in the layer impedance diminish above 3kHz, as shown in Fig.4(d). This is due to the high attenuation indicated in Fig.4(b), which Eq.5 has failed to predict. This could be due to the need for a frequency dependent Young's modulus.

(b) Measurements in soil

As part of an investigation into the effects of moisture and acoustic-to-seismic coupling on the impedance of outdoor ground surfaces, dispersion and attenuation measurements have been taken in soil with two different moisture contents.

Initially, the soil was very powdery, with a moisture content of only 1.2% by weight. After water was added, the soil was thoroughly stirred until the mixture was uniform, and the moisture content was then 8.1%. Figs.5(a) and 5(b) show measured attenuation and phase speeds for these moisture contents. A form of the Biot theory[11] was used to fit the measured data, as the high-porosity approximations for the elastic properties used in Eq.5 are not valid.

The best fit for the dry data was obtained with a flow resistivity of $5x10^4 Nsm^{-4}$, while for the wet mixture it was estimated to be $10^5 Nsm^{-4}$. The most significant change required to fit the data, however, was a decrease of the tortuosity from 3.3, for the dry soil, to 1.3 for the wet case. Apparently this is due to the less convoluted air paths caused by agglomeration of the wet soil during mixing.

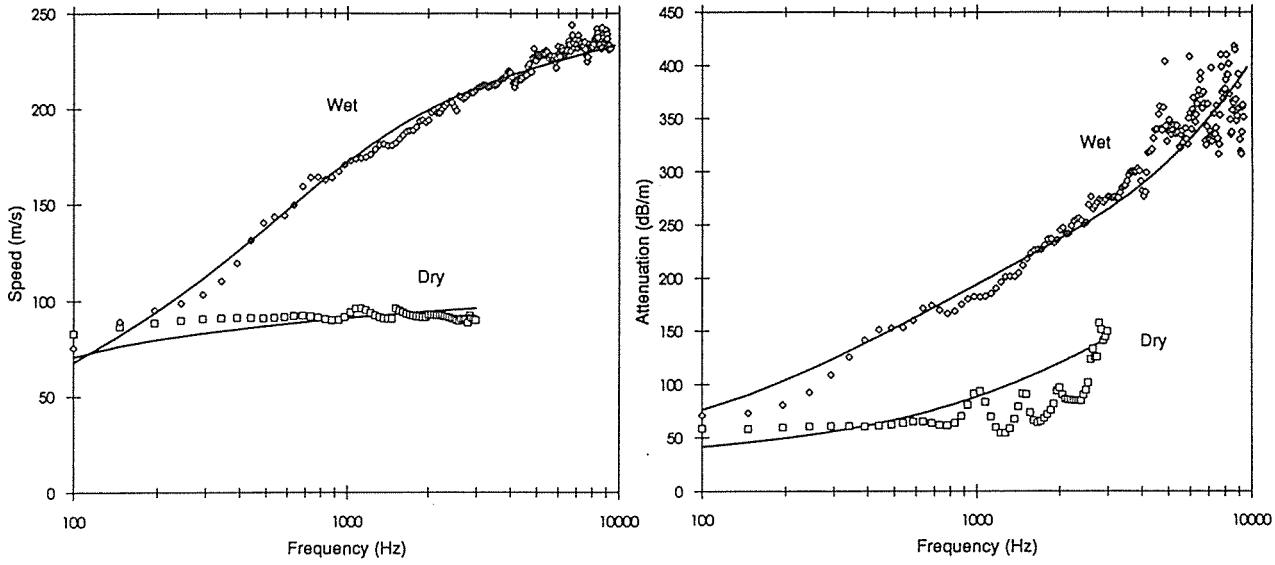

Fig.5. Experimental and theoretical phase speed and attenuation for dry and wet soil.

CONCLUSION

The impulse techniques described above are quick and effective methods for determining the acoustic properties of materials. The high frequency data which arise as a corollary of the impulse technique have proven useful in obtaining estimates of tortuosity and porosity.

The theoretical model, which is an extension of the work of Allard *et al.,* agrees well with the experimental results for foam, altough for foams 1 and 2 there is no advantage over the simpler approach of Attenborough's rigid-frame theory. While the wavenumber and characteristic impedance of foam 1, having a flow resistivity of only $1790 Nsm^{-4}$, are adequately described by the empirical equations of Delany and Bazley, the impedance of a layer is sensitive to the tortuosity even though it varies only slightly from unity.

Foam 3 exhibited some differences from the rigid-frame model which could be predicted when both a frame and fluid wave are permitted (ie. by Eqns.5 and 7). However, the model underpredicts the attenuation at high frequencies, causing the prediction of resonances in the layer impedance which are not observed experimentally.

ACKNOWLEDGMENTS

The authors would like to thank A.Rogers for the use of his sound source, and M.Coates for assistance in obtaining the flow resistivity measurements and for providing many of the foam samples.

REFERENCES

1. L.N.Brekhovskikh, *Waves in a layered media* (Academic, New York, 1960).
2. M.E.Delany and E.N.Bazley, "Acoustic properties of fibrous materials," Appl. Acoust. **3,** 105-116 (1970).
3. K.Attenborough, "Acoustical characteristics of rigid fibrous absorbents and granular materials," J. Acoust. Soc. Am. **73**, 785-799 (1983).
4. J.F.Allard, A.Aknine and C.Depollier, "Acoustic properties of partially reticulated foams with high and medium flow resistance," J. Acoust. Soc. Am. **79**, 1734-1740 (1986).
5. M.A.Biot, "Theory of propagation of elastic waves in a fluid-saturated porous solid," J. Acoust. Soc. Am. **28**, 168-191 (1958).
6. C.G.Don and A.J.Cramond, "Soil impedance measurements by an acoustic pulse technique," J. Acoust. Soc. Am. **77**, 1601-1609 (1985).
7. J.C.Davies and K.A.Mulholland, "An impulse method of measuring normal impedance at oblique incidence," J. Sound Vib. **67**, 135-149 (1979).
8. A.J.Rogers, D.E.P.Lawrence and C.G.Don, "Impulse measurements of acoustic impedance using a microphone on the surface," Proc. A.A.S. Conference, Ballarat, 257-264 (1992).
9. D.E.P.Lawrence and C.G.Don, "Acoustic properties of layered materials," Proc.Internoise 91, Sydney, 419-422 (1991).
10. T.Pritz, "Transfer function method for investigating the complex modulus of acoustic materials: rod-like specimen," J. Sound Vib. **81**, 359-376 (1980).
11. J.M.Sabatier, H.E.Bass, L.N.Bolen, K.Attenborough, and V.V.S.S.Sastry, "The interaction of airborne sound with the porous ground: The theoretical formulation," J. Acoust. Soc. Am. **79**, 1345-1352 (1986).

THE VOLUME VELOCITY METHOD FOR DETERMINING THE SPECIFIC NORMAL IMPEDANCES OF ACOUSTICAL MATERIALS

by

K P BYRNE
School of Mechanical and Manufacturing Engineering
The University of New South Wales
Sydney
Australia

1 INTRODUCTION

The normal incidence specific acoustic impedance and absorption coefficient at the surface of acoustic materials are quantities of fundamental importance whose measurement has been of interest for many years. Numerous methods for measuring these quantities have been developed over the last 100 years. Until recent times the most common method for measuring the normal incidence specific acoustic impedance at the surface of an acoustical material has been by the use of a Kundt tube. This method forms the basis of many national standards, for example [1]. However, with the development of digital signal processing equipment over the last decade the so-called two-microphone method has been developed. This method also forms the basis of various national standards, for example, [2]. The attraction of the two-microphone method is its speed of operation relative to that using the Kundt tube which requires tests to be conducted at a single frequency. A broad classification of the methods used to measure impedance and absorption can be made according to whether or not the sound waves are guided from the source to the surface of the material of interest by a tube. Both of the methods previously mentioned involve the use of a tube. Methods which have been used which do not use a tube range from a free field reflection technique proposed by Ingärd and Bolt [3] in which a heavy steel plate was used as a calibration piece to a two-microphone technique described by Allard and Champoux [4].

Byrne [5] described a tube type technique which was based on digital signal processing of the signal from a single microphone near the surface of the material of interest and the signal from a volume velocity source at the opposite end of a short tube. A relatively crude volume velocity source constructed from a modified horn-driver was used. Subsequently, a more sophisticated volume velocity source was developed and this is described in [6]. The present paper presents a review of the method and an assessment of its performance when this more sophisticated volume velocity source is used. This assessment involves a comparison, for various surfaces, of the impedance

components and the absorption coefficient measured by the volume velocity method with the same quantities measured by the ASTM two-microphone method.

2 THE VOLUME VELOCITY METHOD

The features of the device used to make the measurements are shown in Figure 1.

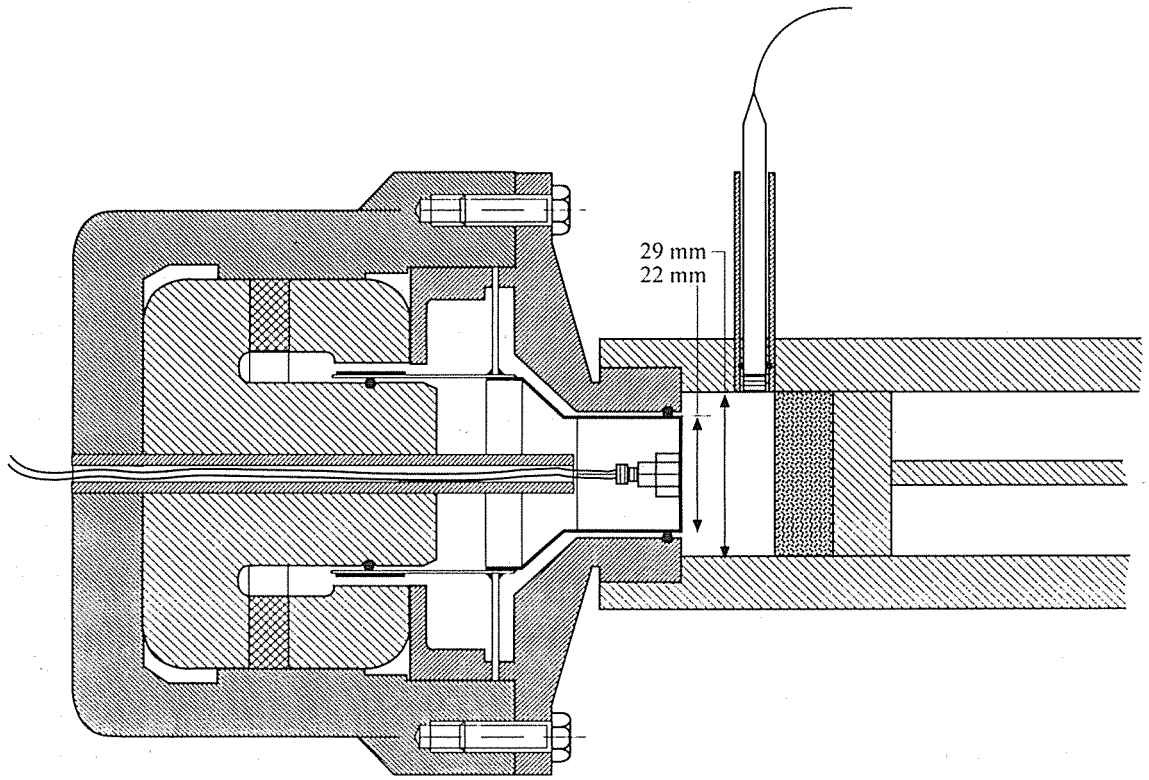

Figure 1: Device for Volume Velocity Measurements

The design shown in Figure 1 was used as it allowed the specimen and its holder to be transferred from the volume velocity source to a Bruel & Kjaer two-microphone tube as shown in Figure 2. Hence the impedance components and the absorption coefficient measured by the volume velocity method could be compared with those measured by the two-microphone method with the certainty that the impedance at the face of the specimen would be unchanged.

The volume velocity method is based on measuring the transfer function relating the pressure sensed by the microphone close to the face of the specimen and the acceleration of the piston of the volume velocity source. This transfer function can be readily found by use of a two-channel frequency analyser when the volume velocity source is driven by a random signal. The model used for the analysis is shown in Figure 3.

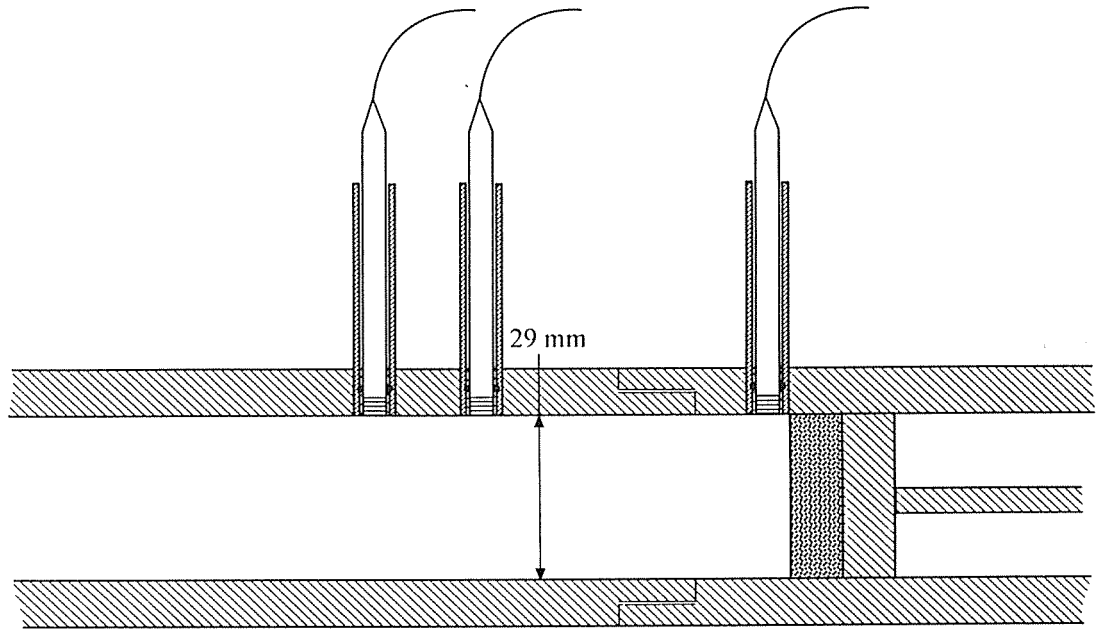

Figure 2: Specimen Holder Fitted to Two-microphone Tube

The positive and negative travelling plane waves in the cavity can be represented in complex form by $\mathbf{p}_+ = \mathbf{P}_+ \exp[\,j(\omega t - kx)]$ and $\mathbf{p}_- = \mathbf{P}_- \exp[\,j(\omega t + kx)]$. The complex reflection coefficient at the surface of the specimen where x = L, the complex representation of the pressure measured by the microphone at x = L–D and the complex representation of the volume velocity at x = 0 can be expressed in terms of these waves.

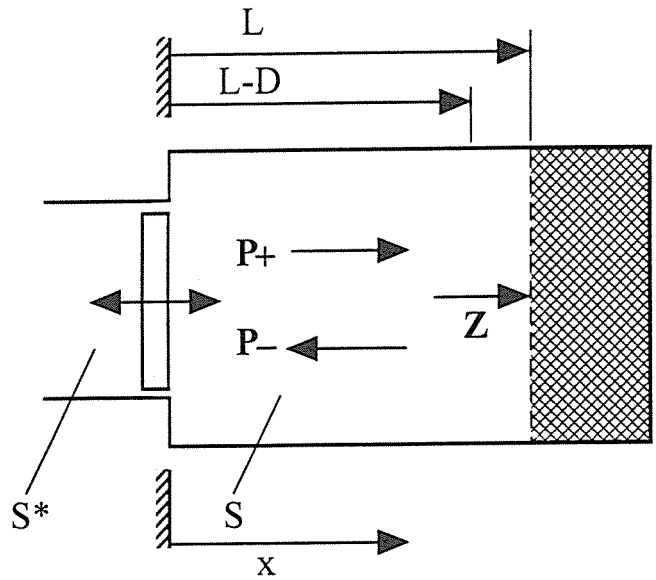

Figure 3: Model for Analysis

The volume velocity produced by the piston of area, S* in terms of the complex representation of its acceleration, **A** is $S^*\mathbf{A}/j\omega$. If the transfer function which relates the pressure measured by the microphone at x = L–D to the acceleration of the piston at x = 0 is denoted $\mathbf{H}(j\omega)$, it can be shown that the complex reflection coefficient, $\mathbf{R}(j\omega)$ can be expressed as below.

$$\mathbf{R}(j\omega) = \frac{(j\omega(S/S^*)\ \mathbf{H}(j\omega)/(\rho c))\exp(+jkL) - \exp(+jkD)}{(j\omega(S/S^*)\ \mathbf{H}(j\omega)/(\rho c))\exp(-jkL) + \exp(-jkD)} \quad (1)$$

The wave number, k is given by ω/c, where ω is the angular frequency and c is the velocity of sound. ρ is the density of the air. Once $\mathbf{R}(j\omega)$ has been found, the normal incidence specific acoustic impedance ratio at the surface of the specimen, $\mathbf{z}/\rho c$ and the absorption coefficient, α can be found from $\mathbf{z}/\rho c = (1+\mathbf{R}(j\omega))/(1-\mathbf{R}(j\omega))$ and $\alpha = 1-|\mathbf{R}(j\omega)|^2$.

3 PRACTICAL ASPECTS

Magnitude and phase errors in the voltages produced by the accelerometer and the microphone will result in the "measured" transfer function, $\mathbf{H}_m(j\omega)$ being different from the "true" transfer function, $\mathbf{H}(j\omega)$ which relates these quantities. The effect of these errors can be minimised by the following procedure. These transfer functions can be related by equation (2).

$$\mathbf{H}(j\omega) = \alpha(j\omega)\mathbf{H}_m(j\omega) \quad (2)$$

$\alpha(j\omega)$, the correction term which should be applied to the" measured" transfer function to obtain the "true" transfer function, can be obtained by measurements made when a hard surface for which $\mathbf{R}(j\omega) = 1$ replaces the surface of the specimen. Suppose that the calibration transfer function measured for this condition is denoted $\mathbf{H}_{mc}(j\omega)$. Equation (1) then leads to the following result.

$$\alpha(j\omega) = \frac{\exp(+jkD) + \exp(-jkD)}{(j\omega(S/S^*)\mathbf{H}_{mc}(j\omega)/(\rho c))[\exp(+jkL) - \exp(-jkL)]} \quad (3)$$

This expression can be used in equation (2) which then can be used in equation (1) to give equation (4).

$$\mathbf{R}(j\omega) = \frac{+\mathbf{H}^*(j\omega)(1-j\cot kL) - (1+j\tan kD)}{-\mathbf{H}^*(j\omega)(1+j\cot kL) + (1-j\tan kD)} \quad (4)$$

Equation (4) is expressed in terms of an "equalized" transfer function, $\mathbf{H}^*(j\omega)$ given by equation (5).

$$\mathbf{H}^*(j\omega) = \mathbf{H}_m(j\omega)/\mathbf{H}_{mc}(j\omega) \quad (5)$$

It is evident that the two key features of the technique are the measurement of an

"equalized" transfer function which allows the effect of the amplitude and phase errors in the transducers to be minimised and the use of this "equalized" transfer function in equation (4). The "equalized" transfer function was measured by use of a Bruel & Kjaer Type 2032 Two-Channel Frequency Analyser and the calculations needed to give $\mathbf{R}(j\omega)$ from equation (4) and then $\mathbf{z}/\rho c$ and α were made using a small computer connected to the analyser.

The internal diameter of the cavity and the specimen holder, being 29mm as shown on Figure 1, results in cross modes in the cavity not being encountered until a frequency of about 6kHz is reached. Thus the transfer function $\mathbf{H}\ (j\omega)$ was measured over a frequency range of 0 to 6.4kHz and the data was plotted over a range 0 to 5kHz. The axis of the microphone was 7mm from the face of the piston of the volume velocity source and the "equalization" transfer function was measured with the hard surface 10mm from the face of the piston. The various materials which were tested were installed therefore, with their surfaces 10mm from the face of the piston.

The two microphones used with the ASTM two-microphone procedure were 20mm apart and the axis of the closest microphone was 43mm from the face of the specimen. The usual procedure of switching the microphones to minimise phase errors was followed.

4 RESULTS

The components of the specific normal acoustic impedance ratio and the absorption coefficient determined by the volume velocity method and the two-microphone method for a number of surfaces are plotted in Figures 4 to 6. The values determined by the volume velocity method are shown by lines while the values determined by the ASTM two-microphone method are plotted as points. Each of the figures contains two diagrams. One covers a frequency range of 0 to 500 Hz while the other is for a frequency range of 0 to 5000 Hz. The absorption coefficients are not plotted on the 0 to 500 Hz diagrams as they are small over much of the range.

The results shown in Figure 4 are for a 25mm deep air cavity. The broken line which refers to the reactance of the 25mm deep air cavity as measured by the volume velocity method is in close agreement with the theoretical value of $-\cot kL$. The theoretical values are plotted as circles on the low frequency diagram. It can be seen that there is a lack of precision with the two-microphone method at low frequencies. This is, of course, to be expected in view of the close microphone spacing.

The results shown in Figure 5 are for a 50mm thick fibreglass specimen backed by a

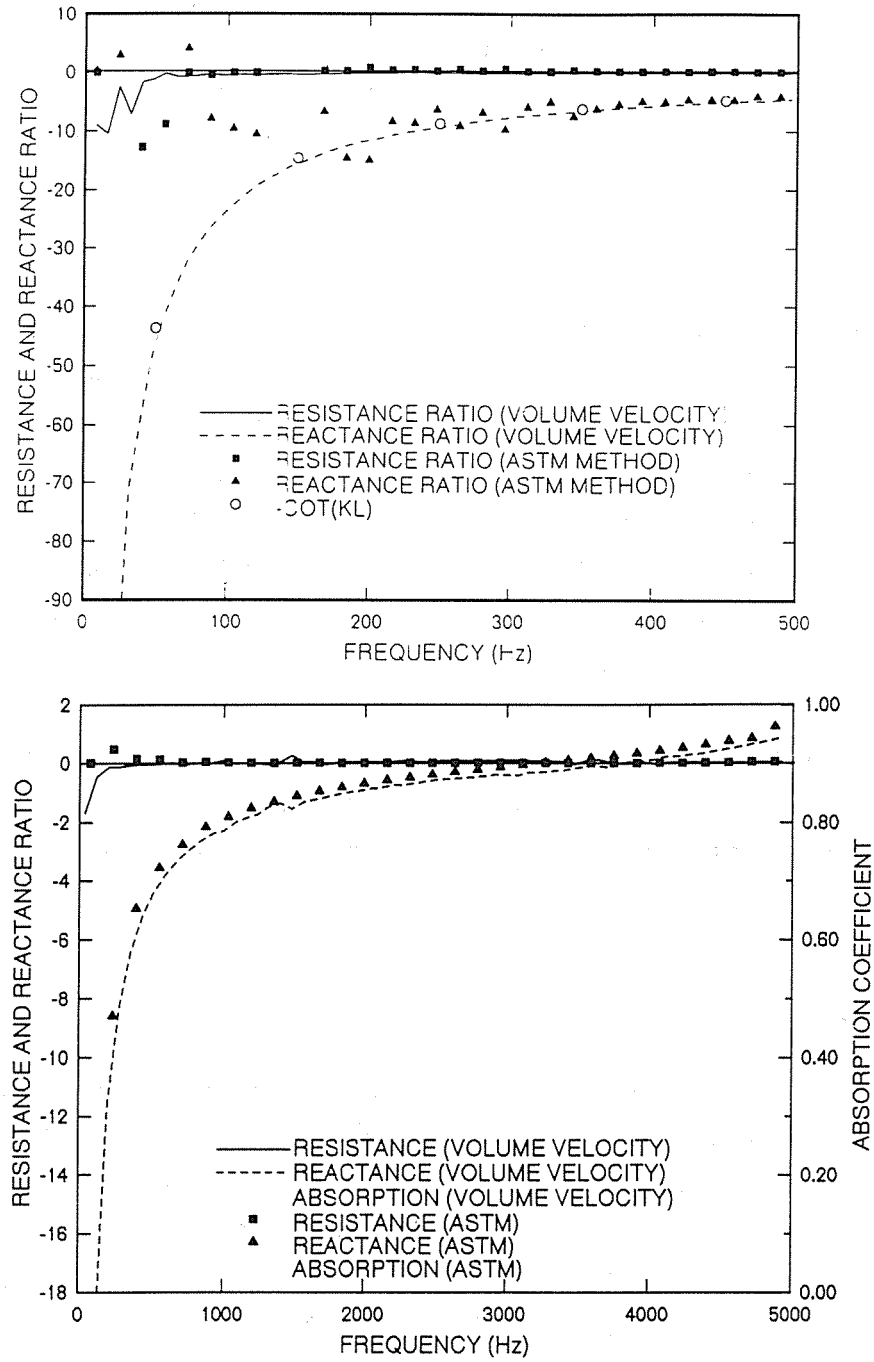

Figure 4: Components of Impedance Ratio and Absorption Coefficient for 25mm Deep Air Cavity

hard surface. It can be seen with regard to the low frequency diagram that, except at low frequencies, there is good agreement between the results derived by the two methods. At high frequencies in the high frequency diagram the agreement is not good between the absorption coefficient results.

The final set of results shown in Figure 6, are for a 25mm thick sample of plastic foam. This sample is in fact the calibration sample supplied with a Bruel & Kjaer two-microphone impedance measuring system. The same features are evident as with the fibreglass sample in that there is poor agreement between the results measured at low

and high frequencies.

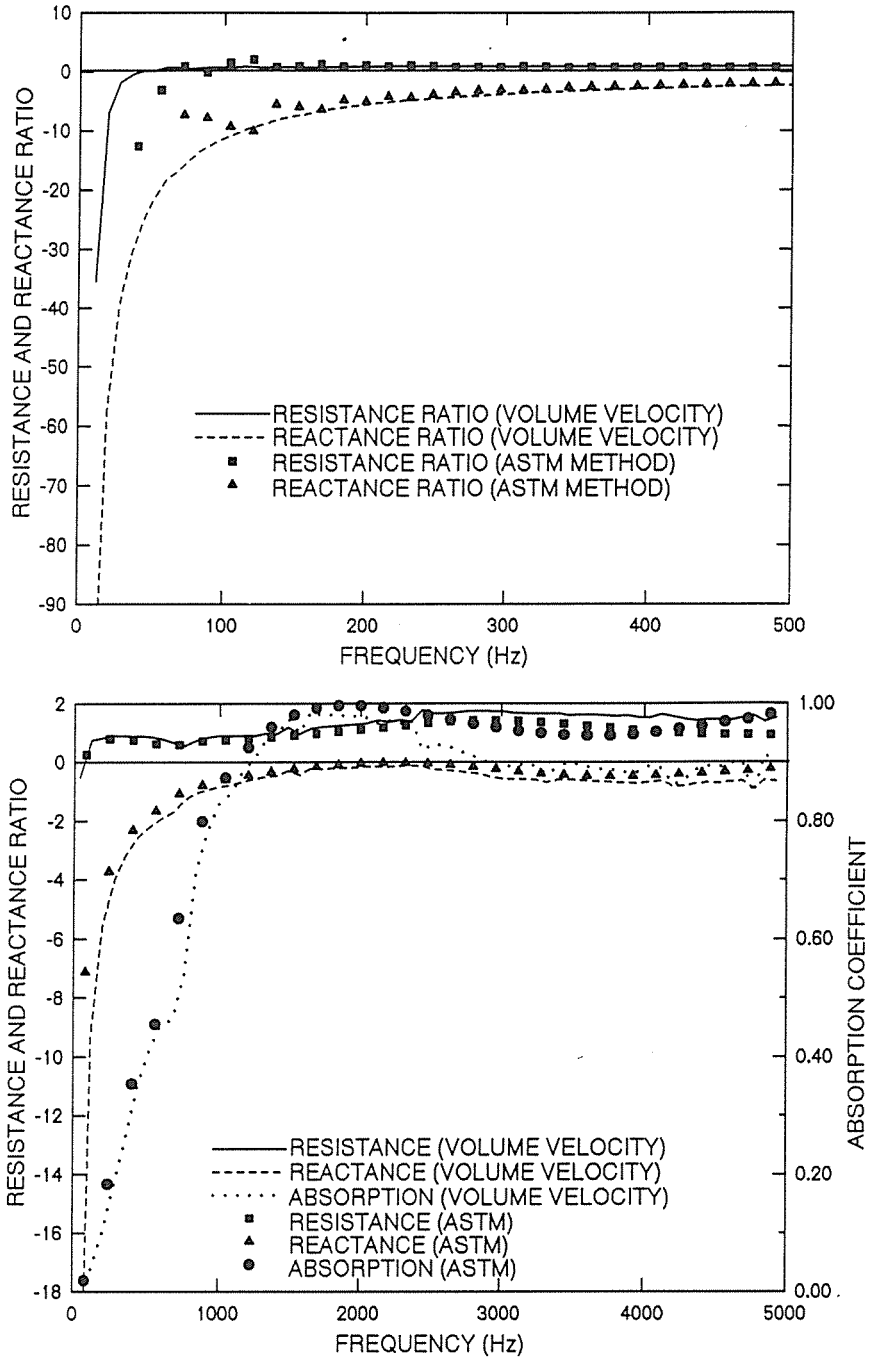

Figure 5: Components of Impedance Ratio and Absorption Coefficient for 50mm Thick Fibreglass.

5. COMMENTS ON THE RESULTS

It can be seen that under favourable conditions the results obtained by both the volume velocity and the ASTM two-microphone method are in good agreement. The value of the volume velocity technique is that it enables accurate values to be obtained at low frequencies. It is likely that the high frequency discrepancies evident in Figures 5 and 6 are due to non-uniformity of the samples. It is possible that this problem could be overcome by rotating, about the cavity axis, the sample holder relative to the microphone.

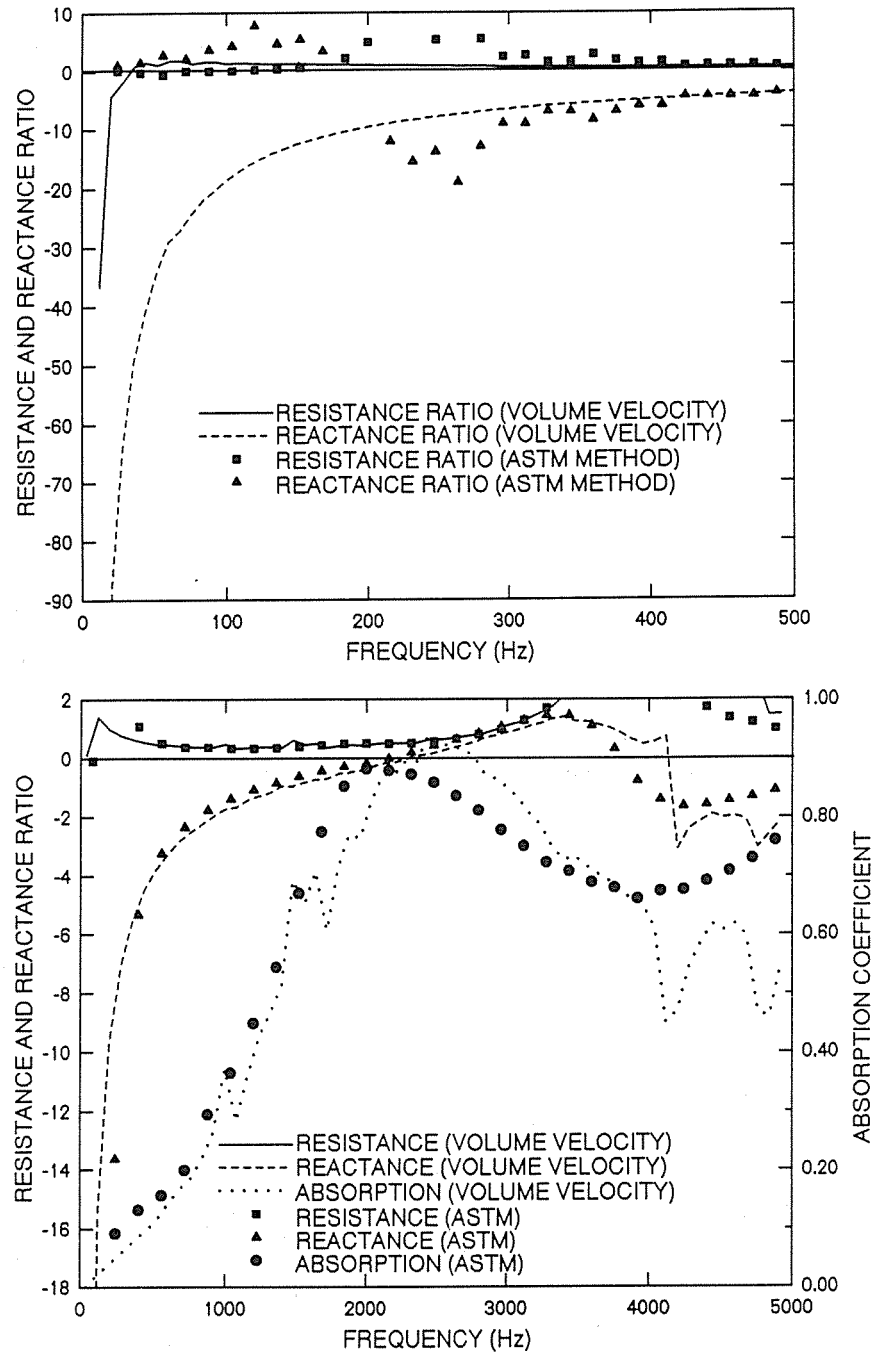

Figure 6: Components of Impedance Ratio and Absorption Coefficient for 25mm Thick Plastic Foam.

REFERENCES

1. Australian Standard 1935–1976, "Method for the Measurement of Normal Incidence Sound Absorption Coefficient and Specific Normal Impedance of Acoustical Materials by the Tube Method". Standards Association of Australia, Sydney, 1976.

2. ASTM E1050–86 "Standard Test Method for Impedance and Absorption of Acoustical Materials Using a Tube, Two Microphones and a Digital Frequency Analysis System".

3. INGÄRD, V. and BOLT, R.H., "A Free Field Method for Measuring the Acoustic Absorption Coefficient of Acoustic Materials". The Journal of the Acoustical Society of America, **23**, 5, 1951, 509–516.

4. ALLARD, J.F. and CHAMPOUX, Y., "In Situ Two–microphone Technique for the Measurement of the Surface Acoustic Impedance of Materials". Noise Control Engineering Journal, **32**, 1, 1989, 15–23,

5. BYRNE, K.P., "Transfer Function Technique for Impedance and Absorption Measurements in a Tube Using a Volume Velocity Source", Proceedings of the International Conference on Noise Control Engineering, Sydney, 1057–1060, 1991.

6. BYRNE, K.P., "The Development of Acoustic Volume Velocity Sources", Proceedings of the Australian Acoustical Society Annual Conference, Ballarat, 61–71, 1992.

Sound power determination in the geometric near field of a source by pressure measurements alone.

by

D. A. Bies and Gareth Bridges

INTRODUCTION

Before the advent of the sound intensity meter there were only two ways of determining the sound power of an acoustic source. If the source was not large the radiated sound power could be determined by placement of the source in a calibrated reverberation chamber and from a determination of the reverberant field level the sound power could be calculated. Alternatively, if the sound pressure level in free far field could be determined over an encompassing surface the radiated sound power could be estimated on the assumption that in the far field the pressure and particle velocity were in phase and consequently the pressure squared was a measure of the sound intensity.

However, situations were often encountered in which a source could not be placed in a reverberation chamber and measurements in the free far field often were not possible but a need still existed for an estimation of the radiated sound power. Consequently, procedures were developed for making sound pressure level measurements in the near field of a sound source over some arbitrarily located measurement surface. Radiated sound power was then estimated by assuming that the squared sound pressure on the measurement surface was a measure of the sound intensity at the surface.

With the commercial availability in recent years of sound intensity measuring equipment the direct determination of radiated sound power has become possible. In principle, the determination of sound power from intensity measurements in the near field of a source is now possible. It has been discovered, however, that the near field of a source can be remarkably complicated and consequently the question may reasonably be asked whether it is possible to determine sound power in the near field of a source using pressure measurements alone. Alternatively, one may ask how great was the likely error incurred by such procedures used in the past and how much has been gained for the purpose of sound power determination by the introduction of the sound intensity meter.

In the investigation to be described here the field of a piston mounted in an infinite baffle is considered. As is well known the extent of the geometric near field of the vibrating piston is determined by the dimensionless quantity $D = a^2/\lambda r$ where a is the radius of the piston, λ is the wavelength of the radiated sound and r is the distance from the center of the piston to the field point in the half space in front of the baffled piston where the observation is made. When the latter dimensionless quantity, D, is greater than one the field point is in the near field and conversely when the quantity is less than than one the field point is in the far field.

The radiated sound power of the piston mounted in an infinite baffle may be calculated in terms of the well known real part of the radiation impedance, *R*, and the piston velocity amplitude, *U*. Consequently, an estimate of radiated sound power based upon field measurements may be compared with the calculated value of the radiated sound power. If the estimated sound power is divided by the known calculated radiated sound power for convenience then a value of one is obtained for the ratio when perfect agreement is achieved while a number for the ratio greater or less than one indicates either an over estimate or an underestimate. The size of the error is indicated by the magnitude of the ratio relative to one.

ANALYSIS

The origin of coordinates is placed at the center of the piston as shown in Figure 1. The piston has radius *a* and vibrates sinusoidally normal to its surface with velocity amplitude *U*. The piston radiates into the half space above the plane of the piston.

It will be supposed that the power radiated by the piston can be determined from the squared pressure distribution over a hemisphere of radius *r* centered at the center of the piston. The hemisphere encloses the piston source in the half space into which the piston radiates sound. The hemisphere will be referred to as the measurement surface and squared sound pressure calculated at field points on the measurement surface will be referred to as measurements. Choice of number, *Q*, of field points will be a variable of the experiment.

Referring to the figure, as the field is symmetric about the central axis of the piston, it is only necessary to consider field points along an arc in the measurement surface extending from the axis of symmetry to the plane of the piston. A further reduction in the computation is possible based upon the observation that source point to field point distances, *r'*, are symmetrical about a plane of symmetry coincident with the the measurement arc. Consequently, it is only necessary to integrate contributions to the sound pressure at the field point over half of the piston surface. The total sound pressure is then determined by multiplication of the integral by 2.

Referring to Figure 1, where the contribution of the piston surface element *dS* to the sound pressure observed at field point *q* is illustrated, the surface element to field point radius, *r'*, divided by the field point radius *r* is given by the following equation.

$$\frac{r'}{r} = \left[1 + \left(\frac{\sigma}{a}\right)^2 \left(\frac{a}{r}\right)^2 - 2\left(\frac{\sigma}{a}\right)\left(\frac{a}{r}\right) \sin\theta \cos\psi\right]^{1/2} \qquad (1)$$

The normalized surface element to field point radius is expressed in dimensionless form as follows.

$$r'_N = \frac{r'}{r} r_N \tag{2}$$

where

$$r_N = \frac{r}{a} \tag{3}$$

Contributions to the pressure, p, observed at field point q are determined by integration over the surface of the piston. Thus where the surface area of the piston is S the pressure at q is expressed in integral form as follows.

$$p = j \frac{\rho c k U}{2\pi} \int_S \frac{e^{j(\omega t - kr')}}{r'} dS \tag{4}$$

The increment of power, ΔP, through a circumferential strip of area $\Delta S'$, at radius $\boldsymbol{r}$ about the axis of symmetry will be approximated as follows.

$$\Delta P = \frac{\rho c k^2 U^2}{8\pi^2} \Delta S' f(k, r') \tag{5}$$

where

$$f(k, r') = \left[\int_S \frac{\cos kr'}{r'} dS \right]^2 + \left[\int_S \frac{\sin kr'}{r'} dS \right]^2 \tag{6}$$

An estimate of the total power radiated, P', is calculated by summing the contributions ΔP given by Equation 5 over the entire hemispherical measurement surface. The estimated total radiated power is

$$P' = \sum_{q=1}^{Q} \frac{\rho c k^2 U^2 f(k, r')}{8Q} \sin \theta_q \tag{7}$$

The integration of Equation 6 is carried out numerically by dividing the area of the piston surface into 2,500 elements distributed uniformly and calculating the contribution of each to the observed pressure at the field point q.

The power, P, radiated by the piston may be calculated in terms of the real part of the

radiation impedance *R(2ka)* and the velocity amplitude *U* of the piston. The power radiated by the piston is

$$P = \frac{1}{2}\rho c\pi a^2 R(2ka)\, U^2 \qquad (8)$$

The normalized estimated radiated power, P_N, is obtained by dividing Equation 7 by Equation 8. The normalized power estimate is

$$P_N = \sum_{q=1}^{Q} \frac{\pi k^2 a^2}{4Q R(2ka)} r_N^2 \sin\theta_q \qquad (9)$$

RESULTS

To ensure that the program provides correct information the cases of a piston of radius *a* which is equal or less than the radiated wavelength λ were first considered. For *Q = 10* in which ten field measurements were simulated the normalized power estimates were all essentially one with errors less than 0.1 or less than 0.5 dB confirming that all of the radiated power was accounted for by the simulated far field measurements.

In Figure 2 the case of a very directional source with an extended geometric near field is considered. In this case the radiated wavelength to piston radius ratio, λ/a, has been set equal to 0.1 or the diameter of the piston is twenty wavelengths across. In this case the boundary between the geometric near field and the far field occurs for a value of field radius to piston radius ratio, *r/a* = 10 as shown in the figure.

It is observed by reference to the figure that both larger and smaller estimates of the radiated power are observed but when the number of simulated measurements is increased from 10 to 20 the departure from 1 is considerably reduced. It is also of interest to note that the worst estimate occurs in the far field for the case of 10 measurements and not in the near field as might have been expected. The figure shows quite clearly that there is no sensible difference between measurements of sound power, using pressure measurements alone, when the measurements are made in either the near or the far fields and that in either case accuracy is improved by increasing the number of measurements.

CONCLUSION

The geometric near field of a radiating source of sound can be quite complicated with extensive constructive and destructive interference effects in the related pressure field.

Sound intensity measurements have confirmed the complexity of such fields and have raised the question whether a determination of radiated sound power based upon pressure measurements alone is even possible in the geometric near field.

The determination of the sound power radiated by a baffled piston from a finite number of pressure squared measurement over an encompassing hemispherical surface has been investigated numerically. It has been shown that the results are independent of whether the measurement surface is in the far field or the geometric near field and in any case the precision of measurement of radiated sound power improves with increasing number of measurements.

Although the investigation reported here is certainly not exhaustive it is considered indicative. Too much information has raised the question whether the measurement is possible whereas the simplistic approach carried out with reasonable care gives the right answer. In fact, the major problem often faced by the engineer is how to reduce a large amount of information to a manageable quantity. Consequently, a greatly expanded measurement capability is not necessarily of itself an asset.

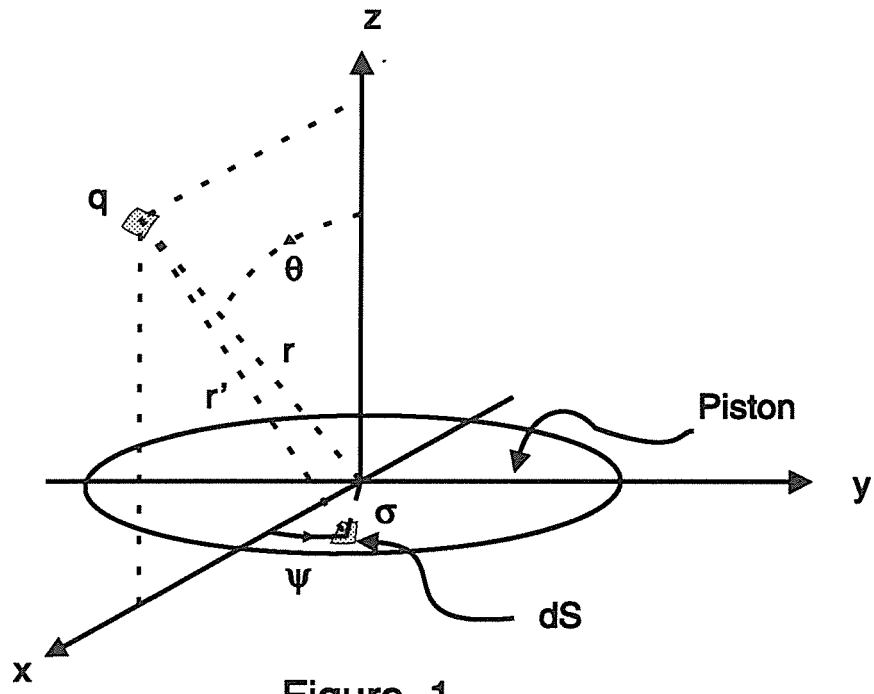

Figure 1.

Piston in an infinite baffle ; Vibrates normal to the x-y plane with velocity amplitude U.

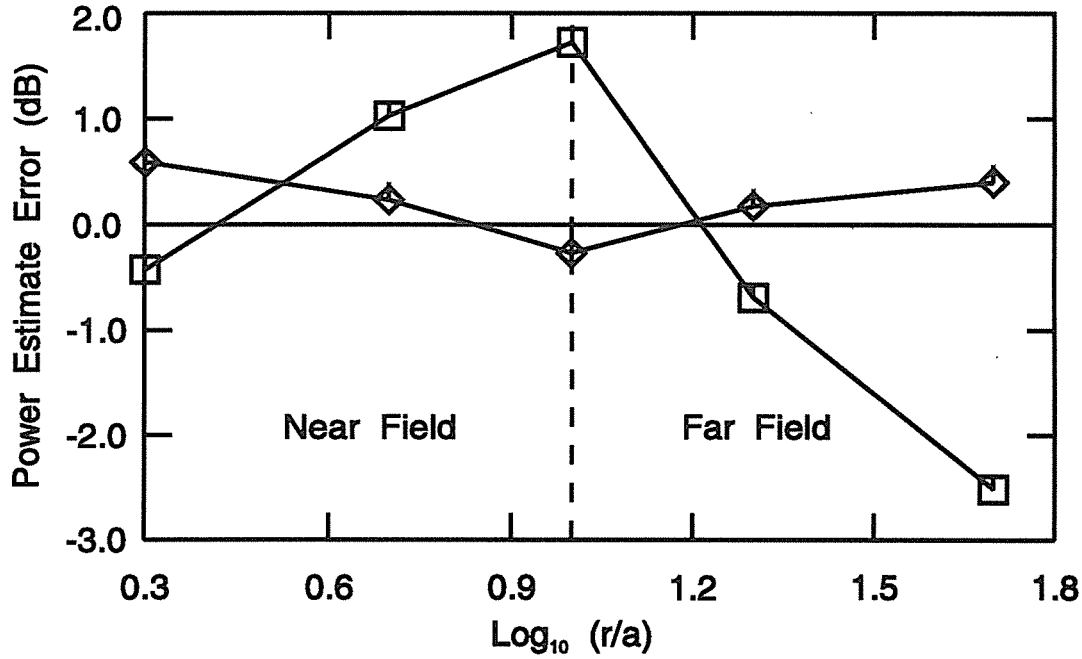

Figure 2.

Power estimate error in decibels vs. normalised field points radius. Boundary between near and far fields at $\log_{10}$ (r/a) = 1. ☐ — 10 Measurement Points, ◇ — 20 Measurement Points.

Single and double pulse propagation in a turbulent atmosphere

I.D.McLeod, G.G.Swenson and C.G.Don
Department of Physics, Monash University, Clayton, Victoria.

1. INTRODUCTION

Sound propagation under outdoor conditions is strongly influenced by meteorological variables and surface impedance values. In many situations, fluctuations in the wind velocity have significant effects on the propagating sound and there is considerable interest in predicting the sound field in terms of models based on readily measured wind velocity parameters. To date most studies have discussed continuous wave investigations[1,2], whereas this work uses pulse propagation as the probe. In this situation the effects of the wind can be manifest as changes in the flight time of the pulse and as alterations in its waveform. Theoretical studies for continuous wave excitation indicate a relation between the RMS value of the pulse pressure and that of components of the wind velocity[3]. Further these studies indicate the RMS value of acoustic parameters should be independent of wind direction. This work seeks to examine the applicability of these ideas to pulses and further seeks to develop a model of propagation in a fluctuating wind derived from properties inherent in the pulse waveform.

2. EXPERIMENTAL SET-UP

In the experiments to be reported here, simultaneous measurements were taken up and downwind over the same region of grassland to see if there were appreciable effects due to wind direction. To this end, identical microphone systems were located 16m away, on either side of an impulse source, and the whole system aligned along the mean wind direction as indicated in Fig 1. This layout enabled upwind and downwind data to be obtained under as near as identical meteorological conditions as possible.

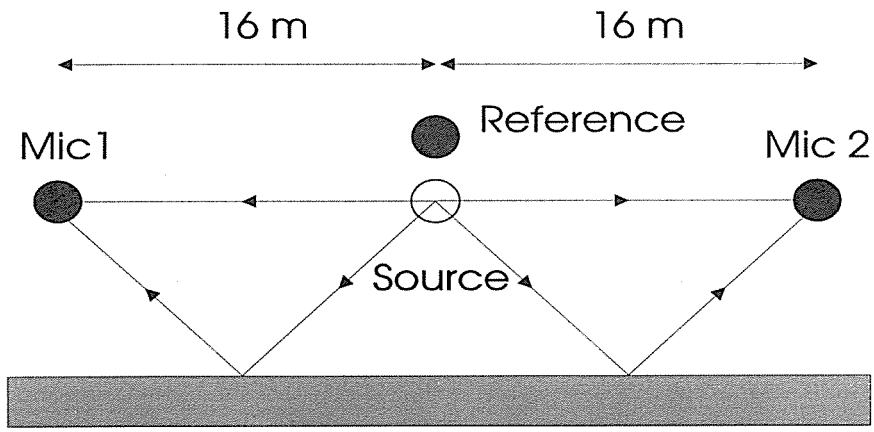

Fig. 1. Experimental setup

Source and receivers were positioned 2.0m above the flat mown grassy surface. This geometry allowed complete separation in time of the direct and ground reflected pulse. Anemometers were placed near both receivers and the source, each output being connected to a digitising system which allowed the wind variations to be stored

in 5ms intervals. The system was triggered by the impulse source, so that 100 data points occurred before and 100 after a particular shot. These data were subsequently averaged over the 50ms interval centred on the instant when the pulse passed the anemometer location. Measurements were only taken when the wind direction, as judged by a number of flags positioned along the propagating path, was within a few degrees of the axis formed by the source and microphones. The anemometers also permitted temperature measurements to be taken, however, it was noted that the variation of temperature over the site and for the data acquisition time was negligible so it is unlikely that this factor could influence the results.

In examining the effects of outdoor wind turbulence, it is useful to establish a reference pulse waveform and to know its spread under zero wind conditions. To achieve this, measurements were taken indoors in a large hall, where there was essentially no movement of the air, and using an identical measurement geometry to that of the outdoor experiments. For the measurements reported here it was also necessary to ensure that the pulse source produced the same amplitude and waveform at equal distances on either side of the source for a given shot. It was found that this condition was closely fulfilled, although there were significant changes to the amplitude between shots. To account for this a reference microphone was positioned 0.50m from the source, but away from the main propagating directions to avoid interfering with these pulse waveforms. This microphone output was used solely to adjust each pulse amplitude to a common value: the philosophy being that even outdoors this microphone was sufficiently close to the source that turbulent effects on its amplitude would be negligible. When such a normalisation was introduced, the distribution of pulse waveforms over twenty or more individual indoor pulses was extremely tight and the ensemble averaged waveform at both measuring receivers was essentially identical and did not vary appreciably between different measuring sets.

3. RESULTS

Measurements from two different regions of a large grass-covered football field are reported. Site 1 was about 8m from, and its axis perpendicular to, a 3m high embankment with trees along its top. The wind was blowing through the trees and then down onto the flat grassland where the experimental measurements were taken. It seemed possible that this geometry could set up turbulent structures which may have preferentially affected the microphone nearer the embankment. The second site was on the flat area, where the wind blew parallel to the embankment and had a fetch length of at least 300m.

3.1 Relationship between Pulse Delay and Meteorological Data.

These measurements follow from those reported earlier,[4,5] where the results were somewhat inconclusive. It was necessary to establish a suitable method for manipulating the anemometer readings to give a representative velocity which would correlate with the measured pulse delays. Three approaches were tested;-

1 take the single result from any one of the anemometers.
2 take an average of the anemometer reading at the source and that at the relevant microphone.
3 fit a quadratic to the three measured values and integrate the function over either the up or downwind path and take the average derived from this integral.

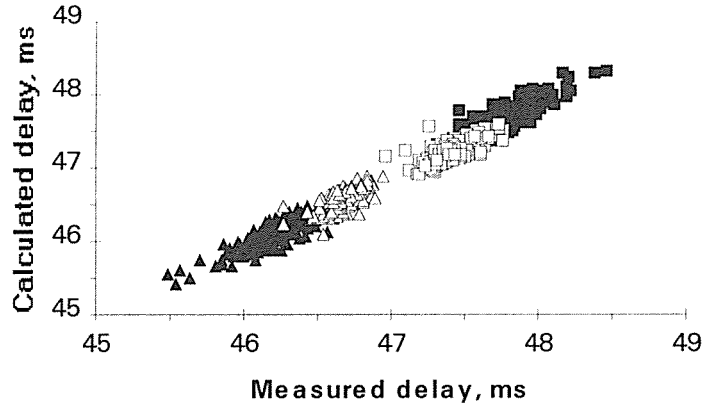

Fig 2. Comparison between calculated and measured delay.

As might be expected, using the individual reading, approach 1, was generally the poorest predictor. Whilst method 3 was marginally better than 2 it is more complex and time consuming and so the second method has been adopted in the remainder of this work. An example of the correlation of measured up and downwind delays with values calculated using this wind parameter is shown in Fig 2.

3.2 Ensemble Average and Distribution Measurements

Fig 3 shows the change in the average impulse waveform between pulses propagating indoors and upwind outdoors under two different wind regimes. While there is a slight increase in the pulse height, the dominant change has been to broaden the pulse. A similar result occurs downwind although the average pulse height is then slightly less than that of the indoor case.

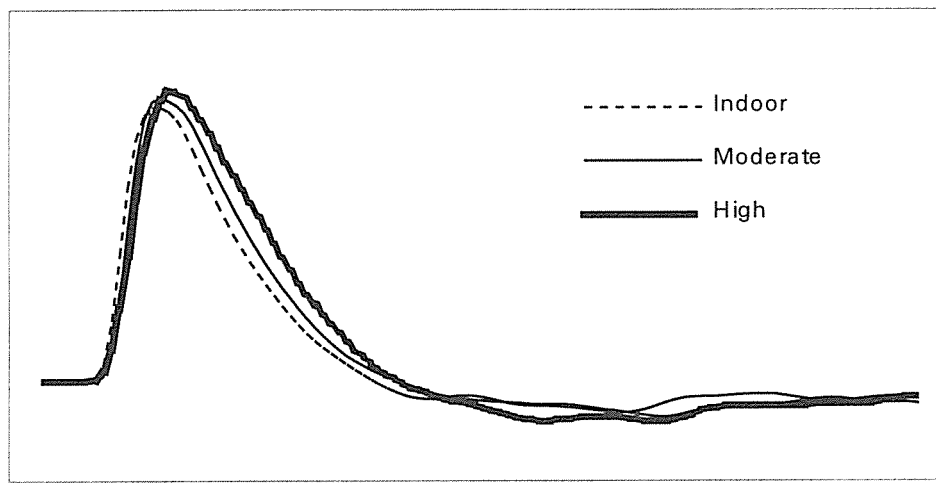

Fig. 3. Averaged pulse shapes.

While individual pulses may have a larger or smaller peak pressure compared to the indoor value, the pulse width is very rarely less and often substantially greater than the width measured indoors. This implies that energy is being scattered into the tail of the pulse, the amount of this scattered energy increasing as the average wind speed increases.

Fig 4 shows the distribution of the peak pressure values (in arbitrary units) for over 200 shots at site 2. Included are the direct and ground reflected pulses, taken simultaneously for both up and downwind propagation. As well, the dotted curve shows the much tighter distribution obtained for 102 indoor direct measurements.

Note this curve was drawn with a different vertical scale. The corresponding reflected pulses from the nearly perfectly reflecting hard wooden floor gave a similar distribution and so has been omitted.

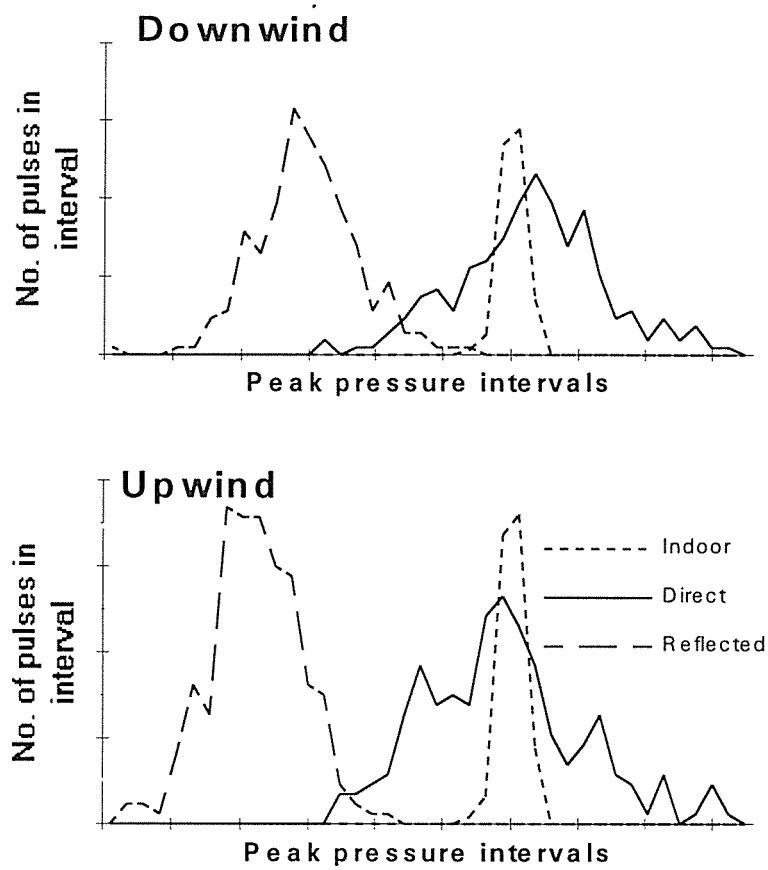

Fig. 4. Peak pressure distributions

The resolution of the above histograms was set by dividing the maximum peak height of the direct pulse into 40 intervals. While it may appear that the reflected pulse distribution is much narrower, this is because their amplitudes are significantly less than the direct pulses. Once appropriately normalised, the direct and reflected distributions, whether up or downwind, are essentially identical.

It is apparent that while the wind fluctuations cause significant changes to the distribution, the effect is essentially independent of wind direction. Further, although the turbulence experienced by the ground reflection could be quite different to that affecting the direct, in fact, the standard deviations of the distributions show negligible difference, in spite of the reflection also being involved. This could not have been established using continuous wave techniques. Based on Fig 2, we might expect a good correlation between the standard deviation of the wind speed distribution and that of the propagation time. However, as shown in Table I, such a relationship is not obtained. Similar findings hold for peak height, width, and energy distributions. Even if the wind speed is broken down into different velocity groups there is no improvement in the correlations. The reason for these discrepancies is not clear at the moment.

	Upwind site 1	Upwind site 2	Downwind site 1	Downwind site 2
Wind speed (m/s)	1.02	1.45	1.01	1.630
Propagation time (ms)	0.157	0.200	0.108	0.192
Peak height*	0.026	0.031	0.020	0.027
Width (ms)	0.067	0.021	0.016	0.020
Energy*	0.111	0.101	0.062	0.102

Table 1. Standard deviation, * refers to normalised units.

The energy of a pulse is related to the sum of the squares of each of the instantaneous pressure values along the length of the pulse. The end point for the computation is difficult to determine due to fluctuations in the tail, however, as the excess pressure region contains 90% of the energy, the overall uncertainty in the energy is minimal. Previous pulse work preformed with considerably lighter wind speeds than in this study revealed that 5% of the received pulses showed energy enhancement[4]. This fraction has significantly increased in the data of Table 2, where the data have been selected if the outdoor energy exceeded 1.09 times the indoor value. There is a marginal increase in the energy of the received pulse when propagating upwind and at higher speeds. To make this consistent with the observation, noted in conjunction with Fig. 3, that the downwind pulse height was smaller than the upwind case, it is necessary to conclude that for downwind pulses the scattered energy tends to arrive later in the pulse.

Site	Mean wind speed (m/s)	Downwind %	Upwind %
Ref. 5	2.0	5	-
1	5.0	36	52
2	7.1	54	64

Table 2. Percentage of pulses with energy greater than average indoor pulse.

3.3 Individual pulse shapes

Major variations occur between individual pulse shapes, either between different shots or between the different propagation directions, as is apparent from the two solid curves in Fig. 5. In an attempt to use the shape information, a simple model has been postulated which assumes that any given pulse can be formed from the linear combination of a number of successively delayed pulses.

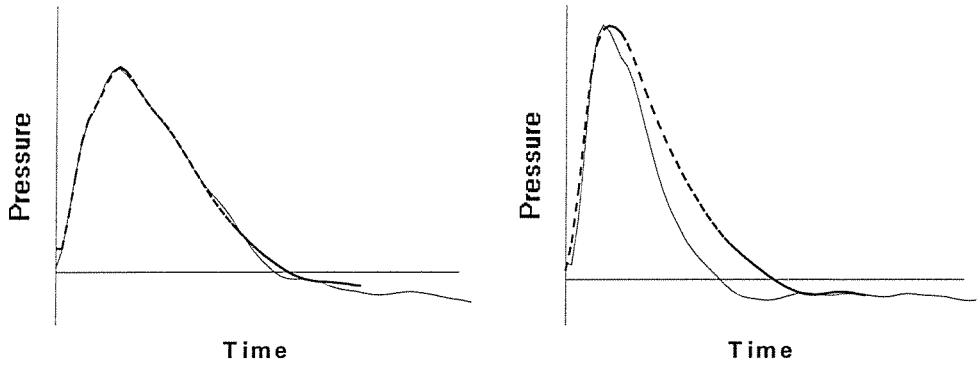

Fig. 5. Example of a good fit and a poor fit, using the pulse reconstruction model.

The shape of each component pulse is assumed to be that of the indoor waveform but its amplitude and starting time can be adjusted as required. It has been found that a maximum of three pulses are required to successfully reproduce all but the tail of the pulse in 95% of the 100 pulses considered. The few exceptions are when the outdoor pulse is narrower than the indoor one and could be explained by allowing the second component to be inverted by a scattering mechanism. An example of a good fit and one of the rare bad fits are indicated by the dashed lines in Fig. 5.

If the required amplitude and delay of each of the three component pulses are plotted, the result is that shown in Fig.6. Not all the first components occur at time zero because of a limitation in the computer matching routine which could not always exactly align the leading edge of the actual pulse and the indoor waveform. Thus the spread of first components into four or five channels is a measure of the current resolution. In some cases the amplitude of the first component exceeds that of the indoor pulse, sometimes it is necessary to add the second component with very little delay while in others a small second component is not required until quite late. However, it is noticeable that the second and third components tend to bunch more tightly in the site 2 results than occurs in the other set. The reason for this difference is unknown, although it may be associated with the different fetch lengths setting up a different pattern of turbulence.

Particularly with the site 2 results, it is tempting to assign three effective paths to the sound reaching the receivers. If it is assumed that the direct path from source to receiver is that followed by the first component, then the second component arriving, on average, 20μs later, can be thought of as being scattered from a region approximately 7.3cm off axis while the third component, which is delayed about 50μ s, would appear to be scattered from a point 11cm off axis. An alternative approach is to consider the components to be delayed as they pass through parts of the turbulent region with different wind vectors.

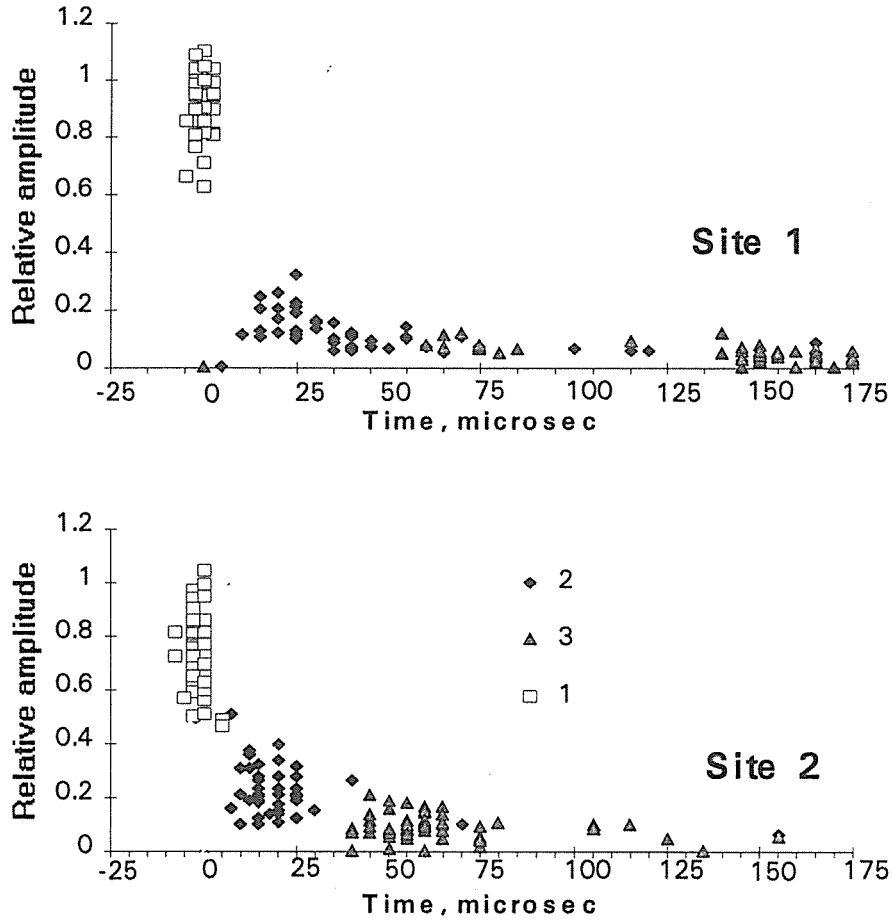

Fig. 6. Amplitude of component verses arrival time.

3.4 Double pulse source

The motivation for using a double pulse source is twofold - to establish that the passage of a pulse does not affect the flow regime significantly and to study the time evolution of turbulence. Two methods of generating double pulse source have been examined[6], double detonation and a single detonation system, see fig 7. The time separation for both methods is achieved by making the exiting gas travel two paths of differing lengths. An additional benefit is the possibility of producing a wider pulse which will contain lower frequencies by having such a small delay that the pulses merge. After testing it was found that system 7b was more acceptable as the interpulse delay was more reproducible between pulses. The lack of reproducibility of either system at the level required, limited the ability to get a consistent wider pulse.

Using a double pulse system in still air, it has been found that for interpulse durations between 0.5 and 4.0ms, changes in waveform for transmission between 1 and 2.5m is negligible when allowance is made for a decrease in amplitude due to distance spreading. Such a finding suggests that the passage of the first pulse does not introduce a flow disturbance and thereby affect the second pulse.

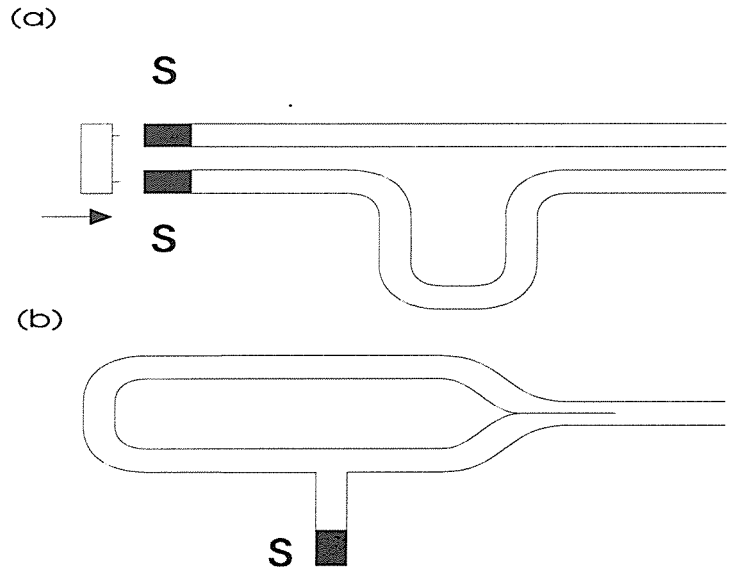

Fig 7 Double pulse source construction.

4. CONCLUSION

Considerable information about the fluctuations of the wind along the propagation path is locked up in the pulse waveform, as is evident from the assortment of observed shapes. The problem is to correctly extract and interpret the results.

This study has considered the average properties of the waveforms by considering groups of several hundred pulses and plotting variations of peak height or calculating their energy content. Further, the standard distribution of such parameters has been compared with that of the wind fluctuation. While good correlation has been achieved with the pulse delay and the meteorological data, the correlation between the standard deviations is relatively poor. At this stage, no adequate explanation is available for this lack of agreement. The development of a model of turbulent behaviour from the way the pulse waveform can be generated by a number of component pulses is in its infancy, however, early results look promising.

REFERENCES

1. G.A.Daigle, J.E.Piercy and T.F.W.Embleton "Effects of atmospheric turbulence on the interference of sound waves near a hard boundary," J. Acoust. Soc. Am. **64**, 622-630 (1978).

2 H.E.Bass, L.N.Bolen, R.Raspet, W.McBride and J.Noble "Acoustic propagation through a turbulent atmosphere: experimental characterisation," Acoust. Soc. Am. **90**, 3307-3313 (1991).

3 L.A.Chernov, "Wave propagation in a random medium" (McGraw-Hill, New York, 1960)

4 I.D.McLeod, G.G.Swenson and C.G.Don "Measurement of atmospheric fluctuations using impulse sound," Fifth international symposium on long range sound propagation, Milton Keynes, England (1992).

5 I.D.McLeod, G.G.Swenson and C.G.Don "Effect of atmospheric fluctuations on impulse sound propagation," A.A.S. National Conference, Ballarat, (1992).

6 C.G.Don, A.J.Cramond, I.D.McLeod and G.G.Swenson "Shotshell primer impulse sources" Appl. Acoust (to be published).

TRANSMISSION OF SOUND THROUGH APERTURES

Kym A. Burgemeister and Colin H. Hansen

Department of Mechanical Engineering
The University of Adelaide
South Australia
5005

Abstract

The prediction of sound transmission through apertures has been the subject of a number of research articles spanning fifty years. Here previous work on this subject is used as a basis for developing a model to calculate the effect of a perforated panel on the sound radiation from a solid panel mounted closely behind it. Experimental data agree well with theoretical predictions for small apertures but agreement becomes worse as the aperture size to wavelength ratio increases.

Introduction and Review

Although vibration actuators can be used to control sound radiation from thin structures (Snyder and Hansen 1990, Meirovich and Thangjitham, 1990) and sound transmission through thin structures (Fuller and Jones, 1987, Eatwell, 1989), the control of vibration of heavy structures with large internal impedances is much more difficult because of the large forces required. For example, the active control of sound radiation from electrical transformers using vibration actuators acting on the transformer tank is generally impractical for this reason. Also the use of sound sources to control the sound radiation on a global basis is impractical because of the large number of sources required. One alternative might be to enclose the transformer in a thin sheet metal enclosure and apply active vibration control to the enclosure. However this would be impractical as the transformer would overheat. Another alternative would be to use a perforated sheet metal enclosure which would still allow cooling by natural convection and which could reduce the radiated sound by appropriate control of its own vibration.

The study of the transmission of sound through single apertures has been the subject of research for many years, mainly with a view to describing the detrimental effects of holes in walls of structures surrounding noise sources. Ritchie (1932) experimentally confirmed some of Lamb's (1931) fundamental statements concerning sound transmission through an aperture, by measuring the intensity of sound transmitted from a source room, through an aperture, into a receiving room. For multi-perforated panels, Ritchie determined an empirical cubic equation to describe the transmission loss for a given number of holes. Mulholland and Parbrook (1967) cast serious doubts on the validity of Ritchie's results because of their belief that the location of the measuring microphone immediately behind the aperture would invalidate them.

Sivian (1935) experimentally determined the acoustic impedance for small orifices, although the results are of little use because they are empirical and thus limited in application. Levine

and Schwinger (1948,1949) provided a rigorous mathematical description of the diffraction of sound by an aperture in a screen. Assuming an incident plane wave they calculated by integral methods the amplitude of the diffracted spherical wave at a given distance from the aperture. This result was used to determine the transmission coefficient of the aperture. However this analysis is too complex to be applied easily to more complicated aperture arrangements.

Cook (1957) calculated the absorption of sound by patches of absorbent materials, and his results were used by Mulholland and Parbrook (1967) to calculate the transmission loss of an aperture based on the assumption that any sound energy absorbed by the patch of air would be re-radiated from the far side of the aperture. However this work was limited to very low frequencies. Gomperts (1965) solved velocity potential equations to model the transmission loss of an aperture, and in particular considered viscous effects within the aperture. Wilson and Soroka (1965) determined the transmission loss of a panel with an aperture by determining the approximate solution for the diffraction of a plane wave incident on an aperture based on the assumption of rigid, massless, infinitely thin, plane pistons in each end of the aperture, with the motion of the pistons modelling the movement of the air particles at the ends of the aperture under acoustic excitation. It was assumed that plane waves propagated in the aperture, which holds true if the wavelength is much larger than the aperture diameter. Wilson and Sorokas analytical results are similar to those of Gomperts but their analysis is much simpler and has been experimentally verified (Oldham and Zhao, 1993; Gibbs and Balilah, 1989)

Mulholland and Parbrook (1966) provided a valuable summary of the theories to that time. In particular, they determined the transmission coefficient of sound through an aperture using the theories of Lamb, Rayleigh, Gomperts, Wilson and Soroka, and Cook as a function of the normalised parameter ka, where k is the wavenumber and a is the radius of the aperture. The various theoretical models showed good agreement at large values of ka (where the transmission coefficient approaches unity) but poor agreement for the case of small ka. Their conclusions, that a modification of Cook's theory best agreed with their experimental results, is in conflict with results of both Gibbs and Balilah (1989) and Oldham and Zhao (1993) who experimentally verified the results of Wilson and Soroka. Mulholland and Parbrook also proposed an interesting solution to the problem of the interactions between the holes in an array. This involved the use of a modified impedance which was determined by the number of neighbours and a "coherence factor" to account for the different relative phases of the vibrating air pistons, but unresolved typographical errors make it difficult to apply.

In 1992 Pan et. al. investigated analytically the feasibility of controlling low frequency sound radiated from a solid, simply supported rectangular panel by mounting in front of it a second actively rectangular panel containing a single large hole. Experimental work (Burgemeister and Hansen, 1993) failed to validate the theoretical model and for this reason the work described in this paper is directed towards providing a more accurate model, and one which can incorporate multiple holes.

A New Theoretical Model

A solid vibrating rectangular panel of dimensions L_x, L_y, thickness h and excited by a point force F_p at $\sigma_p = (x_p, y_p)$ is located on the $z=L_z$ plane as shown in figure 1. In front of the solid panel, a second simply supported panel (the front panel) is installed on the $z=0$ plane and is surrounded by an infinite rigid baffle. The perimeter of the space between the two panels

is sealed by the shim steel used to provide the simple support for the front panel. In this front panel there is an $H_x \times H_y$ array of rectangular holes, each of which has diameter ϕ_h, and centre (for the p, q^{th} hole) at,

$$\left(\left\{\frac{-L_x}{2}+\frac{L_x}{(H_x+1)}p\right\}, \left\{\frac{-L_y}{2}+\frac{L_y}{(H_y+1)}q\right\}\right)$$

Calculation of the far field sound pressure is done by first calculating the response of the solid panel and then calculating the sound field produced by the solid panel at the perforated panel. Once this is done the theory of Wilson and Soroka (1965) is used as a basis for calculating the sound pressure in the farfield. An iterative procedure is used to allow the effect of multiple reflections from the back of the perforated panel to be included in the model.

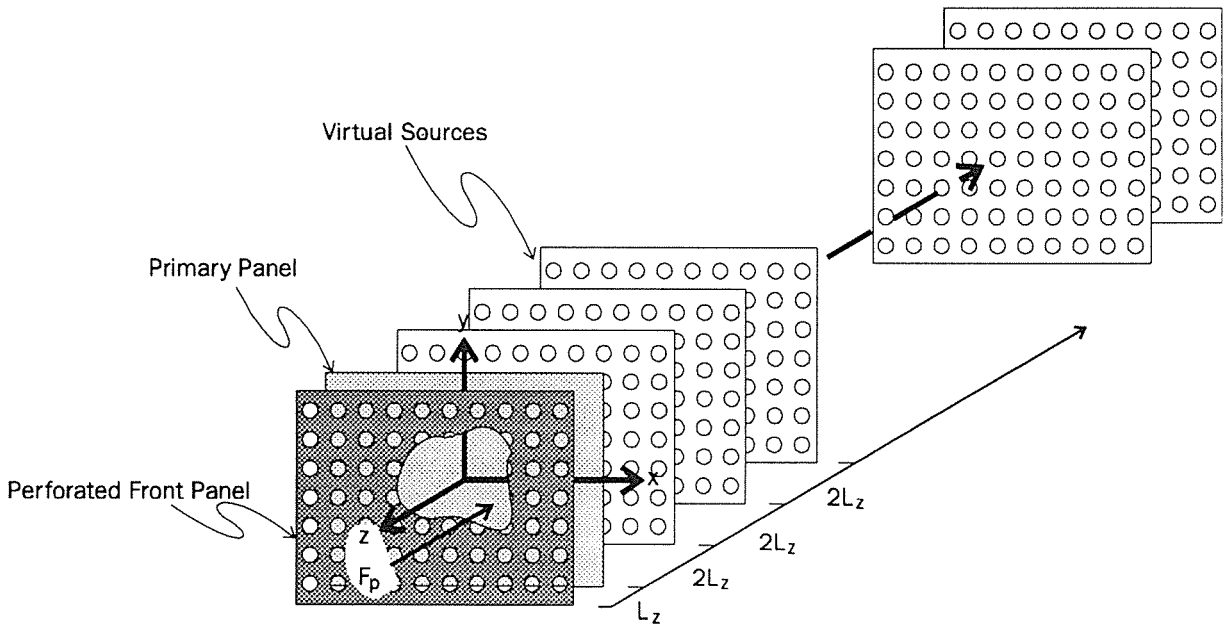

Figure 1 Theoretical Arrangement

Solid Radiating Panel Response

With the origin of the coordinate system in the centre of the panel, the panel displacement due to the *(m, n)* mode is

$$W_{m,n} \approx W^{p}_{m,n}\cos\left(\frac{m\pi x}{L_x}\right)\cos\left(\frac{n\pi y}{L_y}\right)e^{j\omega t} \qquad (1)$$

where the normal mode shape function $\Psi_{m,n}(\sigma)$ is defined as

$$\Psi_{m,n}(\sigma) \approx \cos\left(\frac{m\pi x}{L_x}\right)\cos\left(\frac{n\pi y}{L_y}\right) \qquad (2)$$

where σ=(x,y).

The resonance frequency of the *(m, n)* mode for a simply supported edge panel is given by:

$$f_{m,n} \approx \frac{1}{2\pi}\left(\frac{Eh^2}{12\rho(1-\nu^2)}\right)^{1/2}\left(\left(\frac{m\pi}{L_x}\right)^2+\left(\frac{n\pi}{L_y}\right)^2\right) \tag{3}$$

The panel displacement amplitude matrix $[W^p]$ is an $M\times 1$ array, where M is the total number of panel modes considered.

$$[W^p] = \begin{bmatrix} W_1^p \\ W_2^p \\ \vdots \\ W_M^p \end{bmatrix} \tag{4}$$

It can be calculated, given the driving force F_p as

$$[W^p] = [Y]\left[F_p^t\right] \tag{5}$$

where the panel modal admittance matrix $[Y]$ is an $M\times M$ diagonal matrix with its diagonal element defined as

$$Y_{m,n} = \frac{1}{M_{m,n}(\omega_{m,n}^2 + j\eta_{m,n}\omega_{m,n}^2 - \omega^2)} \tag{6}$$

and the matrix $\left[F_p^t\right]$ is defined as

$$\left[F_p^t\right] = F_p\begin{bmatrix} \Psi_1(x_p,y_p) \\ \Psi_2(x_p,y_p) \\ \vdots \\ \Psi_M(x_p,y_p) \end{bmatrix} \tag{7}$$

where ω is the angular frequency (rad/s) of excitation, $\omega_{m,n} = 2\pi f_{m,n}$ is the angular resonance frequency of the *(m, n)* panel mode, $\eta_{m,n}$ is the loss factor for the *(m, n)* mode,

$$M_{m,n} = \rho h \int_A \Psi_{m,n}^2(\sigma)\, d\sigma$$

is the modal mass of the solid panel and A is the solid panel area.

Sound Pressure Incident on the Perforated Panel

The acoustic pressure on the incident side of the perforated panel is calculated from the

displacement function of the primary panel, $W_{m,n}$, by using the Rayleigh integral as follows

$$p_i = \frac{-\rho\omega^2}{2\pi} \sum_{M} \int_{A_p} \frac{W_{m,n}(\sigma)\, e^{-jkr(\sigma)}}{r(\sigma)}\, d(\sigma) \qquad (8)$$

Where ρ is the density of air, ω is the angular frequency and r is the distance from point $\sigma=(x,y)$ on the primary panel to the centre of the i^{th} hole.

Due to the close proximity of the primary panel to the perforated panel, it is assumed that the sound field incident on portions of the perforated panel not occupied by a hole are reflected, and in this case it is reasonable to assume that there is no absorption by the solid part of the perforated panel. Similarly, it can be assumed that this partially reflected sound field will be re-reflected (with no absorbtion) by the solid primary panel back towards the perforated panel. In theory it is necessary to define an infinite series of virtual sources (reflections) of the primary panel (minus the regions of the holes, where sound will be absorbed and not reflected) stretching behind the primary panel. The n^{th} virtual source is $2L_z$ on behind the primary source, where L_z is the distance between the primary panel and the perforated panel. The pressure field of each virtual source can then be added to the primary source, and its resulting pressure in the far field calculated by using equation (9). Of course only a finite number of virtual sources need be considered in practice, as each has less effect than the previous one because the distance terms in the Rayleigh Integral become larger for each successive virtual source. In this way, all of the sound energy from the primary panel can be seen to eventually make its way out of the perforations. In practice, it was found that using 30 virtual sources provided acceptable convergence of the results.

Wilson and Soroka's analysis is easily applied to calculate the pressure p_r in the far field of an aperture (at some distance r), given the pressure p_i on the incident side of the aperture as

$$p_r = \frac{jka^2 e^{jkr}}{r\left[2R_0(\cos kh - X_0 \sin kh) + j[(R_0^2 - X_0^2 + 1)\sin kh + 2X_0 \cos kh\right]} p_i \qquad (9)$$

where R_0 and X_0 are the radiation resistance and mass reactance functions of a circular piston in an infinite wall given by

$$R_0 = R_0(2ka) = 1 - \frac{2j_1(2ka)}{2ka} = \frac{(2ka)^2}{2\cdot 4} - \frac{(2ka)^4}{2\cdot 4^2\cdot 6} + \frac{(2ka)^6}{2\cdot 4^2\cdot 6^2\cdot 8} - \ldots \qquad (10)$$

and

$$X_0 = X_0(2ka) = \frac{4}{\pi}\left[\frac{(2ka)}{3} - \frac{(2ka)^3}{3^2\cdot 5} + \frac{(2ka)^5}{3^2\cdot 5^2\cdot 7} - \ldots\right] \qquad (11)$$

When the perforated panel contains more than one aperture, the complex sound pressure contributed at some location by each aperture are added together to give the total sound pressure at that location.

To obtain acceptable results when many holes are included in the perforated panel it is necessary to calculate the effect of each hole upon the radiation and mass reactance experienced by nearby holes. Both Pritchard (1960) and Arase (1964) discuss mutual radiation impedance between radiators. Pritchard's results, however, reduce to a simple trigonometric function and hence are vastly simpler to implement numerically. Pritchard states that

$$Z_{12} = (R_{12} + jX_{12}) \approx R_0 \left[\frac{\sin(kd_a)}{kd_a} + j \frac{\cos(kd_a)}{kd_a} \right] \tag{12}$$

where Z_{12} is the mutual impedance between two radiators *1* and *2* and d_a is the distance between them. Hence for an array containing a total of $H_x \times H_y$ holes the radiation impedance of the n^{th} hole is given by the modified radiation resistance and the modified mass reactance as

$$R_n = R_0 + R_0 \sum_{H_x H_y} \frac{\sin(kd_a)}{kd_a} \tag{13}$$

and

$$M_n = M_0 + R_0 \sum_{H_x H_y} \frac{\cos(kd_a)}{kd_a} \tag{14}$$

The major drawback of the theoretical formulation is the vast amount of computing time required, and the high number of calculations involving integrations over extremely small areas also makes this method susceptible to rounding errors.

Experimental and Numerical Results

A rectangular steel panel (primary panel) of dimensions 380mm x 300mm, and thickness 1.98mm was mounted in a heavy steel frame using spring steel shims to approximate simply supported boundary conditions. The panel was placed in the centre of a large wooden baffle and excited using a Brüel & Kjær 4809 electrodynamic shaker at its centre. The acoustic response of the panel was measured with a Brüel & Kjær 1 Inch microphone placed directly in front of the panel at a distance of 1.7m. In front of the primary panel, a second simply supported control panel (perforated panel) of the same dimensions (as the primary panel) was installed. Four different control panels mounted 20mm away from the primary panel were tested. The first panel was constructed to match the panel used in the theoretical analysis of Pan et. al. (1992). It had one 47.5mm square hole, offset 95mm from the centre of the panel. The remaining panels had arrays of holes of different density and size as shown in the table below.

Array Size	Hole Size
1	47.5mm Square
10 by 22	6mm Diameter
55 by 41	3.9mm Diameter
56 by 41	3.25mm Diameter

In figures 2a and 2b, results are shown for the sound radiated from the solid panel with and without the presence of a perforated panel in front of it, with a single square hole. The curves shown in figure 2a represent experimental results as well as numerical results (calculated using a DEC 5000/240 compuserver) for the case including the perforated panel using both the theory of Pan et. al. (1992) and the theory developed in this paper (assuming in both cases a panel loss factor of η=*0.0039* which was determined by measurement of the test panel). It can be seen from the figure that the theory developed in this paper fits the measured data much more closely than the theory of Pan et. al. (1992), especially at low frequencies. In figure 2b two curves represent the experimentally measured sound radiation on axis to the panel with and without the perforated panel and the third curve represents the theoretically predicted sound radiated by the solid panel which can be seen to agree well with the experimental data.

Experimental measurements using other types of perforated panels are shown in figures 3 to 5 where it can be seen that placing the perforated panel in front of the solid panel makes little or no difference to the sound radiation except at higher frequencies.

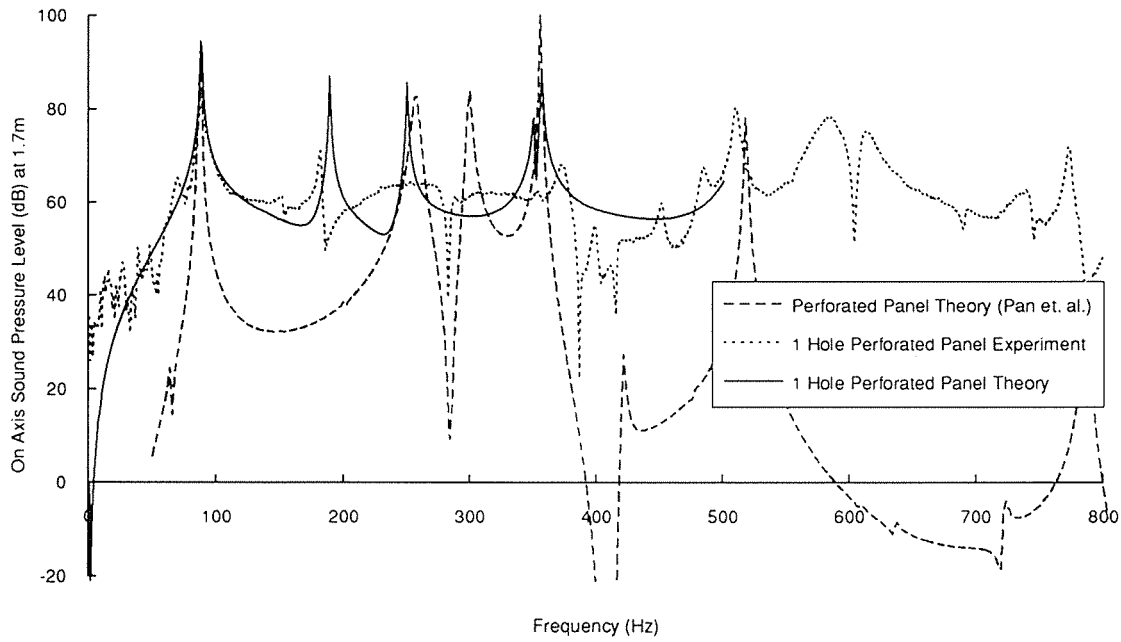

Figure 2a The effect of a panel with a single 47.5mm square hole on the sound radiation from a solid panel mounted 20mm behind it and excited by a 1N point force at its centre.

Conclusions

A theoretical model has been developed to allow the sound field radiated by a solid panel fronted by a perforated panel to be calculated. This is the first step in the analysis needed to calculate the maximum achievable sound reduction as a result of applying active vibration control to the perforated panel. It is of interest to note that by itself the perforated panel only has a small effect on the radiated sound field. However, when actively controlled, preliminary experimental work has shown the potentially achievable noise reduction to be well over 10dB.

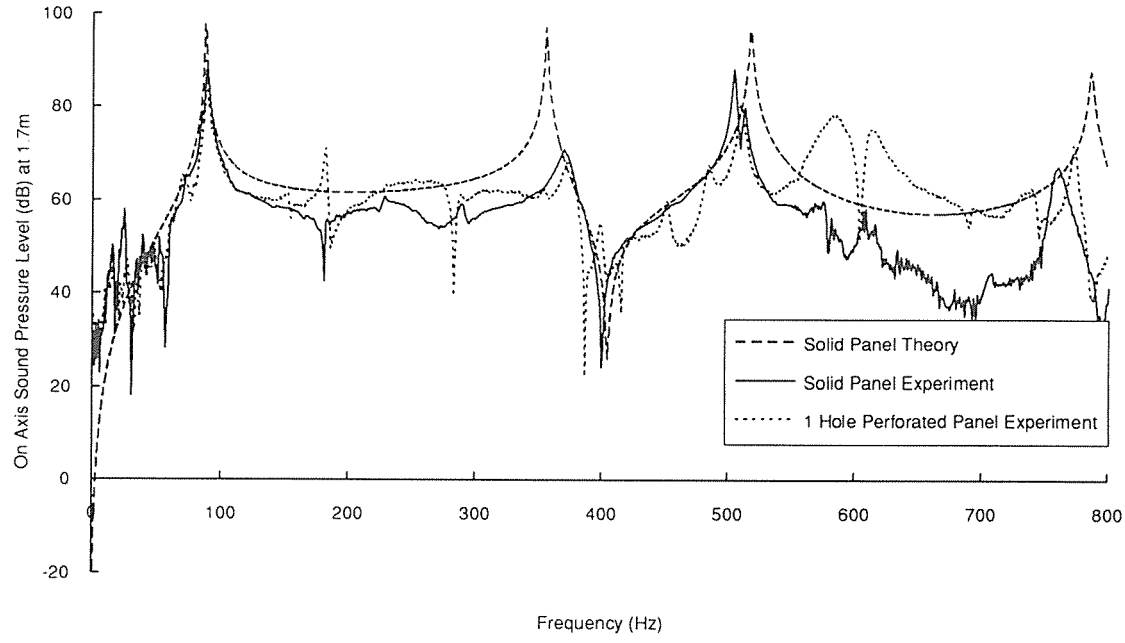

Figure 2b The effect of a panel with a single 47.5mm square hole on the sound radiation from a solid panel mounted behind it and excited by a point force at its centre.

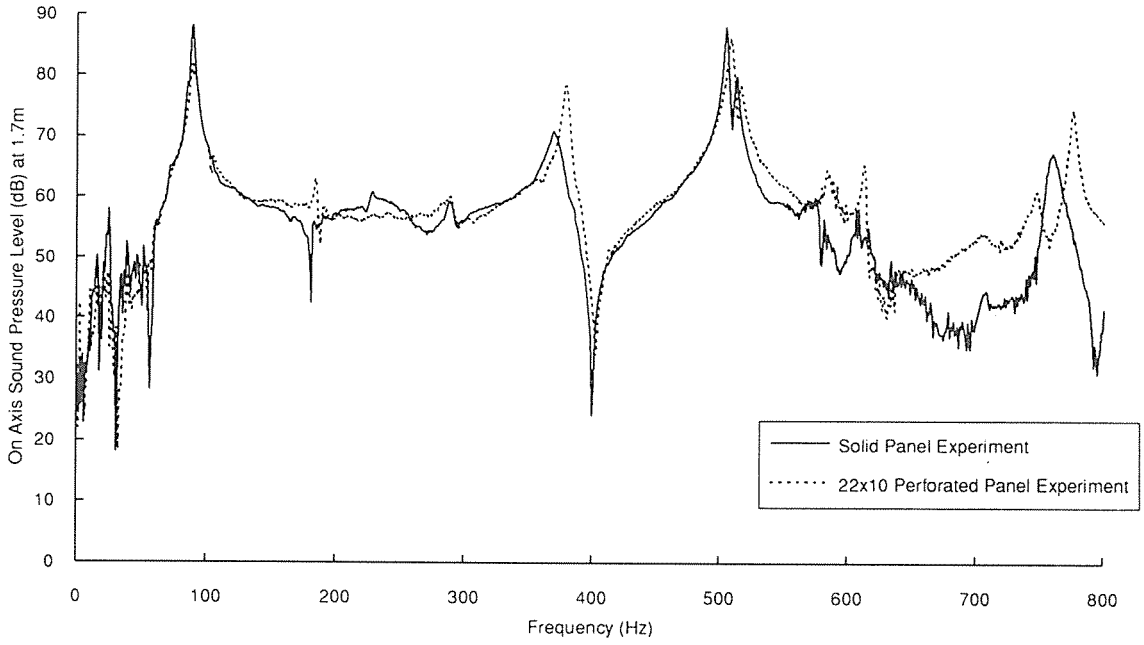

Figure 3 The effect of a panel with an array of 22x10 holes of 6mm diameter on the sound radiation from a solid panel mounted behind it and excited by a point force at its centre.

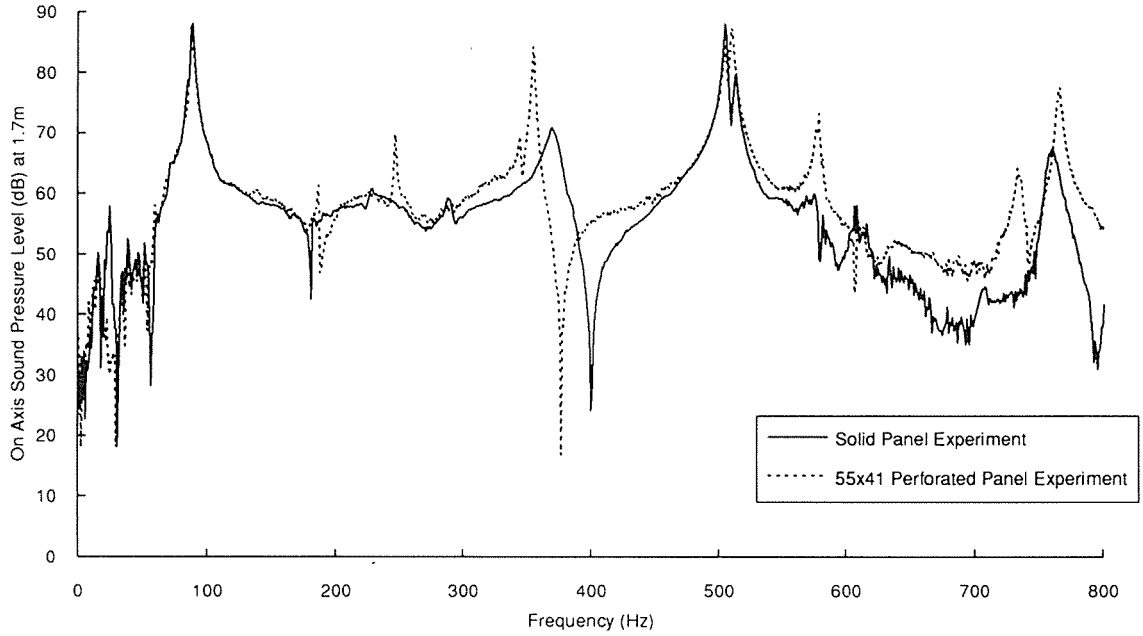

Figure 4 The effect of a panel with an array of 55x41 holes of 3.9mm diameter on the sound radiation from a solid panel mounted behind it and excited by a point force at its centre.

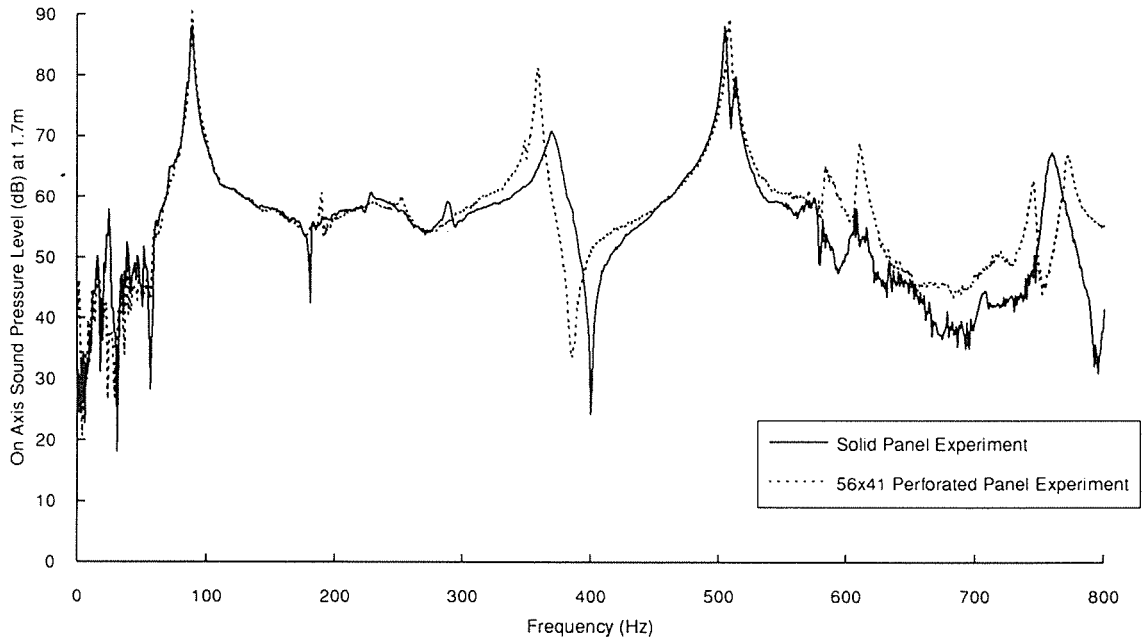

Figure 5 The effect of a panel with an array of 56x41 holes of 3.25mm diameter on the sound radiation from a solid panel mounted behind it and excited by a point force at its centre.

References

Arase, E.M., 1964, "Mutual Radiation Impedance of Square and Rectangular Pistons in a Rigid Infinite Baffle", *JASA*, Vol. 36, No. 8, pp. 1521-1525.

Burgemeister, K.A. and Hansen C.H., 1993, "Use of a Secondary Perforated Panel to Actively Control the Sound Radiated by a Heavy Structure", In proceedings of the American Society of Mechanical Engineers Winter Annual Meeting, New Orleans.

Bouwkamp, C.J., 1949, "On the Transmission Coefficient of a Circular Aperture", Letters to the Editor, *Physical Review*, Vol. 75, p. 1608.

Cook, R.K., 1957, "Absorption of Sound by Patches of Absorbent Materials", *JASA*, Vol. 3, No. 29, pp. 324-329.

Gibbs, B.M. and Balilah, Y., 1989, "The Measurement of Sound Transmission and Directivity of Holes by an Impulse Method", *Journal of Sound and Vibration*, Vol. 133, No. 1, pp. 151-162.

Gomperts, M.C., 1965, "The Influence of Viscosity on Sound Transmission Through Small Circular Apertures in Walls of Finite Thickness", *Acoustica*, Vol. 15, No. 4, pp. 191-198.

Lamb, H., 1931, *Dynamical Theory of Sound*. (Edward Arnold & Co., London, Second Edition.)

Levine, H. and Schwinger, J., 1948, "On the Theory of Diffraction by an Aperture in an Infinite Plane Screen. I", *Physical Review*, Vol. 74, pp. 958-974.

Levine, H. and Schwinger, J., 1949, "On the Transmission Coefficient of a Circular Aperture", Letters to the Editor, *Physical Review*, Vol. 75, p. 1608.

Mulholland, K.A. and Parbrook, H.D., 1967, "Transmission of Sound Through Apertures of Negligible Thickness", *Journal of Sound and Vibration*, Vol. 5, No. 3, pp. 499-508.

Notomi, T. and Namba, M., 1992, "Numerical Calculation of Periodic Viscous Flow Through a Circular Hole", *Journal of Sound and Vibration*, Vol. 157, No. 1, pp. 41-65.

Oldham, D.J. and Zhao, X., 1993, "Measurement of the Sound Transmission Loss of Circular and Slit-Shaped Apertures in Rigid Walls of Finite Thickness by Intensimetry", *Journal of Sound and Vibration*, Vol. 161, No. 1, pp. 119-135.

Pan, J., Hansen, C.H. and Bies, D.A., 1992, "Use of a Perforated Panel for the Active Control of Sound Radiated from Vibrating Structures, I: Low-Frequency Analysis", *Journal of Sound and Vibration*, Vol. 156, No. 2, pp. 349-359.

Pritchard, R.L., 1960, "Mutual Acoustic Impedance between Radiators in an Infinite Rigid Plane", *JASA*, Vol. 32, No. 6, pp. 730-737.

Ritchie, E., 1932, "Transmission of Sound Through Apertures", *JASA*, pp. 402-414.

Sivian, L.J., 1935, "Acoustic Impedance of Small Orifices", *JASA*, Vol. 7, pp. 94-101.

Wilson, G.P. and Soroka, W.W., 1965, "Approximation to the Diffraction of Sound by a Circular Aperture in a Rigid Wall of Finite Thickness", *JASA*, Vol. 37, No. 2, pp. 286-297.

Acknowledgments

The Authors gratefully acknowledge financial support from the Australian Electricity Supply Industry Research Board.

Sound Propagation in Ducts -

Modal Scattering in Rigid-Walled Ducts of Arbitrary Axial Curvature.

Gareth E. Bridges, David A. Bies and Colin H. Hansen
Department of Mechanical Engineering,
University of Adelaide,
South Australia, 5005.

ABSTRACT

Sound propagation in ducts has been a subject of investigation for a very long time. Despite this, a complete theoretical basis from which to design ducting systems with adequate passive noise muffling qualities does not exist. As any practical ducting system may contain curved sections, these form an integral part of any such design. In this paper the results of investigations into the propagation and modal scattering of sound in rigid-walled, curved ducts is presented, with reference to the overall design problem. Experimental data is used to show that the theoretical model of Furnell and Bies (1989) is partially successful in describing the behaviour of sound in curved duct systems. The success the model and its shortcomings are discussed, along with the details of proposed further experimentation.

1. INTRODUCTION

"...any practical waveguide system incorporates couplings of straight sections by means of curved sections..." , Grigor'yan 1969.

The problem of ducting system design, with passive noise muffling qualities has received considerable attention in the literature over the previous decades. The reason for this attention is that ducts can tend to act as perfect waveguides for sound, transmitting sound energy between different locations in buildings with little attenuation. As an example, an industrial exhaust fan which is designed to improve a working environment by removing airborne irritants might simultaneously, by transmitting fan noise, degrade that environment.

The overall design problem has been treated in a piecemeal fashion in the literature. Numerous models have been developed to describe sound propagation in straight ducts lined with sound absorbing material, and in rigid-walled curved ducts. The characteristics of these models have been presented, in some cases, with design curves and occasionally with experimental verification. The models have varied considerably in their generality, and hence range of application.

The aim of the work presently being undertaken is to provide a comprehensive set of design tools for the design of a passive muffling ducting system comprised of straight sections, lined with sound absorbing materials such as rockwool or fibreglass, coupled with sections of arbitrary curvature. Whilst it is recognised that such a set does not encompass the complete range of situations which might be encountered in practice, it

should be sufficient for many commercial and industrial problems. The design tools may be in the form of a comprehensive set of design curves, although user-friendly software packages are a preferable option. The user will then be able to determine the sound propagation properties of a duct specified precisely to their needs. The work toward the development of such software packages is in quite an advanced state in the case of the straight, lined duct problem, but not so in the case of the curved duct problem, which is not as amenable to a user-friendly package due to a number of informed judgments which are required at various stages of the computation process.

In attempting to provide a comprehensive set of design tools, theoretical models of wide range of applicability have been developed, and investigated in an experimental program which has necessarily been more specific.

In the case of the straight, lined duct, theory has been developed which treats either a duct of rectangular cross-section lined on two adjacent walls or a duct of circular cross-section (Bies et. al., 1991). Anisotropy in the performance of the liner due to fibre orientation is included in the model. Mean flow in the airway is treated in an approximate fashion with the assumption that the flow is uniform across the airway, and that there is no flow in the liner. The model exceeds previous models in its precise treatment of the airway-liner interface, which consists of a rigid, perforated wall and a limp, impervious membrane. The membrane is in place to protect the liner material from duct air flow. Experimental verification of the model involved an extensive sound field mapping programme using an experimental duct with variable liner thickness, liner material and airway-liner interface. The theoretical model requires some small adjustment and will be extended to treat rectangular ducts lined on all four walls. A detailed discussion of this model is, however, outside of the scope of this paper.

The basis of the work on rigid walled curved ducts is the theoretical work of Furnell and Bies (1989), which outlined a method for calculating the transmission and reflection coefficients of scattered modes for an arbitrarily curved section of duct of elliptical cross-section. The theory is the most comprehensive in the field, being the only attempt to deal with arbitrary axial curvature. Although the treatment is confined to ducts of elliptical cross-section, of which the circular cross-section is a special case, the treatment may be easily adapted to ducts of rectangular cross-section, or indeed any cross-section which may be described simply in an appropriate co-ordinate system.

An experimental verification programme using ducts of circular cross-section and parabolic axial curvature has been conducted to test the theory of Furnell and Bies. The experiments involved driving a plane wave into each of three curved configurations, measuring the transmission coefficients of modes generated in the curved section, and comparing these with the theoretically predicted values. The experiment was repeated for four different free field wave-number values, chosen so that at each successive value there was an additional propagating or "cut-on" mode in the duct. The results of this investigation show that the theory of Furnell and Bies is qualitatively successful in predicting the transmission coefficients of modes generated in a real curved duct. It is conjectured that the observed discrepancies may be due to the sound field inside the duct coupling with wall modes. To verify this conjecture additional experimentation is currently being conducted.

2. Theory of Sound Wave Scattering in Curves of Arbitrary Axial Curvature.

2.1 A Brief History.

The earliest reference to sound propagation in ducts with axial curvature was made by Lord Rayleigh in 1894, who showed that curvature in piping had an insignificant effect in the limiting case where the axial curvature was much greater than the pipe radius. Very little investigation into this problem was conducted thereafter until comparatively recently. Grigor'yan (1969) was the first in a series of increasingly sophisticated investigations into uniformly curved ducts of rectangular cross-section. The Helmholtz equation was solved in the curved section by use of the separation of variables technique, with a Taylor series expansion of the cross-duct solution. Rostafinski (1972, 1974 and 1976) followed a similar line but used a Bessel function expansion, essentially using a basis set more natural to the system. Non-integer Bessel functions were introduced to deal with the higher order modes. Cummings (1974) provided the first experimental investigation to produce "plausible" design curves - and also initiated work on the toroidal problem (Uniformly curved ducts of circular cross-section), although the investigation in that area was purely experimental. Tam (1976) applied a computational version of the Galerkin method, while Cabelli (1980) applied a finite difference mesh. El-Raheb (1980) and El-Raheb and Wagner (1982) initiated the theoretical analysis of the toroidal problem using finite difference meshes, Green's function techniques and eigenfunction expansions of the Helmholtz equation. Prikhod'ko and Tyutekin (1982) and Ting and Miksis (1983) developed accurate perturbation techniques, although these were restricted to ducts of gentle curvature. Firth and Fahy (1984) treated the torus problem with a mathematically complicated unseparated series solution.

Until 1989, when Furnell and Bies presented their techniques for ducts of elliptical cross-section and arbitrary axial curvature, attempts at solving the curved duct problem had been plagued by a number of recurring problems. All of the methods were ultimately numerical and some of the less elegant methods had very slow convergence rates and difficulties with higher order modes. Most significantly though, all of them lacked generality, dealing with either uniform curvature, or variable but very gentle curvature in the case of the perturbation techniques.

2.2 The Theory of Furnell and Bies.

Furnell and Bies (1989) treat ducts with arbitrary axial curvature by dividing a curved duct into small sections which are each approximately uniform in curvature. Each sub-section has its own transmission scattering matrix (T) and reflection scattering matrix (R), with the state vectors comprised of modal coefficients for a straight duct with the same cross-section. The scattering matrices of the sub-sections are then combined to give transmission and reflection matrices for the complete section. There are two of each corresponding to sound waves incident from each of the two ends of the arbitrarily curved section. If the curved section is entirely in a single plane and there are no discontinuities in the curvature the process of combining the sub-section matrices is relatively simple. Where this is not the case, however, an additional technique must be employed. Where the sign, or the plane of curvature changes from one sub-section to

the next, an additional scattering matrix must be inserted between the two sections, termed the "acoustic potential re-orientation matrix". Thus, completely arbitrary curvature can be treated.

The modes in each duct sub-section are calculated using the Rayleigh-Ritz method on the Helmholtz equation. A large set of basis modes (including evanescent modes) is required to accurately determine the scattering matrices, especially in regions of high curvature. These basis modes are expressed in terms of a set of basis functions. The choice of basis function set greatly determines the rate of convergence of the computation process. As has been discovered by previous authors in this area, finding a basis function set natural to the duct cross-section is necessary to achieve convergence. The scattering matrices (T and R) of each sub-section are calculated by establishing artificial straight duct-sections of infinitesimally small length on both ends of the curved sub-sections and then matching the field and its derivatives at the interface.

3. EXPERIMENT

3.1 Experimental Apparatus.

The curved sections of the test ducts were constructed through various arrangements of two sections of parabolically curved duct of circular cross section. The two sections, precision milled from a hard wood (Eucalyptus Pine), constituted the two halves of a single, symmetrical, parabolically curved section split at the apex. The two sections were rotated 0^{o}, 90^{o}, and 180^{o} with respect to each other about the centre-line axis in the plane of contact, and bolted together to form the "parabolic", "out of plane" and "S shaped" configurations respectively (Figure 1). Each configuration is predicted to have quite distinct sound scattering qualities. The parabolic configuration exhibits virtually a null result in terms of transmission scattering between modes. The S shaped configuration, in contrast, has very large cross mode scattering coefficients, but only between modes of the same parity. The parity of a mode is determined by the symmetry of a mode upon reflecting its sound pressure field with respect to a diametric axis in the plane of curvature (See figure 2). A mode may be symmetric or anti-symmetric on reflection, and is thus termed to have even or odd parity. The out of plane configuration has strong cross mode scattering between modes of like and opposite parity.

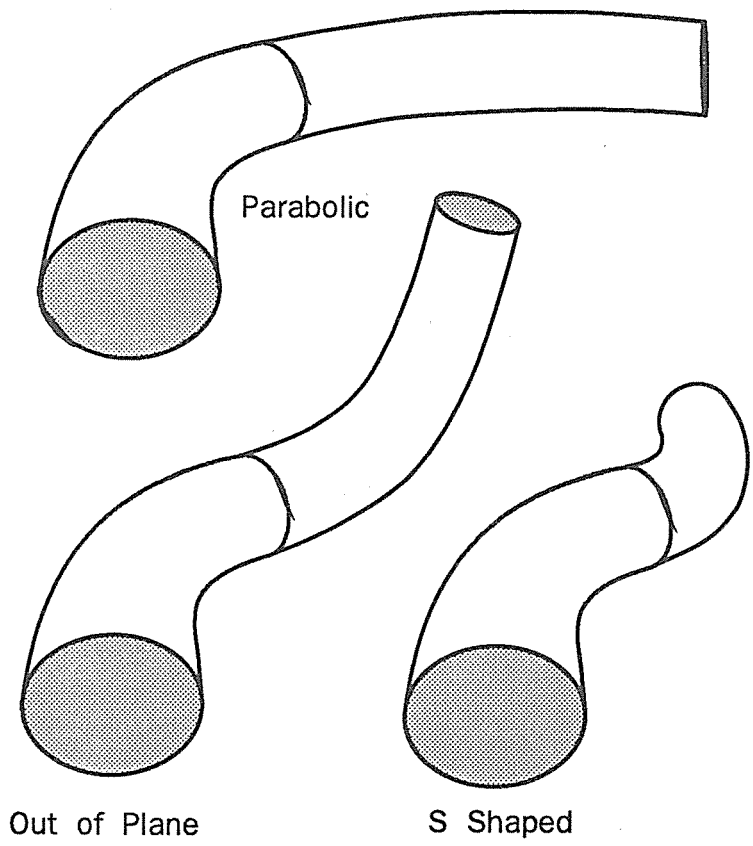

Figure 1. Duct Configurations.

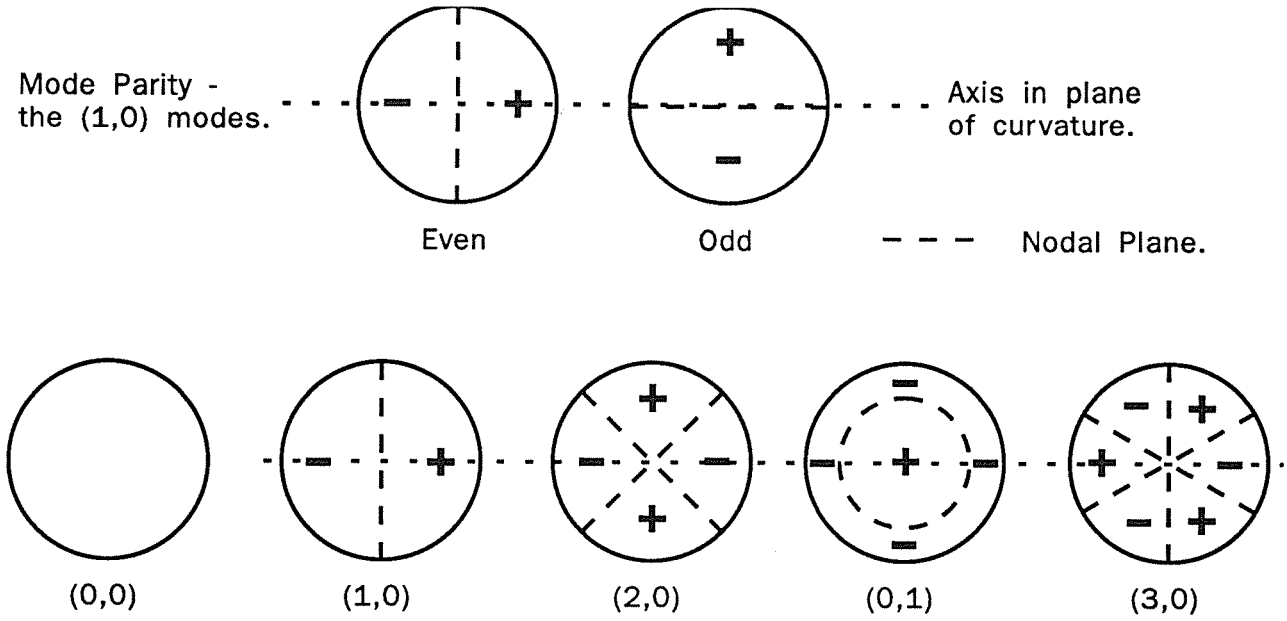

Figure 2. Modes in Straight Rigid Walled Ducts of Circular cross-section.

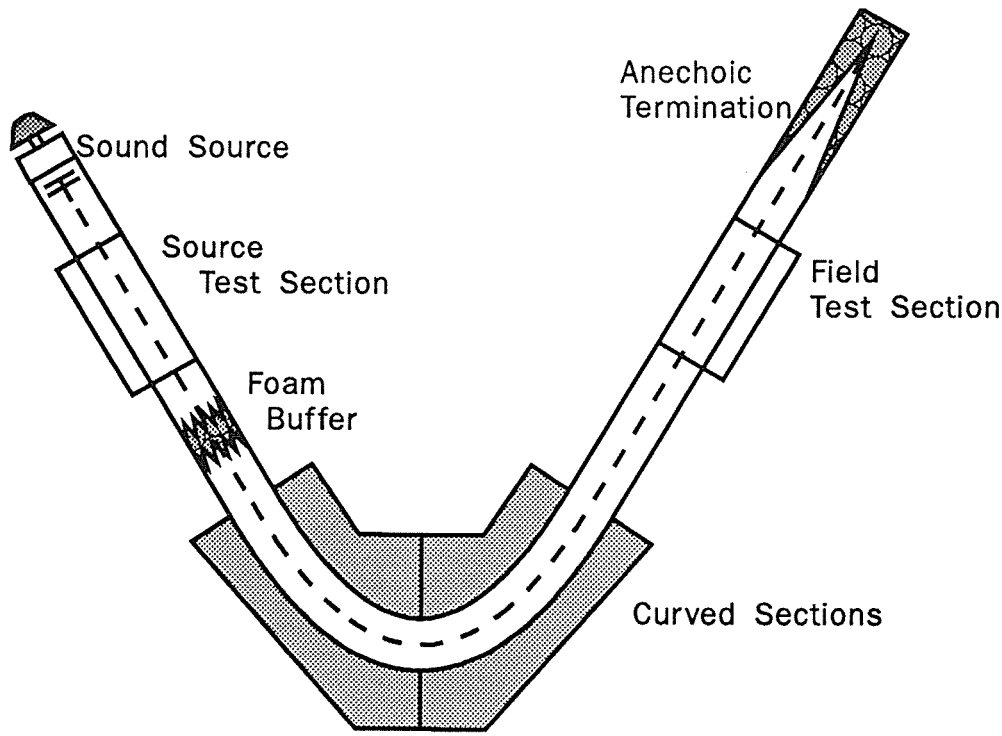

Figure 3. Experimental Apparatus - Parabolic Configuration.

Figure 3 shows how the parabolic sections described are incorporated into the test apparatus. The plane wave source produces a propagating wave which is monitored in the source test section to check that it is indeed a plane wave, as intended. The source microphone can be moved to any location in a cross-sectional plane. The plane wave then propagates into the curved section where it is scattered into higher order modes. The transmitted sound field is measured in the field test section by a small 1/4" diameter electret microphone with three dimensional positioning capability, before being absorbed by the anechoic termination.The buffer before the curved section, displayed in Figure 3,

ensures that any reflected higher order modes incident upon the plane wave source will be less than -40 dB relative to the source signal. A higher order mode of larger amplitude incident upon the source would load it non-uniformly and degrade its performance.

3.2 Experimental Program.

Sound field mapping experiments were carried for each of the three duct configurations, at four different free space wavenumber values as indicated in the following table. The wavenumbers are referred to in dimensionless form as $\kappa = 2\pi a/\lambda$, where "a" is the duct radius and λ the free-space wavelength of the incident field. With each increasing κ value in the table, an additional mode is "cut-on" in the duct.

Experimental κ	Cut on Modes
2.087	(0,0), (1,0)
3.459	(0,0), (1,0), (2,0)
4.015	(0,0), (1,0), (2,0), (0,1)
4.430	(0,0), (1,0), (2,0), (0,1), (3,0)

The straight section modes are labelled by two indices (m,n). The first index, m, specifies the order of Bessel function which describes the radial dependence of the of the sound pressure field and also the number of nodal planes cutting across the duct diametrically. The second index, n, specifies the number of nodal annuli around the duct centre-line (See figure 2). The mode indices both range from $0 \rightarrow +\infty$, although only a small number of these are "cut on" or propagating at the κ values used in the experiment. The (0,0) mode is the plane wave. It should be noted that there is a two fold degeneracy in the modes with $m \neq 0$. That is, for each set of (m,n) indices with $m \neq 0$, there are two orthogonal modes which are identical except for a spatial rotation with respect to each other of $\pi/(2m)$ radians, about the duct centre-line axis. The two modes have even and odd parity respectively. For each configuration/wavenumber combination, the field microphone was used to map the sound pressure field in two cross-sectional planes of the duct, at different axial positions, at approximately 80 positions in each plane.

3.3 Experimental Data Analysis.

The experimental data points in each cross-sectional plane were input into a modal decomposition program which determined the modal amplitudes of the cut-on modes in that plane. Figures 4a and 4b show a typical result of the modal decomposition procedure. The figures show curves synthesised from the modal amplitudes output by the decomposition program, whilst the symbols are actual data points. Figures 4a and 4b show the quality of fit that was achieved by the process. The set of duct modes is mathematically complete in that it is able to describe any sound field within the duct by a suitable linear superposition of the modes. The small subset of modes used in the modal decomposition process (the cut-on modes) is, however, not complete. The fact that the sound pressure field was consistently described so precisely by the few cut-on modes

supports the assumption that a propagating sound field in the duct is composed only of the cut-on modes. Measurements were conducted at two different axial positions so that amplitudes of reflections from the anechoic termination could be identified and accounted for.

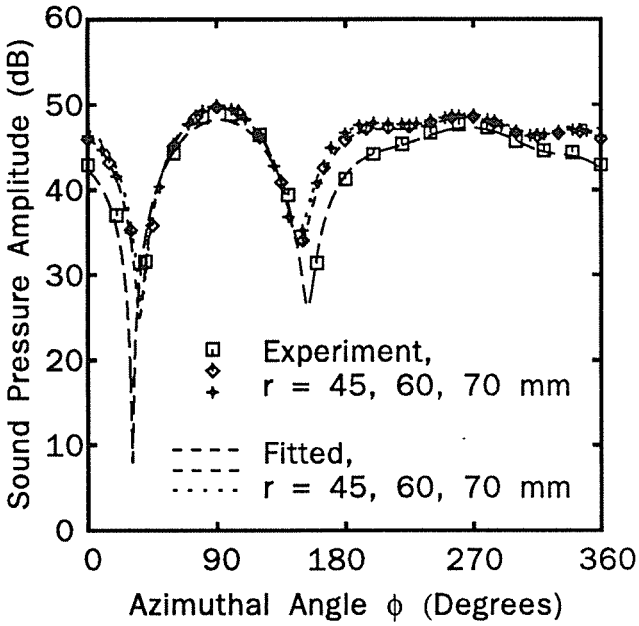

Figure 4a.

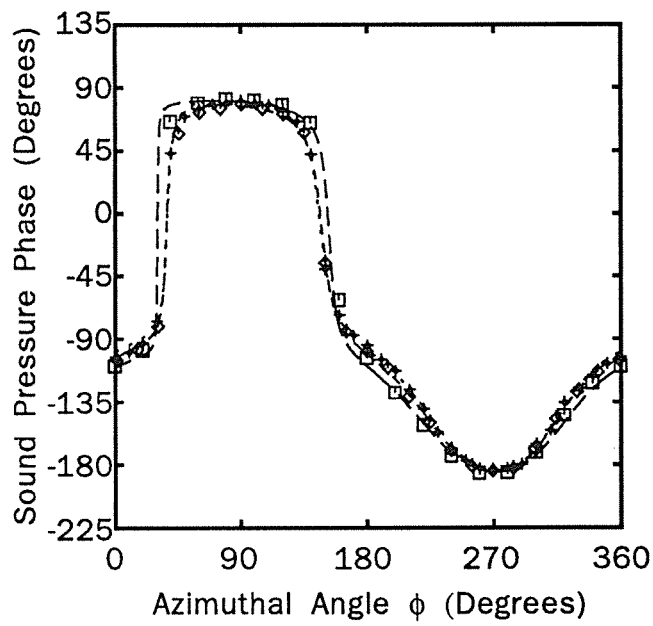

Figure 4b.

Meaured Sound Pressure Field vs. Least Mean Squared Fitted Field for ka = 4.015, using the "cut-on" modes as a basis for the fitted curves.

The final forward scattered modal amplitudes determined by the data analysis process are compared with those predicted by the theory of Furnell and Bies.

4. RESULTS AND DISCUSSION

The results of the investigation are presented in Figures 5-8. As is evident, there is quite reasonable qualitative agreement between the measured scattering coefficients and the theoretically predicted values. The clearly distinguishable behaviour of the three configurations which is theoretically predicted, is clearly present in the experimental data. The largest scattering amplitudes occur for the S shaped configuration, with the out of plane and parabolic configurations following. The out of plane configuration scatters into the even and odd modes with approximately equal amplitude as predicted, and the odd modes are not generated in the two planar configurations, again as predicted.

Quantitatively, however, the agreement is quite poor. For the modes with azimuthal dependence ((m,0) with $m \neq 0$), the scattering transition (0,0) $\rightarrow$ (m,0) is consistently under-estimated by the theory by approximately 6 dB, although there is some scatter in this value. The discrepancies are well outside the scatter error bars of the experiment, which are too small to be shown on the figures.

The scattering transition (0,0) $\rightarrow$ (0,1) fares better, although it is over-estimated by the theory with respect to the experiment in most cases.

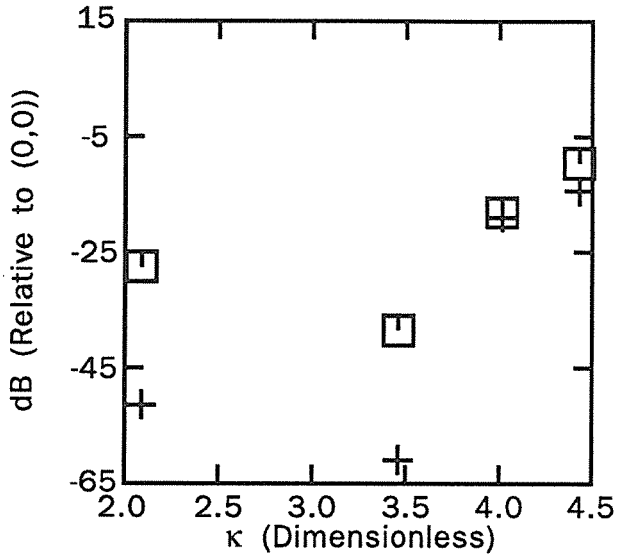

Figure 5a. Parabolic Configuration.

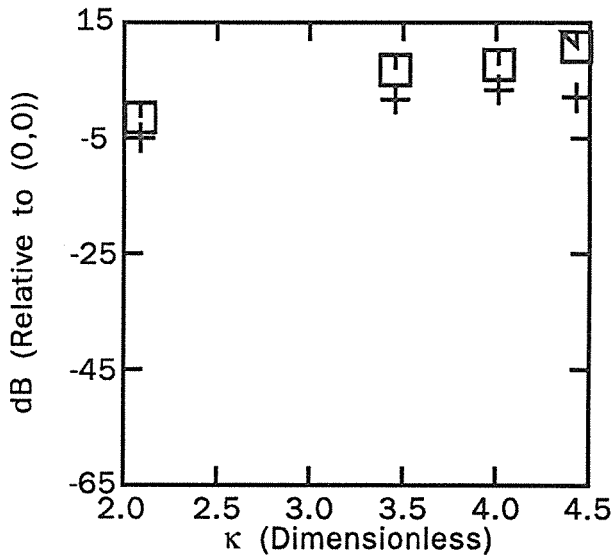

Figure 5b. S Shaped Configuration.

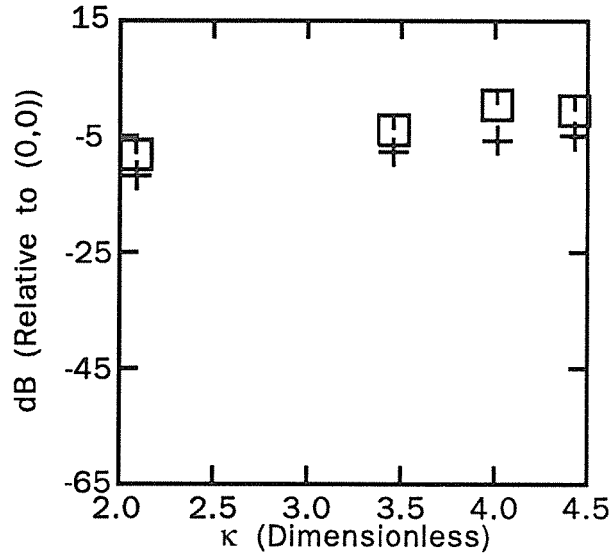

Figure 5c. Out of Plane Configuration. -> (1,0) Even

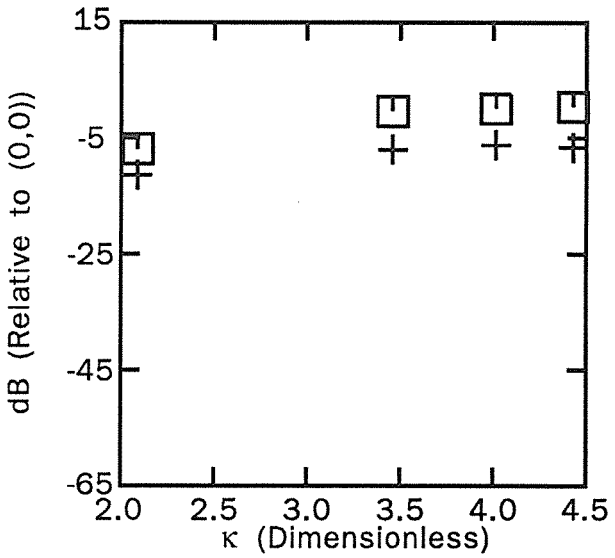

Figure 5d. Out of Plane Configuration. -> (1,0) Odd

Figure 5. (0,0) -> (1,0) Scattering.
+ - Theory ⊡ - Experiment

Assuming that the theory is correct, there is clearly some systematic process occurring which is causing the observed discrepancies. Systematic error would arise from imperfections in the inner surface of the curved duct section, which might result from machining errors. It is unlikely, however, that the machining errors could be large enough to account for all of the discrepancies. Error in the construction of the duct components could also contribute, although again it is unlikely that these are culpable. A more significant contribution might come from variations in the radius of the straight duct sections, although these are only of the order of 0.2% of the mean radius.

It is conjectured that the most likely cause for the observed discrepancies is the strong coupling between duct wall modes and the propagating duct cavity modes. The theory assumes a perfectly rigid wall. In designing this experiment, PVC sewer pipe with a nominal inside diameter of 6" and a wall thickness of 3 mm was chosen for the straight duct sections because it is cheap and readily available, and was judged to be sufficiently

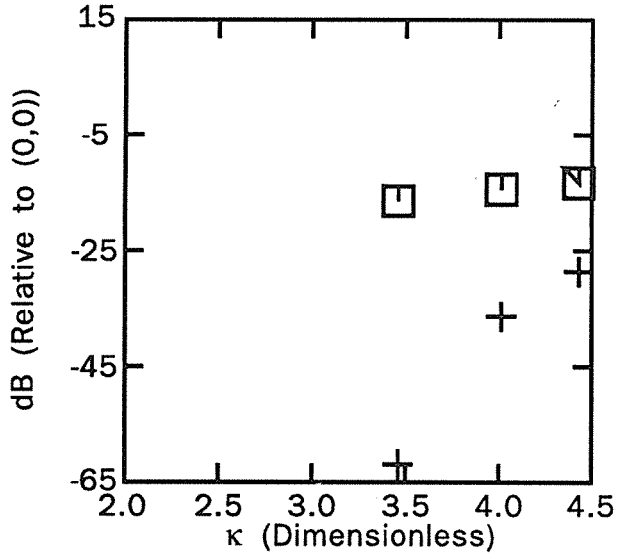

Figure 6a. Parabolic Configuration.

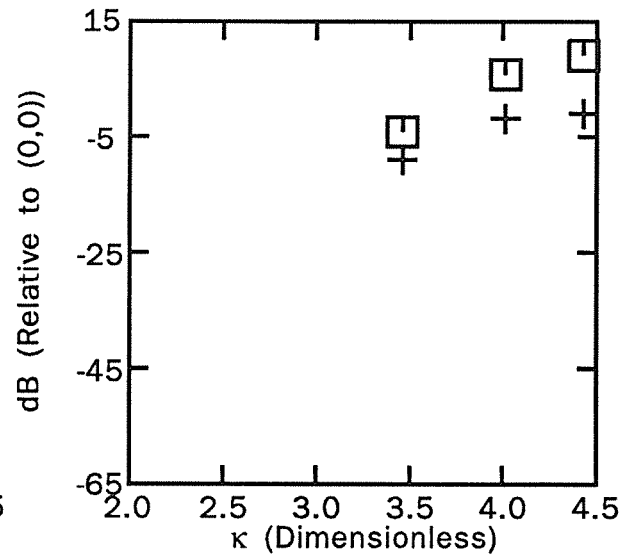

Figure 6b. S Shaped Configuration.

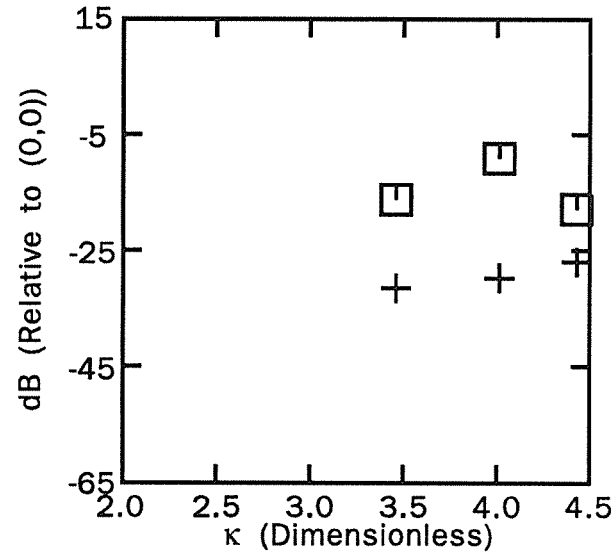

Figure 6c. Out of Plane Configuration.
-> (2,0) Even

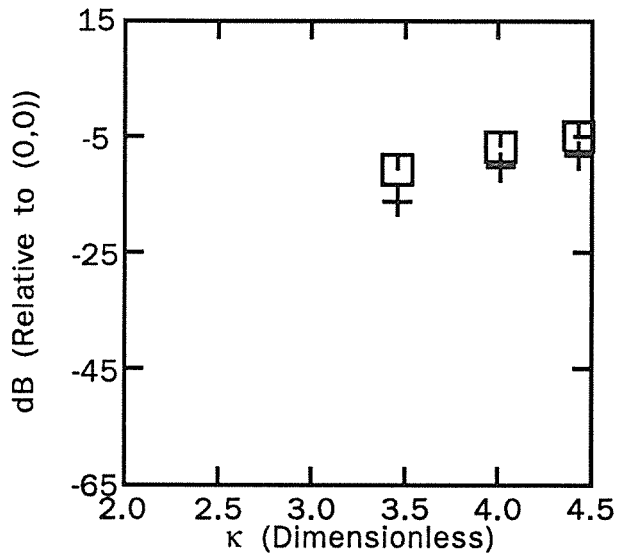

Figure 6d. Out of Plane Configuration.
-> (2,0) Odd

Figure 6. (0,0) -> (2,0) Scattering.
+ - Theory ⊡ - Experiment

rigid to satisfy the boundary conditions of the theory. This may not be the case. Several observations support the conjecture. In setting up the experimental apparatus, the plane wave source did not, initially, perform to anywhere near its theoretical expectations with the (1,0):(0,0) relative excitation as high as 0.1 (10%). Wrapping the straight duct sections with damping tape improved the performance of the source dramatically, although the best performances achieved were still characterised by relative excitation amplitudes, (1,0):(0.0), of the order of 2%, much worse than the expected performance. This tended to indicate a degree of coupling between wall and cavity modes. Also, it is consistent that the (0,1) mode is not as strongly affected as the modes with azimuthal dependence. The (0,1) mode with its purely radial particle motion would need to expand and contract the wall to couple with it. Clearly, the wall would be very stiff with regard to such an excitation. The azimuthal modes, in contrast, do not need to change the cavity volume for small excitations.

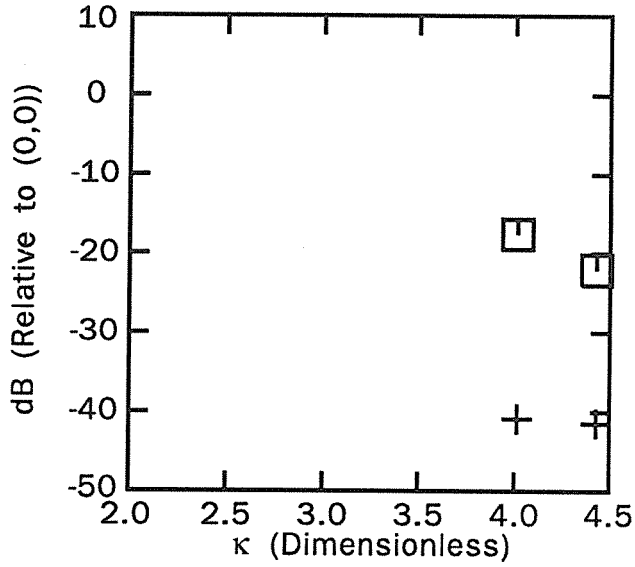

Figure 7a. Parabolic Configuration.

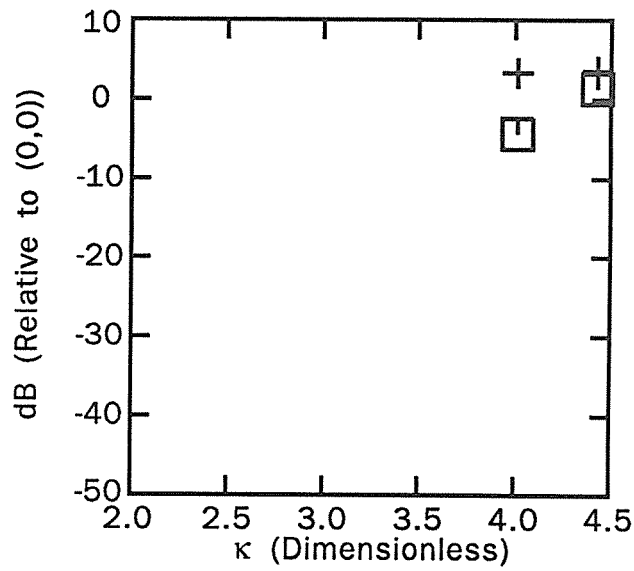

Figure 7b. S Shaped Configuration.

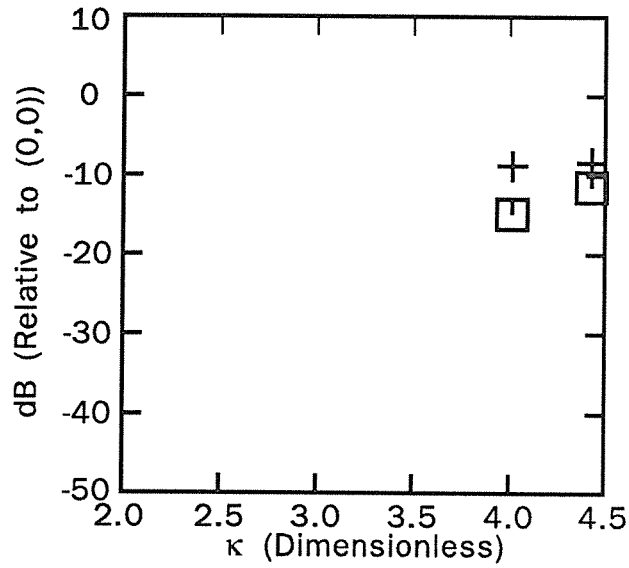

Figure 7c. Out of Plane Configuration.

Figure 7. (0,0) -> (0,1) Scattering.
+ - Theory ⊡ - Experiment

To attempt to confirm the conjecture regarding the discrepant scattering amplitudes, the experimental programme is currently being repeated with straight sections constructed from mild steel with 10mm wall thickness. Such walls would uphold the boundary conditions considerably more accurately. Elucidation regarding this problem should be at hand shortly.

5. CONCLUSIONS

The theory of Furnell and Bies shows reasonable qualitative agreement with the experimental data. In light of the precision with which the experiments were conducted, however, the agreement is poor. The discrepancy between experiment and theory can only be the result of either the theory being incorrect, or some systematic discrepancy

between the assumptions of the theory and the conditions in the experimental apparatus. It has been conjectured that the 3mm PVC walls used in parts of the experimental duct do not satisfy the theoretical criterion of a rigid boundary sufficiently for good quantitative agreement to occur. This conjecture is currently being tested in a duct that uses 10 mm mild steel walls.

In terms of practical ducting systems, the theory in its current form can not be used for quantitative predictions in light weight ducts with flexible walls, although it might be used to provide qualitative estimates.

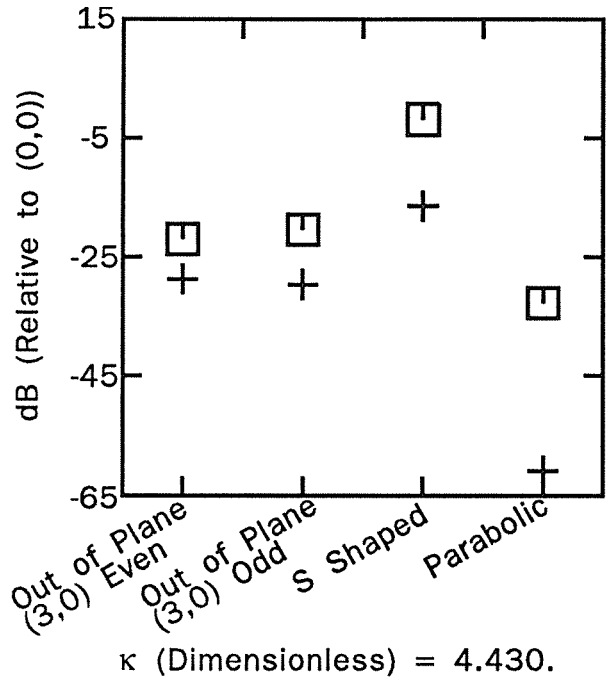

κ (Dimensionless) = 4.430.

Figure 8. (0,0) -> (3,0) Scattering. + - Theory ⊡ - Experiment

It is clear that a duct with a dramatic discontinuity in curvature, such as the S-shaped configuration will strongly redistribute the energy of an impinging plane wave into cross-modes. These cross modes will have significantly higher attenuation rates in a lined section, which may follow the curve.

References.

1. Bies, D. A., Hansen, C. H. and Bridges, G. E. 1991 *Journal of Sound and Vibration* **146**, 47-80. Sound Attenuation in Rectangular and Circular Cross-Section Ducts with Flow and Bulk-Reacting Liner.

2. Cabelli, A. 1980 *Journal of Sound and Vibration* **68** (3), 369-388. The Acoustic Characteristics of Duct Bends.

3. Cummings, A. 1974 *Journal of Sound and Vibration* **35**, 451-477. Sound Transmission in Curved Duct Bends.

4. El-Raheb, M. 1980 *Journal of the Acoustical Society of America* **67** (6), 1924-1930. Acoustic Propagation in Rigid Three-Dimensional Waveguides.

5. El-Raheb, M. and Wagner, P. 1982 *Journal of the Acoustical Society of America* **71**, 1335-1346. Acoustic Propagation in a Rigid Torus.

6. Firth, D. and Fahy, F. J. 1984 *Journal of Sound and Vibration* **97** (2), 287-303. Acoustic Characteristics of Circular Bends in Pipes.

7. Furnell, G. D. and Bies D. A. 1989 *Journal of Sound and Vibration* **130** (2), 405-423. Characteristics of Modal Wave Propagation within Longitudinally Curved Acoustic Waveguides.

8. Furnell, G. D. and Bies, D. A. 1989 *Journal of Sound and Vibration* **130** (3), 245-263. Matrix Analysis of Acoustic Wave Propagation within Curved Ducting systems.

9. Grigor'yan, F. E. 1969 *Soviet Physical Acoustics* **14** (3), 315-321. Theory of Sound Wave Propagation in Curvilinear Waveguides.

10. Prikhod'ko, V. Y. and Tyutekin, V. V. 1982 *Soviet Physical Acoustics* **28** (5), 22. Natural Modes of Curved Waveguides.

11. Rayleigh, J. W. S. 1894 *The Theory of Sound*. London: McMillan

12. Rostafinski, W. 1972 *Journal of the Acoustical Society of America* **52** (5) Pt 2, 1411-1420. On Propagation of Long Waves in Curved Ducts.

13. Rostafinski, W. 1974 *Journal of the Acoustical Society of America* **56** (1), 11-15. Analysis of Propagation of Waves of Acoustic Frequencies in Curved Ducts.

14. Rostafinski, W. 1976 *Journal of the Acoustical Society of America* **60** (1), 23-28. Acoustic Systems Containing Curved Duct Sections.

15. Tam, C. K. W. 1976 *Journal of Sound and Vibration* **45** (1), 91-104. A Study of Sound Transmission in Curved Duct Bends by the Galerkin Method.

16. Ting, L. and Miksis, M. J. 1983 *Journal of the Acoustical Society of America* **74** (2), 631-639. Wave Propagation Through a Slender Curved Tube.

Acknowledgements.

The authors gratefully acknowledge financial support for this work from the Australian Research Council.

MONITORING OF THE SUPPORT CONDITIONS OF BURIED AND SUB-SEA PIPELINES USING A VIBRATING PIG

Dr Uwe G Kopke, VIPAC Engineers & Scientists Ltd.

A method for detecting poor support of buried and sub-sea pipelines has been developed. It utilises vibration excitation and pipe/support response to detect variation the support condition. Variation in pipe-support condition leads to an increased likelihood of pipe damage. Under roadways poorly supported pipes may be damaged by vehicle loading. At sea, spanned and insufficiently covered sections of pipe are vulnerable to ocean-current excitation, and also to snagging by stray anchors in shallow waters.

A vibrating pipe inspection device (pig) has been developed and tested on buried pipelines. Certain features of pipe support, such as hard spots and voids, display characteristic responses to vibration, and these are measured by the vibrating pig which also provides the vibration excitation. The measured vibration data is post-processed to produce a graphical representation of the pipeline support, and certain 'feature characteristics' are identified. In field tests on buried pipelines with deliberately constructed faults, features detected by the vibrating pig are in good agreement with the known construction.

INTRODUCTION

It is advantageous to be able to identify vulnerable sections of a long pipeline before faults occur. Non-uniformity of pipeline support may accelerate degradation if the pipeline is subject to transverse loading. Exposed subsea pipelines are vulnerable to damage by ocean currents and to stray anchors in shallow waters, while voided buried pipes beneath roadways may be damaged by repeated vehicle loading.

An overview of available pipeline pigging technology is given by Cordell [1]. Variation of pipeline-support stiffness is very difficult to detect by existing techniques. For instance, methods such as flux-leakage and ultrasonic techniques which are commonly used for measuring changes in pipe-wall thickness [2] do not 'see' outside the pipe. In an attempt to overcome this problem, devices have been developed that employ radiation backscatter to measure the density of the pipe wall and surrounding material [3]. Variations in back-scattered radiation are interpreted as features of the pipe or the soil, but it is not clear that changes in backscatter always correspond to changes in support stiffness. There are also major practical problems associated with the safe handling of radioactive materials.

There exist curvature-monitoring pigs[1], equipped with a complete six degree-of-freedom inertial navigation system (such as used for aircraft navigation), and these can detect the deflective shape of a voided or spanning pipe. Such an approach will not be able to detect loss of support until sufficient damage has been done to the foundation to produce measurable pipe curvature.

In this paper, a method is described which takes direct account of the variation of pipe stiffness on its foundation by measuring its response to an internally-imposed vibration.

The response of a uniformly-supported pipeline to an applied transverse vibration can be calculated analytically using a model based on the theory of beams on a Winkler foundation [4]. Such a model can only account for bending modes of pipeline vibration, and there is limited scope for producing a realistic foundation model. The use of more-elaborate models based on continuum mechanics is discussed in greater detail by Kopke [5,6].

A vibration pig, designed and built by the author, is used to monitor pipeline responses over a wide range of excitation frequencies and at closely-spaced intervals along the pipe. The pig is equipped with vibration generators, vibration sensors and signal pre-amplifiers. Post-processing of the measured vibration data is used to produce a graphical representation of the pipeline support and certain 'feature characteristics' are identified. This gives an immediate visual indication of the variation of pipe support with distance along the pipe.

PIG DESIGN

Fig.1 shows a vibration pig, constructed at the Cambridge University Engineering Laboratory, that is designed for use in 4- and 6-in pipelines. Testing of this pig was performed in buried cast-iron pipes, for which the frequency range of interest was found to be from 0 to 300Hz. This range encompasses flexural modes of vibration without encountering ovalling modes of the circular pipe section.

The pig generates vertical transverse vibration by means of an electromagnetic shaker moving a brass weight. This weight is supported by a spring located inside the shaker, and the resonant frequency of the mass on its spring limits the lowest frequency of the excitation. In the present design, this is chosen to be 30Hz, which limits the frequency range of excitation to 50Hz and above.

Vibration response of the pipe is measured by four accelerometers located inside the pig. The geometrical arrangement of these accelerometers makes it possible to calculate the vertical and horizontal pig vibration. Torsional vibration can be calculated in two ways, which provides a redundancy to check on the accuracy of the instrumentation. Signal pre-amplifiers, located inside the pig, boost the measured signals to be transferred by shielded cable to an above-ground digital data-acquisition system.

An important design criterion is that vibration measurements made on-board the pig truly reflect the dynamic behaviours of the pipe-soil system. Therefore, the pig structure should not have any resonances near the frequency range of 50-300Hz. This is achieved by making the pig body stiff and light. The pig rests on the bottom of the pipe on three hardened-steel feet, which provide a well-defined and rigid contact between pig and pipe. Extension 'legs' can be placed between the feet and the pig body to configure the pig for larger-diameter pipes, but the elasticity of these legs reduce the lowest resonant frequency of the pig structure. There is a limit to the size of pipe that can be tested in this way with a pig originally designed for use in 4-in pipelines.

The pig is towed through the pipe and the positions of the tow rings and the centre of gravity (CG) relative to the feet ensure that the pig remains upright during towing (for a theoretical treatment of the stability of a pig in a pipe, see Ref.7). In addition, a pendulum sensor monitors the orientation angle of the pig, and vibration measurements are only taken when this angle is within 5° relative to the upright position.

The design of this 4-in pig is described in more detail by Köpke[5]. The method of pipeline-support condition monitoring using vibration is the subject of a patent application[8]. The 4-in pig is a prototype which has been used to validate the method, and it is limited in its applicability to a real-life environment. The 4-in prototype is not 'free-swimming' (i.e. it is not propelled by the product flow in the pipeline), and it is not able to negotiate tight bends. Such features must be built-in to a working design for commercial operation. These are problems that have been solved for several types of intelligent pig, such as flux-leakage pigs, and adapting these solutions to vibration monitoring is the subject of present work.

It is important also to design for a sufficiently stiff contact between the sensors of the pig and the pipe in order to obtain measurements of pipe response that are unaffected by pig dynamics. This may require the vibration sensors to be located outside the pig body to make good contact with the pipe, since the cups that are usually used to support pigs in pipelines have relatively-low stiffness. For larger pipelines, it can be expected that ovalling modes are unavoidably within the frequency range of interest, and by locating several sensors around the circumference of the pipe, it is possible to distinguish between ovalling and transverse modes by standard methods of angular filtering[9]. A pig configured in such a way may be capable of detecting longitudinal defects in the pipe wall, as these will affect the response of the pipe in its ovalling modes.

FIELD TESTING

In the period from June, 1990, to March, 1991, several field tests with the pig were carried out using 4-in buried cast-iron pipelines at a British Gas test facility near Newcastle-upon-Tyne. The support conditions of the pipes tested are believed to be well known. Purpose-built features had been built in to the pipe support, and these include polyurethane voids and concrete blocks; the following Table gives an overview of the pipes tested.

Pipe	*Length tested*	*Date tested*
A	13.0m	November 90
B	16.0m	November 90
C	37.5m	March 91

Test procedure

All testing was performed using the 4-in pig. It has been shown theoretically [5,6] that features of pipe support can be detected by exciting the pipe to vibrate and measuring the response of the pipe. The vibrating pig was inserted into several nominal 4-in cast-iron gas pipes which were buried about 0.7m below the ground surface. The pig generated mechanical vibration within the pipe, and the vertical excitation force was measured. Vertical, horizontal and torsional acceleration responses of the pipe were measured at the point of excitation by accelerometers within the pig, and also at a distance of 1m from the excitation point, by means of an instrumented trailing pig measuring vertical acceleration.

All the measured data was transferred by cable to an above-ground digital data-logging system for further analysis and archiving. The position of the pig in the pipe was measured by means of a surveyor's tape towed through the pipe.

Fig.2 shows the fast sine sweep (chirp), as used by White [10] for dynamic analyses, that was generated by the pig between 50Hz and 450Hz for the force excitation. The responses of pig and trailer were twice sampled at 0.5-m intervals along the pipe, to check for repeatability. The pig and trailer were stationary in the pipe during sampling. In a section of pipe where features such as voids and hard spots were expected, the sampling interval was reduced to 0.25m.

Data analysis

The sampled data was analysed in a IBM PS2-486 computer. The analysis consisted of several steps:

1) calculating frequency response functions (FRFs) and reducing data by smoothing FRFs;
2) optionally, displaying FRFs for all pig locations as contour plots;
3) calculating FRFs of orbital pig motion from vertical and horizontal motion;
4) calculating deviation of FRFs from 'normal' (mean) FRFs, to find changes in support conditions, and reducing data by taking cumulative means over frequency;
5 generating graphs of 'feature characteristics'.

These steps are described in detail in the following sections, using data collected from pipe A as an example.

Calculating FRF

The FRF is the ratio of response to excitation force in the frequency domain. the responses of interest are the vertical, horizontal and torsional responses of the pig, and the vertical responses of the trailer. The excitation force is measured indirectly by an accelerometer situated on top of the brass weight (see Fig.1). Employing the well-known expressions:

action = reaction
and
force = mass x acceleration

yields the excitation force F_{vert} by multiplying the mass of the brass weight by its acceleration. More details of the force generation are given by Köpke[5].

Pipe responses were measures by four accelerometers within the pig. The accelerometers were arranged in a circle and vertical, horizontal and torsional pig accelerations can be calculated from the measured signals by employing simple kinematic relations. In addition, the vertical acceleration was measured at a distance away from the excitation with a single accelerometer inside the trailer.

Fast Fourier transformation (FFT) was used to convert the excitation force signal and pig and trailer accelerations into the frequency domain, where the corresponding FRFs are calculated as FFT_{accel}/FFT_{Fvert}.

Since the procedure of exciting the pipe and measuring responses was carried out twice at each position of the pig in the pipe, the average of the two resulting sets of FRFs is taken for further analysis and display. It has been found that the tests were highly repeatable, and therefore both sets of FRFs are very similar.

Finally, to reduce archiving space and to speed-up further data processing, the averaged FRFs are smoothed and the number of frequency data points at each pig position was reduced.

FRF contour plots

The reduced acceleration FRFs of pig and trailer for different positions of the pig in the pipe are displayed as contour plots in Fig.3. The horizontal axes indicate the position of the pig in the pipe between 1.5 and 13m, the vertical axes correspond to frequency between 50 Hz and 450Hz and the contour levels show FRF magnitudes as different grey shades in 15dB intervals.

By comparing the FRFs with the sketch of the pipe-support conditions shown in Fig.3, it can be observed that hard and soft supports are giving clear signatures. As can be intuitively expected (see Refs 5 and 6 for a rigorous theoretical treatment), vertical FRFs for voids have generally higher magnitudes and a lower resonance frequencies than good soil. For hard supports (concrete foundation and boulder) the opposite is observable.

It is interesting to notice that considerable horizontal and torsional motion occurs, even though only vertical excitation has been applied. This is due to asymmetries in the pipe-soil system which gives rise to mode coupling. In a strictly-symmetrical environment, no horizontal or torsional vibration should be detected, but asymmetry is unavoidable, and very small changes in foundation asymmetry affect the coupled responses dramatically. This mechanism provides an additional powerful tool to detect subtle features of pipe-support conditions, like the crossing pipe at 2.3m. By only considering the vertical pig FRF at 2.3m, no significant signature of a feature is found. However, the horizontal pig FRF more clearly shows a signature, identifying the crossing pipe as a hard spot.

Since vertical and horizontal pig FRFs are both measures of translational motion, they can be combined by calculating the trace of this motion. Fig.4 shows a typical trace; this is an ellipse lying in a plane which is orthogonal to the longitudinal pipe axis.

Calling the major axis of the ellipse (a) and the minor axis (b) ($a \geq b \geq 0$), three important ellipse parameters can be defined:

$$\textit{ellipse radius } r = \sqrt{a^2 + b^2}, \textit{ numerical eccentricity } \epsilon = \frac{\sqrt{a^2 - b^2}}{a}$$
$$\textit{and angle of major axis to the horizontal } \theta.$$

Here, a numerical eccentricity of $\epsilon = 0$ classifies the ellipse to be a circle. When ϵ tends towards 1, the ellipse degenerates to a line with length of the major axis (a). For the ellipse depicted in Fig.4, these parameters are $r = 0.029 ms^2$, $\epsilon = 0.99$, and $\theta = 91°$.

The radius (r) of the FRF ellipse is related to the energy of the translational pig motion if velocity FRF's instead of acceleration FRF's are used to calculate (a) and (b). Recalling basic relations in the frequency domain, it follows that FRF's are calculated by dividing acceleration FRF's by $i\omega$, were $\omega$is the angular frequency $\omega = 2\pi f$.

Fig. 5 shows contour plots for the ellipse parameters r, ϵ and θ calculated at each frequency and position of the pig in the pipe. The horizontal axes indicate the location of the pig in the pipe, and the vertical axes correspond to frequency from 50Hz to 450Hz. By comparing the contour plots with the sketch of the pipe, it is readily seen that the most valuable information about features lies in the FRF ellipse radius r. At some locations, contours corresponding to a certain energy level are shifted towards higher frequencies. This indicates, when compared with the findings of the beam-on-elastic-foundation model (or even a simple vibrating system such as a mass on a spring), a harder support of the pipe which is consistent with a concrete foundation. Similarly, at soft spots, contours corresponding to a certain energy level are shifted towards lower frequencies.

Since the square of the ellipse r calculated from velocity FRFs is proportional to the energy of translational pig motion, and the squares of vertical and horizontal velocity FRFs are proportional to energy of vertical with respect to horizontal pig motions, it can be shown that:

$$r = \sqrt{+|FRF_{vert}|^2 + |FRF_{horiz}|^2}.$$

Hence, the ellipse radius r can be directly calculated from measured FRFs.

FRF deviations

So far, it has been found that features can be identified by examining changes in FRF contour plots. These changes are superimposed on the FRF of the 'normal' pipe, indicating soft spots as 'higher than normal' responses and, consequently, hard spots as 'lower than normal' responses. This demonstrates that the information of interest actually lies in the deviation of FRF from a 'normal' level. This 'normal' level is the mean FRF taken over the pig position. The mean value is calculated using FRF values in dB. This corresponds to the geometric rather than the arithmetic mean of the FRFs in linear units, such as ms^2/N. Consequently, the deviations are calculated using values in dB. Therefore, these deviations correspond to ratios rather than differences of FRFs in linear units.

Fig.6 shows the filtered deviations of ellipse radius, torsional pig response, and vertical trailer response as contours. The horizontal axes indicate the location of the pig in the pipe, the vertical axes correspond to frequency from Hz to 450Hz. Contour heights are spaced in 4-dB intervals of the FRF. A sketch of the pipe is shown at the bottom of the figure.

Since the ellipse radius calculated from velocity FRFs is related to pig energy, in subsequent plots the torsional FRFs of the pig and the vertical FRFs of the trailer are shown as velocity FRFs for compatibility.

A positive deviation indicates a higher-than average-response caused, for example, by a softer support of the pipe. Similarly, a negative deviation indicates a lower-than-average response caused, for example, by a harder support of the pipe.

Features of interest appear as local changes over a few metres only, so global changes in FRF that occur gradually over several metres will spoil the deviations. To overcome this problem, the FRF deviations at each frequency are high-pass filtered along the pipe length in order to remove these global changes. Another problem is caused by bogus changes in FRF that occur at a single location because of bad contact, for instance, between the pig and the pipe. To overcome this problem, the FRF deviations at each frequency are low-pass filtered along the pipe length in order to remove these very-local changes. This does not downgrade the pig's ability to detect very-local features, because at real local features the pipe shows changes in FRF over a length greater than the actual feature size, and the filter cut-off-size has been selected to be smaller than the length of these FRF changes. This is demonstrated for the FRF ellipse in Fig.6 by the signature of the crossing 4-in pipe around 2.5m which has not been filtered out. Fig.7 shows the response of the fourth-order Butterworth band-pass filter, called the 'feature-filter', that performs the high-pass and low-pass filtering.

Cumulative means

A closer inspection of Fig.6 shows that, at a given pig position, the filtered FRF deviations do not change dramatically within certain bands of frequency. Therefore, it is possible to condense the frequency information meaningfully by taking cumulative means of the filtered FRF deviations over frequency up to a limited number of frequencies for each pig position.

Fig.8 shows these cumulative means for ellipse radius, torsional FRF of the pig, and vertical FRF of the trailer. The four different lines in each graph show the cumulative mean for frequencies up to 150Hz (solid), 250Hz (dashed), 350Hz (dotted), and up to 450Hz (dash-dotted). It is interesting to notice that these four lines are generally not too different from each other: this indicates that the choice of the frequencies up to which the cumulative mean is taken is not too critical. Comparing the contour plots in Fig.6 with the cumulative mean plots in Fig.8 demonstrates good agreement between these two methods of data presentation.

Feature characteristics

To make the interpretation of measurements from the pipes easier, it is useful to introduce a new item called *feature characteristics.*

In Fig.8 it can be observed that features of pipe support can be identified mainly by considering cumulative means of filtered deviations of the pig FRF ellipse radius and of torsional pig response. The cumulative means of filtered deviations of vertical-trailer FRF are less conclusive.

Therefore, feature characteristics are solely generated from the pig responses. In Fig.8 it can be seen that the features of pipe support normally cause the cumulative means of filtered deviations of the pig responses to increase above or decrease below certain levels; both FRF ellipse radius and torsional-pig responses show these very similar characteristics.

Therefore, as a first approach for 4-in cast iron gas pipes, the feature characteristics at each pig position are defined to be the mean of the cumulative means of the filtered deviations of FRF ellipse radii for which:

$$|\tilde{r}| > 5dB \text{ and } |\widetilde{tor}| > 3dB \text{ and } sign(\tilde{r}) = sign(\widetilde{tor})$$

where $\tilde{r}$ denotes the cumulative means of filtered deviations of FRF ellipse radius and $\widetilde{tor}$ denotes the cumulative means of filtered deviations of torsional pig FRF. Feature characteristics for pig positions where this relation does not hold are set to zero.

Taking the mean of the cumulative means over-emphasises the low-frequency components in the responses, which is a desired effect. It is shown in the author's thesis [5] that, due to the dynamics of the pig, responses in the lower half of the frequency range of interest are more reliable than those in the upper half.

The threshold values, 5dB and 3dB, have been found by comparing measurements with the known features in the pipe support considering all the tests of 4-in cast iron gas pipes by the author [5]. However, it can be expected that the threshold values are to be modified slightly, based on experience gained with further tests.

Test results

Several 4-in pipes were tested in the period between June 1990, and March 1991 and the results are given below.

Pipe A

A section of this pipe was investigated and Fig.8 shows the cumulative means of filtered deviations of FRF ellipse radius, filtered deviations of torsional-pig FRF, the filtered deviations of vertical-trailer FRF, and the feature characteristics generated from the pig responses. A sketch of the tested pipe with the support conditions is also shown. Features found by measurements are depicted as regions of lighter or darker shades of grey. The locations and types of these features were mainly identified by looking at the plot called feature characteristics. Some features were deliberately built, and are shown labelled as found on construction drawings. Joints are shown at locations specified in these drawings.

The main locations of features of this pipe, with reference to pig position in Fig.8, are:

- 3-4: concrete block (cast *in situ*), which is identified as a hard support;
- 6.2-7.2m: polyurethane void, which is identified as a soft support;
- 8.8m: boulder, which is identified as a hard support. Before and after the boulder, the support is relatively soft. This can be explained by voids that have developed during settling of the pipe because the boulder could not sink as much as the rest of the pipe next to it.

The two other features, the crossing of the 4-in cast iron pipe and the brick wall, do not produce pronounced signatures. The crossing pipe causes only a slight reduction in response, and is therefore not classified as a feature. Behind the brick wall, pig responses are generally lower, indicating harder support; however, the brick wall does not produce a local effect.

It can be observed that the joints in the section of pipe A being investigated do not produce any significant signature in the feature characteristics' plot. This can be explained by the fact that the pipe movement is restricted by the surrounding soil, causing the change of response due to joints to be too small to be identified as features. Theoretical simulations of joints [5] confirm this explanation.

The apparent indetectability of the joints supports the view that joints are not considered to be features of the pipe support that will cause pipe damage. If desired, the locations of joints can be detected by other inspection devices.

Pipe B

This pipe was once used for ground-freezing tests, and the soil surface was covered with a canopy for insulation. It has only one purpose-built feature, a backfilled gravel trench extending from 7.5 to 9m. However, Fig.9 shows more than one feature, and the backfilled trench produces a signature of only one third of the trench width. To clarify this, pipe B was also examined with a testing device that uses a radioactive source to measure density of the pipe-support medium.

The locations of features with reference to Fig.9 are:

- 5m: void, which is identified as a soft support in the feature characteristics' plot, and as an area of low density by the radioactive device;
- 5.5m: hard support; the radioactive device measured high-density, which is interpreted as a joint;
- 8.5-9.5m: void in gravel trench (soft support), which was identified by the radioactive device as an area of lower density. The major part of the trench is assumed to be well compacted, providing good support; this was confirmed by the radioactive device;
- 10-11m: soft support, which was identified as an area of low density by the radioactive device;
- 12.5m: rear wall of the canopy crossing the pipe, identified as a hard support in the feature characteristics, and confirmed by construction drawings.

The joints near 5.5 and 11m cannot be identified as such from the feature-characteristics' plot, which is in agreement with the findings for pipe A. The features identified near these joints might have been generated in the process of making the joints.

Pipe C

This pipe was a fairly-new pipe, and might not have been settled at the time when the tests were made. The graphs in Fig.10 show less-pronounced features than those for pipes A and B. Only one feature, a concrete block near 30m, was built-in to the pipe support. However, the pipe shows more than one feature, although most of the features have fairly-small signatures.

- 11m: soft support that coincides with the location of a joint;
- 30M: concrete block, which is identified as hard support. The radioactive device identified this feature as a low-density water-filled void.

Again, joints cannot identified as such by the feature-characteristics' plot; the feature at 11m coincides with the location of a joint, an effect that is in agreement with findings for pipe B.

CONCLUSIONS

This paper describes a vibrating pig which has been used to monitor the support condition of buried pipelines. It has been shown that the method is viable, and that it can be extended for use in other pipelines, such as those subsea, for the identification of features of the pipe support. A patent application [8] for this technique has been filed.

All data-acquisition and analysis is computerised, and the data analysis follows well-defined steps. Each step condenses information and leads to easier recognition of features in the pipe support. For example, orbital pig motion has been examined and used for condensing information by combining vertical and horizontal pig motion to one parameter, the ellipse radius r.

The final result of the data analysis is the feature-characteristics; plot, which permits an untrained user to spot feature signatures easily. This was demonstrated by identifying features on several pipes. The location of features found using the pig are in agreement with the known position of purpose-built features in these pipes. It was also found that pipe joints do not have very-pronounced signatures compared to other features.

ACKNOWLEDGEMENT

The author is most grateful to his research collegue and former supervisor Dr. Hugh Hunt of Cambridge University Engineering Department for his support.

The author also wishes to acknowledge the assistance of the British Gas Engineering Research Station at Killingworth for providing access to its test facilities in Newcastle.

REFERENCES

1. J.L. Cordell, 1990. Types of intelligent pigs. *Proc.* Pipeline Pigging and Inspection Conference, Houston, 19-22 February, organized by *Pipes & Pipelines International* and *Pipe Line Industry*.

2. J.C. Braithwaite and L.L. Morgan, 1988. Extending the boundaries of intelligent pigging'. *Proc.* Pipeline Pigging and Integrity Monitoring Conference, Aberdeen, 10-12 February, organized by *Pipes & Pipelines International*.

3. R.W.E. Shannon, J.C. Braithwaite, and L.L. Morgan, 1988. Flux-leakage vehicles pass tests for pipeline inspection. *Oil & Gas J.,* 8 August.

4. M. Hetényi, 1946. Beams on elastic foundation, University of Michigan Press.

5. U.G. Köpke, 1992. Condition monitoring of buried gas pipes using a vibrating pig. PhD dissertation, University of Cambridge, May.

6. U.G. Köpke, 1993. Transverse vibration of buried pipelines due to internal excitation at a point, Proc. IMechE Part E, 207 (E1), pp.41-59.

7. H.E.M. Hunt, 1992. The motion of a rigid body resting inside a horizontal cylinder. Presented at the workshop 'Kinematics and Robotics', sponsored by the Zentrum fűr Praktische Mathematik, TH Darmstadt, Ebernburg, 12-17 July.

8. U.G. Köpke and H.E.M. Hunt. 'Pipeline pig and method of pipeline inspection', British Patent Specification 9025394.9, 22 November, 1990.

9. C.H. Hodges, J. Power and J. Woodhouse, 1985. the use of the sonogram in structural acoustics and application to the vibration of cylindrical shells. *J. Sound Vib*, vol.101, pp203-218.

10. R.G. White, 1971. Evaluation of the dynamic characteristics of structures by transient testing. *J. Sound Vib.*, 15, (2), pp147-161.

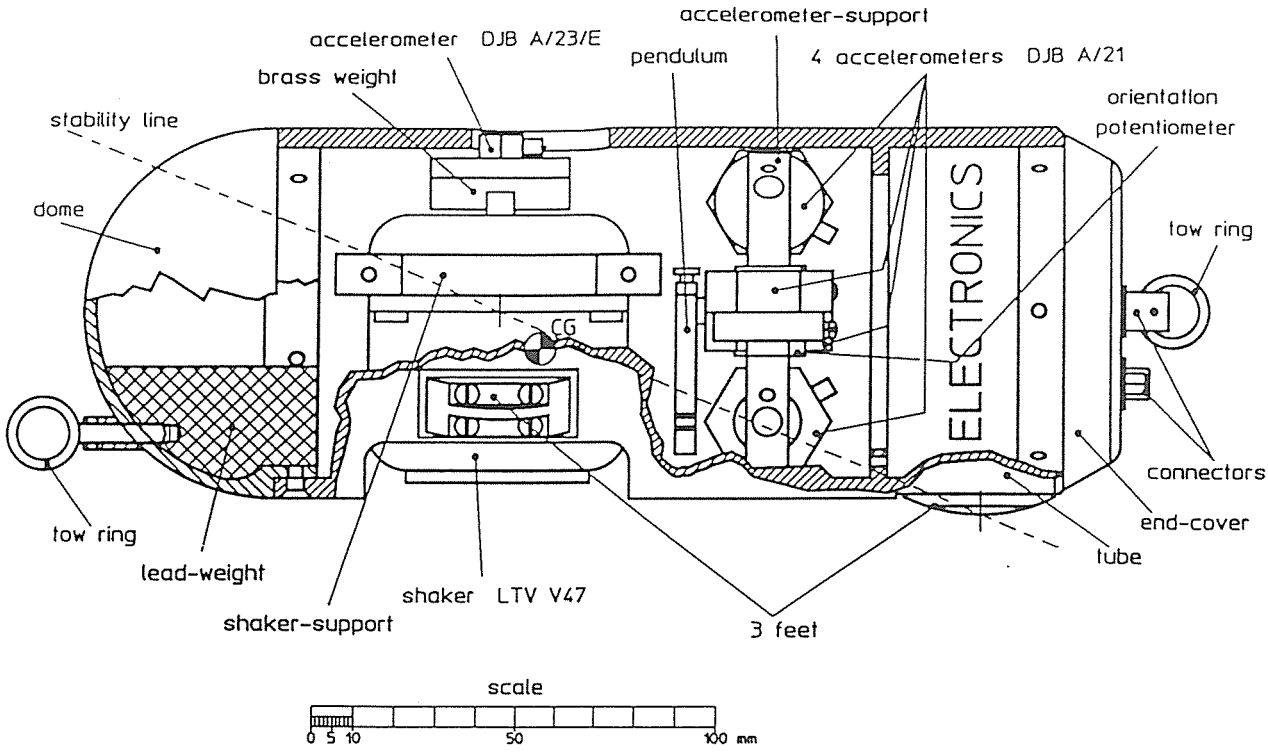

Fig 1. Longitudinal section of the pig showing the location of the shaker and accelerometers.

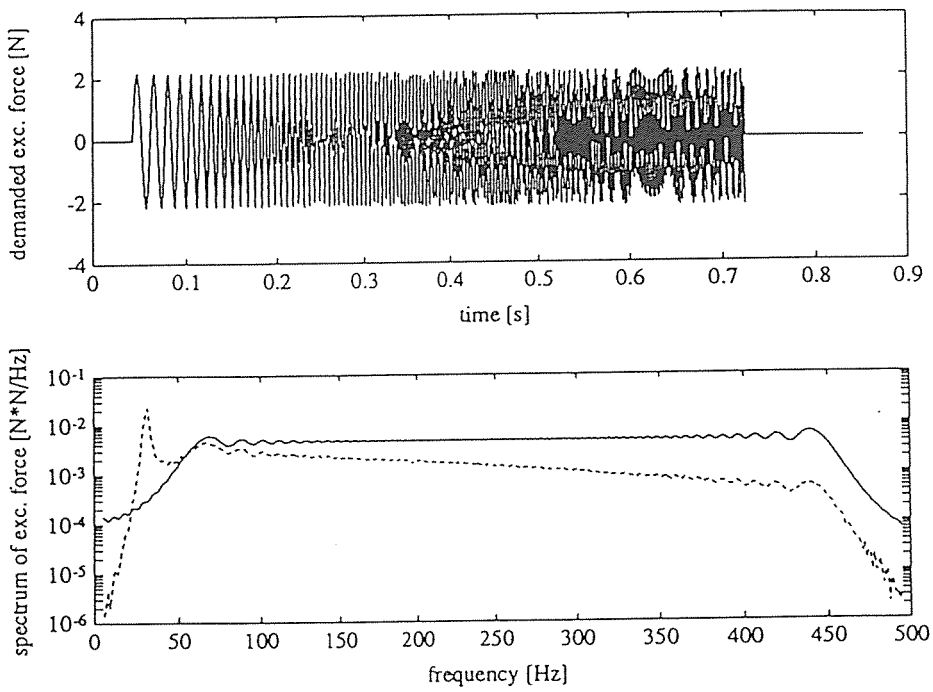

Fig.2. Time-domain plot and spectrum of excitation-force chirp.
The spectral peak at 30Hz and the slope of the spectrum are caused by the dynamics of the brass weight on the shaker spring. The spectrum is reasonably flat between 50Hz and 450Hz.

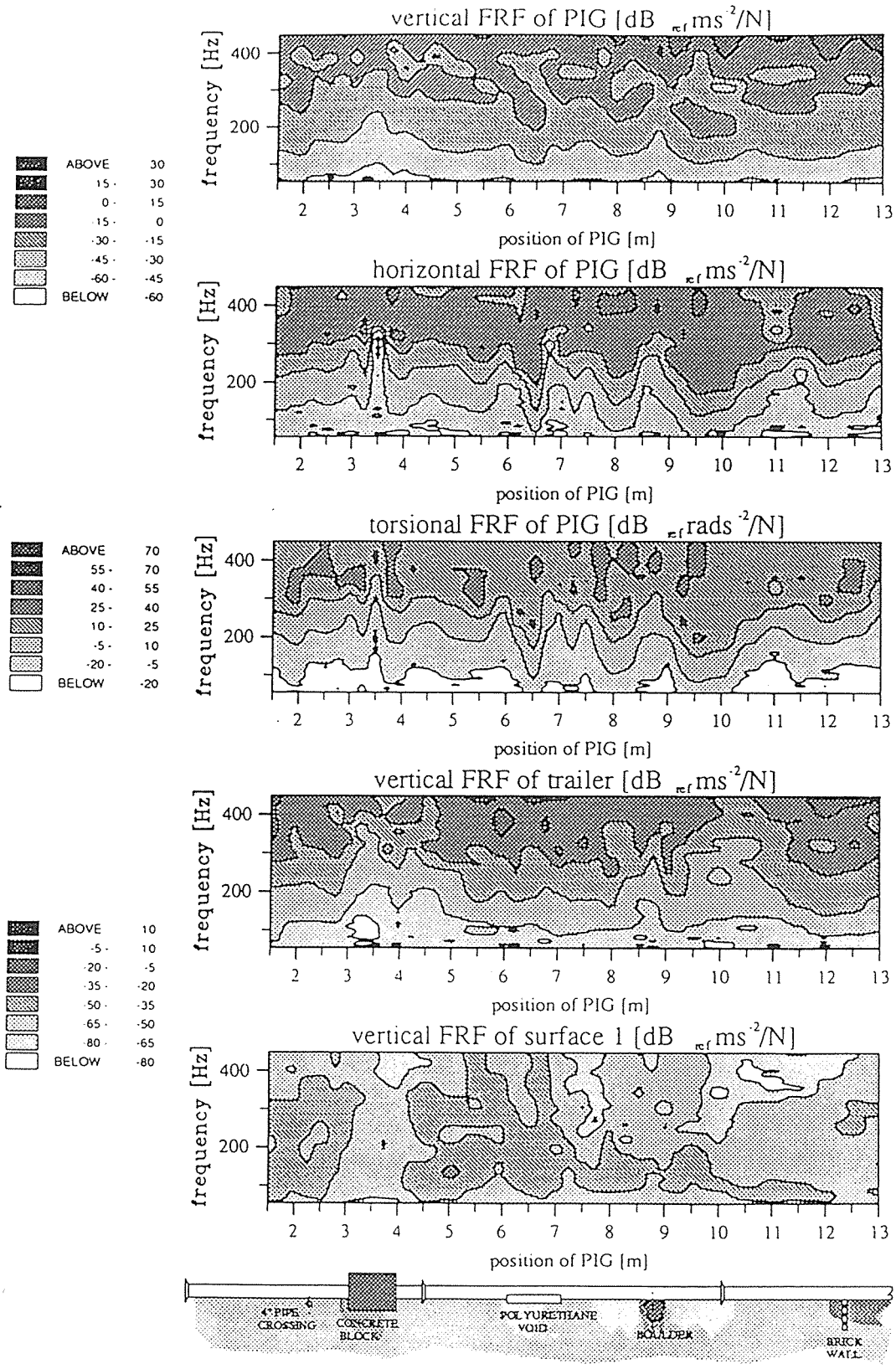

Fig.3. Contour plots of acceleration FRFs of pig and trailer measured at different locations in pipe A. Darker shaded regions in the contour maps indicate increased response. The sketch of the pipe indicates the locations of features obtained from construction drawings.

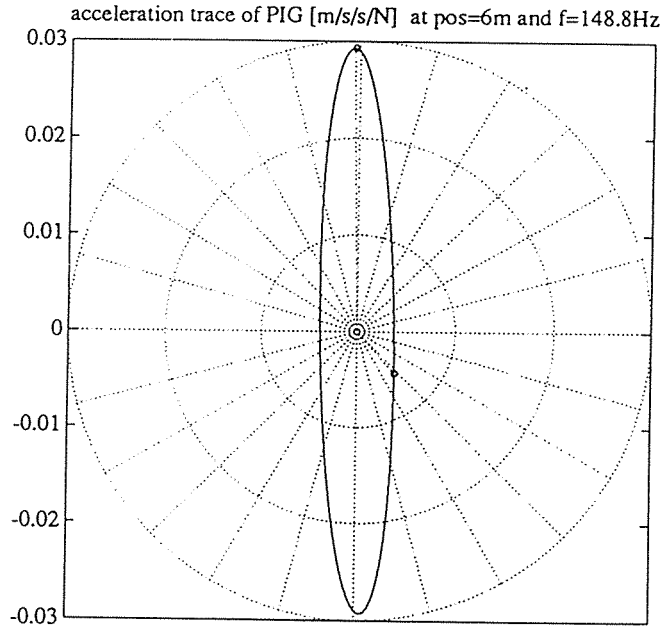

Fig.4. A typical trace of the orbital pig motion in the plane of the pipe cross section, derived from measured vertical and horizontal acceleration data.

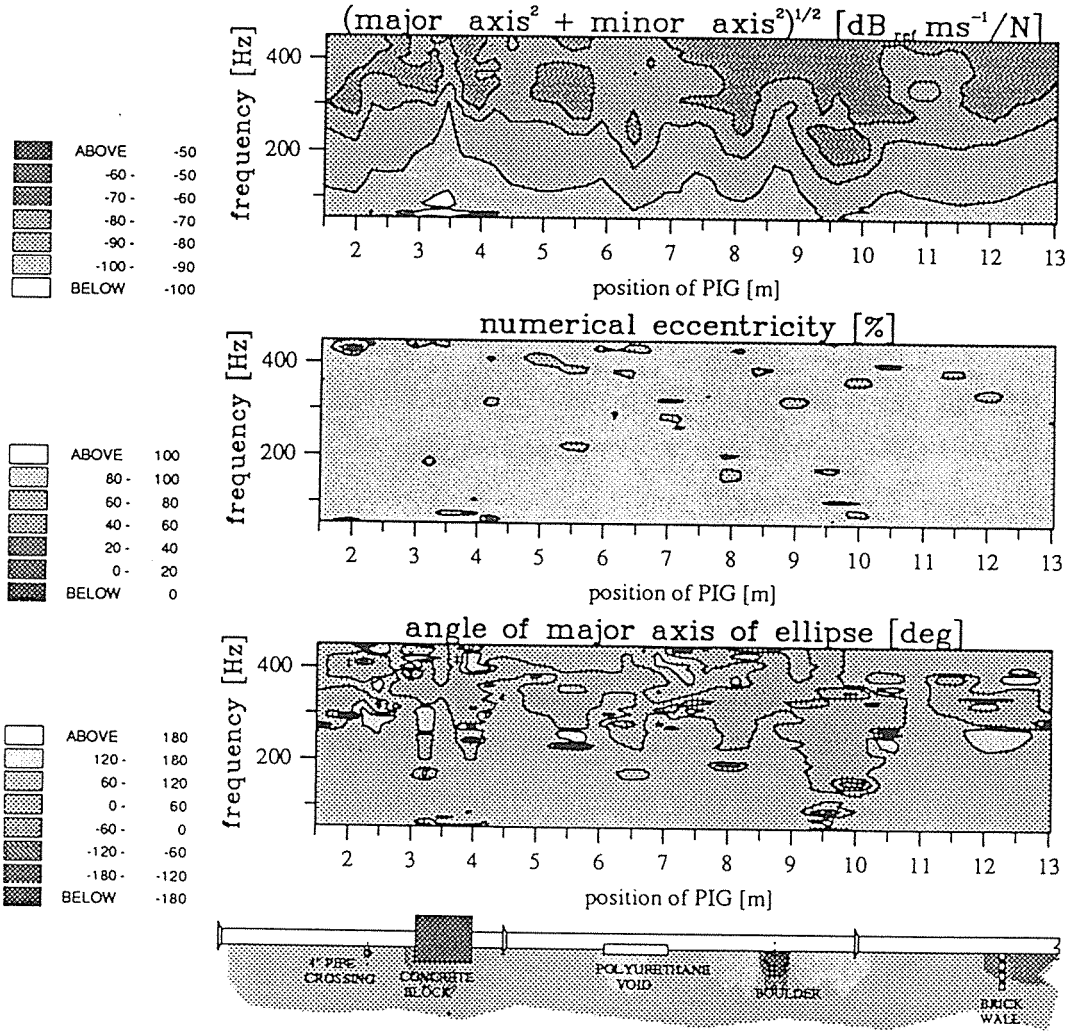

Fig.5. Contour plots of ellipse radius r, eccentricity ϵ, and ellipse orientation angle θ for pipe A. Features are most clearly visible in the ellipse-radius plot.

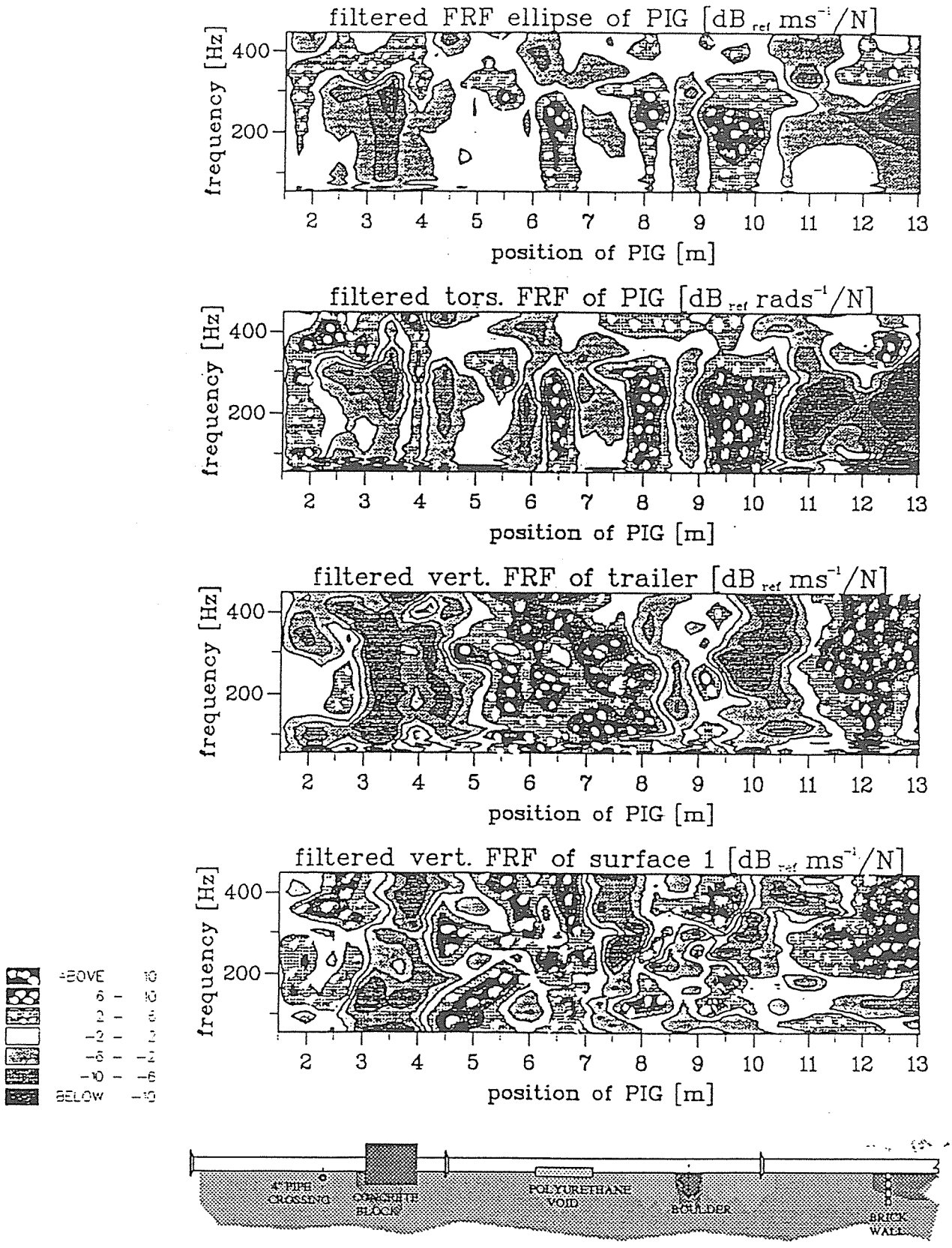

Fig.6. Contour plots showing filtered FRF deviations of pipe A.

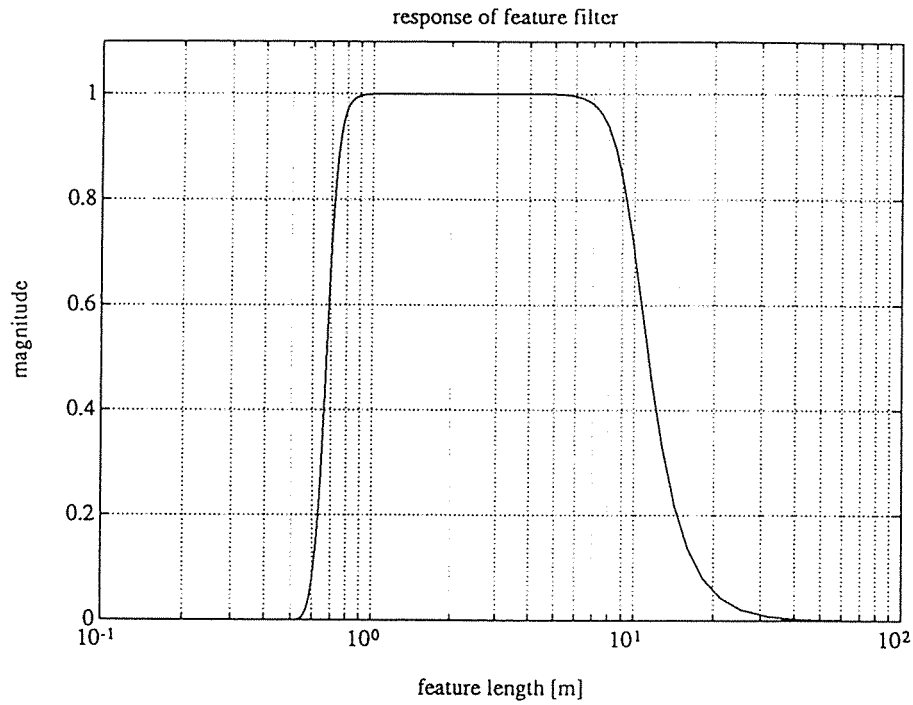

Fig.7. Response function of FRF filter used to highlight features that produce signatures of length between 0.5 and 10m.

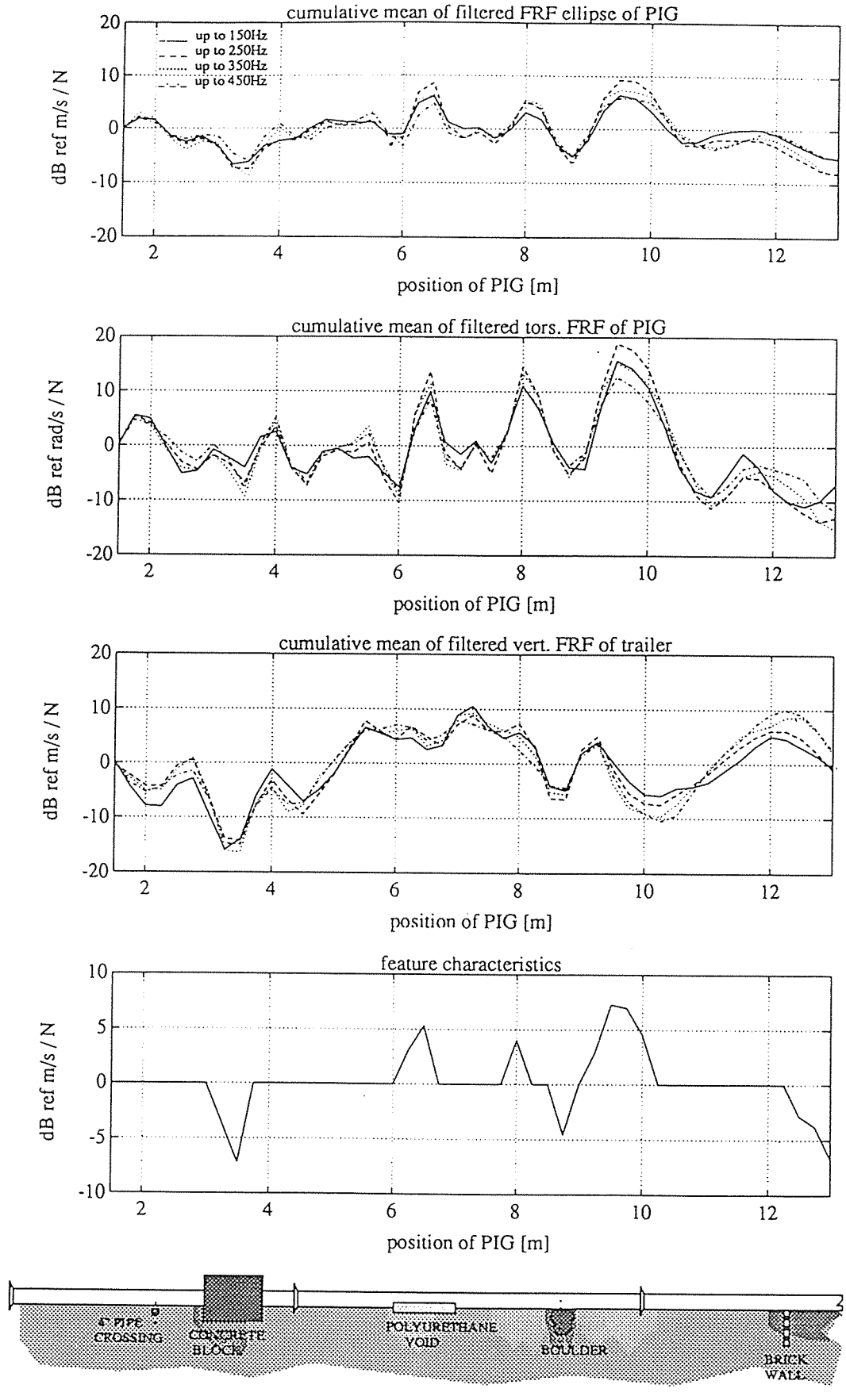

Fig.8. Cumulative mean and feature plots A. In the sketch of the pipe, lighter shades indicate softer support, and darker shades indicate harder support.
The labelled features and the joints are shown as specified on the construction drawings.

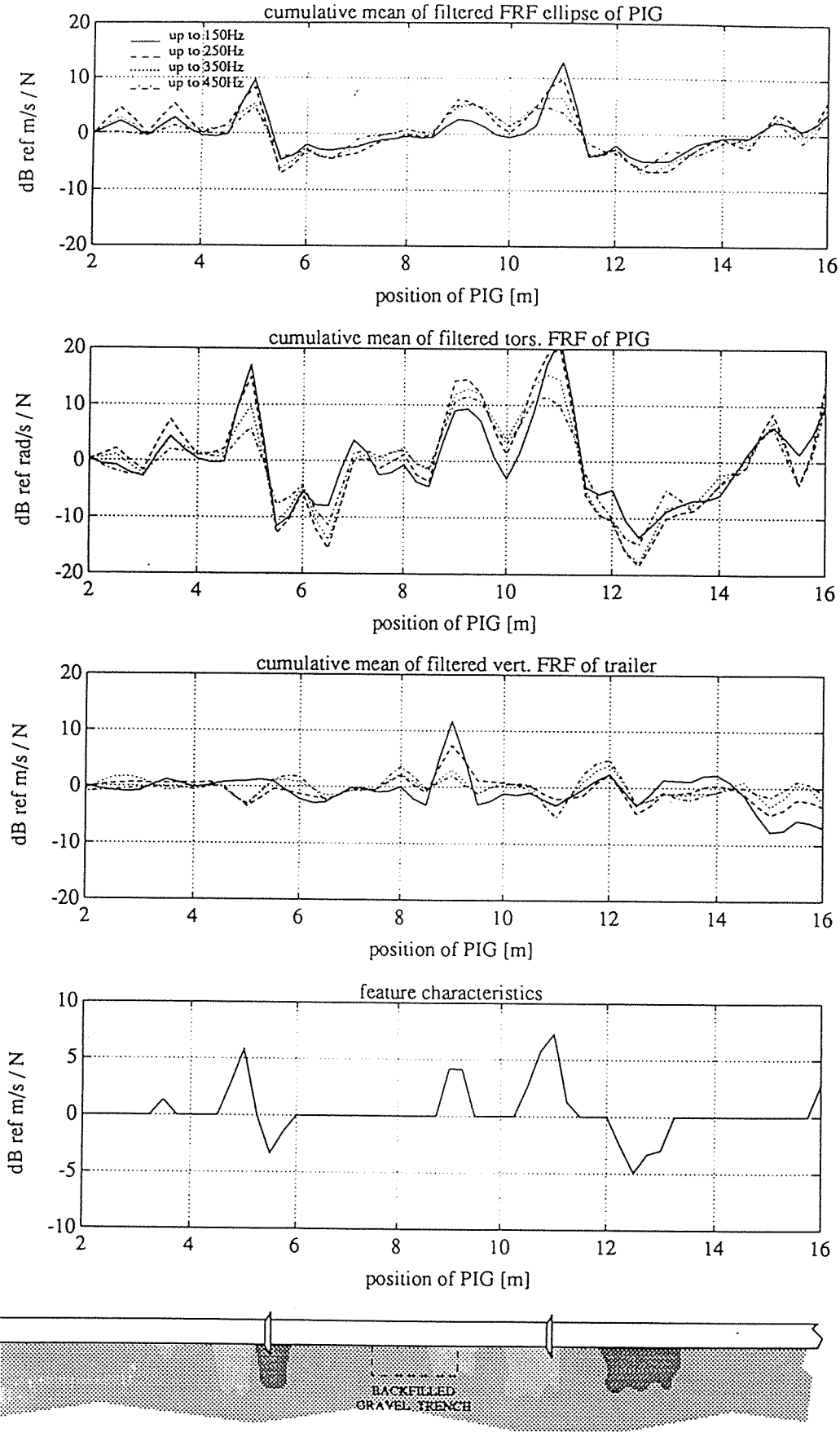

Fig.9. Cumulative mean and feature plots of pipe B.

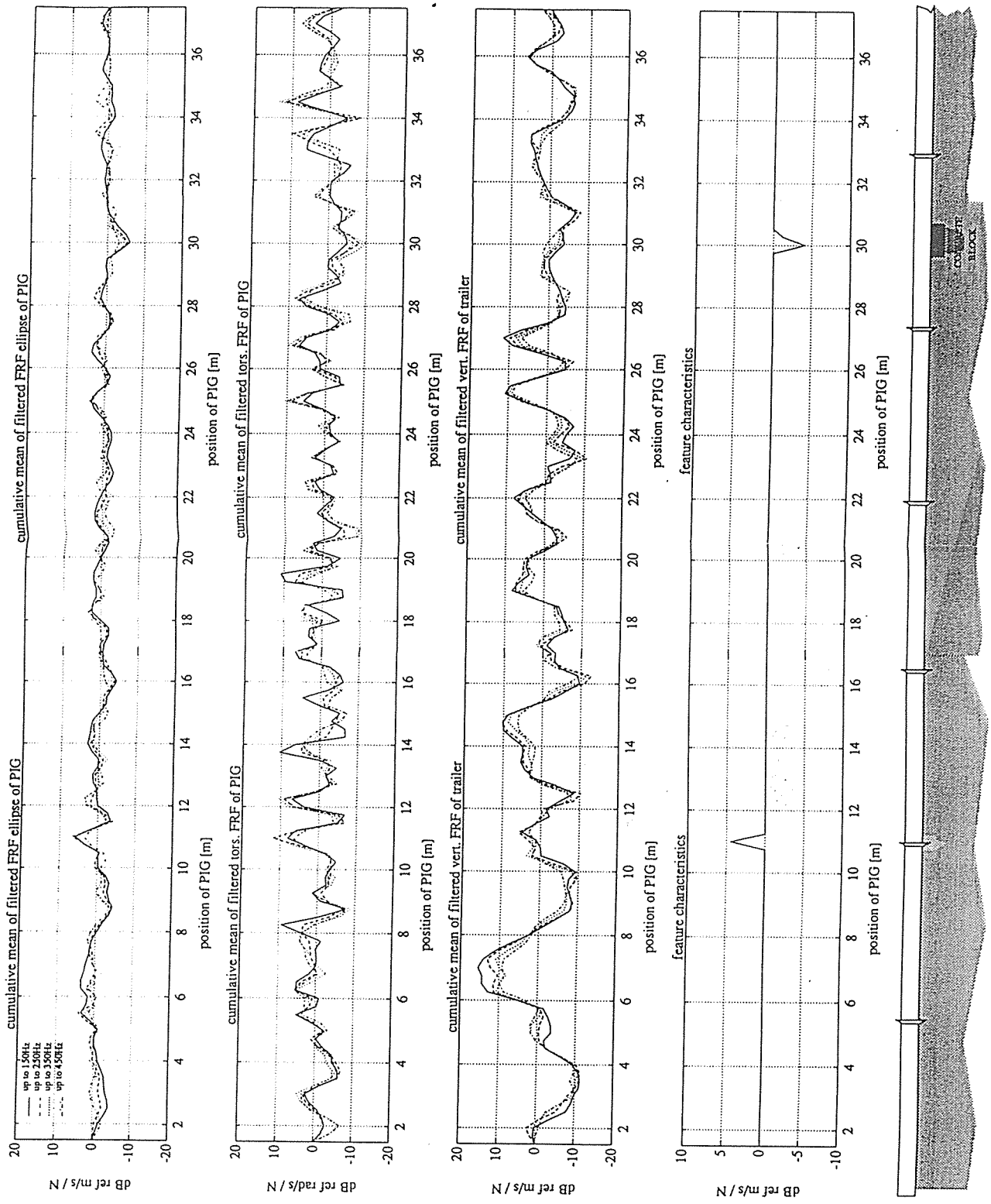

Fig.10. Cumulative mean and feature plots of pipe C.

FOUR POLE PARAMETER CHARACTERISATION OF ISOLATOR ACOUSTIC TRANSMISSION PERFORMANCE

Dickens, J. D., Norwood, C. J. and Juniper, R. G.
Defence Science and Technology Organisation
Materials Research Laboratory
P.O. Box 50, Ascot Vale, Victoria 3032

1. ABSTRACT

This paper discusses the frequency dependent dynamic properties of vibration isolators in terms of their four pole parameters. The expressions relating the isolator four pole parameters and the dynamic properties of the structure above and below the isolator to the isolator effectiveness are presented. The experimental measurement of the four pole parameters is described and the variation of the parameters with different pre-loads for a representative isolator is determined. For a given isolator the effectiveness of isolation and insertion loss depend upon the pre-load and the driving point mobilities of the source and foundation.

2. INTRODUCTION

For naval surface ship and submarine applications, the control of structure borne noise transmission is vital for acoustic signature management. The noise transmitted from machinery via a structure borne path depends upon the dynamic properties of the foundation, the machinery mounting point and the vibration isolator. A knowledge of the frequency dependent dynamic properties of vibration isolators is a necessary part of the acoustic prediction and management process.

Most isolators contain elastomeric material, the stiffness and damping properties of which are both frequency and pre-load dependent. In addition it is possible for standing waves to be set up within the isolator at certain frequencies, which greatly reduce its effectiveness at those frequencies. It is therefore highly desirable to determine the isolator properties under the pre-load conditions and frequency range experienced in normal operation.

The transfer impedance or mobility of an isolator has traditionally been used to describe its dynamic properties and provide a measure of its effectiveness. However, this measure does not necessarily provide a full description, and a more useful description is provided by the four pole parameters, which relate the force and velocity above the isolator to the force and velocity below.

In this paper the dynamic properties of an isolator is expressed in terms of its four pole parameters and the experimental determination of these is outlined. The variation of the parameters for different pre-loads is investigated over the frequency range of 20 Hz to 3.2 kHz.

3. FOUR POLE PARAMETERS

An anti-vibration mount may be modelled as the linear mechanical system shown in Fig. 1, where the input force and velocity are F_1 and V_1, and the output force and velocity are F_2 and V_2, respectively.

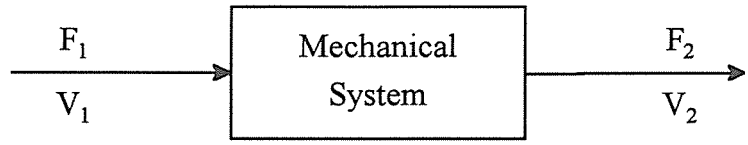

Figure 1
Mathematical model of isolator

The four pole parameters are designated as A, B, C and D, and the performance of the mount is defined by the following two equations:

$$F_1 = A.F_2 + B.V_2 \qquad \text{and} \qquad V_1 = C.F_2 + D.V_2 \tag{1}$$

Expressed as matrices, these become:

$$\begin{bmatrix} F_1 \\ V_1 \end{bmatrix} = \begin{bmatrix} A & B \\ C & D \end{bmatrix} \cdot \begin{bmatrix} F_2 \\ V_2 \end{bmatrix} \tag{2}$$

Equation (2) shows that the four pole parameters characterise the dynamic properties of anti-vibration mounts. They are independent of the systems located before and after the mount. Discussions of four pole parameters may be found in the literature [1], [2], [3]. The four pole parameters are given individually by the following two special cases:
Case (1): The output side is blocked, i.e. $V_2 = 0$:

$$A = \left.\frac{F_1}{F_2}\right|_{V_2=0} \qquad \text{and} \qquad C = \left.\frac{V_1}{F_2}\right|_{V_2=0} \tag{3}$$

Case (2): The output side is unrestrained and is free to vibrate, i.e. $F_2 = 0$:

$$B = \left.\frac{F_1}{V_2}\right|_{F_2=0} \qquad \text{and} \qquad D = \left.\frac{V_1}{V_2}\right|_{F_2=0} \tag{4}$$

In general the following relationship holds true [2]:

$$A.D - B.C = 1 \tag{5}$$

For the case of symmetric isolators i.e. those that behave the same if the input and output sides are interchanged, then:

$$\begin{bmatrix} F_2 \\ V_2 \end{bmatrix} = \begin{bmatrix} A & -B \\ -C & D \end{bmatrix} \cdot \begin{bmatrix} F_1 \\ V_1 \end{bmatrix} \tag{6}$$

Solving equations (2) and (6) gives:

$$A = D \tag{7}$$

The importance of equations (5) and (7) is that only two independent four pole parameters need to be measured for a symmetric isolator in order to completely characterise it.

Effectiveness of an Isolator

Consider that the isolator, having four pole parameters A, B, C and D, is placed between a vibration source and a foundation, as shown in Fig. 2(a). Let the driving point mobilities of the source and the foundation, measured at their connection points with the isolator, be H_1 and H_2 respectively.

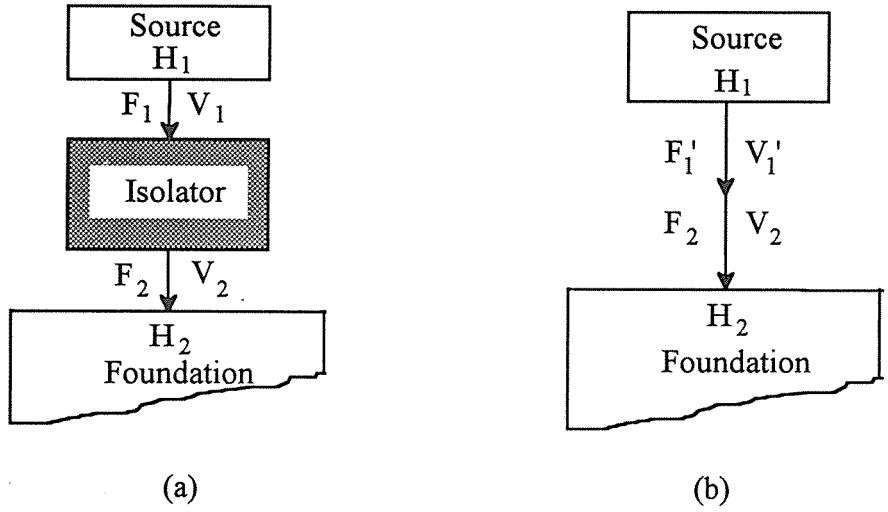

Figure 2
Isolator effectiveness

The velocities at the source / isolator and isolator / foundation interfaces are V_1 and V_2 respectively. The force exerted by the source on the isolator is F_1, and that of the isolator on the foundation is F_2. As before, equations (1) apply. Let V_0 be the free velocity of the source at the connection point, i.e. the velocity with nothing connected to the source. With the isolator connected, this velocity changes to V_1, and by the principle of superposition, V_1 is the sum of the free velocity V_0 and the motion due to the resisting force of the isolator. This resisting force is $-F_1$, and produces a velocity of $H_1.(-F_1)$, and so:

$$V_1 = V_0 - H_1.F_1 \tag{8}$$

If it is assume that the free velocity of the foundation is zero, then:

$$V_2 = H_2.F_2 \tag{9}$$

Solving equations (1), (8) and (9) to obtain V_2 and F_2 in terms of H_1 and H_2 gives:

$$V_2 = \frac{V_0.H_2}{A.H_1 + B.H_1.H_2 + C + D.H_2} \tag{10}$$

$$F_2 = \frac{V_0}{A.H_1 + B.H_1.H_2 + C + D.H_2} \tag{11}$$

Consider the situation that the source and foundation are directly connected across the isolator, as shown in Fig. 2(b). Let the velocities and forces be denoted as above but primed, and the free source velocity as V_0. The isolator has no effect on the motion of the system, and by a similar analysis to that conducted above, we obtain:

$$V_2' = \frac{V_0 . H_2}{H_1 + H_2} \qquad \text{and} \qquad F_2' = \frac{V_0}{H_1 + H_2} \tag{12}$$

The effectiveness of isolation, E, is defined as the ratio between the foundation velocity (or force) obtained when the source and foundation are directly connected across the isolator i.e. Fig 2(b), and the foundation velocity (or force) obtained with the isolator included i.e. Fig. 2(a). Therefore, from equations (10) and (12), E may be expressed in terms of the pole parameters and the source and foundation mobilities, as follows:

$$E = \frac{V_2'}{V_2} = \frac{A.H_1 + B.H_1.H_2 + C + D.H_2}{H_1 + H_2} \tag{13}$$

E is dimensionless and the insertion loss, L, is $|E|$ expressed as dB referenced to $|E| = 1$:

$$L = 20.\log_{10}\left|\frac{A.H_1 + B.H_1.H_2 + C + D.H_2}{H_1 + H_2}\right| \tag{14}$$

For symmetric isolators, by combining equations (6) and (14), we obtain:

$$L = 20.\log_{10}\left|A + \frac{B.H_1.H_2}{H_1 + H_2} + \frac{C}{H_1 + H_2}\right| \tag{15}$$

4. EXPERIMENTAL METHOD

In general the dynamic properties of a vibration isolator are dependent upon its pre-load, and so measurements should be made with a pre-load similar to that experienced in service. This means that the free condition, $F_2 = 0$, cannot be met. However the blocked condition, $V_2 = 0$, can be satisfied with a blocking arrangement, allowing the measurement of parameters A and C to be accomplished using equations (3).

Verheij [4] describes a method for determining the acoustic properties of a resilient mounting in terms of its blocked transfer function, defined as the output force divided by the input acceleration. This paper follows Verheij's experimental approach but characterises the dynamic properties of isolators with their four pole parameters. The schematic of the arrangement used at the Materials Research Laboratory (MRL) is shown in Fig. 3. The test isolator is held between two masses M_1 and M_2, which behave as rigid bodies in the test frequency range. The blocking force is computed by measuring the acceleration of the blocking mass. Although this appears contradictory, Verheij [4] shows that under certain conditions a large mass supported on very soft mounts may be considered as effectively blocked.

The upper mass is driven by the two vibrators via stingers, and provides the input dynamic excitation to the upper side of the test isolator. It also supplies a pre-load to the test isolator to simulate the static load of machinery. The pre-load is adjustable and is applied from the air bag located above the excitation mass. The vibrators are effectively decoupled from the test frame. These details are shown in Fig. 4. The location of the transducers was optimised to minimise the effects of structural modes on the test measurements by performing a modal analysis.

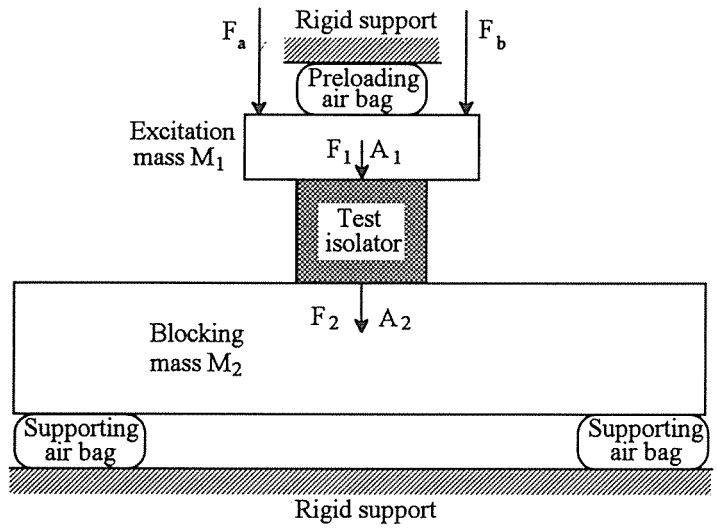

Figure 3
Schematic test arrangement

As previously defined, F_1 is the input force exerted by the excitation mass on the test isolator, and F_2 is the output force exerted by the test isolator on the blocking mass. Let F_a and F_b be the sinusoidal forces exerted on the excitation mass by the two vibrators at the angular frequency ω. A_1 and V_1 are the acceleration and velocity at the excitation mass / test isolator interface, and A_2 and V_2 are the acceleration and velocity at the test isolator / blocking mass interface. We have:

$$F_1 = F_a + F_b - M_1.A_1 \qquad \text{and} \qquad F_2 = M_2.A_2 \tag{16}$$

In this situation, the output velocity V_2 is very small and so the second terms of the equations (1) become small compared to the first ones. This allows the parameters A and C to be approximately calculated as follows:

$$A = \left.\frac{F_1}{F_2}\right|_{V_2 \approx 0} \qquad \text{and} \qquad C = \left.\frac{V_1}{F_2}\right|_{V_2 \approx 0} \tag{17}$$

Therefore the four pole parameters may be determined by measuring F_a, F_b, A_1 and A_2 and using the following relationships derived from equations (5), (6), (16) and (17):

$$A = D = \left.\frac{F_a + F_b - M_1.A_1}{M_2.A_2}\right|_{V_2 \approx 0} \tag{18}$$

$$C = \left.\frac{A_1}{j.\omega.M_2.A_2}\right|_{V_2 \approx 0} \qquad \text{and} \qquad B = \frac{A.D - 1}{C} \tag{19}$$

A digital computerised fast Fourier transform spectrum / network analyser was used to control the tests, and to acquire and analyse the data. It generated an output signal controlling the power amplifier supplying the vibrators, and so controlled the vibratory forcing function applied to the excitation mass.

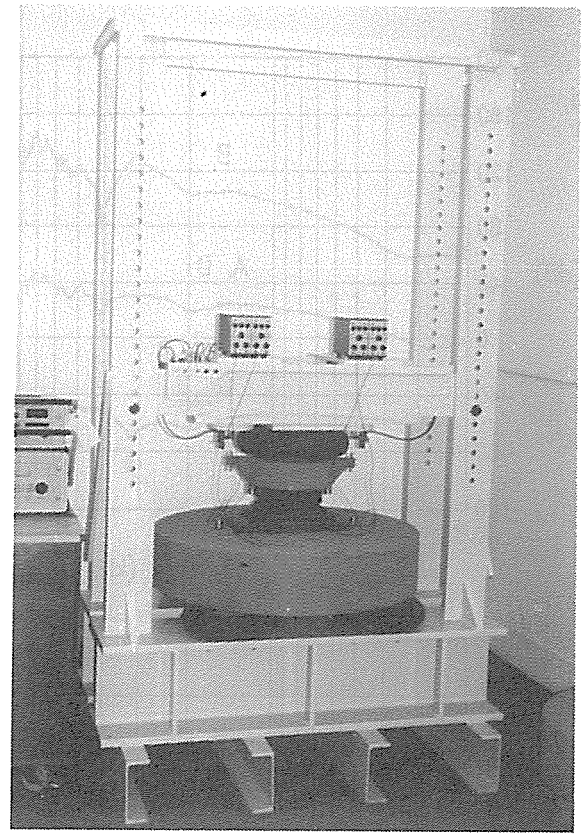

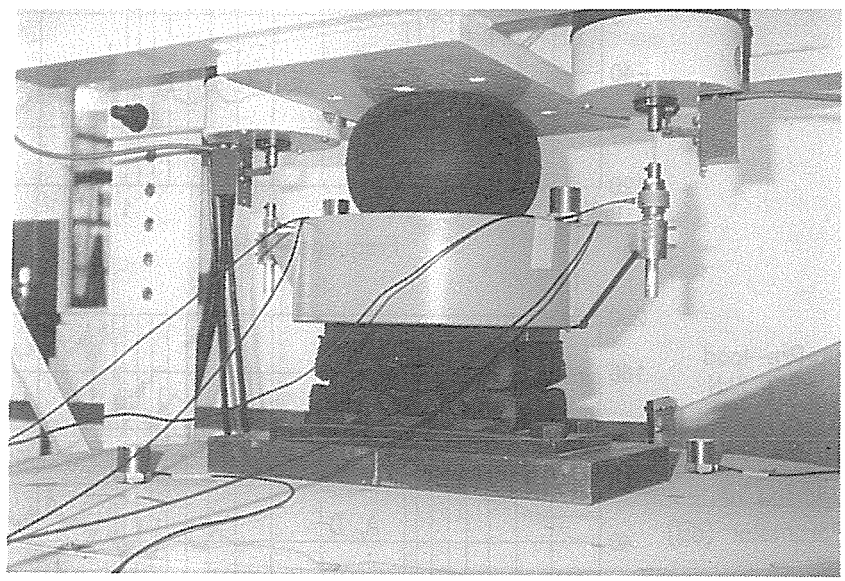

Figure 4
Test rig at the MRL

5. EXPERIMENTAL RESULTS AND DISCUSSION

A representative commercially available elastomeric isolator designed to provide vibration isolation for mechanical apparatus was investigated. Swept sine tests over the frequency range from 20 Hz to 3.2 kHz were conducted on it. The four pole parameters were computed from the experimental results using equations (18) and (19), for pre-loads of 1.5, 2.0 and 2.5 kN. The four parameters are graphed in Fig. 5.

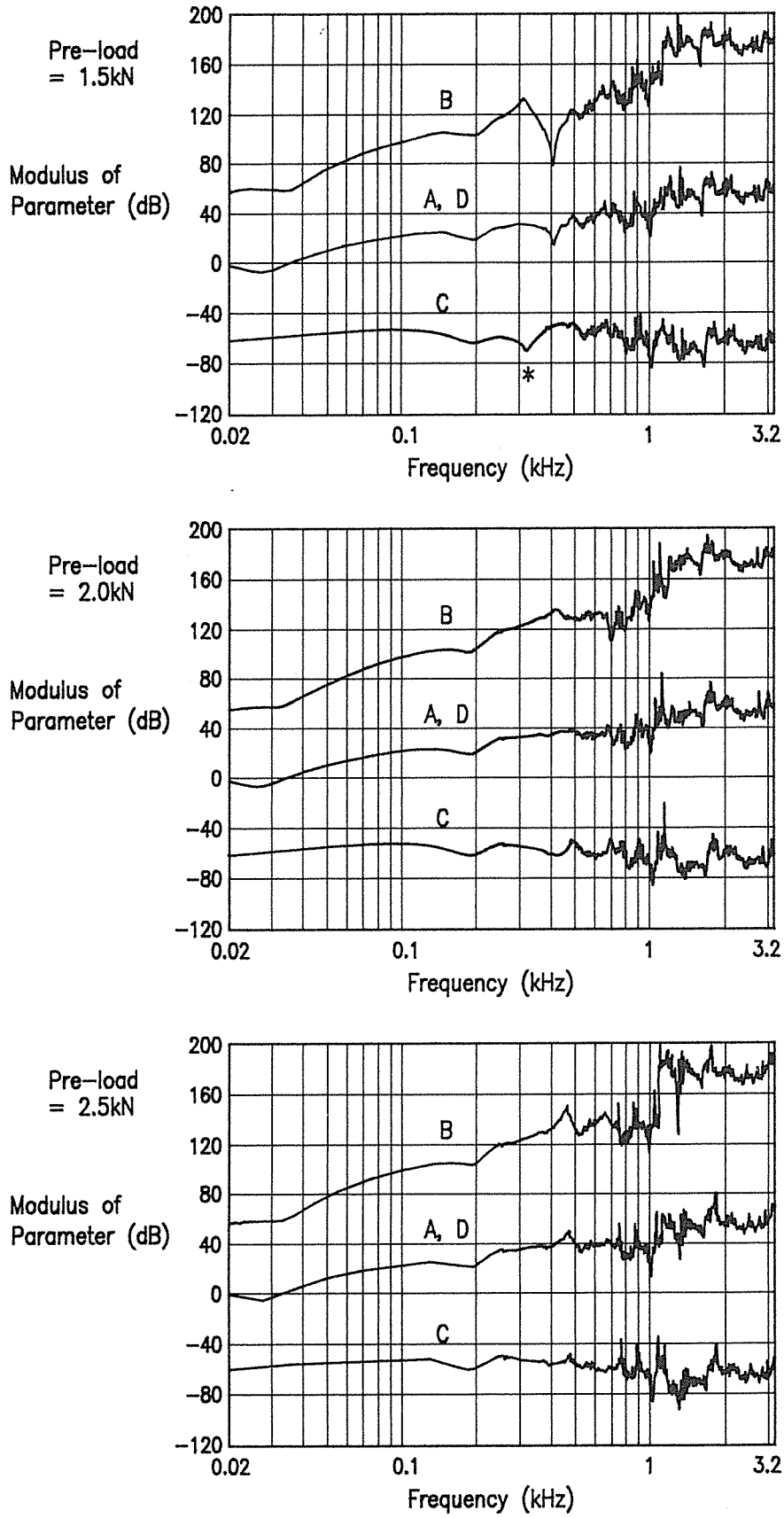

Figure 5
Four pole parameters of representative commercially available isolator

C is the blocked transfer mobility and has a measured slope of 20 dB/decade and phase angle, relative to Fa, of approximately 90 degrees for low frequencies. This indicates massless spring-like behaviour and holds true up to approximately 100 Hz. In addition, this spring-like behaviour implies that $F_1 \approx F_2$ and $V_1 \approx V_2$, and from equations (3) and (7), $A \approx D \approx 1$. This approximation agrees with the measurements for low frequencies. At higher frequencies standing waves within the isolator are evident as indicated by the resonant type peaks in the moduli curves, for example the parameter C peak marked * in Fig. 5.

Furthermore Fig. 5 demonstrates that the parameters depend upon the pre-load and so from equations (14) and (15), both the effectiveness and the insertion loss are functions of the pre-load as well as the mobilities of the source and foundation. The numeric results indicate that at low frequencies the most significant of the three terms in the logarithmic expression of equation (15) is $C/H_1 + H_2$. Therefore for low frequencies C is the most important of the four pole parameters in determining the isolator effectiveness, and to improve isolation for a given H_1 and H_2, C should be increased.

6. CONCLUSIONS

Vibration isolators may be characterised in terms of their four pole parameters, which are independent of the characteristics of other mechanical systems located before and after the isolator. Measurement of two independent parameters is sufficient to determine the dynamic properties of a symmetric isolator.

A representative isolation mount was investigated, and its four complex pole parameters determined over the frequency range 20 Hz to 3.2 kHz for different pre-loads. Spring-like behaviour was observed at low frequencies, and at higher frequencies standing waves were evident. The effectiveness of isolation and insertion loss depend upon the pre-load and the driving point mobilities of the source and foundation. For low frequencies, C is the prime four pole parameter that determines the isolator effectiveness, and for given driving point mobilities of the source and foundation, C should be increased to improve the isolation.

7. REFERENCES

1. Molloy, C.T., "Use of Four-Pole Parameters in Vibration Calculations", Journal of the Acoustical Society of America, pp 842-853, vol. 29, no. 7, July 1957.

2. Snowdon, J.C., "Vibration isolation: Use and characterisation", Journal of the Acoustical Society of America, pp 1245-1274, vol. 66, no. 5, November 1979.

3. Norwood, C., "Vibration Isolator Properties and Performance Prediction", Odegaard & Danneskiold-Samsoe ApS report 87.199, December 1987.

4. Verheij, J.W., "Multi-path sound transfer from resiliently mounted shipboard machinery", Ph.D. thesis, Institute of Applied Physics TNO-TH, Delft, 1982.

THE USE OF THE CEPSTRUM TO SEPARATE SOURCE AND TRANSMISSION PATH EFFECTS

R.B. Randall

School of Mechanical & Manufacturing Engineering
The University of New South Wales
Kensington, NSW

1. INTRODUCTION

There are many situations where it is very difficult to measure a source of sound or vibration, but it is possible to measure the response of a physical system to the excitation. This the case for example with gearboxes, where the main excitation is the varying force at the toothmesh caused mainly by the dynamic transmission error. It is extremely difficult to measure this force in practice, since although it is roughly fixed in space, it is continually moving with respect to the individual gears which are meshing, making it difficult to use strain gauges, for example.

In condition monitoring, vibration measurements are used as a secondary indicator of changes in internal components and processes, but externally measured vibrations are always a compound of the effects of the internal forces and the structural dynamic properties of the transmission path from the source to the measurement point. When changes occur in the measured vibrations, assumptions have to be made about whether these are primarily due to changes in the forcing function or the dynamic properties of the structure, so it would be very advantageous to be able to separate the two effects.

The cepstrum provides this possibility, at least where there is a single dominant source, and where the type of basic excitation satisfies certain requirements. This paper illustrates the basic principles using the example of the response vibrations of a free–free beam excited by hammer blows. A double impact is used to simulate the case of repetitive impulsive impact.

2. THE CEPSTRUM

The cepstrum is a generic term for functions involving a Fourier transform of a logarithmic spectrum [1], and is now most commonly defined as the inverse Fourier transform of the log spectrum (or inverse Z–transform for sampled time functions), ie:

$$C(t) = \mathcal{F}^{-1}\{\mathrm{Log}[F(f)]\} \qquad (1)$$

Where $F(f)$ is complex (eg the direct Fourier transform of a time signal expressed in terms of its amplitude and phase as $A(f)e^{j\phi(f)}$), then $\mathrm{Log}[F(f)]$ is interpreted as $\ell n[A(f)] + j\phi(f)$ and the resulting cepstrum is known as a "complex cepstrum", even though it is real valued because the log amplitude is an even function of frequency, and the phase odd. Where $F(f)$ is real (eg an auto– or power spectrum) the resulting cepstrum is known as a "power cepstrum". By analogy with cepstrum (from spectrum) the time axis is called "quefrency".

For a linear physical system as illustrated in Fig.1, with one dominant input, the output is

derived in the time domain by convolving the input signal with the impulse response of the system. By the convolution theorem, this transforms to a multiplication in the frequency domain (of complex and/or amplitude squared spectra) and thence to an addition in the logarithmic spectra. Because of the linearity of the Fourier transform, the additive relationship remains in the cepstrum, both power cepstrum and complex cepstrum. Thus if the various components of the cepstrum are concentrated in different regions, it is possible to separate them by standard filtering techniques (called "liftering" in the cepstrum domain).

2.1 Cepstrum of a Transfer Function

The transfer function of many physical systems can be represented in the Z–domain in rational form as:

$$H(z) = \frac{|B| \prod_{k=1}^{m_i} (1 - a_k z^{-1}) \prod_{k=1}^{m_o} (1 - b_k z)}{\prod_{k=1}^{p_i} (1 - c_k z^{-1}) \prod_{k=1}^{p_o} (1 - d_k z)} \qquad (2)$$

where $|a_k|, |b_k|, |c_k|, |d_k|$ are all < 1. The a_k and b_k represent zeros inside and outside the unit circle, respectively, while the c_k and d_k represent poles inside and outside the unit circle.

In Ref.[2] Oppenheim & Schafer show that by taking the logarithm of this expression, so that the products become sums, then expanding the individual log terms as power series, the cepstrum can be obtained by an inverse Z–transform as:

$$\begin{aligned} C(n) &= \ell n|B| && , \quad n = 0 \\ &= -\sum_{k=1}^{m_i} \frac{a_k{}^n}{n} + \sum_{k=1}^{p_i} \frac{c_k{}^n}{n} && , \quad n > 0 \\ &= \sum_{k=1}^{m_o} \frac{b_k{}^{-n}}{n} - \sum_{k=1}^{p_o} \frac{d_k{}^{-n}}{n} && , \quad n < 0 \end{aligned} \qquad (3)$$

Note that the poles and zeros outside the unit circle give negative quefrency terms. For a stable, causal system there are no poles outside the unit circle, and likewise there are no zeros outside the unit circle for minimum phase systems [2]. This restriction to minimum phase systems applies to many passive mechanical structures, as it means that the "inverse filter" is stable; in other words finite displacements cannot give rise to infinite forces. With these restrictions, the cepstrum becomes right–sided, or "causal", and has further valuable properties. The most important of these is that the real and imaginary parts of its Fourier transform (the log amplitude and phase of the system frequency response) are related by a Hilbert transform and thus do not have to be separately measured. The complex cepstrum can in fact be derived from the corresponding power cepstrum (obtained from the log amplitude only) by doubling positive quefrency components and setting negative quefrency components to zero [2]. Moreover, since the poles and zeros (except those at zero frequency) occur in complex conjugate pairs, the complex exponential terms can be expressed as exponentially damped cosines, further

damped by the hyperbolic term $1/n$. Thus, Equ.(3) reduces to:

$$C(n) = \frac{2}{n}\left(\sum_{k=1}^{p_{i/2}} A_{ck}^{n} \cos n\omega_{ck} - \sum_{k=1}^{m_{i/2}} A_{ak}^{n} \cos n\omega_{ak} \right) \quad , \quad n > 0 \tag{4}$$

To make this clearer, take the case of a single-degree-of-freedom (SDOF) system, which has no zeros in its transfer function, and a single conjugate pair of poles c and c^* where $c = Ae^{j\omega_c}$. Thus from Equ.(3) the cepstrum is given by

$$\frac{A^n}{n}\left(e^{j\omega_c n} + e^{-j\omega_c n}\right) = \frac{2A^n}{n}\cos(\omega_c n) \tag{5}$$

Since for a SDOF system the impulse response is an exponentially damped sine function, it can be seen that it is very similar in form to the cepstrum, the main differences being the 90° phase shift and the additional hyperbolic damping of the cepstrum. This is illustrated in Fig.2. In multi-degree-of-freedom (MDOF) systems the further differences are that zeros give terms as well as poles (though with opposite sign) and also that the individual terms in the impulse response are scaled by the corresponding residues, whereas the equivalent terms in the cepstrum, the A_{*k}, are all close to unity for low damping.

2.2 The Differential Cepstrum

Using the concept of the differential cepstrum, even the hyperbolic damping can be removed, making the differential cepstrum even closer to the impulse response. The differential cepstrum is defined as the inverse transform of the derivative of the log spectrum (with respect to frequency) and in Ref.[2] it is shown that it is equal to the normal cepstrum multiplied by n; in practice it can be calculated in this way.

3. EXPERIMENTAL RESULTS

Figure 3 shows the experimental set-up used to excite a free-free steel beam, approx. 1m long by 19mm square. A Bruel & Kjaer instrumented hammer type 8202 was used to apply and measure the impact force, and a Bruel & Kjaer miniature accelerometer type 4393 used to measure the response. The accelerometer was left at point 1 at one end of the beam, while the point of application of the impact was at all points 1 through 8. The

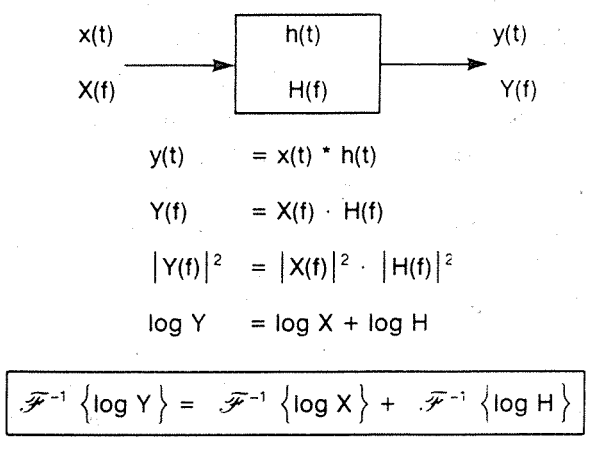

Figure 1 Input-output relationships

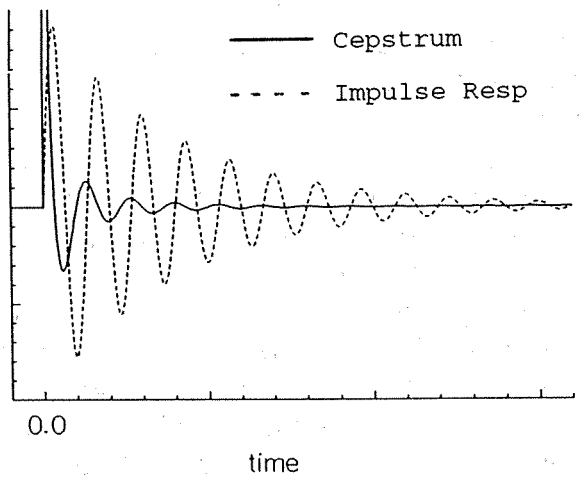

Figure 2 SDOF system response

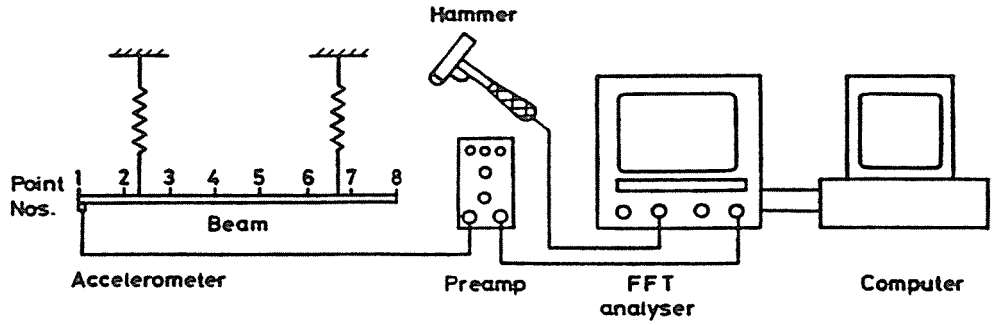

Figure 3 Experimental set-up

hammer used a built-in line drive preamplifier, while the accelerometer was connected to the analyser via a Bruel & Kjaer charge amplifier type 2635. The Bruel & Kjaer dual channel analyser type 2032 was used to digitise all signals with appropriate antialiasing filtering, and to measure frequency response functions for comparison purposes. Much of the signal processing was done in the connected PC, but some was carried out on the UNSW Vax computer.

3.1 The Nonlinear Least Squares Method

Figure 4 shows a typical driving point autospectrum (point 1) and Fig.5 (dotted line) shows the (complex) cepstrum derived from it on the assumption of minimum phase properties. Using a nonlinear least squares optimisation procedure based on the Levenberg-Marquardt method [3] the poles and zeros were extracted by fitting an equation of the form of Equ.(4) to the cepstrum data for quefrencies above 6ms (where the force cepstrum was negligible) [4]. A very good fit was achieved as shown by the solid line in Fig.5. Equally good fits in the cepstrum were achieved for transfer measurements to points 5 and 8.

It had originally been hoped that extraction of the poles and zeros of the transfer function within the frequency range of interest would allow reconstruction of the Frequency Response Function (FRF) over the same frequency range, but as described in Ref.[4] it was found that the effects of out-of-band modes were somewhat different in pole-zero models than in the more familiar pole-residue models. This is illustrated in Fig.6, which compares regenerated with measured FRFs for points 1 and 5. It is seen that there is a

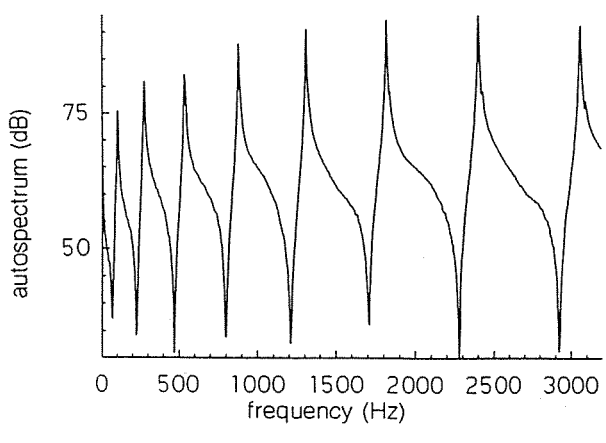

Figure 4 Driving point autospectrum

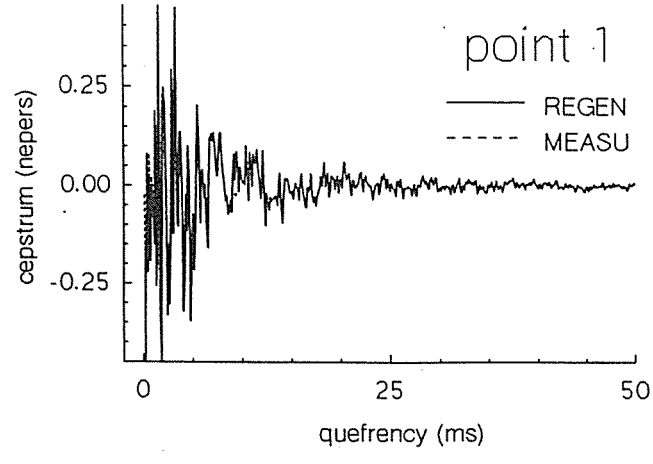

Figure 5 Driving point cepstra

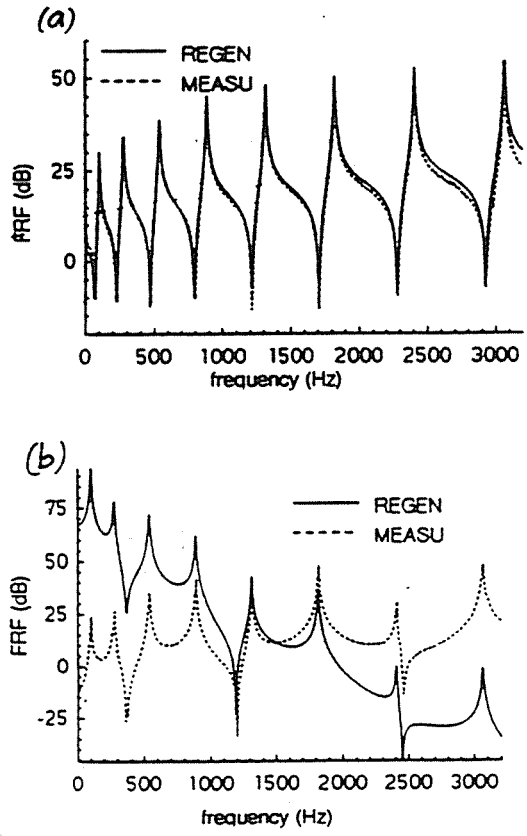

Figure 6 Original FRFs without phantom zeros. (a) Point 1. (b) Point 5.

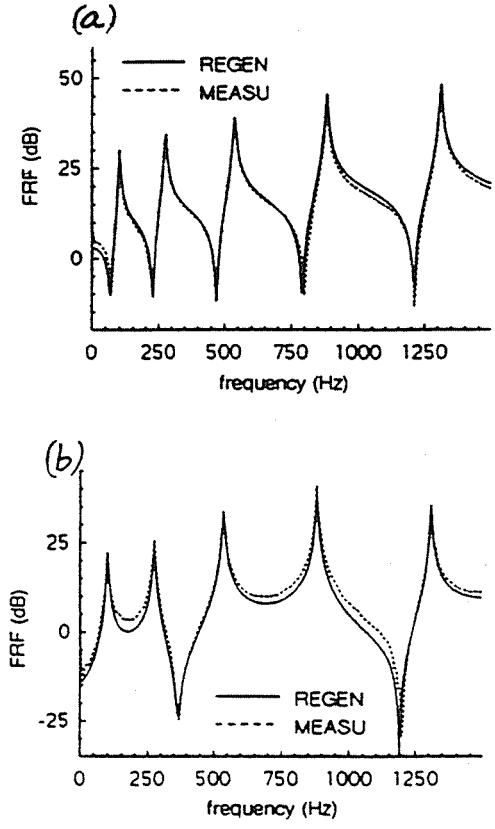

Figure 7 Original FRFs with phantom zeros. (a) Point 1. (b) Point 5.

reasonable match for the driving point measurement (Point 1) but a difference mainly in slope for the transfer measurement (Point 5) with a smaller number of zeros than poles. The difference was even greater for Point 8 as this transfer FRF had no zeros at all. This point was investigated in depth in Ref.[5] where it was shown that it was necessary to compensate for the effects of out–of–band modes by adding "phantom zeros". In this case the phantom zeros were derived by fitting the measured FRF using a modal analysis package based on the Rational Fraction Polynomial technique [6] and the results are shown in Fig.7. Since the phantom zeros are primarily to correct errors in slope of the FRF it is thought that it may be possible to use a theoretical model, such as a finite element model, to derive them, although this has not as yet been demonstrated. It has however been demonstrated that an initial set of phantom zeros can be used when tracking changes in an FRF due to simulated crack development [7]. In this experiment a slot was milled in the middle of the beam, in steps of 2mm to a depth of 10mm, to simulate a developing crack. The initial set of phantom zeros were used in conjunction with the curvefitted poles and zeros extracted from the response cepstra to predict the modified FRF, and as shown in Fig.8, the prediction matched the measurement very well. Fig.9 shows the differences caused by the maximum depth slot.

3.2 Scaling of the FRF

As the scaling of the FRF is contained in the zero quefrency term (as indicated in Equ.(3)) it is lost when curvefitting higher quefrency regions of the cepstrum, and thus some other method must be used to scale the FRF. The results shown in Figs. 7 and 8 were scaled on the basis of the zero frequency values, which for the beam are calculable from its

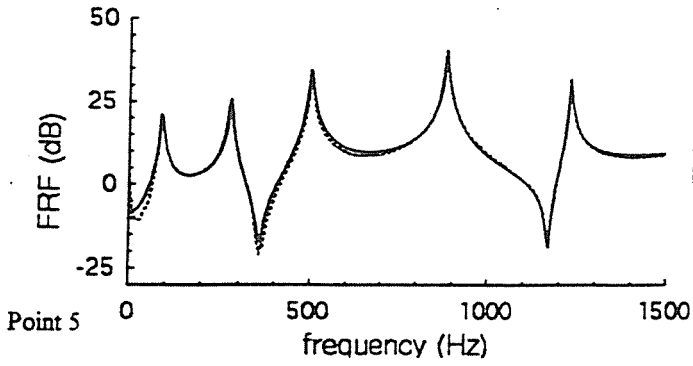

Figure 8 Predicted (—) vs Measured (····) FRFs

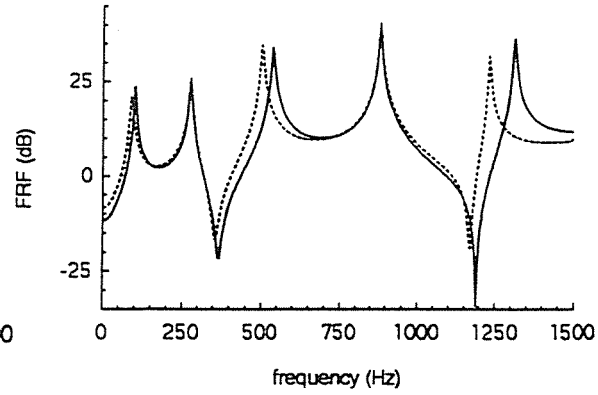

Figure 9 FRFs for zero (—) vs 10mm (····) slot depth

mass, and in the general case could be calculated from the mass and rotational inertia properties. For constrained rather than free–free objects, the FRFs could be expressed in terms of compliance rather than accelerance, and the zero frequency values obtained from measurements of static stiffness.

3.3 The Ibrahim Time Domain (ITD) Method

The ITD method [8] is a standard method of extracting modal properties of systems from free response data (ie sums of impulse responses). It uses an eigenvalue method to extract the damping and damped natural frequencies for each of the modes in the free response. Since the differential cepstrum has the same mathematical form as a sum of impulse responses, it was decided to apply the ITD method to the extraction of the poles and zeros. Even though these in principle have opposite sign, it is not possible to detect this with the ITD method, as there is no zero time reference and the phase relationships between the damped sinusoids are not significant. In Ref.[9] it was shown how the poles and zeros could be extracted from the differential cepstrum by an adaptation of the ITD method, with results equally as good as the Nonlinear Least Squares (NLLS) method as illustrated in Fig.10. The distinction between poles and zeros could be made by comparing the results for the different measurements, keeping in mind that the poles are global properties present in all FRFs, whereas the zeros are local properties present only in a particular measurement.

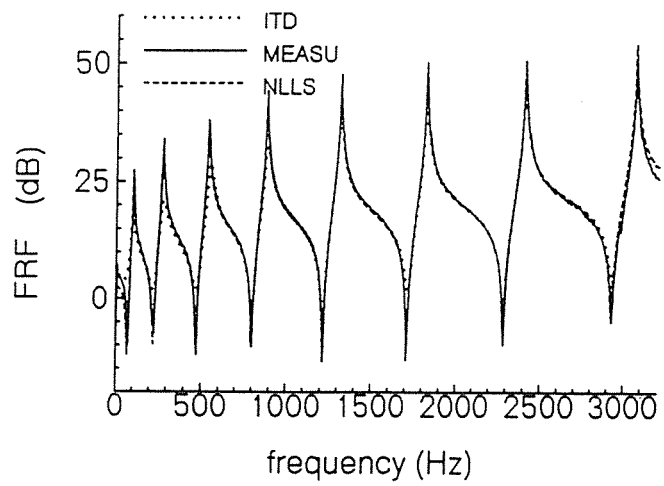

Figure 10 Comparison of results for ITD method with Nonlinear Least Squares (NLLS) and direct measurement

The advantage of the ITD method over the NLLS method is that the latter requires an estimate in advance of the number and approximate location of the poles and zeros to be extracted, whereas the ITD method fits a greatly overdimensioned model and then uses confidence factors to separate the true "modes" from noise or computational modes.

3.4 Double Impact Measurements

A double impact with the hammer was used to simulate such forcing functions, and also periodic forcing functions, which have a very similar effect in the cepstrum. Figure 11(a) shows a typical response autospectrum, with additive ripple due to the double impact, and Fig.11(b) the corresponding cepstrum. Comparing the latter with Fig.5 it is seen that the only difference is the addition of a series of discrete "rahmonics" at intervals of the impact separation time. Fig.11(b) also shows a sine squared function which was used to window out these rahmonics in the NLLS method (as well as allowing for it in the NLLS procedure). The regenerated FRF in this case was virtually identical to that obtained with single impact, and is thus not shown.

With the ITD method a different approach was used because of the difficulty of coping with the sinusoidal modulation. Instead, the discrete rahmonics were simply removed by setting them to zero in the differential cepstrum as illustrated in Fig.11(c). It was found that this disruption could be coped with by the noise rejection properties of the ITD method.

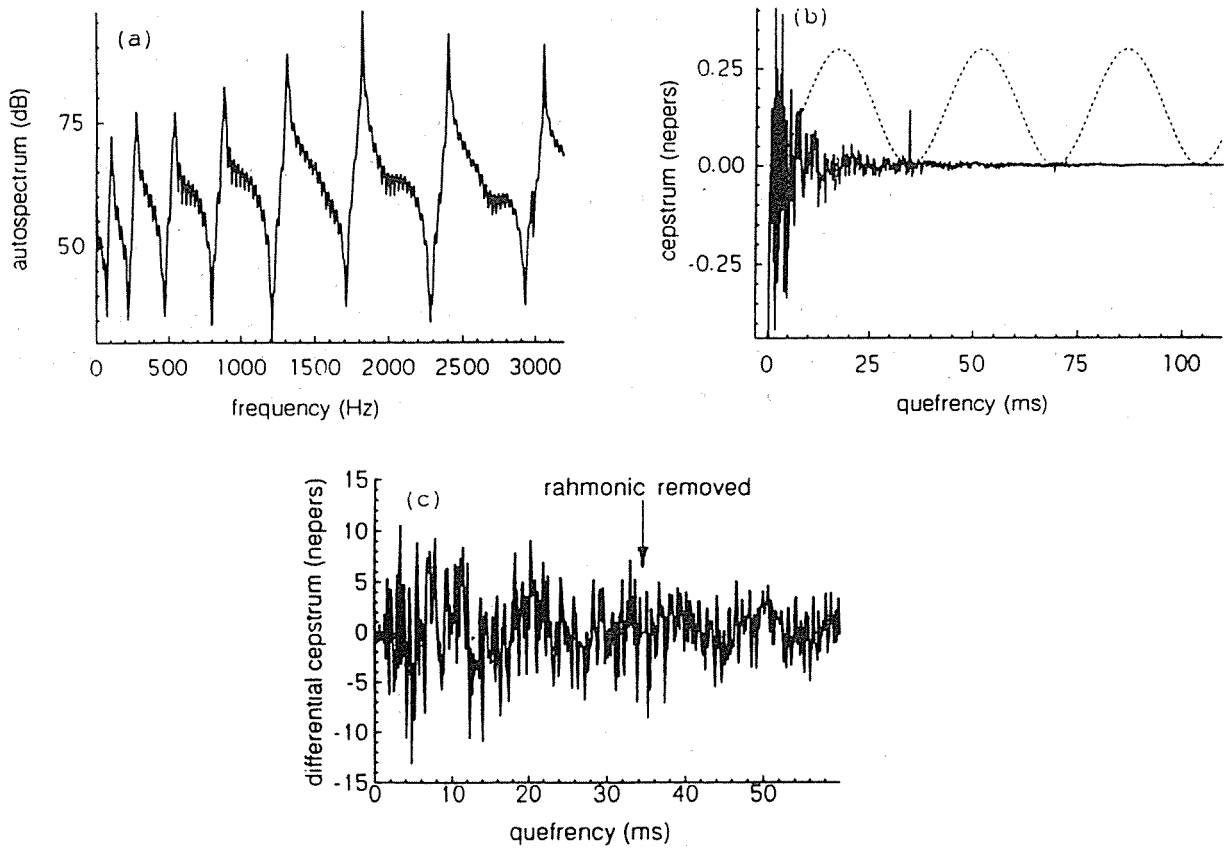

Figure 11 Double bounce measurements, Point 1.
(a) Response autospectrum.
(b) Corresponding cepstrum, showing sine squared weighting.
(c) Edited differential cepstrum.

4. CONCLUSION

The cepstrum is a useful function when applied to response vibration or acoustic signals, since not only are the source and transmission path properties additive, but often also separated into different regions. In principle this gives the possibility of determining whether changes in the measured responses are due to changes in the forcing function or in the structural dynamic properties.

This paper gives two approaches to the extraction of the poles and zeros of the system transfer function from the response cepstrum in the case of impulsive forcing functions, even where these are repeated or periodic. It is yet to be elucidated which method would be best in a given situation. In both cases it is necessary to supplement the poles and zeros actually detected with "phantom zeros" to correct for the effects of truncated out-of-band modes. The method used here to determine the phantom zeros involved an initial measurement of the true FRF but it was shown that the same values could be used to track changes in the FRF from response measurements only. Since the phantom zeros only determine the general slope of the FRF, it is quite possible that they could be determined from a finite element model, or possibly from a simplified measurement (eg with a machine stopped, and then applied with the machine running).

REFERENCES

[1] Randall, R.B. (1987) *Frequency Analysis.* Bruel & Kjaer, Copenhagen.

[2] Oppenheim, A.V. & R.W. Schafer (1989) *Discrete-Time Signal Processing.* Prentice-Hall, New Jersey.

[3] Dennis, J.E. & R.B. Schnabel (1983) *Numerical Methods for Unconstrained Optimization and Nonlinear Equations.* Prentice-Hall, New Jersey.

[4] Randall, R.B. & Y. Gao "Extraction of Modal Parameters from the Response Power Cepstrum". to be printed in Journal of Sound & Vibration, May 1984.

[5] Randall, R.B., Y. Gao & A. Sestieri (1992)"Phantom Zeros in Curvefitted Frequency Response Functions". Proc. 17th IMAS, K.U. Leuven, Belgium, pp503-517.

[6] Richardson, M. et al. (1985) "Global Curve Fitting of Frequency Response Measurements using Rational Fraction Polynomial Method". Proc. 3rd IMAC, Orlando, Florida.

[7] Randall, R.B. & Y. Gao (1992) "Tracking Changes in Modal Parameters by Curve-Fitting the Response Cepstrum". Proc. 17th IMAS, K.U. Leuven, Belgium, pp 55-66.

[8] Ibrahim, S.R. & E.C. Mikulcik (1977)"A Method for the Direct Identification of Vibration Parameters from Free Response". Shock and Vibration Bulletin, Vol.47, part 4, pp183-198.

[9] Randall, R.B. & Y. Gao (1993) "Adaptation of the ITD Method to the Extraction of Poles and Zeros from the Response Cepstrum". Proc. Conf. on Modern Practice in Stress and Vibration Analysis". Sheffield, pp641-653.

Surface Excitation: Surface Mobility

J.Y. ZHAO, H.M. WILLIAMSON and J.P. BAIRD

Department of Aerospace and Mechanical Engineering
Australian Defence Force Academy
Campbell ACT 2600

ABSTRACT

The physical meaning of surface mobility is discussed as a variation of point mobility to cover cases where structures are coupled via large contact areas. Based on alternative concepts, complex power and effective mobility, surface mobilities for an infinite, homogeneous thin plate are derived for uniform, conphase force distributions and uniform, conphase velocity distributions respectively. The contact area considered is circular in shape. The results are compared with the point mobility of the plate showing that for a given net force, a reduction in the transmitted power can be gained by coupling structures via large areas.

1. INTRODUCTION

The point mobility concept has been commonly used to study the vibration transmission of built-up structures [1,2]. To deal with cases of multi-point connections, **Petersson** and **Plunt** [3] introduced the concepts of effective point mobility and effective overall mobility. They considered the mobility of each individual point along with the contributions of all the other points in order to derive a space averaged effective point mobility over all the excitation points. This mobility approach is based on the assumption that the connection point is an area of dimension which is only a fraction of the governing wavelength.

The interest associated with high frequency vibration transmission has increased due to increased machine operating speeds and more flexible supporting structures. Consequently, the assumed point–like connection between a machine and its support becomes invalid since the contact area can be comparable to the governing wavelength. Thus, excitations may have complicated spatial distributions and the power transmitted will differ to that which occurs when the connection is via a 'point'.

Hammer and **Petersson** [4,5] developed the idea of strip mobility based on the concepts of complex power and effective mobility. Strip mobility was derived for infinite, homogeneous thin plates excited with either a uniform, conphase force distribution or a uniform, conphase velocity distribution along a finite strip. It was shown that for the two cases investigated, a reduction of power transmission can be gained by using a strip coupling for a given net force. It was also shown that the difference between the obtained strip mobilities using either the complex power or the effective mobility concepts is insignificant disregarding the difference in the spatial difference of force distributions.

Presented here are the results of a theoretical study to determine the effective surface mobility of large contact areas following on the concepts of **Hammer** and **Petersson** [4,5]. The supporting structure is theoretically idealized as an infinite, homogeneous thin plate with no losses. The contact area considered is circular in shape, however, the theory is applicable to any arbitrary shape.

2. SURFACE MOBILITY

It is assumed that the systems under consideration are linear and passive. The mobility of a mechanical system is defined as:

$$\underline{Z} = \frac{\underline{V}}{\underline{F}}, \tag{1}$$

When the force acts at a region whose dimension is considerably smaller than the governing wavelength of interest, the mobility is determined from the velocity and force at that point, and this mobility is referred to as the driving point mobility. In the following sections, a variation of the point mobility is presented to incorporate large contact area cases based on the complex power approach and the effective mobility approach respectively.

2.1 Complex Power Approach

Figure.1 schematically shows an interface of large contact area S between a machine and its support. The net complex power transferred through the contact area S is:

$$\underline{Q} = \frac{1}{2} \int\int \underline{\sigma}^*(x, y) \cdot \underline{v}(x, y) \cdot dxdy. \qquad (2)$$

The harmonic time factor $e^{i\omega t}$ is omitted here for the sake of brevity. The surface mobility defined on the complex power basis can be obtained as [4]:

$$\underline{Z}^s = \frac{1}{|F|^2} \int\int \underline{\sigma}(x, y)^* \cdot \underline{v}(x, y)\, dxdy. \qquad (3)$$

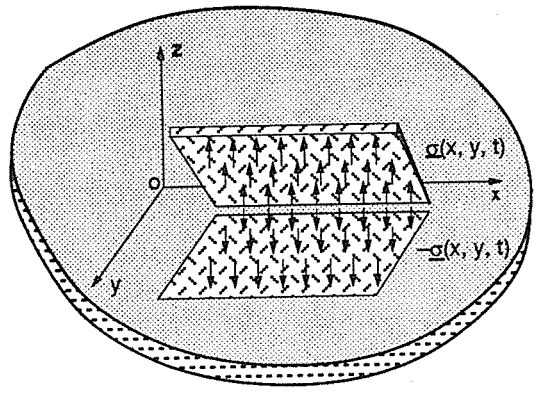

Figure.1 Schematic of Large Contact Area

2.2 Effective Point Mobility Approach

From the concept of effective point mobility for discrete point connection [3], the effective point mobility for a continuously distributed force can be written as:

$$\underline{Z}^e(x, y) = \frac{\int\int \underline{Z}(x, y)|(\zeta, \eta) \cdot \underline{\sigma}(\zeta, \eta)\, d\zeta\, d\eta}{\underline{\sigma}(x, y)}. \qquad (4)$$

This double integration is taken over the contact area S. The total power transferred through the contact area S is then written as:

$$\underline{Q} = \frac{1}{2} \int\int |\sigma(x, y)|^2 \cdot (\underline{Z}^e(x, y))\, dx\, dy. \qquad (5)$$

Finally, the surface mobility based on the effective point mobility can be obtained as:

$$\underline{Z}^s = \frac{\int\int |\sigma(x, y)|^2 \cdot (\underline{Z}^e(x, y))\, dx\, dy}{\left|\int\int \sigma(x, y)\, dxdy\right|^2}. \qquad (6)$$

To implement the above development, one has to specify the force distribution at the interface. This is a rather difficult task. Firstly, the dimension of the contact area can be comparable to the governing wavelength of interest, thereby resulting a spatial force distribution. Secondly, it is very difficult to exactly specify the contact condition between a machine and its support. The next two sections assume an idealized firm contact condition with either a uniform, conphase force distribution or a uniform, conphase velocity distribution prescribed at the contact area.

3. ASSUMPTIONS AND GOVERNING EQUATIONS

In built-up structures such as ships, buildings and aircraft, power units are often connected to plate–like supporting structures via isolators. These structures are often finite, inhomogeneous and complex. However, it is feasible to consider the plate-like structures as infinite and homogeneous when studying high frequency vibration transmissions [6]. In addition, the following assumptions are made:

a. loses in the plate and local damping are neglected;
b. the plate vibrates in pure bending (flexural) mode;
c. rotational inertia and shear deformation are neglected; and
d. the plate thickness is assumed to be only a fraction of the governing wavelength and bending wave equation for homogeneous, thin plate is valid.

The forced bending motion of a plate is governed by [7]:

$$\Delta\Delta\underline{v} - k^4\underline{v} = \frac{j\omega}{B}\underline{\sigma}(x, y). \qquad (7)$$

The solution to this equation is the combined zero-order Hankel function of the second kind. As given in [7], the ordinary point mobility of an infinite, homogeneous thin plate is:

$$\underline{Z}_0 = \frac{\underline{v}_0}{\underline{F}_0} = \frac{\omega}{8Bk^2} = \frac{1}{8\sqrt{Bm}} = \frac{8c_B\rho h}{k} \quad , \tag{8}$$

which is real and independent of frequency.

Figure.2 shows the response at point (x, y) due to a force at point (ζ, η). The net response at point (x, y) due to a distributed force over the area S is [7]:

$$\underline{v}(x, y) = \int\int \underline{\sigma}(\zeta, \eta) \cdot \underline{Z}_0 \cdot \Pi(kr)\, d\zeta d\eta. \tag{9}$$

Under the assumptions of no loses and no local damping effect, the active power transferred through the excited region should be equal to the 'far-field' power flow through a circumference $2\pi R$. If one considers the 'far–field' case, the imaginary part of the combined Hankel function can be neglected completely. Using the asymptotic expansion for $H_0^{(2)}(kr)$ ($kr >> 1$), one obtains the far-field velocity distribution as [7]:

$$\underline{v}(x,y) = \frac{\underline{Z}_0\sqrt{2}}{\sqrt{\pi kr}} e^{j\pi/4} \int\int \underline{\sigma}(\zeta, \eta)\, e^{-jkr}\, d\zeta d\eta. \tag{10}$$

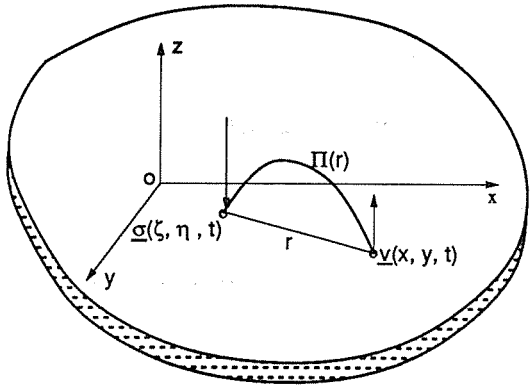

Figure.2 Response at (x, y) due to a Force at (ζ, η)

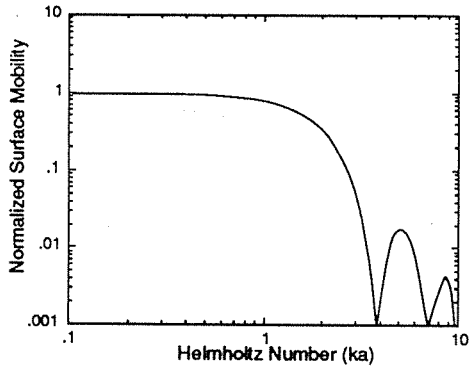

Figure.3 Surface Mobility vs Helmholtz Number

4. SURFACE MOBILITY: UNIFORM, CONPHASE FORCE DISTRIBUTION

For soft isolators, the forces at the interface can be assumed to be conphase and uniformly distributed. The surface mobility of the infinite plate excited with a conphase force uniformly distributed over a circular area will be derived using the complex power and effective mobility respectively.

4.1 Complex Power Approach

Since the force ($\underline{\sigma}_0 = \underline{F}/\pi a^2$) is conphase and uniformly distributed over a circular area of radius, a, the velocity in the far-field can be written as [7]:

$$\underline{v}(R) = \underline{\sigma}_0 \pi a^2 \frac{\sqrt{2}}{\sqrt{\pi kR}} \underline{Z}_0 \frac{2J_1(ka)}{ka} e^{-jkR + j\pi/4} \quad , \tag{11}$$

The power flow through the circumference in the 'far-field' is given by [7]:

$$Q = c_B\, 2\pi R\rho h\, |\underline{v}|^2 = \frac{1}{4}\pi Rk\, \mathrm{Re}(\underline{Z}_0)\, |\underline{v}|^2 = \frac{Z_0}{2}\, |\underline{\sigma}_0 \pi a^2|^2 \left[\frac{2J_1(ka)}{ka}\right]^2 , \tag{12}$$

which should be equal to the active (real part) power transferred through the contact area of $S = \pi a^2$. Thus, one obtains the real part of surface mobility by dividing equation (12) using $\frac{1}{2}|\underline{\sigma}_0 \pi a^2|^2$:

$$\mathrm{Re}(\underline{Z}^{s}) = Z_0 \left[\frac{2J_1(ka)}{ka}\right]^2, \tag{13}$$

which shows that the surface mobility depends on the Helmholtz number, which is the product of the governing wavenumber, k, and the radius, a, of the circular area.

Figure.3 shows the variation of the real part of the surface mobility (normalized by Z_0) with Helmholtz number. It can be seen that the real part of the surface mobility decreases as Helmholtz number increases, implying an increase in the rigidity of the plate. The decrease in the surface mobility also indicates a reduction of power transmission for a given net force. The real part of the surface mobility also shows oscillating behaviour with Helmholtz number. Zero mobilities occur at the zeros of $J_1(ka)$, ie. at ka = 3.8317, 7.0156, 10.1735.

4.2. Effective Mobility Approach

The effective mobility at (R, φ) taking into account the effect of a conphase, uniformly distributed force can be written as:

$$\underline{Z}^{e}(R, \varphi) = a^2 \int_0^1 \int_0^{2\pi} \underline{Z}(R, \varphi)|(\rho, \theta)|\, \rho\, d\rho\, d\theta. \tag{14}$$

The transfer mobility can be written as [7]:

$$\underline{Z}(R, \varphi)|(\rho, \theta) = \underline{Z}_0\, \Pi(kr) = \underline{Z}_0\, (H_0^{(2)}(kr) - H_0^{(2)}(-jkr)), \tag{15}$$

$$\text{with} \quad r = a\sqrt{\rho^2+R^2-2\rho R\cos(\varphi-\theta)}\,.$$

The real part of this transfer mobility can be approximately written as [8]:

$$\mathrm{Re}(\underline{Z}(R, \varphi)|(\rho, \theta)) = \underline{Z}_0\, J_0(kr). \tag{16}$$

Hence, one has the real part of the effective point mobility as:

$$\mathrm{Re}(\underline{Z}^{e}(R, \varphi)) = a^2 \int_0^1 \int_0^{2\pi} \underline{Z}_0\, J_0(kr)\, \rho\, d\rho\, d\theta. \tag{17}$$

As the force is uniform and conphase, the effective point mobility does not depend on the angle φ. Figure.4 shows the variations of effective point mobilities (normalized by $\pi a^2 \underline{Z}_0$) at R = 0.0, 0.5 and 0.9 with Helmholtz number. It can be seen that the three mobility curves coincide at ka = 3.8, which is the zero of J_1 - the first order Bessel function of the first kind. Moreover for ka < 3.8, the effective point mobility is the largest at the centre-point (R = 0.0) and decreases substantially as R increases. At higher ka values, these mobilities also oscillate with ka. For 3.8 < ka < 6.8, the mobility at the center point becomes negative and this implies that the power is transmitted back to the machine from the plate at this particular point.

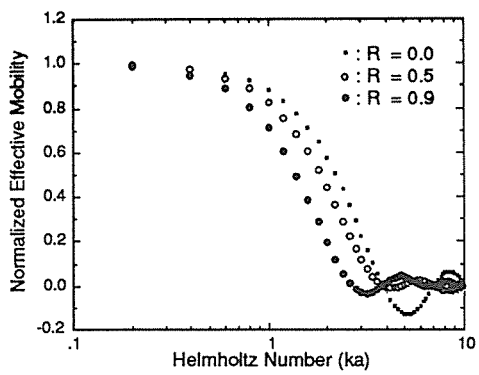

Figure.4 Effective Point Mobility vs Helmholtz Number

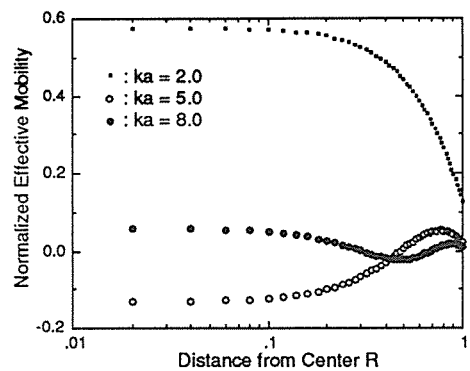

Figure.5 Effective Point Mobility vs Distance from Center

Figure.5 shows the variation of the real part of the normalized effective point mobility with the distance R for three different values of Helmholtz number. For ka = 2.0, it is clearly shown by the little squares that the effective point mobility decreases monotonously with R. While for ka = 5.0 and 8.0, the spatial oscillating behaviours are clearly shown by the open and closed circles.

The real part of the surface mobility normalized by the ordinary point mobility, based on the effective mobility concept, can be written as:

$$\mathrm{Re}(\underline{Z}^s) = \frac{Q}{\frac{1}{2}|F|^2} = \frac{Z_0}{\pi^2} \int_0^{1} \int_0^{2\pi} \int_0^{1} \int_0^{2\pi} J_0(kr)\, \rho\, d\rho\, d\theta]RdRd\varphi. \tag{18}$$

The numerically integrated results are within a few percent of those obtained using the complex power approach as shown in Figure.3.

4. SURFACE MOBILITY: UNIFORM, CONPHASE VELOCITY DISTRIBUTION

When the isolators are relatively stiff compared to the supporting plate, it is reasonable to assume a uniform, conphase velocity distribution at the interface. In order to derive the surface mobility in this case, however, one needs to know the force distribution. This section uses a discretized model to determine the force distribution, surface mobility and effective point mobility.

The transverse velocity of an infinite, homogeneous thin plate is given in equation (7). For a uniform, conphase velocity distribution, one has the following boundary conditions:

$$\begin{aligned} &\underline{\sigma}\,(\zeta, \eta) = 0, && \text{for } \sqrt{\zeta^2 + \eta^2} > a; \text{ and} \\ &\underline{v}(\zeta, \eta) = \underline{v}(0, 0), && \text{for } \sqrt{\zeta^2 + \eta^2} \le a. \end{aligned} \tag{19}$$

These equations define a linear integral equation of Fredholm type of the first kind in terms of unknown stress distribution. Solving this integral equation problem, a stress distribution must be assumed which should be consistent with the boundary conditions.

Hereafter, a discretized model as shown in Figure.6 is used to find the stress distribution [9]. The circular region is divided into MxN sub-regions with constant intervals $\Delta r = a/M$ and $\Delta\varphi = 2\pi/N$ in radial and tangential directions respectively. If M and N are large enough, the effect of the forces at each sub-region can be approximated by the effect of a point force

$$\underline{P}_{kl} = \int_{\rho_k}^{\rho_k+\Delta r} \int_{\varphi_l}^{\varphi_l+\Delta\varphi} \underline{\sigma}(\rho_k, \varphi_l)\, d\rho d\varphi, \tag{20}$$

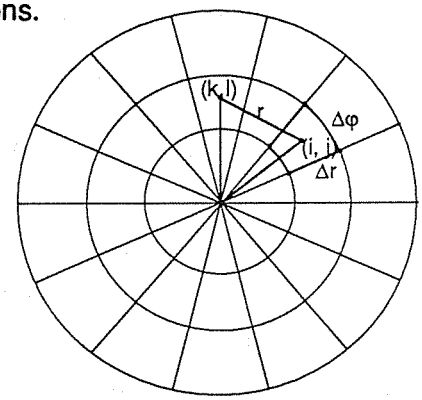

Figure.6 Discretised Model of a Circular Area

acted at the center of the sub-region.

The velocity at the center of sub-region (k, l) due to a point force acting at the center of sub-region (i, j) is given by:

$$\underline{v}\,(k, l)|(i, j) = \underline{Z}_0\, \underline{P}_{ij}\, \Pi(kr), \tag{21}$$

and

$$r = \frac{a}{M}\sqrt{(k-0.5)^2\,(i-0.5)^2 - 2(k-0.5)(i-0.5)\cos(j-l)\Delta\varphi}.$$

Thus, the velocity at the center of sub-region (k, l) taking into account forces acting at the centers of all the sub-regions becomes:

$$\underline{v}\,(k, l) = \underline{Z}_0 \sum_{i=1}^{M} \sum_{j=1}^{N} \underline{P}_{ij}\, \Pi(kr), \tag{22}$$

which can be written in a matrix form of

$$\{\underline{v}\} = \{\underline{T}\}\{\underline{P}\}^T, \tag{23}$$

where $\{\underline{v}\}$ and $\{\underline{P}\}$ are vectors of MxN elements, and $\{\underline{T}\}$ is a square matrix of $(MxN)^2$ elements. Due to the axially symmetric force and velocity distributions, the force and velocity will only depend on the radial coordinate. Thus, equation (23) can be reduced to:

$$\{\underline{v}\} = [\underline{U}]\{\underline{P}\}, \tag{24}$$

$$\{\underline{v}\} = \{\{\underline{v}(1), \underline{v}(2), \underline{v}(3), \ldots.\underline{v}(M)\},$$

$$\{\underline{P}\} = \{\{\underline{P}(1), \underline{P}(2), \underline{P}(3), \ldots.\underline{P}(M)\},$$

$$\{\underline{U}\} = \{\{\underline{U}(1,1), \underline{U}(1,2),\underline{U}(1,3),\ldots\ldots\underline{U}(1,M),$$
$$\{\underline{U}(2,1), \underline{U}(2,2),\underline{U}(2,3),\ldots\ldots\underline{U}(2,M),\ldots\ldots,$$
$$\{\underline{U}(M,1), \underline{U}(M,2),\ldots\ldots\underline{U}(M,M)\} \text{ and}$$

$$\underline{U}_{ij} = \frac{1}{N}\sum_{k=1}^{N}\sum_{l=1}^{N}\underline{T}(ixN+k, jxN+l).$$

After this reduction, only M linear equations are needed to be solved for M unknowns. Once $\underline{P}(i)$ for i=1 to M are determined, one has $\underline{P}(i + jxM) = \underline{P}(i)$ for i = 1 to M and j = 1 to N-1. The total force is written as:

$$\underline{F} = \sum_{i=1}^{MxN}\underline{P}(i) = A\sum_{i=1}^{MxN}\underline{G}(i), \tag{25}$$

where A is the force amplitude and $\underline{G}(i)$ is the force distribution. If A = 1, the normalized force $\underline{P}(i)$ becomes:

$$\underline{P}(i) = \frac{\underline{G}(i)}{\left|\sum_{j=1}^{MxN}\underline{G}(j)\right|}, \tag{26}$$

This gives $|\underline{F}| = 1$. The total complex power at the excited region may be written as:

$$\underline{Q} = \frac{1}{2}\sum_{i=1}^{MxN}\sum_{j=1}^{MxN}\underline{G}(j)\,(\underline{G}(i)\cdot\underline{T}(i,j))^{*} \tag{27}$$

Hence, the surface mobility on the complex power basis is:

$$\underline{Z}^{s} = \frac{\sum_{i=1}^{MxN}\sum_{j=1}^{MxN}\underline{G}(j)\,(\underline{G}(i)\cdot\underline{T}(i,j))^{*}}{\left|\sum_{i=1}^{MxN}\underline{G}(i)\right|}. \tag{28}$$

In order to describe the detailed transmission process at the interface, it is advantageous to use the effective point mobility which is defined as:

$$\underline{Z}^{e}(\rho_i) = \sum_{j=1}^{MxN}\underline{T}(i,j)\frac{\underline{G}_j}{\underline{G}_i}, \tag{29}$$

which is independent of the angular coordinate. In the process of finding the force distribution, one can starts with MxN discrete elements. The surface mobility is then calculated from the obtained force distribution. The above procedure is then repeated for (M+1)x(N+1) elements. Thereby, the relative error with respect to the surface mobility is calculated and the complete process is terminated when the error is smaller than a given value.

Figure.7 shows the force distribution determined using the above method for different Helmholtz numbers (ka). In the figure, the arrows point in the direction of increasing ka. It can be seen that, independent of ka, the forces at $r < 0.7a$ compared with those at $r > 0.7a$ are very small

and are out of phase. This implies compressive forces and tensile forces respectively. As ka increases, the forces tend to become uniform. Hence, as Helmholtz number increases, ie. a/λ becomes large, the region affected by the boundary conditions becomes small.

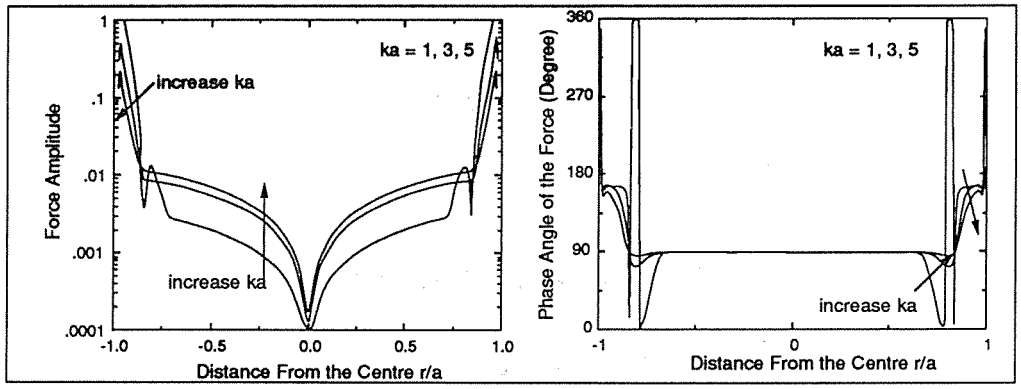

Figure.7 Spatial Variation of the Force Distribution for ka = 1, 3 and 5

Figure.8 shows the spatial variation of normalized effective point mobilities for various Helmholtz numbers. From this figure it can be seen that the maximum effective mobility occurs at the centre and the effective point mobility decreases rapidly as approaching the boundary. It can also be seen that the effective point mobility decreases rapidly as Helmholtz number increases. For r < 0.7a, there is no change in the phase angle of the effective point mobility, independent of ka. However, towards the boundary, the phase angle varies significantly.

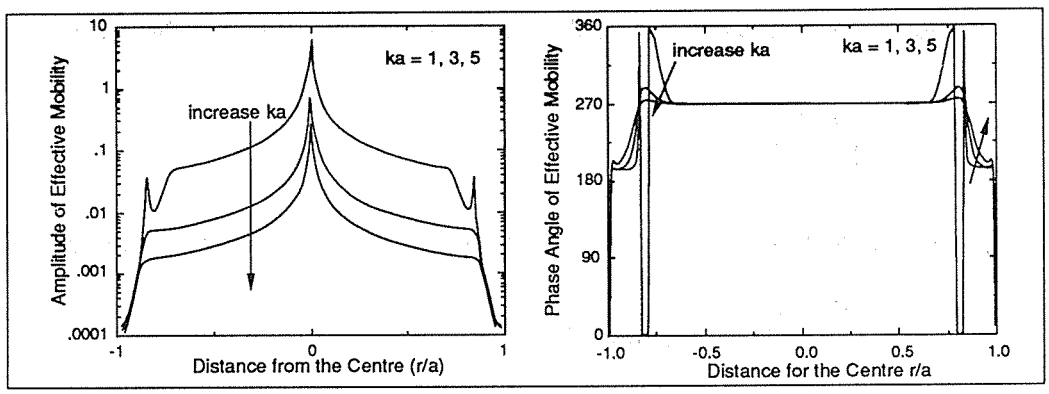

Figure.8 Spatial Variation of Normalized Effective Mobility for ka = 1, 3 and 5

The real part and imaginary part of the normalized surface mobility are shown in Figure.9. It can be seen from this figure that the real part of the surface mobility and hence the active power decreases as ka increases. The imaginary part of the surface mobility reaches a minimum at ka = 0.9. However, the real part surface mobility obtained using the uniform, conphase velocity distribution does not show any oscillating behaviour at high Helmholtz numbers.

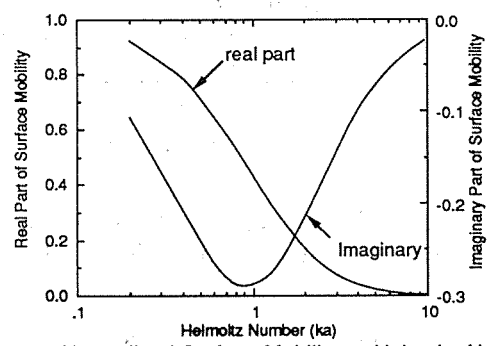

Figure.9 Normalized Surface Mobility vs Helmoltz Number

6. CONCLUSIONS

Using the complex power approach and the effective mobility approache, an attempt has been made to introduce the surface mobility concept to the study of high frequency vibration transmissions for built-up structures coupled via large contact areas. Surface mobilities of an infinite, homogeneous thin plate were derived for a uniform, conphase force distribution and a uniform, conphase velocity distribution respectively. For the latter case, a discretized model was utilized to determine the force distribution with the constraints given by the prescribed velocity distribution at the interface. Although only circular contact areas were considered, the adopted numerical approaches can be applied to contact areas of arbitrary shape.

It is found that the surface mobility decreases very quickly as Helmholtz number increases. This implies a reduction of power transmission can be gained by coupling structures via large contact areas for a given net force. The comparison of the surface mobilities obtained for the two cases shows that the difference in the surface mobility is insignificant, apart from the difference in the force distributions.

It is also interesting to note that the surface mobility obtained using a uniform conphase force distribution oscillates with Helmholtz number. The effective point mobility is the largest at the centre-point and decreases to zero as approaching the boundary. In case of the uniform, conphase velocity distribution, the forces at the central area are very small and are out of phase in comparison with those near the boundary. This implies compressive forces and tensile forces respectively. At high Helmholtz numbers, the forces tend to distribute uniformly.

7. ACKNOWLEDGEMENTS

The financial support received from the Material Research Laboratory of DSTO is gratefully acknowledged. The Authors would also like to acknowledge the support of Mr. C. Norwood of MRL for his interest in this project.

8. REFERENCES

[1] **Harris, C. M.** (1987) " Shock and Vibration Handbook - Third Edition", McGRAW-HILL.

[2] **Ungar, E. E.** and **Dietrich, C. W.** (1965) "High Frequency Vibration Isolation", Journal of Sound and Vibration, pp. 224-241.

[3] **Petersson, B.** and **Plunt, J.** (1982) "On the Effective Mobilities in the Prediction of Structure–borne Sound Transmission between a Source Structure and a Receiving Structure, Part I: Theoretical Background and Basic Experimental Studies", Journal of Sound and Vibration, Vol. 82, No. 4, pp. 517–529.

[4] **Hammer, P.** and **Petersson, B.** (1989.a) "Strip Excitation, Part 1: Strip Mobility", Journal of Sound and Vibration, Vol. 129, No.1, pp. 119–132.

[5] **Hammer, P.** and **Petersson, B.** (1989.b) "Strip Excitation, Part 2 : Upper and Lower Bounds for the Power Transmission", Journal of Sound and Vibration, Vol. 129, No.1, pp. 132–142.

[6] **Skudrzyk, E.** (1958) "Vibrations of a System with a Finite or an Infinite Number of Resonances ", Journal of the Acoustical Society of America, Vol. 30, pp. 1140–1152.

[7] **Cremer, M., Heckl, L.** and **Ungar, E.** (1973) "Structure–borne Sound", Berlin : Springer–verlag

[8] **McLachlan, N. W.** (1955) "Bessel Functions for Engineering", the Oxford Engineering Science Series.

[9] **Holzlohner, U.** (1980) "Vibrations of the Elastic Half–space due to Vertical Surface Loads", Earthquake Engineering and Structural Dynamics, Vol. 8, pp. 405–414.

9. NOTATION

a	= radius	A	= constant
c_B	= velocity of bending wave in plate	B	= bending stiffness
C_{LI}	= velocity of longitudinal wave in plate	$\underline{F}$	= force
$\underline{G}$	= spatial force distribution	h	= thickness of plate
$\overline{H}$	= Hankel function	J	= Bessel function
k	= governing wavenumber	ka	= Helmholtz number
m	= mass per unit area	$\underline{Q}$	= transmitted power
Q	= active power	$\underline{P}_{kl}$	= point force
r	= radius	R	= r/a, far-field radius
r	= distance from excitation point to observing point	$\{\underline{U}\}$	= matrix
		$\underline{v}$	= velocity
$\{\underline{v}\},\{\underline{P}\},\{\underline{T}\}$	= vectors and matrix	x, y, z	= cartesian coordinates
$\underline{Z}$	= complex mobility	$\underline{Z}^s$	= surface mobility
$\underline{Z}_0$	= ordinary point mobility of infinite, homogeneous thin plate	λ	= bending wavelength
		$\underline{Z}(R,\varphi)\|(\rho,\theta)$	= transfer mobility
$\underline{Z}^e$	= effective point mobility	φ, θ	= angular coordinates
ρ	= density; radial coordinate	$\underline{\sigma}(x, y)$	= stress distribution
ω	= angular speed	$\overline{\Pi}$	= combined Hankel function

A.A.S. ANNUAL CONFERENCE 1993, PROGRESS IN ACOUSTICS, NOISE AND VIBRATION CONTROL
NOVEMBER 1993, GLENELG, SOUTH AUSTRALIA

PVDF noise-control source in liquid-filled pipes.

M. Podlesak and R. G. Juniper

Ship Structures and Materials Division, Materials Research Laboratory, DSTO, P.O. Box 50, Ascot Vale, Victoria 3032, Australia.

Abstract

In this paper, we present the results of a study of a PVDF-based sound source for the control of noise propagating in liquid-filled pipes. The advantage of using PVDF(Polyvinylidene fluoride) film lies in its mechanical strength, flexibility and adaptability to mounting on curved surfaces. Our experiments were performed in approximately 100 mm diameter pipe sections, where the required noise control bandwidth ranged from 20 Hz to 2 kHz. The noise control source was designed to achieve sound pressure levels of up to 160 dB (re: 1 μPa) at frequencies as low as 50 Hz. To achieve the required volume velocity of the source, which is relatively large at low frequencies, we resorted to a multilayer PVDF-film design. The need for large signal voltages, normally required to drive the PVDF-based source at low frequencies, was significantly reduced through multilayering and maximisation of the active area size.

1. Introduction

The object of this work is to control noise propagation in water-filled pipes. The type of control under investigation is based on active adaptive techniques. Such techniques utilize an adaptively controlled actuator which either reflects the water-borne noise back to its source through destructive interference and/or absorbs it [1, 2]. The total reflection approach may be thought of as providing a zero impedance boundary or pressure release condition, whereas the absorption approach may be thought of as providing a boundary whose impedance is perfectly matched with the characteristic impedance of the noise propagation medium. In practice, however, the active control actuator may both reflect and absorb energy from an impinging sound field.

Active noise control systems may be based on a feedback or feedforward principle (see for example [2,3]). Fig.1 shows a schematic diagram of a feedforward-type system applied to noise control in a one-dimensional duct. It illustrates the basic elements of such a system, where the signal from a reference sensor provides the control system with information required to regulate the output of the control source to minimize the signal from the error sensor. This results in minimising the noise propagating down the duct past the control source. Our work is based around a similar system, but is applied to water-filled pipes. Much work has been done with active noise control in air-filled ducts (e.g. [1-6]) and finds widespread commercial applications. However, the water-borne counterpart is less frequently encountered and has not received as much attention [6, 7].

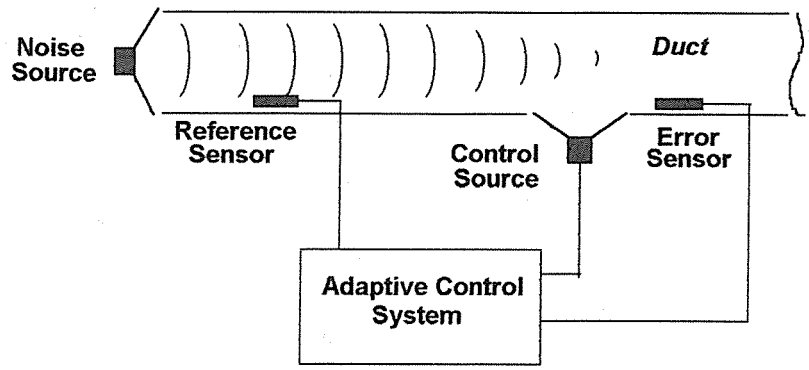

Figure 1. A schematic diagram of a single channel feedforward system applied to noise control in a one-dimensional duct.

Because of relatively high incompressibility and density of water, large variation in hydrostatic pressure levels, high flow rates as well as likely corrosive nature of the fluid medium, the design of the control source transducer needs to be robust. Moreover, the control source needs to have sufficiently broadband response in the frequency range of interest and be able to produce sufficient acoustic volume flows.

In view of the above performance requirements, we have decided to test the viability of PVDF (polyvinylidene fluoride) film in the development of a suitable control source. PVDF, after suitable processing and electrical polarization, displays useful piezoelectric characteristics [8]. Some of the advantageous properties of PVDF film are its mechanical strength, flexibility, and considerable chemical resistance as well as high signal bandwidth (approximately dc - 1 GHz) and low Q. The chief disadvantages, however, are its low threshold level of temperature-induced degradation (approximately 100 °C) and low piezo-strain constant (of the order of 10^{-11} m/V).

In this paper, we report on the development and testing of a PVDF-based noise-control source.

2. PVDF actuator design

The essential design criteria for our PVDF actuator design were:

(i) Suitability for in-line installation of transducer within a water-filled steel pipe and negligible inhibition of fluid flow within the pipe (the wall thickness of the pipe used in our concept demonstrator was 6 mm and the inner diameter 100 mm);
(ii) ability to control broadband noise at levels up to 100 Pa over a frequency range of 20 Hz to 2 kHz;
(iii) electrical, chemical and mechanical robustness.

The first requirement was met by attaching the PVDF film to the inner walls of the pipe as shown schematically in Fig.2. The film electrodes and connections to the driving amplifier are not shown, but these can be readily made flat so as not to interfere with the fluid flow in the pipe. The second requirement is met through matching the acoustic parameters of the control source performance and the PVDF performance specifications. The third requirement is accomplished through the application of a protective coating over the PVDF film surface.

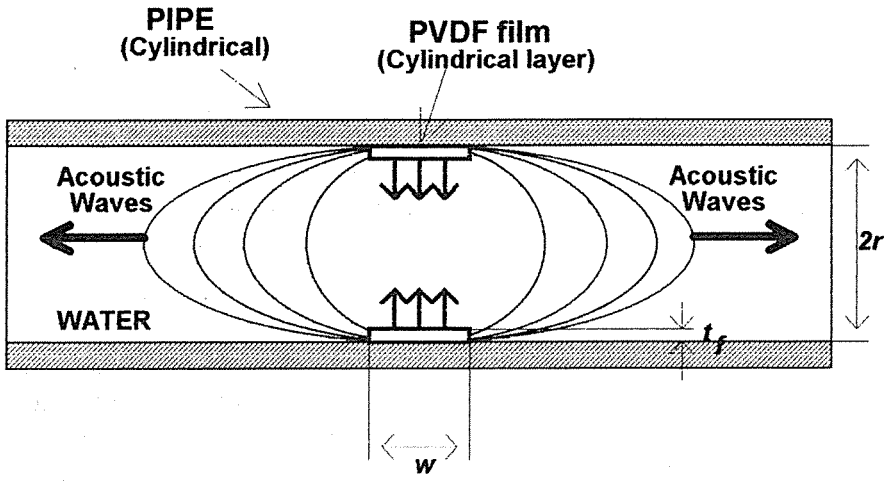

Figure 2. A Schematic diagram of the PVDF film installed within a cylindrical pipe. The film is shown in a sound generation mode without a background noise field.

In the control mode, the control source will mainly provide a pressure release boundary to the noise propagating down the pipe (duct). Hence it is important to focus on the PVDF film as an acoustic volume velocity source rather than a pressure source [9].

In the derivations below, we assume a perfectly rigid duct and only plane wave propagation within the frequency range of interest.

The acoustic volume velocity amplitude Q_s of a simple harmonic plane wave of angular frequency ω, propagating down a duct of cross-sectional area A, is given by

$$Q_s = \frac{Ap}{\rho c} \qquad (1)$$

where ρ and c are the density and speed of sound in water and p is the corresponding acoustic pressure amplitude. Provided that the wavelength is large compared to the duct cross-section, then in the control mode the wave will be almost totally reflected by the control source and the volume velocity at the control source Q_c will be approximately twice that of the incident wave.

In order to determine the necessary voltage level across the PVDF film which is to produce the required control volume velocity Q_c, we need to use the acoustic volume displacement U_c. Using (1) and $Q_c \approx 2Q_s$ and $U_c = Q_c / \omega$, we obtain

$$U_c \approx \frac{2Ap}{\omega \rho c} \qquad (3)$$

The voltage-displacement relation for a PVDF film working in the thickness mode is given by

$$u_f = t_f d_{33} E_f = d_{33}(V_f / t_f) = d_{33} V_f \qquad (4)$$

where u_f is the film displacement along the thickness axis, V_f the voltage applied across the film of thickness t_f, giving rise to an electric field E_f. The term d_{33} is the piezo-strain constant with both electric field and strain along the 3-axis (thickness axis of the film).

For zero order mode waves in the duct, approximately plane waves can be generated by the PVDF film actuator in the cylindrical configuration as portrayed in Fig.2. The volume displacement due to the applied voltage V_f is

$$U \approx 2\pi rw\delta r = 2\pi rwu_f = 2\pi rwd_{33}V_f \qquad (5)$$

where r and w are the film cylinder radius and width, respectively, and δr is the change in the cylinder radius due to the voltage-induced thickness strain in the film. By equating (3) and (5), and using $A = \pi r^2$ and $\omega = 2\pi\nu$, then for a given harmonic noise-pressure-amplitude p of frequency ν, the required control voltage amplitude $V_c = V_f$ is

$$V_c = \frac{pr}{2\pi\nu\rho cwd_{33}} \qquad (6)$$

For very low frequencies, the required voltage across the film may be too high and exceed practical system limitations such as dielectric breakdown of the PVDF film or driving capabilities of the control signal source. This can be overcome by using several layers of the PVDF film connected electrically in parallel. Hence for the same volume displacement, n layers of film yield

$$V_c = \frac{pr}{2\pi\nu\rho cwd_{33}n} \qquad (7)$$

3. PVDF actuator construction

The design of our actuator was based on a 200 mm long flanged section of steel pipe of 100 mm inner diameter and 6 mm wall thickness. The inner surface was lined with a 110 mm wide 10-layer PVDF film stack. The PVDF film selection criteria included reliability, robustness and ability to control noise pressures of the order of 100 Pa at realistic driving voltages. The piezo-strain constant of the film* was specified as $d_{33} \cong 33 \times 10^{-12}$ m V^{-1} and the dc dielectric breakdown strength as 7.5×10^7 V m^{-1}. We have chosen 110 μm thick PVDF film which provided both excellent dielectric breakdown strength (this is expected to be lower as the signal frequency increases) as well as mechanical strength. The film was coated with silver-loaded conducting ink with surface resistivity $R_\square \cong 0.5\ \Omega$.

Using (7) with $\rho \cong 1.0 \times 10^3$ kg m^{-3}, $c \cong 1.5 \times 10^3$ m s^{-1}, $r \cong 5.0 \times 10^{-2}$ m, $w \cong 1.0 \times 10^{-1}$ m, $p \cong 1.0 \times 10^2$ Pa, $d_{33} \cong 33 \times 10^{-12}$ m V^{-1}, and $n = 10$, we obtain the required control voltage as a function of driving frequency ν:

$$V_c = \frac{1.61 \times 10^4}{\nu} \qquad (8)$$

A special assembly fixture was constructed to fix the layers of PVDF film within the pipe using a suitable adhesive. Flat copper tape leads were attached to the film electrodes with a conducting adhesive. The adjacent film layers had electrodes of the same polarity facing one another, so no potential difference existed between them. Also, to avoid mechanical strain cancellation, care had to be taken that the electrode polarity was the same with respect to the film poling direction for all the PVDF film layers.

4. Performance evaluation

* The PVDF film was supplied by INTAQ International, Sydney, and was manufactured by Atochem Sensors, Inc., U.S.A.

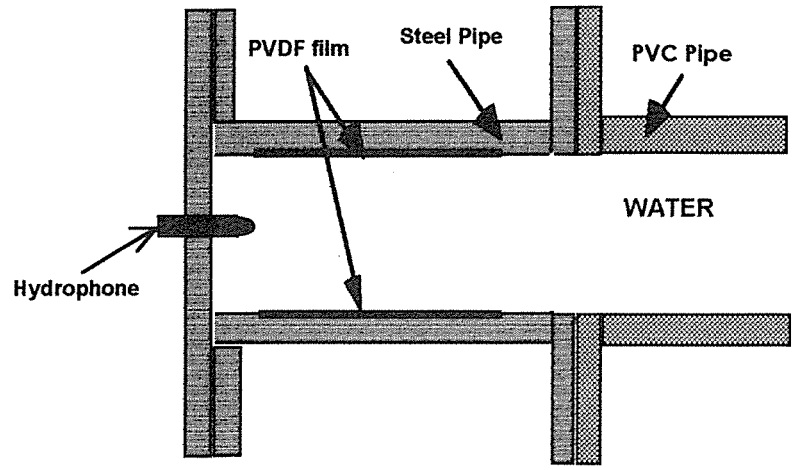

Figure 3. Schematic diagram of the dynamic test set up.

Two types of tests were carried out, static and dynamic. The static test provided the calibration of volume displacement U_c as a function of applied voltage V_c. In the dynamic test, we connected the PVDF actuator to a 40 m long water-filled PVC pipe, shown schematically in Fig.3, which provided an anechoic termination.

The static test was performed by blocking the PVDF actuator pipe-cell, terminated by a narrow glass tube with 2.3 mm inner diameter. Dc voltage was applied to the film in steps of 200 V from 0 to 1400 V. The change in the water level of the tube (approximately 1 mm per 100 V) was measured within an uncertainty of ±0.25 mm, from which the corresponding volume displacement was calculated. The resultant film displacement is plotted as a function of voltage in Fig.4. The gradient of the line in Fig.4 yields the aggregate piezo-strain constant for the ten layers of PVDF film. Using a least square fit for data obtained from film expansion and film contraction tests, we obtained a slope of 1.19×10^{-3} μm V^{-1}. For a single film layer, this represents an effective value of $d_{33} \cong 1.2 \times 10^{-10}$ m V^{-1}, which is 3.64 times greater than the nominal value stated by the film manufacturer. Because of the wide frequency response of PVDF film, we used the new value of d_{33} to amend relation (8) to

$$V_c = \frac{4.43 \times 10^3}{\nu} \qquad (9)$$

The dynamic test was carried out using an Ono Sokki CF-350 dual channel FFT analyser, driving the PVDF film with the analyzer's built-in pseudo-random signal generator via an amplifier with a gain of 10. A Brüel and Kjaer 8103 hydrophone (connected to a Type 2635 charge amplifier) was placed in the centre of the blocked cell as shown in Fig.3, to monitor the acoustic pressure level of the PVDF actuator. The resultant frequency response function is presented in Fig.5, showing the frequency response in terms of the ratio of acoustic pressure and applied voltage. The response is not a simple function of frequency and we suspect that it is strongly affected by the structural modes of vibration of the steel flanged pipe-section. Also, the position of the hydrophone may become critical at high end of our frequency range because of acoustic impedance mismatch between the steel pipe section and the PVC pipe.

Measurements of the wave propagation velocity in the water-filled PVC pipe indicated a wave speed of approximately 300 m s^{-1}, which yields a corresponding characteristic impedance of approximately one fifth of the value for a rigid-walled pipe [7, 10]. This effect is due to the compliant nature of the PVC pipe walls.

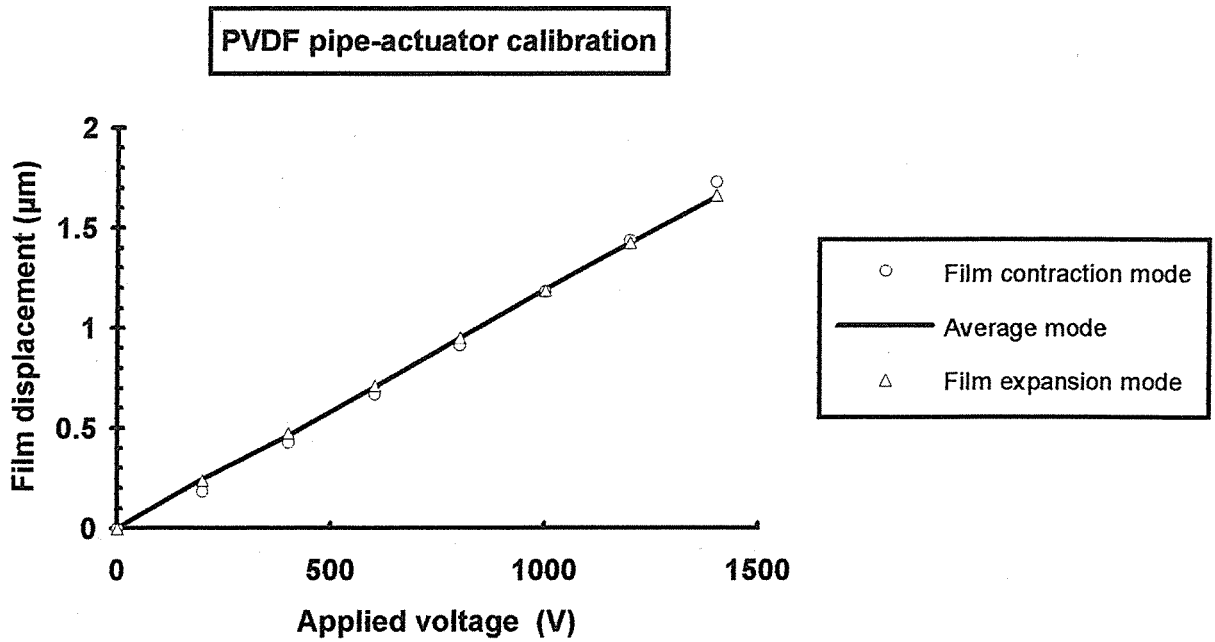

Figure 4. PVDF actuator: Static calibration

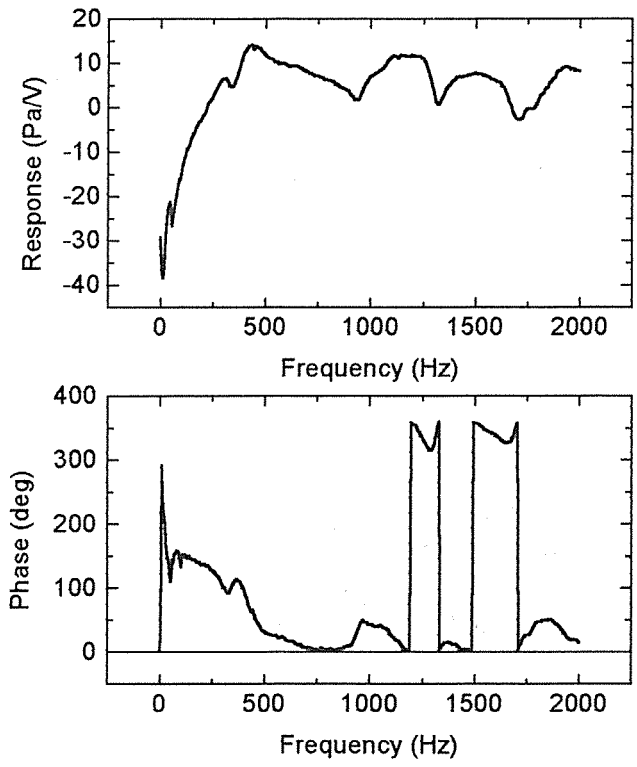

Figure 5. Frequency response function of the PVDF control source connected to a 40 m long PVC pipe filled with water.

The velocity relationship for wave propagation in a duct with yielding walls is described in Reference 10, which shows its characteristics. This dispersive behaviour is expected to affect the actuator's dynamic test response in addition to any modal effects of the actuator assembly.

The performance of the control source may be assessed in terms of the voltage required to control a given noise propagating down a pipe according to (7). This is illustrated in Fig.6, which shows three calculated voltage-frequency relationships for the control of a 100 Pa simple harmonic wave propagating down a water-filled rigid pipe. The first relationship shows the calculated response based on the PVDF manufacturer's data (8) and the second on data obtained from static calibration (9). The third is an estimated response based on the dynamic test, using an acoustic impedance value of approximately $\rho c / 5$. The new impedance value of

the acoustic load changes the outcome of relation (1), giving a five-fold increase to the volume velocity for a given acoustic pressure amplitude. Taking this into account, as well as the fact that we need an acoustic control volume velocity Q_c which is twice the value of the noise volume velocity Q_s, then we have to multiply the experimental frequency response function of the PVDF actuator by a factor of 2.5 in order to obtain its performance characteristic as a noise control device. However, while this is expected to be approximately true in the low frequency region (0 - 300 Hz), the wave impedance changes dramatically as the frequency approaches the ring resonance of the water-loaded tube wall (we estimate this to be $\cong$ 900 Hz for our PVC pipe). Therefore, in the neighbourhood of the ring resonance frequency of the PVC pipe, the acoustic volume velocity may be considerably higher than estimated and would result in lowering the required applied voltage level shown in Fig.6. Resonant modes of the actuator assembly will also affect this voltage level, though further work is required to determine their contribution.

In order to explain the differences between the results from the dynamic tests and the simple relation predicted by (9), we need to fully characterise the acoustic load of the test pipe and the modal behaviour of the actuator assembly. However, the results obtained so far indicate that our prototype of the PVDF control source is capable of generating sufficient volume velocities for the control of noise within the specified frequency and amplitude range at practically achievable voltage levels. Particularly at the high frequency end (1-2 kHz), where our dynamic response predictions may show the greatest deviation from actual behaviour, even a gross error of one order of magnitude would result, at worst, in control-voltage levels not higher than 50 V.

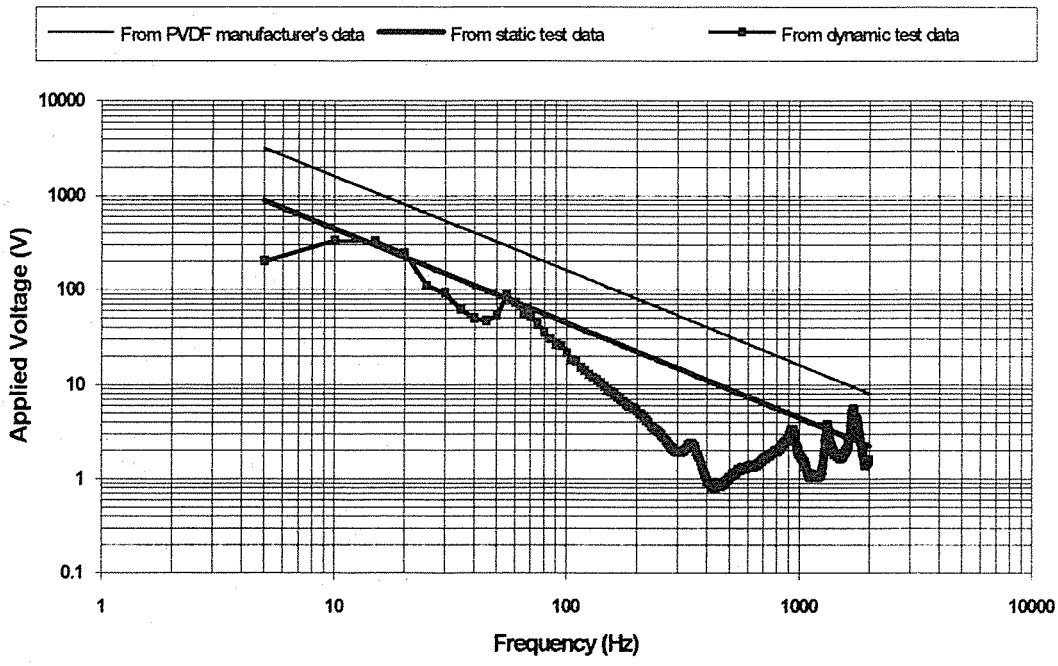

Figure 6. The three graphs illustrate the PVDF actuator voltage required to control a 100 Pa simple harmonic wave propagating down a water-filled rigid duct. The graphs were derived from the manufacturer's data (relation (8)), the static test (relation (9)), and dynamic test respectively.

5. Conclusion

Our performance predictions and test results portrayed in Fig.6 demonstrate that our prototype of the PVDF-based active control source should be capable of blocking 160 dB (re: 1 μPa) noise propagating down a water-filled steel pipe (100 mm inner diameter and 6 mm wall thickness). A number of irregularities have been observed in the actuator's frequency response which are thought to be due to the complex response characteristics of the actuator assembly and the type of acoustic load used during the dynamic testing. However, these types of irregularities are expected to be compensated for by the adaptive filter in an active noise control system.

Future work will involve full characterisation of the dynamic test method and performance tests of the PVDF actuator in an adaptive noise control system.

6. References

1. Orduna-Bustamante F., and Nelson P.A., "An adaptive controller for the active absorption of sound", J. Acoust. Soc .Am., 91 (5), 2740-2747, 1992.

2. Mackenzie Neil C., and Hansen Colin H., "A Review of Controller Hardware and Control Algorithms for Active Noise and Vibration Control", Acoustics Australia, 20 (1), 5-10, 1992.

3. Nelson P.A. and Elliott S.J., Active Control of Sound, Academic press, London 1992.

4. Eriksson L.J., and Allie M.C., "A Practical System for Active Attenuation in Ducts", Sound and Vibration, February 1988.

5. Curtis A.R.D., Nelson P.A., Elliott S.J., and Bullmore A.J., "Active suppression of acoustic resonance", J. Acoust. Soc. Am., 81(3), 624-631, 1987.

6. Hansen Colin, "Active control of noise propagating in ducts", in course notes on Active Control of Noise and Vibration, Volume 1, ed. C. Hansen, Department of Mechanical Engineering, University of Adelaide, Australia, December 1991.

7. Culbreth William G., Hendricks Eric W., and Hansen R.J., "Active cancellation of noise in a liquid-filled pipe using an adaptive filter", J. Acoust. Soc. Am., 83(4), 1306-1310, 1988.

8. Pointon A. J., "Piezoelectric devices", IEE Proc., 129 Pt. A (5), 285-307, 1982.

9. Shepherd I.C., Cabelli A., and LaFontaine R.F., " Characteristic of loudspeakers operating in an active noise attenuator", J. Sound and Vibration, 110(3), 471-481, 1986.

10. Morse Philip M., and Ingard K. Uno, Theoretical Acoustics, Princeton University Press, New Jersey, 1986, pp 475-477.

SENSING VIBRATION TO CONTROL STRUCTURAL RADIATION

Scott D. Snyder
Department of Mechanical Engineering
University of Adelaide, SA 5005

ABSTRACT

The use of shaped piezoelectric polymer film vibration sensors in a vibration source-based adaptive feedforward control system targeting attenuation of acoustic power radiated from a structure is considered. The questions of what should be measured by the sensor to minimise acoustic power, and how the adaptive feedforward active control system should incorporate the measurements, are first addressed. Experimental implementation of an adaptive feedforward control system using optimally shaped piezoelectric polymer film error sensors is then described.

INTRODUCTION

Feedforward active control of structure-based disturbances using a force or moment input, targeting either the vibration explicitly or the resultant acoustic radiation, is a topic of increasing research interest. In structural/acoustic problems, the use of vibration control sources offers several potential advantages over the use of more conventional acoustic control sources, one of these being system compactness; bulky speakers and cabinets can be replaced by compact control sources such as surface mounted or embedded piezoelectric ceramic actuators, creating a "smart structure". A potential hindrance to realising this advantage is the use of acoustic sensors, microphones, to provide an error signal to the control system. Microphones are typically placed in the farfield of a radiating structure to insure that global sound attenuation accompanies the reduction in acoustic pressure at the sensor. Clearly an improvement would be had if vibration error sensors were used in conjunction with vibration control sources.

The use of vibration error sensors in systems targeting a reduction in structural vibration is commonplace. Such systems can be designed to explicitly reduce structural modal amplitudes, measured using some form of spatial filtering. Minimising the velocity of structural modes is not, however, always the best approach to minimising acoustic radiation from the structure, especially when only a limited number of actuators are being used. There are, in fact, two ways in which vibration sources can reduce acoustic power radiation. The first of these is velocity, or modal, control. The second is essentially acoustic control, where the velocity distribution of the structure is altered so as to optimise the inherent (acoustic) pressure reduction phenomena, such as intercellular cancellation in plates. It has been demonstrated, both theoretically and experimentally, that in this instance an *increase* in structural velocity may accompany a reduction in radiated acoustic power [1,2]. Clearly a control system which is constrained to reducing structural velocity is inappropriate for control of structural radiation.

This paper considers the problem of sensing some measure of structural vibration to provide an error signal to an adaptive feedforward active control system to attenuate radiated acoustic power. The first questions to be addressed are, what should be sensed to maximise the levels of global attenuation of the error criterion of interest, radiated acoustic power, and how should an adaptive feedforward active control system using these vibration-based error signals be implemented? Once these concerns are answered, experimental implementation of an adaptive feedforward control system using optimally shaped piezoelectric polymer film error sensors, targeting both harmonic and random noise disturbances, will be described.

GENERAL THEORY

Consider some generic structure, subject to harmonic excitation by an unspecified primary forcing function. The aim of active control is to globally attenuate some measure of the system response, normally expressible as a quadratic function of the structural modal velocities. This measure may be vibrational, such as the kinetic energy of the structure, or acoustic, such as radiated acoustic power or sound transmission into a coupled enclosure. Limiting consideration to a finite number of modes, each of these quantities, or global error criterion, can be expressed in the form

$$J = \mathbf{v}^H \mathbf{A} \mathbf{v}, \tag{1}$$

where J is the global error criterion of interest, $\mathbf{v}$ is the vector of complex modal velocity amplitudes, ^{H} is the matrix Hermitian (conjugate transpose), and $\mathbf{A}$ is some real, symmetric, positive definite transfer matrix. As $\mathbf{A}$ is a real symmetric matrix it can be diagonalised by the orthonormal transformation

$$\mathbf{A} = \mathbf{Q} \Lambda \mathbf{Q}^{-1}, \tag{2}$$

where $\mathbf{Q}$ is the orthonormal transform matrix, whose columns are the eigenvectors of the transfer matrix $\mathbf{A}$, and Λ is the diagonal matrix of associated eigenvalues. The form of $\mathbf{A}$ dictates that the eigenvectors in $\mathbf{Q}$ will be orthogonal. If the transformation of equation (2) is substituted into equation (1) the generic global error criterion expression becomes

$$J = \mathbf{v}^H \mathbf{A} \mathbf{v} = \mathbf{v}^H \mathbf{Q} \Lambda \mathbf{Q}^{-1} \mathbf{v} = \mathbf{v}'^H \Lambda \mathbf{v}', \tag{3}$$

where the vector of transformed modal velocities $\mathbf{v}'$ is defined by the expression

$$\mathbf{v}' = \mathbf{Q}^{-1} \mathbf{v} = \mathbf{Q}^T \mathbf{v}. \tag{4}$$

Observe that the orthonormal transformation has decoupled the global error criterion expression, so that it is now equal to a weighted summation of the form

$$J = \sum_{i=1}^{N_m} \lambda_i |v_i'|^2, \tag{5}$$

where λ_i is the ith eigenvalue of $\mathbf{A}$, v'_i is the ith transformed modal velocity of the vector $\mathbf{v}'$, and the summation is over the N_m structural modes being modelled. The important point to note about the error criterion as expressed in equation (5) is that v'_i is not necessarily equal to the velocity amplitude of the ith structural mode v_i, but is rather equal to some orthogonal grouping of modal contributions, defining the ith principle axis of the error "surface" (the plot of error criterion as a function of modal velocity) defined by the quadratic criterion of equation (1).

Consider now the problem of implementing an adaptive feedforward active control system to attenuate the global error criterion of equation (1), where the control source provides a direct input to the structure (such as via an electro-dynamic shaker or a piezo-electric ceramic actuator). The desired error signal, to be minimised by the control system, is some measure of structural velocity, which can be decomposed into a set of orthogonal constituents by, for example, the use of a custom sensor such as shaped piezoelectric polymer film. One approach to the decomposition of the error signal is to base it upon the *in vacuo* mode shape functions of the structure. However, using this data in its "raw" form may not produce the desired result, as strictly speaking the value of the global error criterion is based not solely upon individual *in vacuo* modal contributions but rather upon these terms in conjunction with modifications resultant from other coexisting modes; simplifying this holistic view by considering only individual contributions is often detrimental to system performance, as will be demonstrated later in this paper. A better approach is to

resolve the orthogonal transformed modal velocities in v' and simply weight the contributions by the associated eigenvalues. Not only does this implicitly account for the off-diagonal, or cross-coupling, terms in the transfer matrix $\boldsymbol{A}$ but it may also reduce the number of error signal inputs to the controller required to obtain a satisfactory result, as some eigenvalues may be so small as to make contributions to the error criterion by the associated transformed modal velocities negligible.

MINIMISING ACOUSTIC POWER vs. MINIMISING VIBRATION

The error criterion of interest here is minimisation of radiated acoustic power. In order to fit this criterion into the general form of equation (1), it can be shown [3] that for an infinitely baffled planar structure

$$A(i,\iota) = \frac{\omega\rho_o}{4\pi} \int_S \int_S \psi_i(\vec{x}') \frac{\sin kr}{r} \psi_\iota(\vec{x})^T \, d\vec{x}' \, d\vec{x}. \tag{6}$$

From the defining relation for the terms in the transfer matrix $\boldsymbol{A}$ given in equation (6) is immediately apparent that in this instance $\boldsymbol{A}$ is *not* constrained to be a diagonal matrix. This result can be contrasted with that obtained for systems specifically targetting a reduction in vibration levels, where $\boldsymbol{A}$ *will* be a diagonal matrix. It is therefore fundamentally incorrect to design a control system targeting a reduction in structure borne sound which is constrained to minimise the amplitudes of the individual structural modes.

To study further the problem of controlling radiated acoustic power it will be useful to specialise the discussion to a specific structure, the one chosen here being a baffled, simply supported rectangular panel. For a simply supported rectangular panel of length L_x and width L_y the structural mode shape function is

$$\psi_{m,n}(x,y) = \sin\frac{m\pi x}{L_x} \sin\frac{n\pi y}{L_y}, \tag{7}$$

where m, n are the modal indices in the x and y directions, respectively, and $\vec{x}=(x,y)$. At low frequencies, such that $(kL_x/m\pi)<<1$, $(kL_y/m\pi)<<1$, where k is the acoustic wave number, it can be shown that the terms in the transfer matrix $\boldsymbol{A}$ can be written in terms of modal radiation efficiencies as [3]

$$A(i,\iota) = \frac{\rho_o c_o L_x L_y}{8} \frac{\left(1+(-1)^{m_i+m_\iota}\right)\left(1+(-1)^{n_i+n_\iota}\right)}{4} \frac{\frac{m_i n_i}{m_\iota n_\iota}\sigma_i + \frac{m_\iota n_\iota}{m_i n_i}\sigma_\iota}{2}, \tag{8}$$

where σ_i and σ_ι are the radiation efficiencies of the ith and ιth modes. While using radiation efficiencies as described by [4] to calculate the terms in the transfer matrix $\boldsymbol{A}$ is strictly only acceptable at low frequencies, the relationship between the terms which is described by equation (8) reveals interesting characteristics about the eigenvalues and eigenvectors of this matrix. Firstly, note that only modes with like index pairs, such as (odd,odd) modes, with exert a mutual influence on each other, as would be expected. Secondly, observe the terms in $\boldsymbol{A}$ will be highly frequency dependent, the same as radiation efficiencies. However, a closer inspection of the problem in light of the data given in reference [3] shows that while the absolute values of the terms will vary significantly with frequency, the relative (to each other) values of the terms, which are governed by the ratio of two modal radiation efficiencies, will vary much more slowly. It is the relative values which will be important in determining the eigenvectors, and hence the

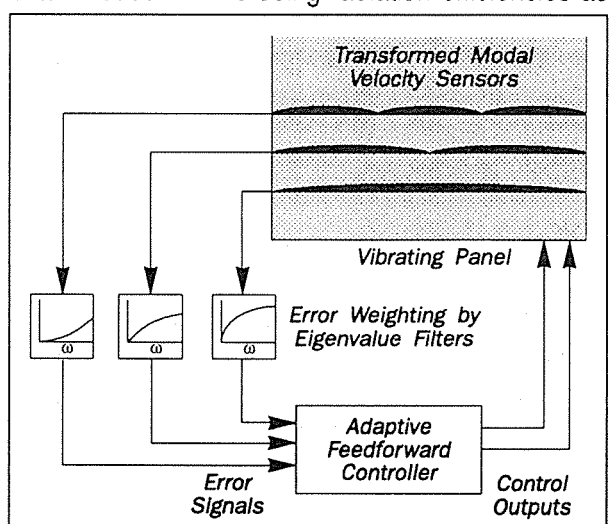

Figure 1 Outline of feedforward control system using shaped error sensors.

transformed modal velocities V_j, while the absolute values will dictate the value of the eigenvalues. Therefore, at some given frequency ω_1 it may be possible to sense a transformed modal velocity (eigenvector) which is strictly only correct at some other frequency ω_2, weight it by the ω_1 frequency-correct eigenvalue, and obtain a satisfactory result. This would enable the use of a shaped (to measure a transformed modal velocity) piezoelectric polymer film sensor, the shape of which is strictly only optimal at a single frequency, to provide satisfactory levels of acoustic power attenuation over an enlarged frequency range. The adaptive feedforward control arrangement would then look something like what is shown in figure 1, where the output of the shaped piezoelectric polymer film "transformed modal velocity sensors" are passed through "eigenvalue filters" and provided to the controller as an error signal. The frequency response of a given eigenvalue filter is defined by the magnitude of the associated eigenvalue as a function of frequency. In fact, the eigenvalues can be viewed as defining the "radiation efficiency" of a given (orthogonal) set of radiating structural modes, the constituents of which are defined by the eigenvectors of the transfer matrix.

EXPERIMENTAL INVESTIGATION

To investigate this further, consider now a steel panel of dimensions 1.8m x 0.88m x 10.1mm, subject to harmonic excitation within the frequency band 30Hz - 200Hz. In this range there are seven modal resonances, as outlined in table 1. If the transfer matrix is calculated at any given frequency in this band using 60 structural modes and then decomposed as outlined in equation (2) it is found that at low frequencies only three acoustic power modes may be considered as "significant", significance being defined by the associated eigenvalue which will weight the influence which the transformed mode has upon the calculation. These transformed modes are, in order of importance, based upon orthogonal groupings of (odd,odd), (even,odd), and (odd,even) structural modes, and will be referred to as transformed modes w(o,o), w(e,o), and w(o,e), respectively. As the frequency increases, two more modes, based upon a second grouping of (odd,odd) modes and a grouping of (even,even) modes, become important. A plot of the variation in eigenvalues of these transformed modes as a function of frequency is given in figure 2. The interesting point to note here is that while the eigenvalues of these transformed modes vary greatly with frequency, the constituent components of the eigenvectors vary by a relatively small degree. Consider for example the w(o,o) mode, which is shown in figure 2 to have the greatest radiation potential. Table 2 lists the values of the five most significant contributions from the first 60 structural modes to this transformed mode at 30Hz and 100Hz. This mode is dominated by the (1,1), (3,1) and (1,3) structural modes, with the proportional contributions changing only slightly.

Table 1 Experimental and theoretical panel resonances below 200 Hz.

Mode	Experimental Resonance Frequency (Hz)	Theoretical Resonance Frequency (Hz)
1,1	40.5	39.5
2,1	64.0	62.3
3,1	101.5	100.4
1,2	132.5	135.0
4,1	153.5	153.7
2,2	155.5	157.9
3,2	195.0	195.9

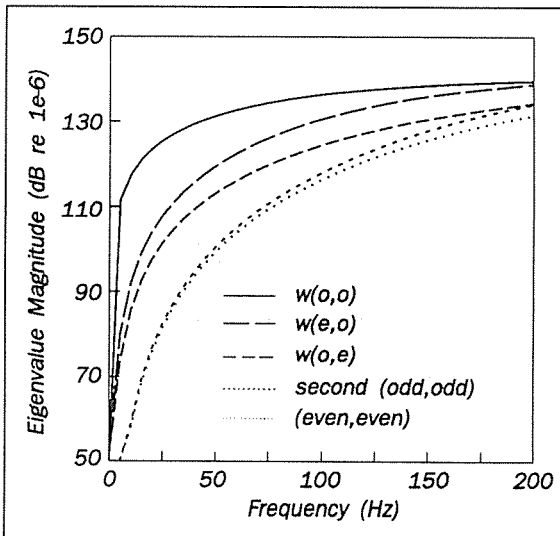

Figure 2 Eigenvalues of the first five transformed modes.

EXPERIMENTAL INVESTIGATION

To implement the above outlined feedforward active control system, shaped piezoelectric polymer film sensors can be used to measure transformed modal amplitudes, with the constituents of the transformed modes

defined at a single frequency. These signals could then be passed through "eigenvalue filters", filters which have the frequency response characteristics defined by the eigenvalues associated with each transformed mode, and used as error signals for an adaptive feedforward control system to minimise. The experimental work presented here, however, will consider the minimisation of *unweighted* transformed modal velocities, thereby avoiding the need to build a set of "eigenvalue filters". Simulation results [5] have shown that such an approach is only slightly sub-optimal with the control source at (0.9m,0.24m), and it will simplify this initial investigation. The experiments will have two basic aims: to compare the effect of minimising the amplitude of an *in vacuo* structural mode and a transformed mode at both discrete frequencies (pure tone excitation) and over a frequency band, and to examine broadband control of radiated acoustic power by minimising the amplitude of transformed structural modes.

Table 2 Constituents of the first transformed mode w(o,o) as defined at 30 Hz and 100 Hz.

Mode	30 Hz Value	100 Hz Value
1,1	0.913	0.919
3,1	0.229	0.199
5,1	0.138	0.117
1,3	0.233	0.241
1,5	0.141	0.143

Shaped piezoelectric polymer film sensors will be employed to measure both the *in vacuo* and transformed structural modes used in the experiments. Such sensors will output a charge proportional to the second (spatial) derivative of the mode shape function. As both *in vacuo* and transformed structural modes are orthogonal (with other *in vacuo* or transformed structural modes), and separable in the *x* and *y* directions, modal responses could be approximately measured by fabricating separate sensors to be orientated in the *x* and *y* directions whose width is described by the *x* and *y* components of the modes (neglecting lateral excitation of the sensor). The output from sensors in the *x* and *y* directions could be multiplied in the frequency domain or convolved in the time domain to give a total mode output. In the experiments presented here, however, only one component, *x* or *y*, was measured for each mode, and fed directly into a time domain adaptive feedforward control system (errors in this simplified approach will be discussed further shortly).

In the experiments a 1.8m x 0.88m x 10.1mm meter steel plate is clamped on knife edges mounted in a heavily damped enclosure to simulate simply supported boundary conditions, and situated in a semi-anechoic room. The experimental resonances of the plate below 200 Hz are given in table 1. A primary

Table 3 Acoustic power outputs and reductions for pure tone excitation with the feedforward control system minimising the signal from the (3,1) mode sensor and the w(o,o) transformed mode sensor.

Frequency (Hz)	Primary Power Output (dB)	(3,1) Mode Controlled Power Output (dB)	First Transformed Mode Controlled Power Output (dB)	(3,1) Mode Controlled Power Reduction (dB)	First Transformed Mode Controlled Power Reduction (dB)
40	101.0	84.3	66.3	16.7	33.7
45	83.4	99.8	63.2	-16.4	20.2
85	64.4	81.5	66.1	-17.1	-1.7
95	79.0	80.3	74.2	-1.3	4.8
101	99.6	82.1	80.7	17.5	18.9

source electrodynamic shaker, mounted in the enclosure, is attached to the plate at (0.35m, 0.64m). A singlecontrol source was used in the experiments, located at (0.9m, 0.24m) or (1.35m, 0.24m) as described. A traverse was mounted above the plate, which moved an acoustic intensity probe over a 24 x 12 (288) point grid, measuring acoustic intensity 100mm above the plate in 1/12 octave bands. The acoustic power output of the plate was calculated from these measurements. The control signal was generated by an adaptive feedforward controller. For the pure tone excitation experiments to be described, a simple 4-tap FIR filter, adapted using the filtered-x LMS algorithm, was used. For the broadband experiments, an IIR filter with 35 feedforward taps and 20 feedback taps was used, adapted using a similarly modified gradient algorithm.

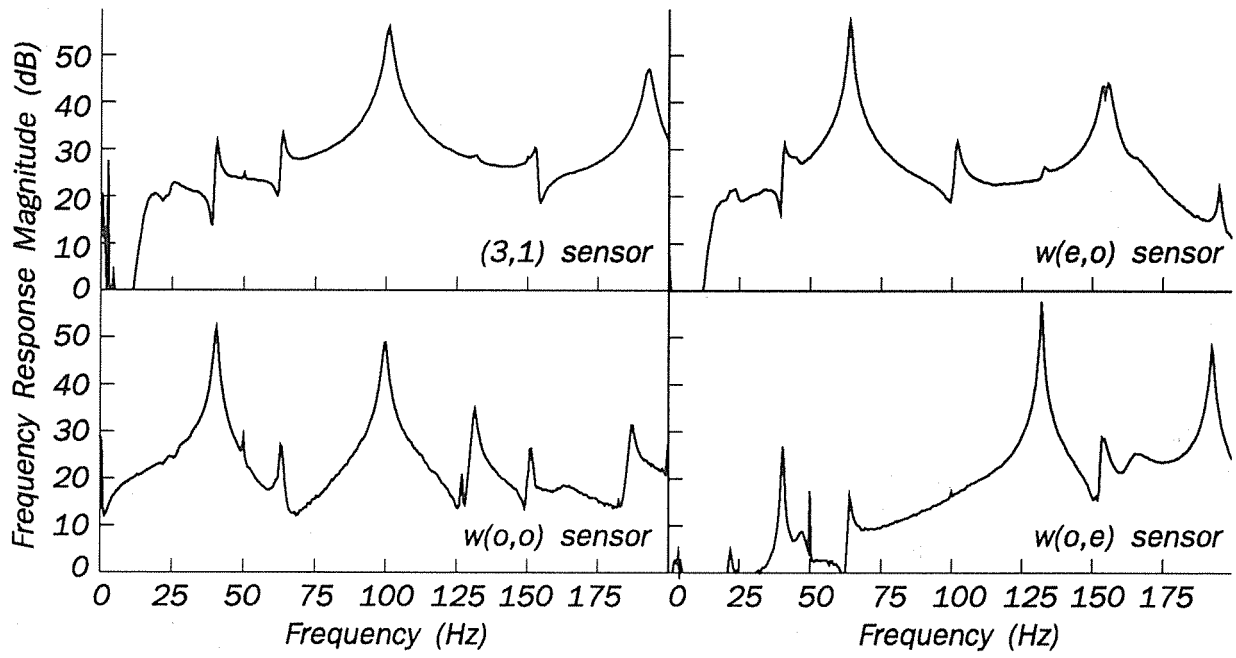

Figure 3 Frequency response magnitude of experimental shaped sensors.

The modes which are to be minimised by the feedforward control system are the (3,1) structural mode and the w(o,o), w(e,o) and w(o,e) transformed modes as defined at 30 Hz. Only one direction of these quantities will be measured in the implementation, as discussed, to simplify the experiments. For the (3,1) structural mode and the w(o,o) and w(e,o) transformed modes it will be the *x* direction, while for the w(o,e) mode it will be the *y* direction. These were chosen so as to most closely approximate the desired response with a single measurement. The strips were located close to the center of the plate to help filter out unwanted modal components. The experimental frequency response characteristics of the four sensors are shown in figure 3. With the (3,1) modal sensor, note that the response of the desired mode is approximately 25 dB above that of the neighbouring (1,1) and (2,1) modes. The only other peak is at the (3,2) resonance, which would be eliminated if the *y* component of the mode had been taken into account. With the first transformed modal sensor, the (1,1) and (3,1) modal resonances are dominant, which is the desired response of the sensor. The (1,2) and (3,2) resonances are also present, approximately 15 dB below the amplitude of the dominant modes. These modes are undesired, and would again be eliminated if the *y* component of the transformed mode was accounted for. With the second transformed mode sensor, the (2,1) mode is dominant, with a significant level of the (4,1) mode, which is desired. Unfortunately, the (2,2) is also present, which would again be eliminated if the *y* component of the mode was measured. Finally, with the third transformed mode sensor the (1,2) and (3,2) modes are clearly dominant, which is the desired feature. In light of this data, the principal error in the experiments to be described which is introduced by measuring only part of the transformed modes is the (2,2) contribution to the response of the second sensor.

The first set of experiments is aimed at comparing minimisation of the (3,1) structural mode and the w(o,o) transformed mode with the control source at (0.9m, 0.24m). Table 3 lists the acoustic power output of the panel at various discrete frequencies under primary, (3,1) controlled, and w(o,o) controlled conditions. At every frequency, including the resonance of the (3,1) mode at 101 Hz, minimisation of the w(o,o) transformed

mode produced a result superior to that obtained by minimisation of the (3,1) modal amplitude. This was the characteristic predicted by the simulation of the previous section.

There are, however, a few differences between theory and experiment. Firstly, at the (1,1) resonance of 40 Hz minimisation of the (3,1) mode sensor error signal produced 17 dB of attenuation, while the theoretical work of the previous section predicted a significant increase in the acoustic power output. This is due to the limitations of the sensor in filtering out unwanted modal responses, such as the (1,1) mode resonance peak. Secondly, the off-resonance performance of the (3,1) mode sensor is *worse* than predicted by the theoretical studies of the previous section. It is presumed that this is due to contamination in the error signal, which was extremely small at these frequencies. Despite these discrepancies, the qualitative agreement between the theoretically predicted and experimental performances obtained by minimising the sensor signals is good.

Illustrated in figure 4 is the result of minimising the (3,1) mode sensor signal and the first transformed mode sensor signal for broadband excitation up to 200 Hz. Observe that when minimising the (3,1) sensor signal the acoustic power output at the (3,1) mode resonance frequency is significantly reduced, as would be expected. There is also some reduction at the (3,2) resonance frequency, as the sensor is also sensitive this mode as shown in the frequency response characteristics of figure 3. This, however, is the extent of the positive results achieved, and the benefit is offset somewhat by a significant increase in the power output at the (1,2) resonant frequency. When minimising the first transformed mode sensor signal, however, there is significant attenuation of the acoustic power output at both the (1,1) and (3,1) resonance frequencies, without a significant increase at any frequency. Clearly the latter result is superior.

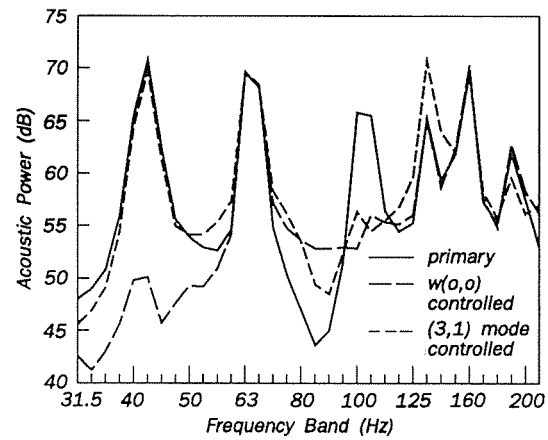

Figure 4 Radiated acoustic power with random excitation, minimisation of w(o,o) transformed mode, and minimisation of (3,1) mode.

The second stage of the experimental work is targeted at broadband control of radiated acoustic power using the shaped sensors. Figure 5 illustrates the acoustic power output of the panel under primary excitation, and under the action of a control system which minimises the w(o,o) transformed mode, and the w(o,o) and w(o,e) transformed modes, with a control source located at (0.9m,0.24m). Observe that when the first transformed mode sensor signal is minimised there is significant attenuation of the power output at the (1,1) and (3,1) resonance frequencies, while the inclusion of the third transformed mode sensor results in significant attenuation at the (1,2) and (3,2) resonance frequencies as well. Note that with this particular control source arrangement (located halfway along the *x* direction of the panel) it is not possible to change the amplitude of any mode having an even index in the *x* direction.

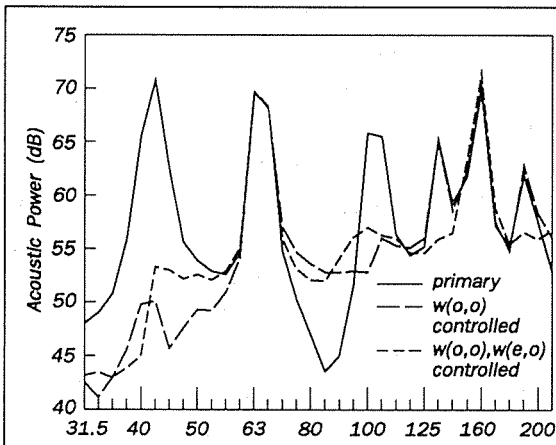

Figure 5 Radiated acoustic power with broadband excitation, minimisation of w(o,o) transformed mode, and minimisation of w(o,o) and w(o,e) transformed modes.

The final experimental result to consider is that obtained when the excitation frequency band is increased to 400 Hz. From the characteristics of the eigenvalues shown in figure 2, it can be concluded that many more transformed modes are significant radiators, casting doubt on the ability of a control system which minimises only three transformed modes to produce any real levels of acoustic power attenuation. There are also 17 structural modes resonant at frequencies below 400 Hz, further complicating the problem. Illustrated in figure 6 are the primary and

controlled acoustic power outputs for this case, where the control source is now located at (1.35m,0.24m), and all three transformed modes are being minimised. Observe that there is significant attenuation at lower frequencies, with reduced levels of attenuation at higher frequencies, although still notable in many bands. Perhaps more importantly, note that there is no noticeable increase in the acoustic power output of the panel at any frequency, a problem which is common at higher frequencies with the use of microphone error sensors. This suggests that with broadband excitation, the use of shaped piezoelectric polymer film sensors to provide an error signal for a feedforward adaptive controller is superior to the use of microphones when vibration control sources are used, whether compactness is an issue or not.

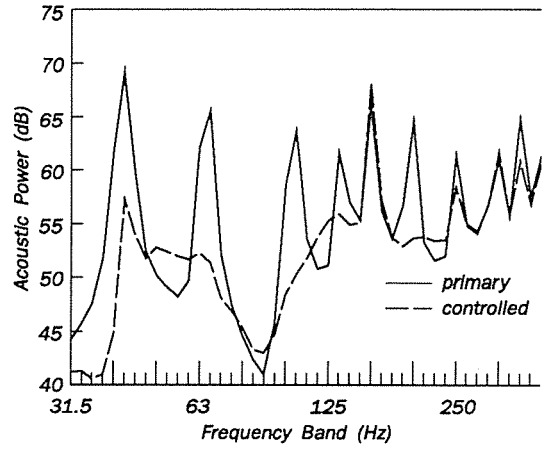

Figure 6 Radiated acoustic power with broadband excitation and minimisation of w(o,o), w(e,o) and w(o,e) transformed modes.

CONCLUSIONS

The design of optimally shaped piezoelectric polymer film sensors to provide error signals for an adaptive feedforward active control system targeting a reduction in free field structural radiation using vibration sources has been considered. It was shown that by performing an orthonormal decomposition on the governing relationship for acoustic power it is possible to define transformed modes, which are orthogonal sets of structural modes radiating as a single unit. If these transformed modes, weighted by the eigenvalues associated with them from the orthonormal decomposition, are minimised in amplitude, radiated acoustic power will be minimised. For low frequency excitation, typically only a few transformed modes are important, greatly decreasing the error sensing requirements. The transformed modes are only mildly frequency dependent, a dependence which can often be neglected at low frequencies in practice without adverse effects. Experimental results minimising transformed modes as measured by shaped piezoelectric polymer film sensors show that significant levels of acoustic power attenuation can be obtained using this approach when the structure is subject to low frequency sinusoidal or broadband excitation.

BIBLIOGRAPHY

1. Snyder, S.D. and C.H. Hansen 1991 "Mechanisms of active noise control using vibration sources", *J. Sound Vib.*, **147**, 519-525.
2. Pan, J., S.D. Snyder, C.H. Hansen, and C.R. Fuller 1992 "Active control of far field sound radiated by a rectangular panel - a general analysis", *J. Acoust. Soc. Am.*, **91**, 2056-2066.
3. Snyder, S.D. and N. Tanaka 1992 "Calculating total acoustic power output using modal radiation efficiencies", *J. Acoust. Soc. Am.*, submitted for publication.
4. Wallace, C.E. 1972 "Radiation resistance of a rectangular panel", *J. Acoust. Soc. Am.*, **51**, 946-952.
5. Snyder, S.D., N. Tanaka, and Y. Kikushima 1993 "The use of optimally shaped piezo-electric film sensors in the active control of free field structural radiation, part 1: Feedforward control", *J. Vib. Acoust.*, accepted for publication.

GENETIC ALGORITHM ADAPTATION OF NON-LINEAR FILTER STRUCTURES

Corey T WANGLER and Colin H HANSEN

Department of Mechanical Engineering, University of Adelaide, South Australia 5005, Australia.

ABSTRACT

This paper examines the use of a genetic algorithm for active sound and vibration control, where the genetic algorithm is used for the adaptation of the filter weights of non-linear filter structures. Non-linearities introduced by electro-acoustical and electro-mechanical transducers can considerably reduce the overall levels of attenuation that can be achieved in actively controlled sound and vibration systems. Such non-linearities can be compensated for by the use of non-linear filter architectures to produce control signals from the given reference signals. Use of a genetic algorithm for adaptation of filter weights eliminates the need to know the transfer function between the control source input and the error sensor output, which is essential knowledge for a conventional algorithm to remain stable. This enables the use of complex filter structures which would normally not be practical when combined with 'standard' gradient descent-type adaptation algorithms (such as the filtered-x LMS). For active sound and vibration control several modifications to the standard genetic algorithm are necessary to produce the required operating performance and these are also discussed. The operation of the algorithm is experimentally verified using a polynomial filter structure for the non-linear control of a vibrating beam, where the piezoceramic control actuators introduce additional frequency components.

INTRODUCTION

Active sound control is the process of attenuating unwanted noise by introducing additional sources of sound. These additional sound sources act to reduce the sound power output of the existing primary source by absorption, by reflection, or by changing the impedance experienced by the sound source. In some cases, none of the preceding control mechanisms occur and destructive interference results in the reduced sound levels in some locations at the expense of increased levels in others, with an overall increase in total sound power. Similar attenuation mechanisms apply to active vibration control where additional structural excitation forces are applied. An active control system is used to generate the control signals required to drive these additional control sources, whether they be acoustic or vibration.

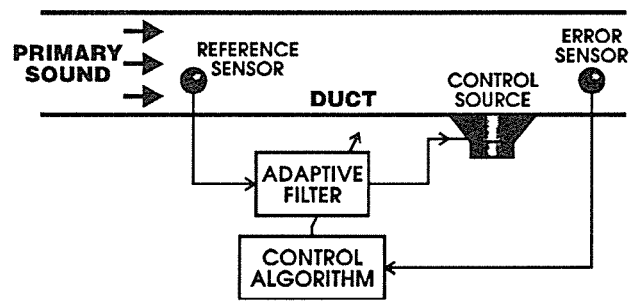

Figure 1: Single channel adaptive sound control system.

To be practical, an active control system must adapt to changes in the environment in which it is operating. An adaptive single channel active control system applied to sound propagating in a duct is shown in Figure 1. A reference sensor samples the incoming sound, with the resulting electrical signal being passed through a digital adaptive filter to the control source. The weights of the adaptive filter are adjusted by

the control algorithm to minimise the signal detected by the error sensor.

The simplest adaptive filter in general use is the finite impulse response (FIR) filter, which is sometimes referred to as a transversal filter. The FIR filter, shown diagramatically in Figure 2, is a tapped delay line with single sample (τ) delays between taps. Each output sample from the filter is a weighted sum of the tap values at the given instant in time.

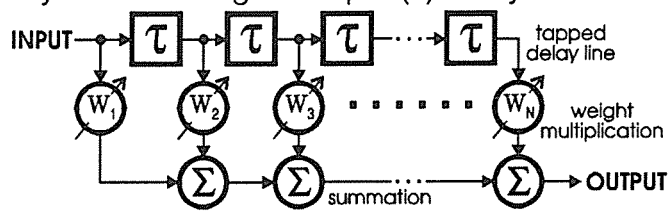

Figure 2: FIR filter.

Updating of the filter weights is usually done using a least squares algorithm which, to be stable, requires knowledge of the cancellation path (control source input to error sensor output) transfer function to a phase accuracy of better than 90°. With the FIR filter structure it is not possible to generate any frequencies in the control signal which do not appear in the reference signal. Thus any non-linearities in the physical system or control source cannot be compensated for. One way of controlling a non-linear system is to use a non-linear filter structure. However, it is not practical to use a standard LMS algorithm in this case. Also, it is desirable to avoid another disadvantage of the LMS algorithm and that is the need to know the cancellation path transfer function. One such algorithm which can adapt the weights of a non-linear filter structure and which is stable with no knowledge of the cancellation path transfer function is the genetic algorithm, and this is the subject of this paper.

The genetic algorithm is an optimisation/search technique based on evolution, and is essentially a guided random search. It has been applied to many optimisation problems, but in the field of active sound and vibration control it has so far been restricted to optimising the placement of control actuators in actively controlled structures (Rao et al, 1991). In this paper it is shown how the genetic algorithm may be used to adapt the coefficients of a digital filter. A general control system schematic arrangement for application of the genetic algorithm to filter weight adaptation is depicted in Figure 3.

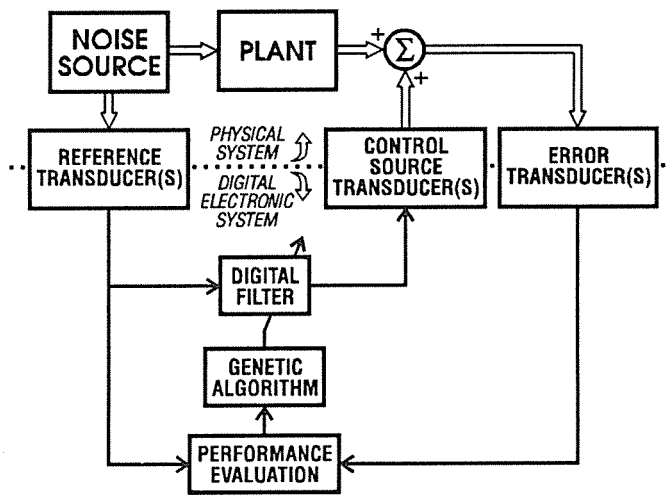

Figure 3: Control system arrangement.

Use of the genetic algorithm enables any filter structure to be treated as a 'black box' that processes reference signals to produce control signals, based on different sets of filter weights. Basic genetic algorithm operation requires the testing of solutions (sets of filter weights), which involves loading the filter weights into the filter and subsequently evaluating the performance of the filter in minimising a cost function based on the error sensor outputs. The genetic algorithm in essence combines high performance solutions while also including a random search component.

Although the arrangement shown in Figure 3 allows for multiple input, output and error transducers, this paper only discusses the validation of the operation of the genetic algorithm for the single-input, single-output, single-error-sensor case.

ALGORITHM IMPLEMENTATION

Implementation of the genetic algorithm described in this paper has three basic stages: fitness evaluation, selection and breeding. Fitness evaluation requires the testing of the performance of all individuals in the population. Here an individual is considered to be a separate set of filter weights, with the fitness of the individual being a measure of the filter's performance when these weights are being used for filter output calculation. The population then consists of a collection of these individuals. Selection involves killing a given proportion of the population based on probabilistic 'survival-of-the-fittest'. Killed individuals are replaced by children, which are created by breeding the remaining individuals in the population. Typically 70% of the population are killed, with the remaining 30% forming the mating pool for breeding. For each child produced, breeding first requires probabilistic selection of two (possibly the same) parent individuals, with fitter individuals being more likely to be chosen. Application of the crossover and mutation operators on the parent pair produces the new child. The crossover operator combines the information contained in two parent strings (or two sets of filter weights) by probabilistic copying of information from either parent to each corresponding string element (or single filter weight) of the child being produced. Mutation introduces random copying 'errors' during the information copying stage of crossover, and gives the algorithm a random search capability.

Mutation plays a minor role in the 'standard' implementation of the genetic algorithm, in that it is used to replace lost bits in the binary encoding of the problem. As binary data has only two states, small mutation probabilities work well with the 'standard' implementation where data loss is minor. This is not the case in the implementation used in this paper, where a weight string is used instead of binary encoding. Here mutation is necessary to maintain population diversity (differences between individuals) and also to allow 'homing in' on optimal solutions, as the population data corresponding to one weight in the string will not fully represent the weight's entire data range.

Two selection processes are carried out during the operation of the genetic algorithm, namely the choice of individuals to be killed, and the choice of parents during breeding. Both selection processes have been implemented using a simulated roulette wheel, where each segment (or slot) on the roulette wheel is allocated a size proportional to the individual's probability of being chosen (selection probability). Each spin of the roulette wheel results in one "winner" being selected. Selection probabilities are assigned such that low performance individuals are more likely to be killed, and such that high performance individuals are more likely to be chosen as parents for breeding. Selection without replacement is used for killing, where once an individual is chosen it is removed from the roulette wheel. For breeding, selection with replacement (no removal) is used for choosing the parents, hence the entire mating pool is used in the selection of each parent individual.

Many aspects of the 'standard' genetic algorithm implementation have been changed to give the desired on-line optimisation performance required in this application. These changes are listed below.

- Killing selection instead of survivor selection
  Choosing individuals to be killed rather than those to survive allows higher survival probabilities to be realised for the higher performing individuals. This enables greater selective pressure (bias towards survival and breeding of the higher

performance individuals) to be applied, which can be used to give faster convergence when high levels of mutation are used to sustain population diversity. Use of killing selection also allows the best performing individual to be assigned a killing probability of zero to ensure its survival.

- Weight string instead of binary encoding

  The "genetic code" of each individual is normally encoded as a binary string (from the problem variables), with the crossover and mutation operators working at the single bit level. Mutation of the upper bits of weight variables results in large jumps in weight values when filter weights are encoded in this way, which significantly degrades on-line performance. To alleviate this problem a weight string has been used, with the crossover and mutation operators applied using whole weight values as the smallest operational element. This modification was used by Ichikawa and Sawa (1992), who reasoned that crossover of weight fragments is "almost meaningless" and did not consider on-line performance.

- Mutation probability and amplitude

  Application of mutation to whole weight values enables a limit to be placed on the deviation of filter weight values about their current values, which gives control over the spread of the filter's performance. Mutation has been applied to all child string variables at a given probability (mutation probability, typically 20 to 30%). The weights chosen to be mutated are modified by a random change in value, which is limited to a specified range (mutation amplitude).

- Rank-based selection (killing and breeding)

  Rank-based selection removes the scaling problems associated with fitness proportionate selection (assigning selection probabilities proportional to fitness values), and gives exceptional control over selective pressure (Whitley, 1989; Whitley and Hanson, 1989). Rank-based selection was used by Whitley and Hanson (1989) for breeding (parent selection). This has been extended here to include killing selection. Selection (choosing) probabilities, for both killing and breeding, have been assigned here based on the rank position of each individual's performance. This essentially means that the individuals have been sorted into order from best to worst performance, then each allocated a fixed selection probability (probability of being chosen) based on their position in this list. The performance evaluation method used thus becomes irrelevant as long as the rank positions are the same (or similar). Separate (adjustable) probability distributions have been used for killing and parent selection, with killing being more probable for lower ranked individuals and selection to be a parent being more probable for higher ranked individuals.

- Uniform crossover

  Uniform crossover nearly always combines the information of two parent strings more effectively than one or two point crossover (Syswerda, 1989). One point crossover is where a position along the string is selected at random, and information is copied (to the child being created) from one parent for the first part of the child string and from the other parent for the second part. Similarly two point crossover involves selecting two points along the string, and copying from one parent between these two points, and from the other parent for the rest of the child string. In uniform crossover each position along the child string is produced by randomly copying from either parent, with both parents being equally likely to be chosen as the information source. In this paper a modified form of uniform crossover has been used, where the probability of copying information from the lower ranked parent is supplied, and whole weight values are the smallest elements that are copied (compared to single bits for binary encoded strings).

- Genetic algorithm parameter adjustment

  As suggested by De Jong (1985), adjustment of the operating parameters (probabilities, population size, etc) can improve the performance of the algorithm. The adjustable parameters used in this implementation (population size, survival ratio, killing and breeding rank-probability distributions, crossover probability, mutation probability, and mutation amplitude) provide good control over the stages of adaptation needed when good on-line performance is required. While manual adjustment between a fixed set of parameter setups has been used in the present implementation, dynamic adjustment (using population fitness values) will be examined in future work.

The use of a genetic algorithm for adaptation of filter weights requires a suitable filter performance measure to be obtained when comparing sets of filter weights. This has been achieved by using a moving average of the squared error obtained from the error sensors. The resulting performance measure can also be modified by scaling with another similarly obtained moving average of the reference signals to give improved comparison accuracy when the source level is not stationary. Testing of the filter performance by using moving averages removes the need for identification of the cancellation path transfer functions, thus producing a robust algorithm and simplifying its implementation.

EXPERIMENTAL RESULTS

The experimental work was undertaken using an aluminium beam with a cross-section of 25mm x 50mm, and a length of 3896mm. The beam was fixed at both ends, and driven on the 50mm face by a shaker at 167Hz. The piezoelectric control actuators were connected out of phase, to "bend" the beam in the same direction. An accelerometer was used as an error sensor, with the resulting signal being low-pass filtered at 550Hz before reaching the error input of the controller. The sampling frequency of the controller was 2.5kHz.

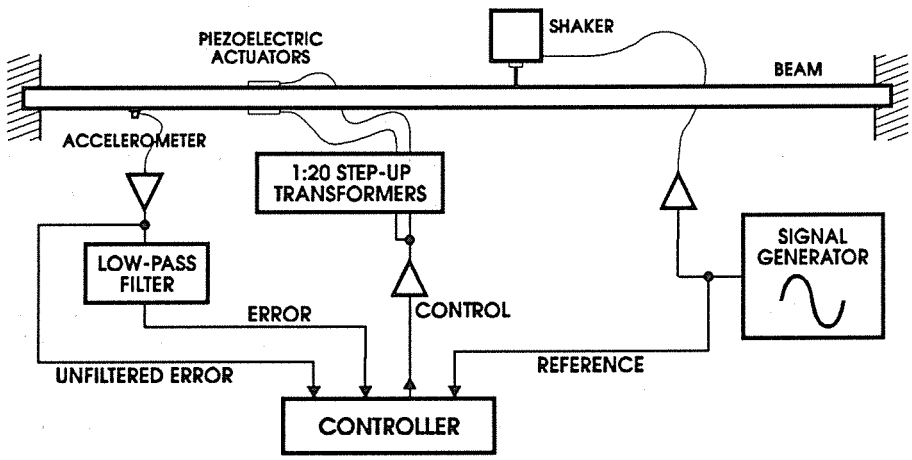

Figure 4: Experimental setup.

The experimental setup is shown in Figure 4, and the filter structures used in these experiments are shown in Figure 5. The first filter shown in Figure 5 is a finite impulse response (FIR) filter, which is linear and consists of a tapped delay line as illustrated in Figure 2. The tapped delay line gives a history of the reference signal, and acts as a buffer with sample values shifting from left to right. The second filter shown in Figure 5 is a polynomial filter, with only the cubed term present. This filter is essentially a FIR filter with the reference samples raised to the third power, and will be referred to as a P3

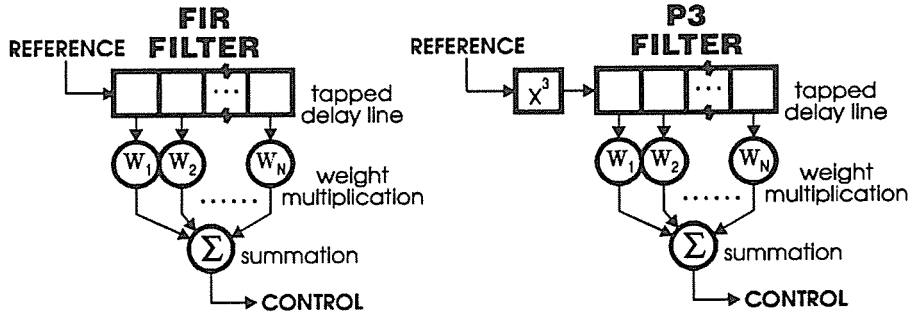

Figure 5: Filter structures used in the experiments.

filter. Raising the reference samples to the third power introduces third order harmonics of the reference signal, while also keeping the original signal frequency content. Thus the P3 filter is able to generate frequencies appearing in the reference signal along with third order harmonics of the reference signal content.

The filter weight performance measurement for the genetic algorithm was taken over a period of 60 samples. A 60 sample delay was introduced before the start of each measurement to allow any transient vibration (produced when changing the filter weights to new values) to subside. The value of the performance measure was calculated as the fraction of mean squared error (MSE) reduction, with the initial MSE being measured over a period of one second before control was applied. The MSE is found by averaging (over a given interval of time) the error signal samples after squaring.

The power spectrum of the unfiltered error signal when FIR and P3 filters are used is shown in Figures 6 and 7 respectively. In both cases, the piezoelectric control actuators introduce harmonics of the reference signal. The even harmonics are most likely caused by mismatch in the control forces produced by the two piezoelectric actuators, although the sixth harmonic also coincides with a beam resonance near 1000Hz. The odd harmonics arise due to non-linear output (harmonic distortion) from the piezoelectric actuators, with the third harmonic corresponding to a beam resonance at 500Hz.

In the FIR filter case (Figure 6), attenuation of the fundamental peak at 167Hz is limited by the introduction of the third harmonic caused by the inherent harmonic distortion of the piezoelectric actuators. Noting that the error signal is low-pass filtered, it can be seen that the controller has made a compromise between attenuation of the fundamental and the introduction of the third harmonic. This gives the best overall attenuation possible for the FIR filter structure, which can only generate frequencies that are present in the reference signal (which here only contains the fundamental frequency of 167Hz).

The power spectrum results for the P3 filter (Figure 7) show that both the fundamental and third harmonic have reached the same level as the second harmonic. The fundamental has been reduced by 37dB, compared to only 29dB reduction when using the FIR filter (Figure 6). Also, the third harmonic has only risen by 4dB compared with an increase of 27dB for the FIR filter. The genetic algorithm adapted FIR filter gave a maximum of 17dB MSE reduction within 40 seconds. Given the same period of time the P3 filter had achieved 20dB MSE reduction, with a maximum of 30dB MSE reduction attained within 8 minutes.

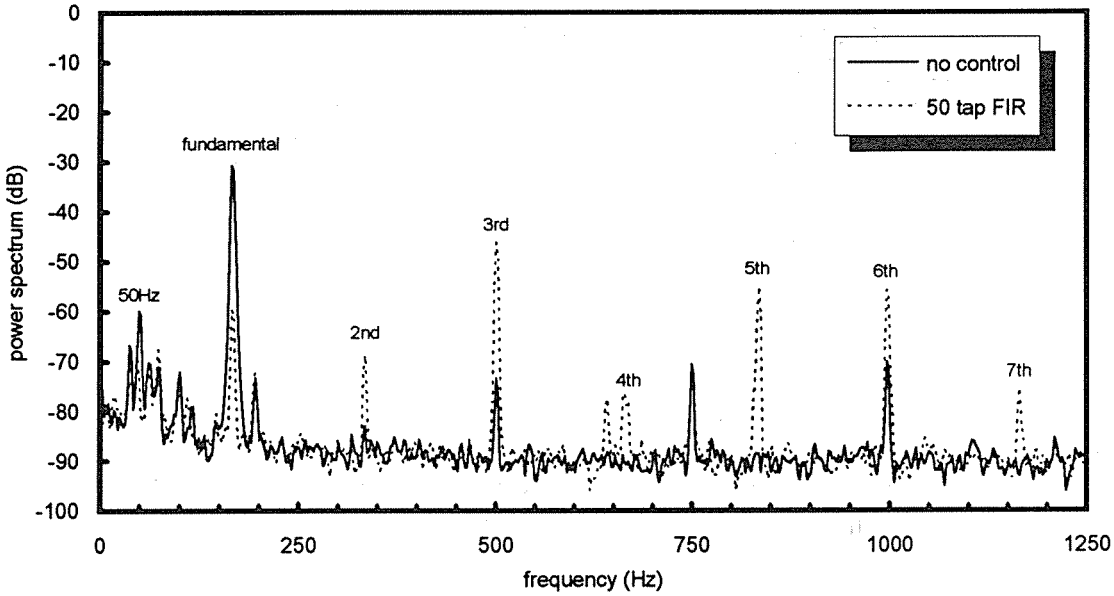

Figure 6: Power spectrum of the unfiltered error signal, with linear control (FIR filter).

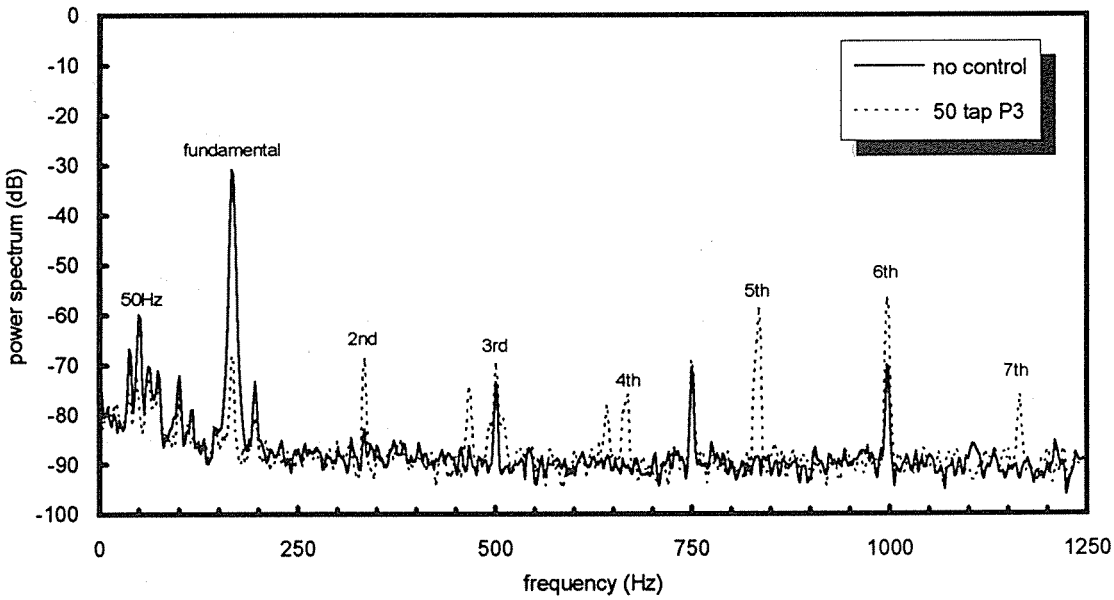

Figure 7: Power spectrum of the unfiltered error signal, with non-linear control (P3 filter).

Introduction of harmonics of order four and higher occurred almost identically for both filter structures, the only difference being that the level of the fifth harmonic was 3dB lower for the P3 filter. Note that these frequencies are not present in the low pass filtered error signal used for control performance evaluation. The appearance of all odd and even harmonics (observable up to the seventh order with a 2.5kHz sampling rate) confirms that these additional frequency components arise due to the piezoelectric control actuators.

Use of the P3 filter has, by counteracting the rise of the third order harmonic, enabled an increased amount of control to be applied. This increase in control level is displayed by an increase in the piezoelectric actuator (control source) driving voltage from 51V RMS for the FIR filter to 54V RMS for the P3 filter.

Both filters were unable to prevent the introduction of the second harmonic, with a 14dB rise occurring in both cases. To remove all of the harmonics it is expected that a more complex filter such as a neural network will be needed.

CONCLUSIONS

The experimental results show that the non-linear filter and genetic algorithm combination can control non-linear systems, and can increase attenuation levels in cases where control actuators introduce additional harmonic content.

The use of a genetic algorithm with moving average performance evaluation results in an increase in stability and robustness over gradient descent algorithms. The main reason for this is that identification of the cancellation path transfer function is not necessary when using this method of filter weight adaptation. A major advantage associated with the genetic algorithm is that the error signals are not required to be linearly correlated with the reference signals (as required by gradient descent algorithms), thus allowing easy application to non-linear systems. Another advantage is that various filter structures can be used with virtually no change to the adaptation algorithm, which allows quick selection of appropriate filter structures for the problem at hand.

The major disadvantage of the genetic algorithm compared to gradient descent algorithms is slower convergence and less ability to track environmental changes, due to the averaging time required for the moving average performance measurement which is approximately half the period of the lowest frequency encountered in the error signals. This limits application to systems that are steady state or only slowly changing.

REFERENCES

Kenneth De Jong (1985) Genetic algorithms: A 10 year perspective, *Proc. of the 1st International Conference on Genetic Algorithms and Their Applications*, pp 169-177.

Rao, S.S., Tzong-Shii Pan, and Venkayya, V.B. (1991) Optimal placement of actuators in actively controlled structures using genetic algorithms, *AIAA Journal*, 29, 942-943.

Syswerda, G. (1989) Uniform crossover in genetic algorithms, *Proc. 3rd International Conference on Genetic Algorithms*, pp 2-9.

Whitley, D. (1989) The genitor algorithm and selection pressure: Why rank based allocation of reproductive trials is best, *Proc. 3rd International Conference on Genetic Algorithms*, pp 116-121.

Whitley, D. and Hanson, T. (1989) Optimising neural networks using faster, more accurate genetic search, *Proc. 3rd International Conference on Genetic Algorithms*, pp 391-396.

Yoshiaki Ichikawa and Toshiyuki Sawa (1992) Neural network application for direct feedback controllers, *IEEE Transactions on Neural Networks*, 3, 224-231.

ACKNOWLEDGMENTS

The authors gratefully acknowledge financial support for this work from the Australian Research Council.

ACTIVE CONTROL OF AIRCRAFT INTERIOR NOISE WITH A VIEW TO APPLICATION IN LIGHT AIRCRAFT

Marc T. Simpson and Colin H. Hansen

Department of Mechanical Engineering
University of Adelaide, S. A. 5005

Abstract

The need for active noise control in aircraft has been driven by recent advances in fuselage construction and turboprop engine technology of medium sized passenger aircraft. However, application of this noise control technique to light aircraft has been largely overlooked. The purpose of this paper is to review the development of active noise control in aircraft and to assess previous analytical models to determine their applicability to light aircraft structures. The difficulties of analysing and optimising an active noise control system in a light aircraft fuselage is discussed and modelling procedure capable of overcoming these difficulties is proposed.

Introduction

The parallel development of advanced composite materials for use in aircraft fuselage structures and more fuel-efficient turboprop engine technology have dominated contemporary propeller aircraft design. However, the lighter and stiffer fuselage structure has created the potential for increased interior noise levels. Conventional passive means of noise control sufficient to address the low frequency propeller noise would increase the mass of the structure, and may negate the advantage of using composite materials. Aircraft acousticians are now looking to more advanced, lightweight methods of noise control, such as active noise control, to provide the required reductions of interior noise.

The excessive interior noise levels in light aircraft are well documented. However, weight constraints characterise the overall lack of success of passive noise control techniques for these aircraft. In this paper, the current stage of development of active noise control in aircraft will be reviewed, with a view to assessing its potential application to light aircraft. The problems which have hindered the development of active noise control in light aircraft fuselage structures may now be overcome and ongoing research into this area will be described briefly.

Active Control Of Aircraft Interior Noise.

To design an active noise control system for a particular aircraft application requires a detailed understanding of the basic underlying mechanisms of how the control is achieved. Much of the initial research into this field has been undertaken using simplified analytical fuselage models. More recently however, numerical techniques, such as finite element analysis have been used to model the complex structural/acoustic behaviour of realistic fuselage structures. These advanced models have been used to investigate the use of active noise control in production aircraft. They were undertaken as feasibility exercises rather than as research into the factors that affect active noise control. In the following sections, both approaches will be reviewed to gain a greater understanding of the current development of active noise control in aircraft structures and to assess their potential application to light aircraft.

A feedforward active noise control system may be divided into two parts (figure 1): the physical control system (layout of control sources and error sensors) and the electronic control system. The physical control system has three major components. First, the control sources (consisting of speakers or shakers) provide the controlling or cancelling disturbance. Next the error sensors (consisting of microphones, accelerometers etc.) provide a measure of the residual disturbance. An optional third component, the reference sensor, provides a measure of the impending disturbance. The electronic control system uses the signals obtained from the reference and error sensors to calculate the relative amplitudes and phases of the control sources, to achieve sound attenuation.

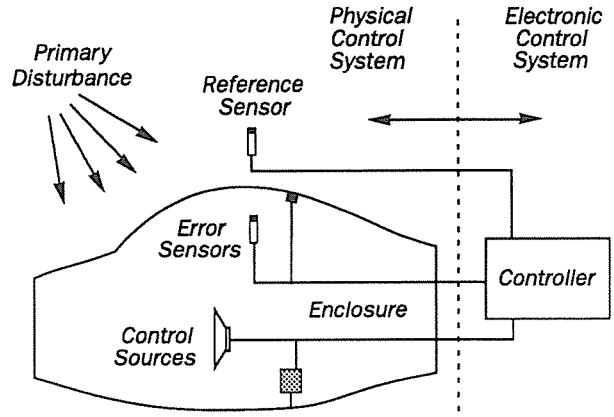

Figure 1. Feedforward active noise control system layout

The maximum noise reduction achievable by an active noise control system is dependent upon the layout of control sources and error sensors. The electronic control system simply optimises the noise levels to a minimum achievable level which is determined by the physical system layout. Therefore, a detailed understanding of the physical system behaviour and mechanisms are required to optimally design the overall system.

Simplified Analytical Models

Simplified analytical fuselage models have been used extensively in active noise control research to gain an understanding of the mechanisms involved in active noise control of aircraft interior noise. The unnecessarily complex and little understood features of realistic fuselage structures have the effect of masking the underlying mechanisms of active noise control (Zalas and Tichy, 1984). More simplistic analytical representations have therefore been pursued; the most commonly used fuselage model being a plain isotropic cylindrical shell (Bullmore et al, 1990; Elliott et al, 1989; Elliott et al, 1990; Fuller and Jones, 1987a; Lester and Fuller, 1986; Silcox et al, 1989; Fuller and Jones, 1987b). With this model, the shell mode shapes and interior acoustic mode shapes are calculated separately and then coupled together using modal coupling theory. The response of the coupled system to an external excitation field incident on the cylinder wall is then calculated. Thus, this configuration is a useful first approximation for the analytical simulation of propeller noise transmitted through the fuselage walls into the aircraft cabin.

Initial work by Bullmore et al (1990) examined the nature of the noise environment and the placement of acoustic control sources within an acoustic volume. They concluded that the acoustic control sources within the volume must be positioned so they can couple effectively with the dominant modes excited by the primary force. This should be done whilst simultaneously ensuring that the amplitudes of previously unexcited modes are kept to a minimum level under controlled conditions. This undesirable effect of exciting previously unexcited modes is commonly termed 'control spillover'. Good levels of reduction were achieved and these were confirmed further in flight test comparisons (Elliott et al, 1989; Elliott et al, 1990).

Fuller and Jones (1987a) demonstrated that only selected structural modes couple well with the interior acoustic modes. Lester and Fuller (1986) showed that this selected structural/acoustic coupling may be modelled, and they analytically evaluated the

performance of active noise control in a simple fuselage model. Silcox et al (1989) performed an initial experimental validation of Lester and Fuller's work (1986) as well as investigating further the mechanisms which govern the operation of active noise control in an enclosure of finite extent. This was done using an array of equally spaced acoustic control sources arranged on the interior of the cylinder. It was found that to achieve significant global noise reductions, the number of acoustic control sources must be equal to at least twice the circumferential order of the cavity mode to be controlled.

The performance of vibration control sources mounted on the fuselage to reduce the sound transmitted through the fuselage wall has also been investigated. In one study (Fuller and Jones, 1987a) it was demonstrated that up to 15 dB attenuation could be achieved by using a single control force on a plain cylinder model. Although the amplitudes of the dominant cylindrical modes responsible for passing energy into the dominant acoustic mode were reduced, control spillover was experienced with some of the control energy being shifted to higher order structural modes. These higher order modes were not able to couple well with the interior acoustic modes, thus reducing the interior sound levels. When additional control sources and error sensors were added (Fuller and Jones, 1987b), it was found that the control sources needed to be located at the anti-nodal positions of all the modes to be controlled. In addition to this, the error sensors needed to be located at positions where the responses of all modes to be controlled were strong.

More recent research has been orientated towards fuselage models which include the effect of an integral floor structure in a cylindrical model. This has been found to more accurately reflect realistic fuselage structures. The cylinder with floor structural model combines the motions of the plain cylinder and the plate structure using a Rayleigh-Ritz procedure outlined by Peterson and Boyd (1978). The interior acoustic field is solved in two dimensions using the finite difference technique and then extended to three dimensions analytically (Pope et al, 1983).

Snyder & Hansen (1991), using vibrational control sources, contrasted the difference between the mechanisms of control in the cylinder and the cylinder with floor models. They found that an extra control mechanism was at work in the cylinder with floor model enabling greater reductions to be achieved. The joint mechanism of control common between the two models was *modal control* where the amplitudes of the primary radiating structural modes were reduced. The extra mechanism of control which existed in the cylinder with floor structure was that of *modal rearrangement*, where the relative amplitudes and phases of the radiating structural modes were altered. For this to occur, there must be at least two structural modes coupled to a single acoustic mode (as with the cylinder with floor case). However, with the plain cylinder, only one structural mode is able to couple with one acoustic mode, thus preventing modal rearrangement from occurring.

It is the mechanism of modal rearrangement which offered the most scope for active noise control, as it had the effect of altering the overall vibration pattern of the structure. This created the potential to control a large number of structural modes using very few vibration control sources. Global interior noise reductions of up to 20 dB were achieved for single frequency excitation.

Realistic Fuselage Models

Most of the research reviewed so far has concentrated on simplistic fuselage models. These models have proved to be adequate for the study of active noise control mechanisms and the influence of various system parameters on the maximum achievable noise reductions. However they are an unrealistic representation of a practical fuselage structure, as structural complications such as ring and stringer

stiffening, structural damping and variations in cross-sectional shape have not been considered. These features are difficult to include using the modelling procedures just discussed and numerical modelling procedures (that is, finite element analysis) must therefore be adopted to enable their influence on the structural response to be determined. This has the advantage of replicating the true nature of the structural/acoustic interactions which allows realistic predictions of the interior sound field to be obtained.

In recent years, there has been a major thrust from an European consortium (Advanced Study of Active Noise Control in Aircraft - ASANCA) (Borchers et al, 1992; Van der Auweraer, 1993; Emborg and Ross, 1993) to implement active noise control systems in several medium sized passenger aircraft. In these studies, testing and theoretical work has been undertaken for 4 different partner aircraft (that is, Dornier 228, Saab 340, ATR 42, & Fokker 100). They were selected to identify general noise control information and demonstrate that active noise control was feasible in aircraft that have large differences in acoustical character.

The ASANCA consortium (Borchers et al, 1992; Van der Auweraer, 1993; Emborg and Ross, 1993) implemented active noise control using a fixed array of acoustic control sources, located in the interior trim and ceiling of the aircraft. A fuselage test cell (Hackstein et al, 1992) of a Dornier 228 was subsequently used to experimentally verify the results obtained from the analytical results. Reductions of 15 and 16 dB were achieved for the blade passage tone and first harmonic, respectively.

Additional flight tests (Emborg and Ross, 1993) were performed using a similar system in a Saab 340 aircraft. A total of 48 error sensors and 24 loudspeakers were installed. Reductions in this aircraft were 10 dB and 3 dB for the blade passage tone and first harmonic, respectively. These results were not as good as predicted for the Dornier 228 aircraft, but this is probably a result of differences in the fuselage structure and the presence of cabin furniture and passengers. It is expected that a production system will be available in this aircraft by late 1994.

Other analytical and experimental active noise control studies have involved the McDonnell Douglas MD-80 (jet) aircraft (Paxton et al, 1993) and the Saab 2000 aircraft (Green, 1992).

In the analytical studies just mentioned (Borchers et al, 1992; Van der Auweraer, 1993; Emborg and Ross, 1993; Paxton et al, 1993; Green, 1992), coupled finite element analyses were used to model the fuselage structures. This enabled the discrete modelling of important structural and acoustic characteristics that influenced the overall fuselage response. In general, the structure was modelled as a small length of fuselage adjacent to the propeller, where the sound transmission is at its highest. No consideration was given to the effect of wing attachments and the potential for structure-borne excitation via that path. The excitation input into the structure was primarily represented as a propeller blade passage pressure distribution on the fuselage surface. The interior acoustic finite element model used in these studies occupied the internal space of the structural models. Both the structural and acoustic modes were calculated separately and then combined, creating a single large coupled model. The resulting interactions between the excitation field, structural vibrations and the interior acoustic field enabled interior noise levels resulting from a specified external excitation field to be calculated. The additional input of control sources thus enabled the reductions in the interior sound field to be determined.

Light Aircraft Interior Noise

There has been considerable research done in an attempt to understand the problem of interior noise in light aircraft (De Metz, 1988; Hayden et al, 1983; Jha and

Catherines, 1978a; Jha and Catherines, 1978b). It has been reported (De Metz, 1988) that the interior noise levels in general aviation aircraft often exceeded comfortable conversational noise level (82 dBA) by 12-18 dB. In addition, cockpit noise levels in a single engine light aircraft often exceed permissible noise exposure standards by 4-8 dB for flights lasting three hours or more.

The major contributors to light aircraft interior cabin noise have been identified (Hayden et al, 1983; Jha and Catherines, 1978a; Jha and Catherines, 1978b) and the reproducability of these sources in a laboratory fuselage has been evaluated (Jha and Catherines, 1978b). It was found that the interior noise levels in both single and twin engine light aircraft were dominated by the blade passage frequency (100Hz and its lower harmonics) and were usually 10-15 dB higher than any other contributing components. It was determined that the bare fuselage structure can offer up to 10 dB reduction (Jha and Catherines, 1978b) in sound transmission, although this reduction is much smaller for the lower frequency region (50-100Hz).

A commonly used method to reduce cabin noise is that of lining the interior cabin surfaces with an absorptive acoustic trim. This treatment is known to be effective for high frequencies, but its performance is greatly reduced at lower frequencies. The weight of additional treatment required to attenuate low frequency sound is too great, and would hinder the flight performance of the aircraft.

An alternative method to reduce cabin noise levels is to modify the design of the aircraft to address the interior noise levels (De Metz, 1988; Hayden et al, 1983). This involves modifying the aircraft structure significantly (increasing panel and glass thickness, using an advanced multi-bladed propeller, etc.) to address the noise generation mechanisms. In most cases, these changes are not feasible to implement in the vast majority of light aircraft flying today.

With no other alternatives, occupants of light aircraft resort to using personal devices such as noise reducing headsets or earplugs to protect themselves from the unacceptably high cabin interior noise. However, the emergence of active noise control as a practical noise control technique, especially for periodic, low-frequency sound, shows promise as a much more attractive alternative.

Active Control of Light Aircraft Interior Noise

While there are many light aircraft world-wide exposing people to uncomfortable noise levels, active noise control has yet to be applied in any of these types of aircraft. The major reason for lack of work in this area is attributed to the complexity of analytically modelling the sound transmission into the fuselage. This step forms an important part of active noise control design, providing a basis for the optimisation of the control source and error sensor locations for maximum noise reduction.

Most of the early simple analytical fuselage models were easily described in terms of existing structural and acoustic theories. However, for large fuselage structures, a coupled finite element analysis has been used in the past to enable the modelling of more complex features. This involved accurately modelling the combined structural/acoustic properties of a section of fuselage and determining the interior noise levels as a result of the primary excitation field (Green, 1992). Although this latter approach is capable of modelling a light aircraft fuselage, the computing resources required are too great. Therefore a need exists for the development of a cost effective method of analysis, which will allow an economical evaluation and optimisation of the multitude of possible physical arrangements of the control sources and error sensors.

Work currently being undertaken at the University of Adelaide is orientated towards addressing these problems. An analytical procedure for the prediction of the effect of active noise control in three dimensional enclosures of general shape has been

proposed. It is based upon an existing procedure (Snyder and Hansen, 1991) used to analyse a cylinder and cylinder with floor enclosure. The difference is that the structural and acoustic mode shapes and resonance frequencies are calculated using finite element analysis in which use is made of an existing displacement-pressure analogy to enable a structural finite element package to be used for analysis of the acoustics space (Lamancusa, 1988).

Once the modal properties have been determined using finite element analysis, the structural and acoustic modal vectors are coupled together outside of the finite element package using modal coupling theory (Pope, 1971). This involves determining the energy transfer between the structural modes and the interior acoustic modes. For the calculation of the structural modal properties, the structure is assumed to be lightly damped and vibrating 'in vacuo'. For the calculation of the acoustic modal properties, the enclosure boundaries are assumed rigid. The effect of active control on the interior noise is calculated using quadratic optimisation theory (Nelson et al, 1985). This enables the interior sound field to be minimised given a fixed number of vibration control sources and error sensors. However, optimisation of the number and location of vibration control sources and error sensors presents a more difficult problem. The sound reduction achieved is not a linear function of control source location, and the optimal error sensor locations are dependent upon the control source locations. This presents some difficulty for conventional numerical search routines which possibly may have been used to optimise layouts. However, advanced randomised searches such as those based on genetic algorithms (Katsikas, 1993) will be assessed to overcome this problem.

Conclusion

A review of existing active noise control research shows that significant reductions are possible in aircraft fuselages. Advanced analytical and numerical modelling techniques have been used to predict the interior noise reduction in realistic, large fuselage structures. However the economical application of these techniques to the problem of optimising active control system design to minimise cabin noise in small, light aircraft requires considerable changes to existing modelling procedures and is the subject of on-going research.

References

Borchers, I.U., Emborg, U., Sollo, A., *et al* (1992) "Advanced study for active noise control in aircraft (ASANCA)", *Proceedings of DGLR/AIAA 14th Aeroacoustics Conference, Aachen, Germany,* 130-141.

Bullmore, A.J., Nelson, P.A., and Elliott, S.J. (1990) "Theoretical studies of the active control of propeller-induced cabin noise", *Journal of Sound and Vibration* 140, 191-217.

De Metz, F.C. (1988) "Cockpit noise generation mechanisms in light aircraft", Paper presented at the 116th Meeting of the Acoustical Society of America, Honolulu, Hawaii.

Elliott, S.J., Nelson, P.A., Stothers, I.M., and Boucher, C.C. (1989) "Preliminary results of in-flight experiments on the active control of propeller induced cabin noise", *Journal of Sound and Vibration* 128, 355-357.

Elliott, S.J., Nelson, P.A., Stothers, I.M., and Boucher, C.C. (1990) "In-flight experiments on the active control of propeller induced cabin noise", *Journal of Sound and Vibration* 140, 219-238.

Emborg, U., and Ross, C.F., (1993) "Active control in the Saab 340", *Proceedings of the Recent Advances in Active Control of Sound and Vibration, Blacksburg, Virginia,* 100-109.

Fuller, C.R., and Jones, J.D. (1987a) "Experiments on reduction of propeller induced interior noise by active control of cylinder vibration", *Journal of Sound and Vibration* 112, 389-395.

Fuller, C.R., and Jones, J.D. (1987b) "Influence of sensor and actuator location on the performance of active control systems", *Paper presented at ASME winter annual meeting, Boston.*

Green, I.S. (1992) "Vibro-acoustic FE analyses of the Saab 2000 aircraft", *Proceedings of the 4th NASA/SAE/DLR Aircraft Interior Noise Workshop, Friedrichshafen, Germany,* 44-69.

Hackstein H.J. *et al* (1992) "The Dornier 328 acoustic test cell (ATC) for interior noise tests and selected test results", *Proceedings of the Recent Advances in Active Control of Sound and Vibration, Blacksburg, Virginia,* 35-43.

Hayden, R.E., Murray, B.S., and Theobald, M.A. (1983) "A study of interior noise levels, noise sources and transmission paths in light aircraft", *NASA CR*-172152.

Jha, S.K., and Catherines, J.J., (1978a) "Interior noise studies for general aviation types of aircraft pt1: field studies", *Journal of Sound and Vibration* 58, 375-390.

Jha, S.K., and Catherines, J.J., (1978b) "Interior noise studies for general aviation types of aircraft pt2: Laboratory studies", *Journal of Sound and Vibration* 58, 391-406.

Katsikas, S.K. *et al* (1993) "Genetic algorithms for active noise control", *Proceedings of NOISE-93, St. Petersburg, Russia,* 167-171.

Lamancusa, J.S., (1988) "Acoustic finite element modelling using commercial structural analysis programs", *Noise Control Engineering Journal,* March-April, 65-71.

Lester, H.C., and Fuller, C.R. (1986) "Active control of propeller induced noise fields inside a flexible cylinder", *AIAA Paper* 86-1957.

Nelson, P.A., Curtis, A.R.D., and Elliott, S.J. (1985) "Quadratic optimisation problems in the active control of free and enclosed sound fields", *Proceedings of the Institute of Acoustics,* 7, 45-53.

Paxton, M. *et al* "Active control of sound in a MD-80", *Proceedings of the Recent Advances in Active Control of Sound And Vibration, Blacksburg, Virginia,* 67-73.

Peterson, M.R. and Boyd, D.E. (1978) "Free vibrations of circular cylinders with longitudinal, interior partitions", *Journal of Sound and Vibration* 60, 45-62.

Pope, L.D. (1971) "On the sound transmission of sound through finite closed shells: statistical energy analysis, Modal coupling, and non-resonant transmission.", *Journal of the Acoustical Society of America,* 50, 1004-1018.

Pope, L.D., Wilby, E.G., Willis, C.M., and Mayes, W.H. (1983) "Aircraft interior noise models: sidewall trim, stiffened structures, and cabin acoustics with a floor partition", *Journal of Sound and Vibration* 89, 371-417.

Silcox, R.J., Lester, H.C., and Abler, S.B. (1989) "An evaluation of active noise control in a cylindrical shell", *Journal of Vibration, Acoustics, Stress, and Reliability in Design* 111, 337-342.

Snyder, S.D., and Hansen, C.H. (1991) "The effects of modal coupling characteristics on one mechanism of active noise control", *Proceedings of Recent Advances in Active Control of Sound and Vibration,* 708-727.

Van der Auweraer, H. *et al* (1993) "Aircraft interior sound field analysis in view of active control: results from the ASANCA project", *Proceedings of NOISE-CON 93, Williamsburg, Virginia,* 219-224.

Zalas, J.M., and Tichy, J. (1984) "Active attenuation of propeller blade passage noise", *NASA CR*-172386.

Acknowledgments

The authors gratefully acknowledge financial support for this work from the Sir Ross and Sir Keith Smith Fund and the Australian Research Council.

Commercial Application of Active Noise Control in Ducted Systems

Peter B Swift
Principal Acoustical Engineer
Bassett Consulting Engineers, Adelaide SA

It appears that there is a potentially bright future for the use of active noise control systems for the control of duct-borne noise,however the commercial availability of such systems may be some time away in Australia. Is it that Australia is seen as a relatively minor market or are there practical problems in providing a reliable product?

1 INTRODUCTION

The concept of active noise and vibration control has been known for most of this century. Over the last two decades, developments and improvements in adaptive filters and the ongoing progress in very fast computers technology have allowed the theoretical concepts to be realised, resulting in some commercial applications, at least for the more simple systems, and continuing vigorous research and development in many areas of active noise and vibration control.

This paper is not a technical review of active noise control methods. It is presented mainly to raise awareness of active noise control methods from a user or consultant perspective and to pose the questions

how ready are such systems for general commercial use?

and

how long before they are available in Australia?

2 CONTROL OF DUCTBORNE NOISE

Active noise control is more easily achieved for one dimensional, low frequency applications and becomes increasingly more difficult to achieve for two and three dimension systems and at higher frequencies. Given this, it seems reasonable to assume that the application to the reduction of low frequency ductborne noise is that most likely to be developed for commercial use.

The following generally describes the concept used in most systems applied to the attenuation of duct-borne noise.

Microphone sensors are used to provide an input signal to loudspeakers in order to generate an equal and opposite sound signal in the duct to cancel the unwanted noise as it passes the loudspeaker. The difficulty in the past has been in providing the appropriate signal to the loudspeaker, allowing for phase variations to the signal which are imposed by the microphone, amplifier, loudspeaker system and also for the time delay as the noise travels within the duct system between the noise sensing microphone and the loudspeaker. An additional problem was that some of the system characteristics alter with time causing an unstable noise cancelling system.

Various advances made in the technology over the past decade and used in present commercial systems include the Infinite Impulse Response (IIR) adaptive filter. This system has the ability to adapt to the changes in the duct system and the elements of the control system and basically is the reason for the step forward in commercial usage in the past decade. The effectiveness has been partially limited by variation in the characteristics of the sensing system itself comprising the error microphone, amplifier and loudspeakers. Recent advances in the late 1980's, have incorporated a second system to monitor a random noise source, allowing changes in the error system to be tracked more accurately (Eriksson 1991). This data is fed into the main adaptive system, hence increasing the ability of the system to reduce the in-duct noise. The figure below shows a block diagram of a typical active control system applied to in-duct noise reduction.

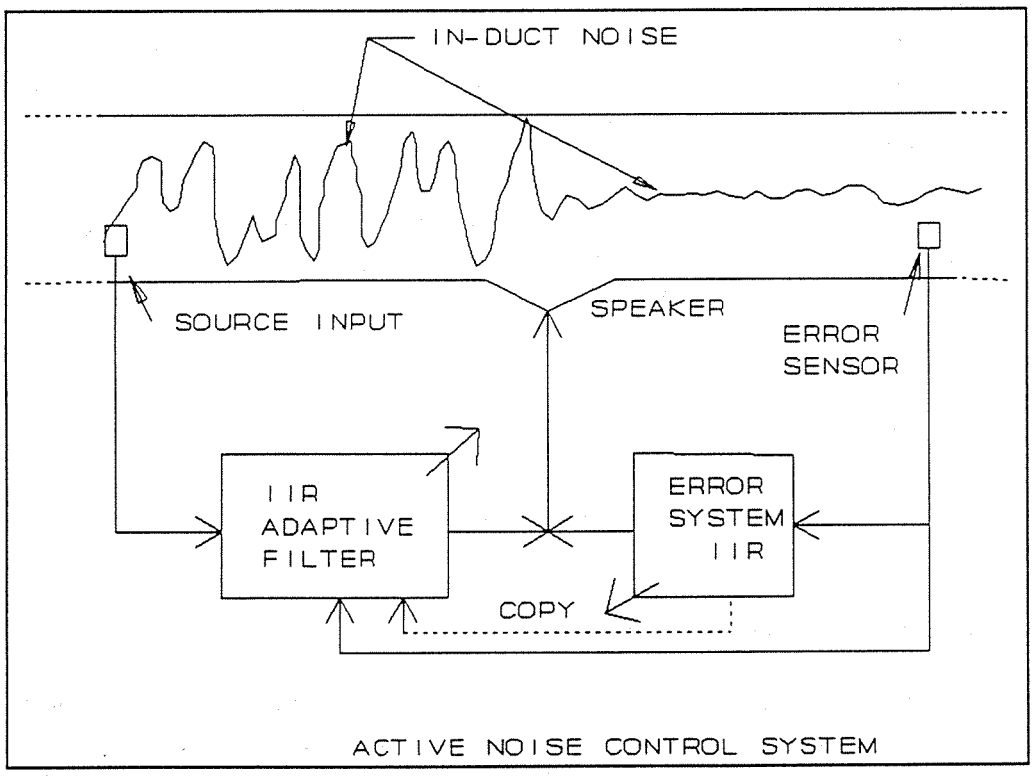

The application of the active noise concepts is very effective for narrow band noise control and less so for random broad band noise control. The upper frequency limit for simple systems increases with reducing duct size. The system elements and control hardware are similar for all duct applications including exhaust noise control for internal combustion engines, inlet and discharge paths for air compressors and vacuum pumps. The commercial application to the control of noise propagation along larger ducts in industrial plant and heating, ventilation and air conditioning (HVAC) systems in building services is the main concern of this review.

Although the acoustical control of plant noise is generally considered by most designers, certain aspects, mainly duct low frequency breakout noise, are still overlooked in many systems. There have been recent reviews of room noise design criteria leading to Room Criteria (RC) and Balanced Noise Criteria (NCB) room criteria curves (Beranek 1988) where the "rumble" component associated with plant noise is set at a lower level compared with the well known Noise Rating (NR) and Noise Criteria (NC) curves. As the RC and NCB curves gain increasing acceptance, the low frequency noise component of the mechanical plant will require greater attenuation. This is especially applicable to large building systems and for specific low noise spaces, but is also relevant to smaller systems on separate floors where often offices are located close to plantrooms and suffer from duct breakout noise. As the major area of application of active noise control is for low frequency noise reduction, in particular for tones within a random noise background, then it appears that there should be a bright commercial future for the application of active noise control products in the control of ductborne noise.

3 DESIGN CONSIDERATIONS

At present, the frequency range of application is dependent on the duct size, but generally is effective from around 30 Hz to 250 or 300 Hz. This is the range where normal acoustic lining is least effective. Passive duct silencers can be designed to reduce low frequency noise but they generally increase the duct resistance, are large and over-attenuate in other frequency ranges.

At present, active systems generally require at least 1.5 m and preferably 2.5 m to 3 m distance between the input microphone and the loudspeaker system. Acoustic duct lining is usually incorporated to achieve some attenuation by passive control in the middle and upper frequencies. The duct system between the noise source and the loudspeaker generally would require some noise break out assessment as the in-duct noise level in this section is increased.

The desirable length of around 3 m is a restriction to their use for many smaller HVAC installations. Improvements in the next generation of controllers are likely to relieve this length constraint such that the overall length will be controlled by the physical size of the speakers required rather than the speed of the controller.

The obvious benefit is that low frequency noise reduction can be achieved with minimal restriction to airflow. This is most valuable in industrial plant with either solids in the air stream where use of conventional silencers are impractical or where

conventional silencers create significant back pressure, in which case use of an active system results in potential savings in operating cost. Other benefits compared with conventional low frequency HVAC silencers are the reduction of regenerated noise from the splitters (or pod) and the elimination of the need for large cross section ducts required to achieve suitable low passage velocities. The reported attenuations achieved generally are around 20+ dB for tones and 12 - 15 dB with more broad spectrum noise. The characteristic of an active noise control system is that it tends to reduce tones and raised sections of a broad spectrum more effectively than at the other frequencies, hence it results in a broad spectrum of relatively even sound power level. This is desirable in achieving a non tonal system noise but does cause difficulties in attempting to predict the attenuation which will be achieved.

For a ducted system, assuming that

- there is good correlation between signals at the sensor and error microphones (no regenerated or other noise sources downstream of the source reference microphone)

- there is sufficient space to locate the loudspeakers

- the problem noise is within the duct and not controlled by other flanking paths,

then it appears that the active duct silencer should give good results and we would expect there would be much interest in the use of these systems in building services and industry.

4 REVIEW OF COMMERCIAL USE

As a consultant interested in the application of active noise control in building services, I took the opportunity to inquire about its status during a recent trip to Internoise 93. My inquiries were not exhaustive but the majority of those to whom I spoke should have had a reasonable knowledge of the status of commercial use in their local area.

The investigation which was undertaken indicates:

- there appears to be only one commercial group advertising and installing their active noise control product for ductborne noise control in HVAC systems. This is Digisonix which is based in the United States (Wisconsin) and also has a European office located in London.

- the great majority of installations are in industry and generally for environmental control of low frequency tonal noise.

- the great majority of installations are retrofit

- there are only three systems where active noise systems have been included at the design stage

    - ABC studios in Washington

- new office complex in Tampa Florida incorporating over 80 separate active silencers on the large HVAC systems; project due for completion around November 1993

- new clean rooms in Germany to be installed around December

- A French group, Boet Systeme Actif, is marketing a system which is aimed at engine, compressor and pump noise control, where the system is applied to the small exhaust, discharge or inlet pipes, in lieu of high back pressure reactive (and absorptive) mufflers. At present, they do not appear to be interested in the HVAC market.

- some installations are carried out on a research basis generally by research institutions and some consulting groups, however the majority of the research appears to be concentrating on the more difficult problems of two and three dimensional applications and higher modes, and the controllers required.

- discussions with consultants in Europe and Canada seemed to indicate generally a lack of confidence in the technology, or the application of the technology. It was not made clear what the problems were but in general, the comments were that "it has always turned out that it did not seem to be suitable" for their application or "that system does not work".

- although there is presently only one Digisonix system (about to be) installed in Europe, many of their research controllers are in use in Europe.

- There are no immediate plans by Digisonix to support their active noise control systems in Australia (or Asia).

Given the above, the question that must be asked is whether the systems are suitable for general use as an engineering tool for HVAC noise control at the design stage. Obviously, the minimum performance cannot be specified in the same way as one specifies for absorptive attenuators.

At present, Digisonix provides its own personnel from Wisconsin to install and set up the systems. This is understandable for a retrofit application where some assessment of sensor and actuator locations must be made. However, provided that the proposed location in the duct system is acceptable (away from bend or other sources of turbulence), it seems reasonable that the active attenuator should be able to be installed and activated by reasonably skilled personnel in the local area, and not have to require specialists from the parent company. If there is such a requirement for specialist installation, then it may explain the relatively slow penetration into HVAC designs in the last few years.

According to published advertising literature, active noise control in ducted systems is successful and there is no reason to doubt the data. What we do not know is how many designs were not successful and whether these were the few difficult cases, or whether the published successful cases are the minority where it just happened to work well. If the success of the system is very sensitive to the location of the system elements for relatively simple duct systems, then active noise control is not likely to be readily accepted, hence will not be considered at the design phase.

5 CONCLUDING COMMENT

Given the development over the last ten years and the number of reported successful installations, it seems reasonable to expect that the use of active silencers, in combination with conventional acoustic lining in the duct, should become a common approach to the reduction of duct-borne noise in industrial and commercial fan powered ducted systems. This is likely to be the case provided that it can be installed following a few guidelines and that the system performance does not depend on sensitive adjustments to the hardware.

From a viewpoint here in Australia, the impact of active noise control in the acoustical engineering design field in United states, Canada and Europe, where it is commercially available, does not appear to be as marked as I would have expected it to be. Is this because of a general wariness of the concept and the product, lack of awareness of the product and its potential benefits, or are there still unresolved difficulties which are not immediately obvious from afar.

It is unlikely that there will be any move to make the product available in Australia until the European market is penetrated more effectively, and, until there is local support for a commercial product, it is not very practical to attempt to incorporate active noise control in building services in Australia.

6 REFERENCES

Beranek L.L. (1988)
Noise Criteria Curves for Enclosed Spaces
Section 18.3, Noise and Vibration Control, Revised Edition
INCE, Washington

Eriksson L.J. (1991)
Application Considerations and Case Histories for Active Noise Control in Ducts, Chapter 17, Active Control of Noise and Vibration, Course Notes, University of Adelaide, Edited by C.H. Hansen, Adelaide

AUSTRALIAN ACOUSTICAL SOCIETY

1993 ANNUAL CONFERENCE

Establishment of an outdoor learning environment for young deaf children in an acoustic climate dominated by road traffic noise.

J. North
Head of Early Childhood
Royal NSW Institute for Deaf & Blind Children
North Rocks, NSW

S.E. Samuels
Head of Transport Engineering
School of Civil Engineering
University of NSW
Kensington, NSW

ABSTRACT

It is essential that young deaf children receive the earliest possible educational assistance to enable them to develop to the maximum extent. The majority of parents of deaf children choose oral communication methods for their children. This means that children need to learn to use their residual hearing to listen and to develop speech. Since a good acoustic environment is necessary for the acquisition of listening skills, preschool programs for deaf children must provide a better acoustic environment than regular schools.

The present paper is concerned with one aspect of the planning process leading to the construction and operation of a new preschool facility for deaf, oral children on the North Rocks campus of the Royal NSW Institute for Deaf and Blind Children. It commences with a brief outline of the educational processes occurring in such a centre. Particular emphasis is placed on outdoor activities which form a major part of each student's school day. The outdoor acoustic environment on the campus is dominated by road traffic noise. Consequently the paper then proceeds to describe how this was assessed and allowed for in planning the new preschool. Given the specific acoustic requirements of the preschool, a somewhat novel approach to traffic noise assessment was required which may have application to similar situations elsewhere.

INTRODUCTION

Ninety percent of children with hearing impairment are born to hearing parents. Most of these parents initially wish to develop their child's ability to use verbal communication rather than embrace the world of sign language. Under this philosophy, the earliest education of children with hearing impairment begins in the home and involves teachers informing parents how to provide the best listening environment for the acquisition of language and assisting the family to learn techniques to promote listening and oral language skills in the children. The aim is for parents to work to ensure that listening becomes integrated into the child's personality so that he/she becomes a "listener" in all circumstances. Work that is begun in the home is extended in the Preschool where teachers continue to pursue the goal of a complete, complex understanding and use of oral English for the chid with the hearing impairment.

The Early Childhood Department of the Royal New South Wales Institute for Deaf and Blind Children begins working with babies when they are first diagnosed as hearing impaired. The home program continues until babies are three years of age when they may enter the Rockie Woofit Preschool. The Preschool, established in 1989, is staffed with regular early childhood educators and specialist staff including a full time teacher of the deaf and an audiologist/speech pathologist, a apecial music educator and a psychologist who provide regular services to the Preschool.

Until the end of 1991, the Preschool program was primarily conducted indoors and withdrawal of children into an acoustically treated room for individual auditory/verbal work was an important part of the program. Under this model the playground was used for recess from teaching activities. In 1992 it was decided to alter the program to adopt a model of education which both eliminated the withdrawal of children except in special circumstances and broadened the curriculum to include a much wider range of experiences for children. It was felt that expanding the program into the outdoors would significantly increase the range of possible language experiences for children. Use of the outdoor environment would also capitalise on the natural interests and energies of children.

The move from withdrawal to full inclusion was prompted by the understanding that the most effective learning for little children occurs when the content to be learned is integrated into as many daily activities as possible. The inclusion model would also enable more opportunity for peer interactions to be used in the teaching process. The move to broaden the curriculum stemmed from the understanding that children with hearing impairment need to have first-hand experience from which to learn. They need to explore, to manipulate, to problem solve and to discover things for themselves. They need to link their experiences to language in order to arrive at a full understanding of concepts.

The existing preschool was unsatisfactory to accommodate the changes in program emphasis. Whilst the playroom had excellent acoustics for the type of program that had previously operated, it was unsatisfactory to cater for the new full inclusion model where up to 16 children and three teachers could be working in small groups. Even more unsatisfactory was the playground which was located beside Pennant Hills Road, one of the busier arterial roads in Sydney, where traffic noise made listening conditions poor. It was therefore proposed that a new preschool facility be constructed on the North Rocks campus of the Institute for Deaf and Blind Children. The facility was to comprise a single story building opening onto a large outdoor area which would be landscaped to provide the ideal environment for a substantially outdoor program.

Consideration of the locality of the facility within the campus was, therefore, very much focussed on ensuring that an appropriate acoustic environment exists in the outdoor area. In particular, possible adverse effects of a freeway, known as the Northwest Transport Link, which is proposed to be constructed adjacent to the campus have been of some concern. Road traffic represents the major source of background noise in the campus grounds at present. Consequently the paper commences by quantifying this acoustic environment and then goes on to demonstrate how it might change once the Northwest Transport Link becomes operational. An assessment of the ensuing acoustical amenity of potential sites for the preschool was then undertaken using a somewhat novel approach. The means by which a satisfactory outdoor learning environment were achieved are then discussed.

EXISTING ACOUSTICAL ENVIRONMENT

The existing acoustical environment in the campus grounds is dominated by road traffic noise and is, according to Centre staff, reasonably uniform throughout each day and consistent from day to day throughout the week. Typical existing traffic noise is shown in Fig. 1, reproduced from Wilkinson Murray Griffiths (1991A). Shown here are the various noise indices usually adopted to quantify traffic noise. Note that the well known relationship of Eqn (1) for traffic noise is also apparent in Fig. 1, thereby supporting the subjective observation of the dominance of traffic as the major source of environmental noise on the campus.

$$L_{10}(1h) = L_{eq}(1h) + 3 \quad \text{.....(1)}$$

Seven potential sites for the preschool facility had been proposed and these are indicated in Fig. 2. Also shown in Fig. 2 are five locations where free field measurements of the acoustic environment were made. Samples of both the $L_{10}(1h)$ and $L_{eq}(1h)$ were monitored at each location on a mild and calm afternoon and these data appear in Table I. Note firstly that these data conform to the Eqn (1) relationship. Again this shows objectively that the measured levels originated from traffic noise. Secondly, it is important to observe that the levels at Site M1 are very similar to those of Fig. 1 which were measured in the vicinity of M1. Minor differences between these two sets of data are due to site and traffic effects.

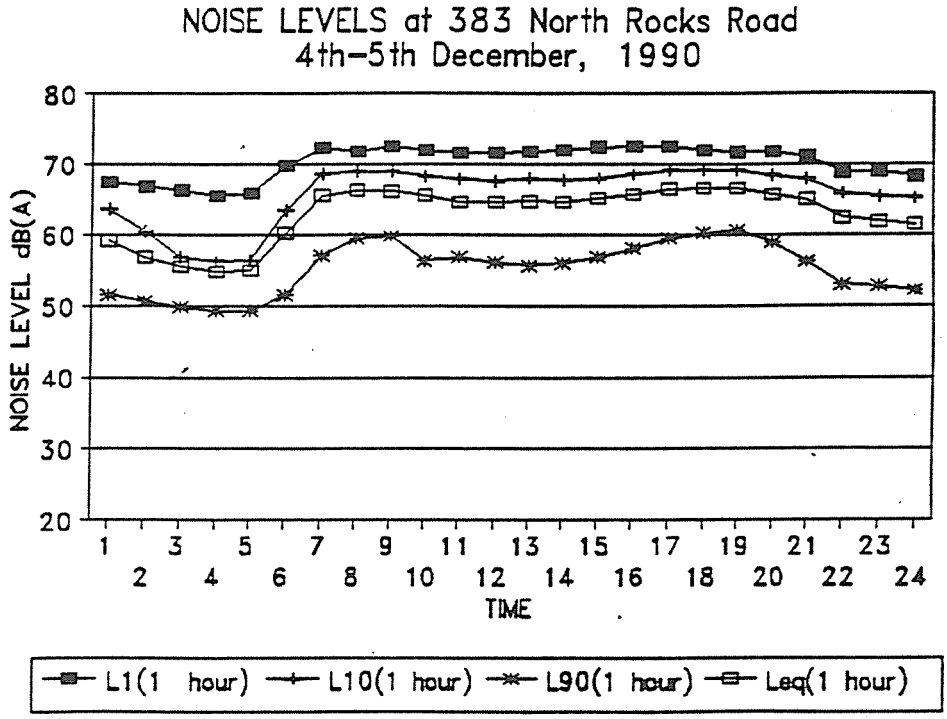

Figure 1. Existing traffic noise. (Reproduced from Wilkinson Murray Griffiths (1991A).)

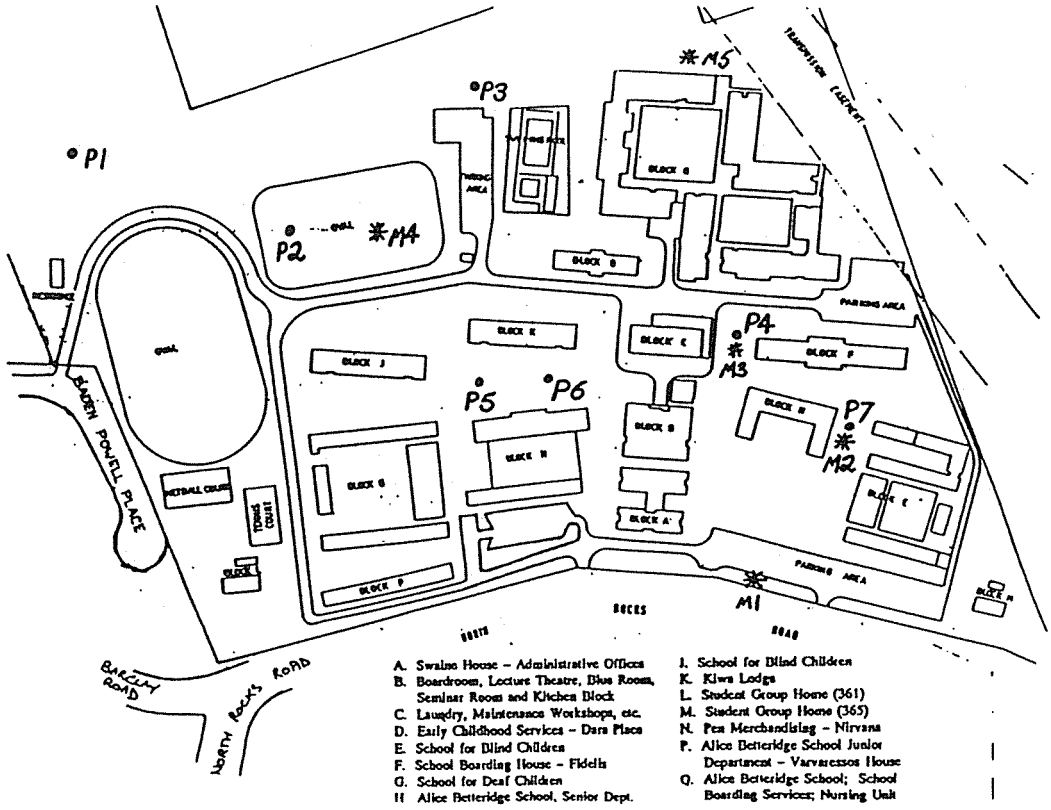

Figure 2. Campus showing potential sites for preschool (P1 to P7) and noise measurement locations (M1 to M5).

TABLE I - MEASURED NOISE LEVELS IN CAMPUS GROUNDS

MEASUREMENT LOCATION	NOISE LEVEL (dB(A)) L_{10} (1h)	L_{eq} (1h)
M1	71.5	68.4
M2	52.0	49.3
M3	49.0	47.0
M4	52.5	49.3
M5	49.0	46.0

ASSESSMENT CRITERION

An assessment was required in order to quantify the acoustical amenity of potential sites for the preschool facility. Essentially such a criterion represents the relationship between the level of (traffic) noise and the possibility of successfully undertaking the preschool outdoor activities. It was subjectively obtained by an expert panel comprising three of the Institute staff - two teachers of the deaf and an audiologist. During each of the five measurement samples already reported herein, the panel familiarised themselves with the acoustic environment at each site and then the panel arrived at a consensus if the suitability of that environment as far as the preschool outdoor activities are concerned.

To assist in this somewhat difficult process, both qualitative and quantitative rating scales were employed. Quality range was set from good to unacceptable and was mirrored in a 10 point numerical rating scale. Results of this exercise appear in Fig. 3 where the measured noise levels of Table I are graphed against the panel's ratings. The curve is merely an eyeballed line of best fit - insufficient data precluded regression analysis or the like. It indicates well what was mentioned previously that low noise levels are required for the preschool outdoor area. Overall it would appear that the appropriate assessment criterion is an L_{10} (1h) of 50 dB(A).

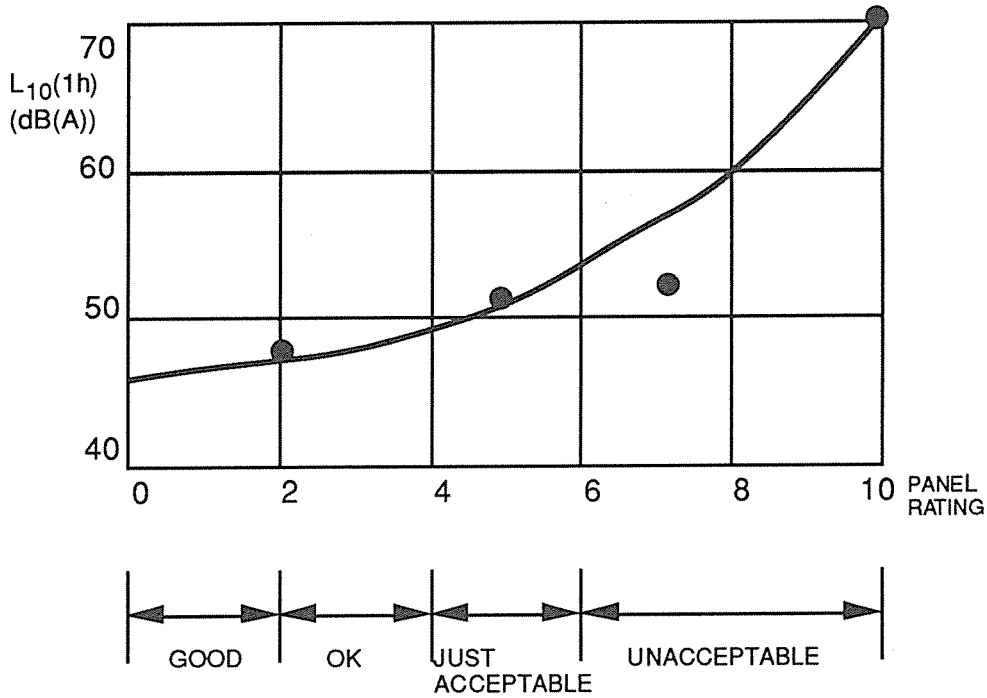

Figure 3. Panel ratings of traffic noise environment for preschool outdoor activities.

FUTURE ACOUSTIC ENVIRONMENT

Traffic noise impacts associated with the Northwest Transport Link are dealt with in the Environmental Impact Statement (Roads and Traffic Authority 1992) and in two of the accompanying support documents (Wilkinson Murray Griffiths 1991A and 1991B). Although considerable information is provided in these documents, insufficient is available for the present purposes. Consequently a series of traffic noise predictions was undertaken to estimate the traffic noise levels from the Northwest Transport Link at the potential sites for the preschool outdoor area.

Prediction of traffic noise is a complex procedure which requires knowledge of parameters such as traffic conditions, topography and the presence of shielding. For the present predictions a method widely used and accepted throughout Australia (UK Department of Transport 1988) was adopted. A different method was employed by Wilkinson Murray Griffiths (1991A) so as a first step a check prediction was done to ensure both methods were producing the same results in the vicinity of the campus. Details of this procedure are provided in Samuels (1992). In summary it was found that good agreement (within 1dB(A)) was obtained between the present predictions and those of the WMG (1991A). On this basis, future predictions were undertaken with UKDoT (1988) and compared subsequently as appropriate with other data from WMG (1991A) and RTA (1992).

Predictions of the Transport Link L_{10} (1h) noise levels at each potential site for the preschool were undertaken. These were conducted for a typical, average hour during the school day and for a morning peak hour situation. However it was apparent (Samuels 1992) that there were negligible differences between these two sets of predicted levels. This was consistent with the expectation that the Transport Link will carry reasonably uniform traffic volumes throughout the day. Subsequently in the present paper only the average hour levels will be considered.

Once the Transport Link becomes operational, the acoustic environment in the campus grounds will result from noise produced by the existing roads and by the Transport Link. Future noise levels from the existing roads were estimated on the basis of the measurements reported in WMG (1991A) and adjusted appropriately to the traffic volumes as projected after the Transport Link becomes operational (Samuels 1992). These were then combined with the Transport Link predicted levels to estimate the future, overall acoustic environment as presented in Table II.

TABLE II ESTIMATED FUTURE ACOUSTIC ENVIRONMENT AFTER OPENING OF TRANSPORT LINK FOR AN AVERAGE HOUR DURING DAY

PRESCHOOL POTENTIAL SITE	L_{10}(1h) (dB(A))		
	EXISTING ROADS	TRANSPORT LINK	OVERALL ACOUSTIC ENVIRONMENT
1	48.5	51.5	53.5
2	48.5	48.0	51.3
3	45.0	51.5	52.4
4	45.0	41.6	46.6
5	30.0	40.2	40.6
6	30.0	40.2	40.6
7	48.0	40.2	48.7

ACOUSTIC ENVIRONMENT FOR OUTDOOR LEARNING ACTIVITIES

An assessment criterion of 50 dB(A) was developed previously. Applying this to the future acoustical environments of Table II indicated that Sites 1, 2 and 3 would be unsuitable for the preschool. Sites 5 and 6 would be clearly good while Sites 4 and 7 would be reasonable, with Site 7 possibly being marginal. Sites 5 and 6 rated well primarily because of the good shielding provided by buildings adjacent to these two sites. The other sites would all experience some form of direct exposure to the traffic noise and this is reflected in the resultant noise levels. From other aesthetic considerations, Sites 1, 2 and 3 offered what appeared to be good settings for the preschool. They are somewhat distant from the other buildings on the campus and have a pleasant outlook over the trees and bushland of the Darling Hills State Forest. However these sites would be clearly unacceptable on acoustic grounds.

Some consideration was given to the possibility of improving the acoustic environment at Sites 1, 2 and 3 by treatments such as a barrier along the Northern boundary of the property (Samuels 1992). Theoretically a 3m high barrier would improve the situation at all three sites. Sites 1 and 2 would then become marginally suitable with Site 3 very satisfactory. However, this solution was expected to be difficult and expensive to implement. On this basis, and given the predicted acoustical environment at the 7 potential sites, it was concluded that the new preschool facility should be located at Sites 5 or 6 or possibly at Sites 4 or 7. Each of these sites would provide an acoustical environment satisfactory for the outdoor learning activities of the young deaf children in the preschool.

THE PRESCHOOL

Construction of the Preschool began in May 1993 and was completed, along with landscaping of the grounds, in the last week of September. Located at Site 7, it was designed to fit neatly into the space available between two existing buildings. The main playroom is approximately three times as large as that in the previous Preschool and its internal space is organised to provide a number of "quiet" areas where small groups of children or individuals can attend to tasks uninterrupted by the noise of their

peers. Acoustic treatments such as ceiling tiles and carpeting of floors in conjunction with the architectural design features have ensured an excellent internal acoustic environment.

The outdoor area consists of a large undercover area and a variety of play spaces such as sandpits, a stream, a bridge, a jungle and flower gardens which are very attractive to young children. All have been designed to provide quiet places which attract children's interest and engage them in language development activities. Because of the large number and variety of quiet spaces available, children are always busily occupied in small groups or alone. Teachers are finding that they are readily able to set up appropriate educational activities within the play spaces. The Preschool was occupied on 11th October , 1993 and the 16 children attending have flourished in their ideal new environment. It is firmly anticipated that this situation will continue once the North West Transport Link has been constructed and becomes operational.

REFERENCES

ROADS AND TRAFFIC AUTHORITY (1992). Environmental Impact Statement - North West Transport Link, Pennant Hills Road to Old Windsor Road. Roads and Traffic Authority, Sydney, NSW.

SAMUELS, S.E. (1992). Assessment of traffic noise impacts on a proposed preschool in the Royal NSW Institute for Deaf and Blind Children, North Rocks, NSW. Report 92-158R1.811. P.R. Knowland & Associates, North Sydney, NSW.

UNITED KINGDOM DEPARTMENT OF TRANSPORT (1998). Calculation of road traffic noise. HMSO, Welsh Office, UK.

WILKINSON MURRAY GRIFFITHS (1991A) Northwest Transport Link Western Section - Noise Investigation. Specialist working paper for Environmental Impact Statement. Wilkinson Murray Griffiths, Sydney, NSW.

_____ (1991B) Northwest Transport Link Western Section - Noise Investigation: assessment of tollway. Specialist working paper for Environmental Impact Statement. Wilkinson Murray Griffiths, Sydney, NSW.

ATTITUTDES OF RESIDENTS, CURRENTLY EXPOSED TO AIRCRAFT NOISE, TO AMELIORATION MEASURES

M.A. Burgess[*] and R.B. Zehner[†]

[*] Acoustics and Vibration Centre
University College, The University of New South Wales
Australian Defence Force Academy
Canberra ACT 2600

[†] School of Town Planning
The University of New South Wales
PO BOX 1, Kensington NSW 2033

1. INTRODUCTION

The increase in jet aircraft operations over recent decades has led to increasing concern about the effects of aircraft noise on the communities surrounding airports. Amelioration of aircraft noise has been an important priority for the administration of civil aviation in Australia. Actions in relation to the various recommendations of the House of Representatives Select Committee on Aircraft Noise [HORSCAN, 1985] are being taken by the Commonwealth Government. Major steps have been taken by the various authorities to reduce the amount of aircraft noise exposure.

While it is important to reduce the noise at the source, there are a number of amelioration measures which can be adopted to minimise the impact of the aircraft noise for those communities in the vicinity of existing airports, or of proposed airports. These measures range from property acquisition and relocation assistance to provision of monetary compensation and soundproofing for buildings. This paper reports the findings of a social survey conducted in the areas around Sydney Airport and designed to investigate the attitudes of residents to various aircraft noise amelioration measures.

2. AMELIORATION MEASURES

In this study, the term *Aircraft Noise Amelioration Scheme* is considered to refer to a scheme which is applicable to communities in the vicinity of an airport to reduce the impact of aircraft noise. Many such schemes have been adopted in other countries and the essential elements are:

- **Planning** - use of town planning restrictions and other control measures to limit incompatible development in the areas around an airport. This can involve not allowing certain types of developments or requiring special construction to minimise the intrusion of aircraft noise.
- **Acquisition and Relocation** - the building occupier is given financial and other assistance to move to a location in a less noisy area.

- **Soundproofing of Buildings** - the building owner is provided with a grant for the specific purpose of improving the sound reduction of the building envelope. Alternatively the work can be undertaken by an authority, with the approval of the home owner.
- **Fiscal Compensation** - the building owner is given a one-off payment as a compensation for the reduction in property value, change in lifestyle or as reimbursement of costs which could be incurred for additional soundproofing of the building.

The questionnaire was designed to investigate the attitudes of residents, currently exposed to aircraft noise, to the latter three amelioration measures.

3. SURVEY DESIGN

A complete picture of the attitudes of Australians to aircraft noise and its effects on their lifestyles, and their views of noise amelioration alternatives, should, ideally include interviews with residents in the vicinity of all Australian airports. As is the case for most studies, however, budget limitations for this project limited the amount of fieldwork that was feasible. It was decided to interview a larger number of respondents in the vicinity of one airport with the hope that further surveys could be undertaken around other airports should additional funding be available.

People living in a community where aircraft flight and noise patterns had been the subject of continuing recent discussion seemed more likely to have views on noise amelioration issues and a decision was made to focus the social survey on areas in the proximity of Sydney's Kingsford Smith Airport. Plans for a parallel runway (commonly referred to at that time as a third runway) had generated considerable discussion about possible impacts of those changes on the surrounding community.

Specifically, the survey concentrated on those living within two aircraft noise exposure groups, on the basis of current Australian Noise Exposure Forecast (ANEF) contour maps:

Low aircraft noise	ANEF 20-25
High aircraft noise	ANEF >30

People living in the ANEF 25-30 zone were not included in the survey primarily because responses from the ANEF 20-25 and ANEF 30+ groups could be expected to bracket those in the 25-30 zone, and also because of limited resources for fieldwork. Those outside the ANEF 20 zone were also excluded as it was essential that those interviewed had adequate experience of aircraft noise exposure.

Next, because the social survey was to focus on the residential environment and amelioration measures for dwellings, an attempt was made to obtain representative responses from two main housing situations within each of the ANEF zones:

Single family dwellings	(lower density housing)
Multifamily dwellings	(higher density housing)

The sample addresses were selected randomly for each of the four cells and just over 100 face to face interviews were obtained giving a total of 431 completed questionnaires. The survey was undertaken between March and June 1992.

4. ATTITUDES TO AMELIORATION MEASURES

4.1 General

Of the responses to the 65 questions in the questionnaire, only the responses to those directly related to amelioration measures are discussed in this paper. The full report on the study is given in Burgess and Zehner (1993).

4.2 Attitudes to neighbourhood and noise

It is important to consider the attitudes of the residents to their local environment and their sensitivity to noise in general and to aircraft noise in particular. Irrespective of aircraft noise exposure, the majority of the residents were satisfied with their environment, with convenience being given as the main reason for liking their area. The main reasons for disliking the area were aircraft noise and traffic noise. An extreme annoyance reaction to being unable to hear TV or having a disrupted telephone conversation was reported by around two fifths of those in the lower ANEF strata and three fifths of those in the higher ANEF strata. Over 70% of the total sample indicated that aircraft noise had been a problem in their living rooms and over half indicated that it had been a problem in the bedrooms and in the kitchen.

Between a fifth and a quarter closed their windows because of aircraft noise and almost as many closed their windows because of other noises. An overwhelming majority of all respondents in both the low and high noise exposure zones make use of their outdoor space at least occasionally. Only one person indicated aircraft noise as the reason the outdoor space was not used, although from half to four fifths of the respondents reported disturbance by aircraft noise the last time the outdoor space was used.

4.3 Changes to Dwellings

Several approaches to reducing the effects of aircraft noise were posed to respondents during the interview. These ranged from making various alterations to the dwelling structures on to an option to leave the area entirely. While the emphasis in the interview was on what residents would like to see happen in the future, the respondents were also asked what, if anything, had already "been done to this building specifically to reduce the effect of aircraft noise." The answer to that was, generally, very little.

The interview pursued the issue of making such changes by asking those who owned (or were buying) their dwelling that if someone else paid for the cost would they be willing to have gaps around doors and windows sealed, double glass windows or insulation in the roof/ceiling. Then respondents were asked if they would be willing to have the work done under three funding options. Responses to these items are shown in Figures 1 and 2. For these and subsequent figures the strata are referred to as:

high/multi	ANEF >30 and multifamily dwellings
high/single	ANEF >30 and single family dwellings
low/multi	ANEF 20-25 and multifamily dwellings
low/single	ANEF 20-25 and single family dwellings

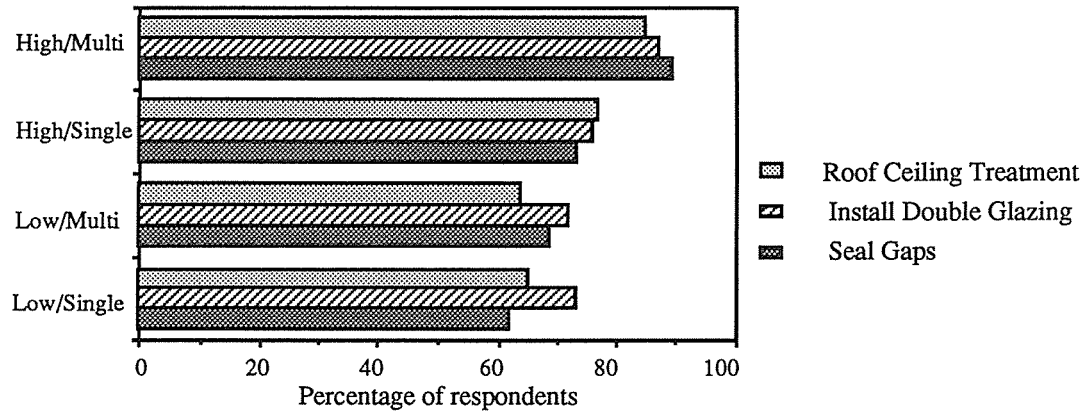

FIGURE 1 Willingness to have alterations done to dwelling.

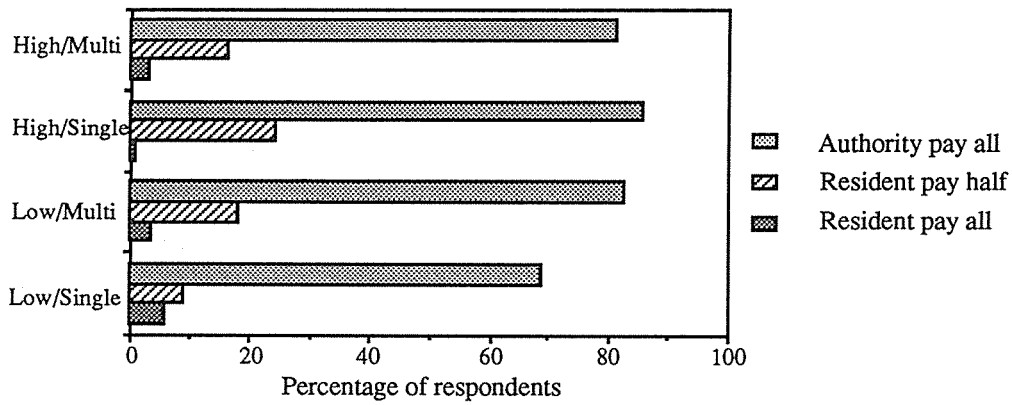

FIGURE 2 Willingness to have alterations done to dwelling under different funding options.

The responses indicate a broad willingness to have structural changes made to dwellings, but a very decided lack of enthusiasm for having them done unless the costs were assumed by someone else ("an authority"). It seems unlikely that many would volunteer to pay for such alterations if there was a possibility that another party would pay part or all of the cost.

The interview included an opportunity for those who were not interested in having one or more of three alterations done to their dwellings to indicate why they preferred not to have the work carried out. In each case (sealing gaps, double windows, under roof insulation), the main reasons for not wanting to proceed were an impression that the alterations wouldn't have much effect and that such changes were not necessary at this time.

As windows need to be kept closed to achieve high noise reduction, another form of ventilation must be used. Two alternative systems, window fans and air conditioning, were presented to the residents. More than half the respondents in each strata indicated they would want neither ventilation system even if the costs were borne by "an authority", as shown on Figure 3. The main reason, given by about a third, for not wanting any form of alternative ventilation was a desire for fresh air. Around a half of those willing to have air conditioning were willing to contribute half of the installation costs.

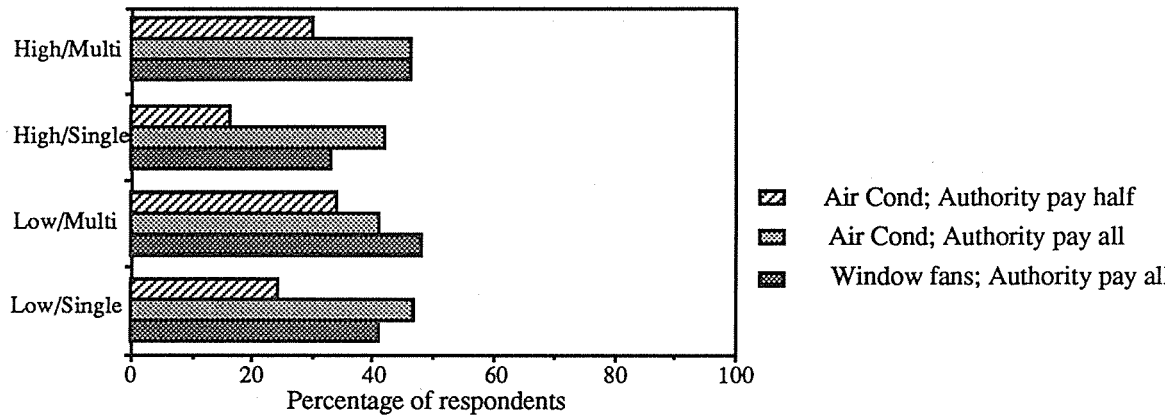

FIGURE 3 Willingness to have fan units or air conditioning

In the high/multi strata there was a clear preference for the work to be implemented by an authority rather than by the home owner. In the other strata both options were almost equally preferred. If work was only to be done to one room then there was a clear preference across all strata for the work to be done to the living/family room. In the multifamily dwellings, a sizeable minority (over 30%) preferred to have changes made to their bedroom.

4.4 Fiscal Compensation

Over half of all strata would be willing to accept a lump sum payment instead of having the work done, although about a third of these would not be willing to have the deeds stamped. The main reason for not accepting the payment was concern about the implications of accepting the payment.

4.5 Purchase and Relocation

With the exception of the high/single strata, a majority of owner/buyers indicated they would be willing to sell their homes to an authority. However, only around one in six of all owner/buyers were willing to sell at a price set by an independent valuer. Sizeable numbers in all strata indicated they would prefer not to sell in any event, especially those in the high/single strata.

For most residents, aircraft noise had not led them to seriously consider moving. While the cost of moving was an important deterrent for some respondents, a number cited the positive aspects of the neighbourhood and that the noise was not bad enough to consider moving. Cost reimbursement would be much more likely to have an effect on those households who have already considered moving at some point in the past.

5. PREFERENCES AND PRIORITIES

The questionnaire also sought to identify the preferred amelioration measure from the main options, i.e., changes to the building, lump sum payment, assistance with moving expenses and sale to an authority. The reactions to these options did not suggest overwhelming support for any one of the choices, see Figure 4. However, it is apparent that the most popular alternative was to have changes and modifications made to the home owner's house/building. Approximately two-fifths of the respondents opted for that alternative, except in the low ANEF multifamily households where that choice was preferred by about one-fourth of the residents. A similar proportion in that strata said that they would prefer the lump-sum alternative.

The prevalence of building modification preferences was especially notable in the higher ANEF areas. A probe of those who said "none of these choices" indicated, in aggregate, that roughly half of those people were not sure what choices might be appropriate (and might well have been put into the "Unsure, don't know" category), roughly one in six felt that no help was needed, and some ten per cent felt that nothing could realistically be done to help.

When the first and second preferences were combined, the difference between the "building modification" and "lump-sum" alternatives was virtually eliminated, except in the case of those living in multifamily situations in the higher ANEF areas where more than twice as many residents preferred the building modifications. Also noteworthy is that, with the inclusion of second choices, the multifamily respondents were much more likely to want to sell their homes to an authority than were those living in single family accommodation and that, in the low ANEF areas, that choice ended up as the most popular option.

As funds to meet the needs of aircraft noise amelioration programs will be limited there would be a need to establish guidelines to coordinate the expenditure of available resources. With this in mind, the interview asked residents to indicate if the extent of assistance should be related to level of aircraft noise, the ability to pay themselves and which of homes, schools and hospitals should be given the highest priority.

The responses indicate a preference across all groups to have the degree of assistance related to the amount of aircraft noise experienced, tempered by a sizeable minority (approximately 30 per cent) who would like to see assistance distributed evenly, regardless of the level of noise exposure, see Figure 5. Somewhat unexpected was the finding that those living in the higher ANEF areas were no more likely to want assistance related to the noise level experienced than those living in the ANEF 20-25 areas.

While from approximately one-fifth to one-fourth of the respondents in each area felt that the degree of assistance should be related to the ability of residents to share the cost of changes, there was a clear preference that the level of assistance not be dependent on the financial situation of the resident, see Figure 6 . As shown in Figure 7, residents were more likely to indicate that hospitals should be given the highest priority in the use of program funds to reduce the effects of aircraft noise, followed by homes, then by schools. Those who nominated homes as the highest priority were more likely to place schools as their second preference; those who

nominated schools first decisively ranked hospitals as next most deserving of assistance; a reaction which was reciprocated by those who chose hospitals as their highest priority. They tended to place schools as next in line for noise amelioration work.

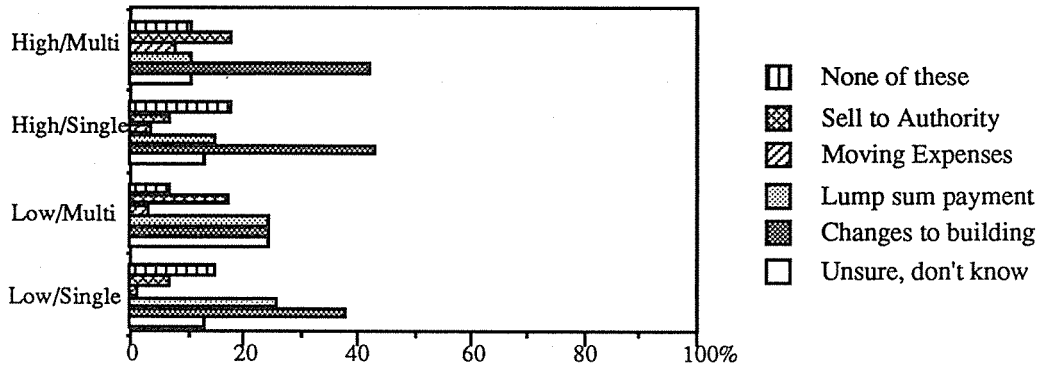

FIGURE 4 First preferences for amelioration measures

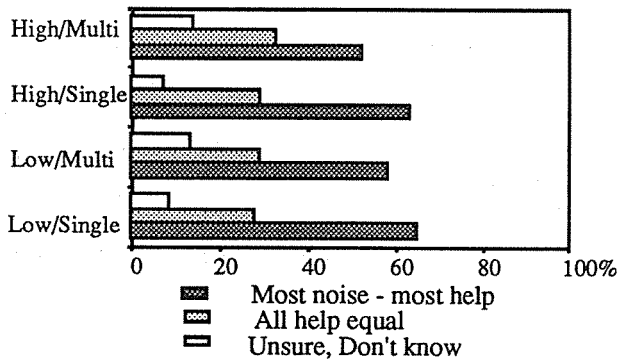

FIGURE 5 Preferences re noise exposure

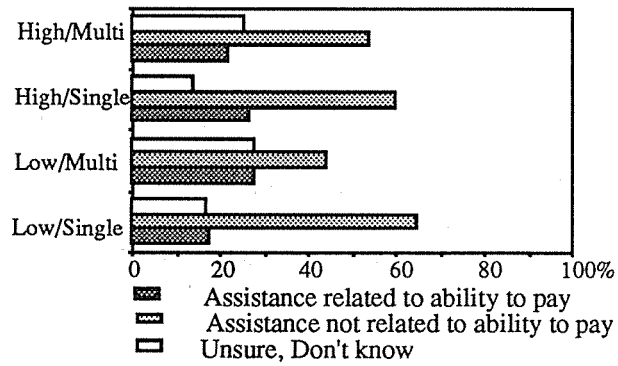

FIGURE 6 Preferences re ability to pay

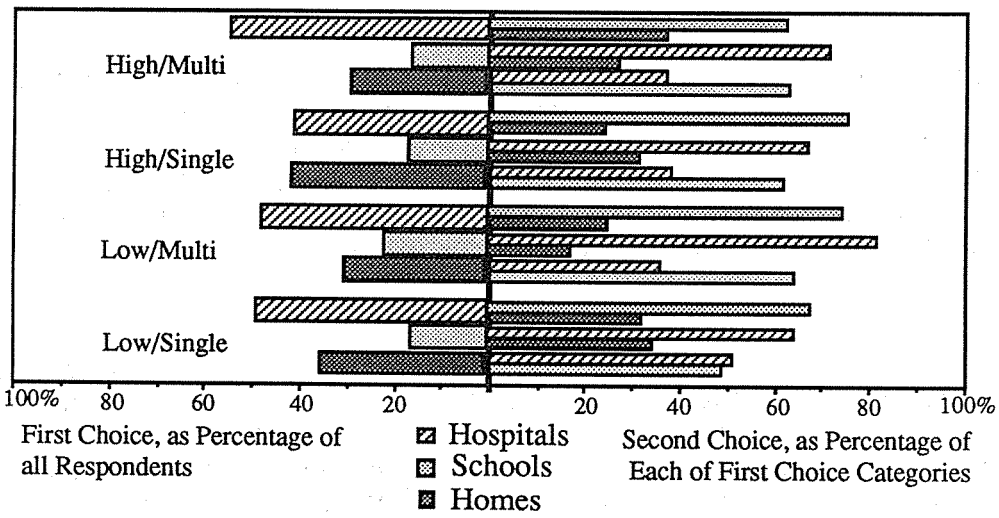

FIGURE 7 Preferences for work to be done

6. CONCLUSION

The primary aim of any aircraft noise amelioration scheme should be to improve the quality of life for those exposed to high levels of aircraft noise. Many schemes have been implemented in other countries but there have been no reported systematic studies on attitudes of residents to various types of schemes. There have been few studies on assessments of satisfaction once the schemes have been implemented.

The survey of resident attitudes, carried out around Sydney Airport, provides information on the degree of community acceptance of various types of schemes. While caution should be used in applying the results of this survey to the areas around other airports in Australia, three particularly relevant findings are that there is a strong preference for schemes which allow the resident to remain in their home, that the residents are reluctant to contribute to the costs associated with the scheme and that they consider those exposed to the most noise should receive the most assistance.

A significant finding from the social survey was a lack of knowledge of the likely benefits of building modifications and a lack of acceptance by more than half the sample of air conditioning which would be needed to provide alternative ventilation. An education program would be an essential part of the community liaison associated with the implementation of any scheme.

The survey response indicated the first choice for priority for amelioration measures was hospitals followed by homes and then schools. The extent of work and nature of applicable public buildings would need careful consideration to avoid overlap with commercial buildings. Each public building would need individual assessment of the work necessary. It may be more appropriate for this work to be undertaken in parallel with the implementation of an amelioration scheme for residential dwellings.

7. REFERENCES

M Burgess and R Zehner (1993) *Report on Aircraft Noise Amelioration Study*, prepared by Unisearch (UNSW) for the Commonwealth Department of Transport and Communications

Commonwealth of Australia (1990) *Response to "Aircraft Operations and the Australian Community" (Report of the House of Representatives Select Committee on Aircraft Noise, HORSCAN)*, Commonwealth of Australia.

HORSCAN (1985) *Report of the House of Representatives Select Committee on Aircraft Noise,* AGPS, Canberra.

8. ACKNOWLEDGEMENTS

The findings reported in this paper were part of a larger study which was undertaken on behalf of the Department of Transport and Communications in accordance with the Government's response to Recommendation Number 6 of the HORSCAN Report.

CRITERIA FOR RAIL TRAFFIC NOISE

Robert B. Bullen and Sarah E. Banks

Mitchell McCotter and Associates Ltd Pty, 24 Falcon Street, Crows Nest, NSW 2065

INTRODUCTION

Noise from rail traffic can be a cause of serious disturbance for residents living near rail lines, resulting in disturbance to sleep, conversation and other activities as well as general annoyance. In Australia, NSW and Queensland have specific guidelines for assessment of rail traffic noise, namely:

- For planning purposes, $L_{eq(24hr)}$ levels should not exceed 55 dB(A) and L_{max} levels should not exceed 80 dB(A).
- Maximum acceptable levels are 60 dB(A) $L_{eq(24h)}$ and 85 dB(A) L_{max}

Other States rely on the provisions of Australian Standard AS 2107, which sets recommended maximum internal L_{eq} noise levels of 30 - 35 dB(A) for sleeping areas in suburban houses. If external windows are open, this would imply external night-time noise levels of 40 - 45 dB(A), which is considerably more stringent than the guidelines above.

In this paper, results from international studies of community response to rail traffic noise are compared, and used to assess the implications of the above guidelines. The guidelines are also compared with those used for other noise sources such as aircraft and road traffic, and with rail traffic noise criteria used in other countries. The feasibility of meeting various criteria is also discussed. Assessment criteria are then suggested which are considered to provide acceptable protection for residents, to be in line with international practice, and to provide an achievable goal for management authorities.

FINDINGS REGARDING ANNOYANCE DUE TO RAILWAY NOISE

A number of studies of community reaction to railway noise have been carried out in various countries over the last two decades. In this paper, attention will be focussed on results concerning general annoyance with rail traffic noise and sleep disturbance due to the noise, although many studies have also considered other effects such as interference with conversation or television listening.

It is agreed by most researchers that the most appropriate noise measurement unit for assessing annoyance due to railway noise is $L_{eq(24hr)}$. This represents the total noise energy due to train passbys over a single day. Fields and Walker (1982), after a thorough comparison, conclude that annoyance reactions to railway noise are more closely related to $L_{eq(24hr)}$ than to various alternative noise indices.

The percentage of people found to be highly annoyed by railway noise has been plotted against $L_{eq(24hr)}$ for a variety of studies in Figure 1. It can be seen that generally the results cluster together reasonably well. The Richards (1975) data stands out as being significantly different: these data are an estimate for annoyance in the UK due to the new Channel Tunnel rail link, and are clearly quite conservative.

A cubic regression curve fitted to all data except Richards' is also shown in Figure 1. The correlation co-efficient for this regression was 0.74. The regression curve indicates that at 55 dB(A) $L_{eq(24hr)}$ - the "planning" criterion used in NSW and Queensland - around 8% of people are likely to be highly annoyed by the noise. At 60 dB(A) $L_{eq(24hr)}$, around 10% of people are likely to be highly annoyed.

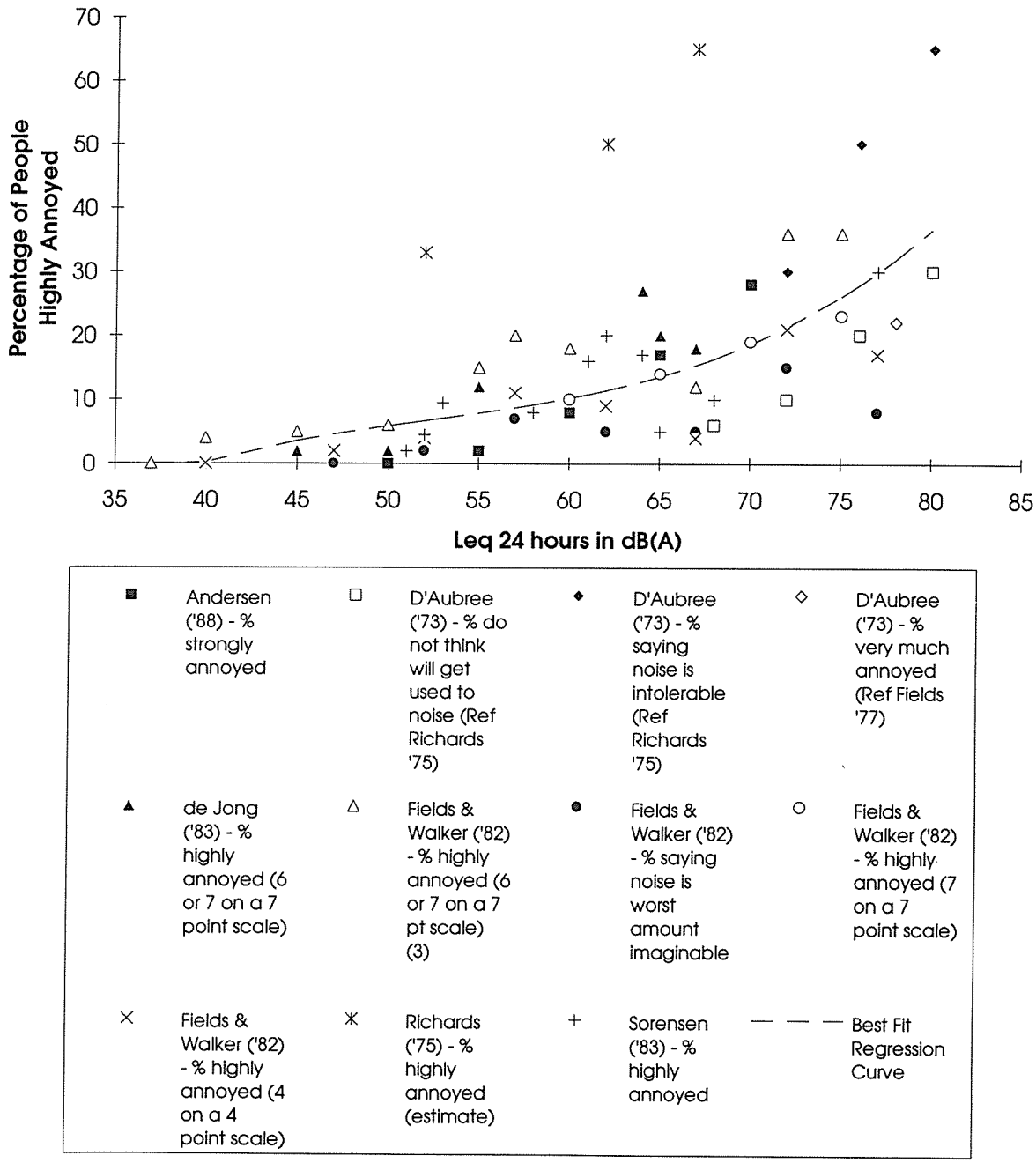

Figure 1 SUMMARY OF DATA ON ANNOYANCE DUE TO RAIL TRAFFIC NOISE

Similar data can be used to estimate the proportion of people annoyed to any extent by rail traffic noise. This indicates that at 55 dB(A) $L_{eq(24hr)}$ around 30% of people are likely to be annoyed to some extent, and at 60 dB(A) $L_{eq(24hr)}$ around 40% of people are likely to be annoyed.

Two surveys of response to noise from a new railway line were conducted by de Jong (1983) at intervals of 4 and 16 months after the line opened. These results indicate that reaction to a newly-opened rail line is likely to be stronger than for an existing line, for the same noise level. This result has also been found for road traffic noise (Langdon and Griffiths 1982). Fields and Walker (1982) also found a relationship between length of residence in the area and annoyance, longer term residents being less annoyed by the railway noise.

De Jong (1983) suggests that the lessening of very high annoyance in the community with time is not due to individuals becoming habituated to the noise, but rather to noise-sensitive residents moving from the area and being replaced with less sensitive people. This is consistent with results found for road traffic noise by Langdon and Griffiths (1982).

Results from a number of surveys indicate that noise from maintenance operations such rail grinding, and from shunting and similar operations, cause annoyance to more people than noise from through trains. It is suggested that this effect requires research in the Australian context, since it indicates that the current concentration on criteria for limiting noise from through trains may be misplaced. There may also be implications for possible ameliorative measures, since one method of reducing through train noise would be more regular rail grinding, which would increase the level of maintenance noise.

FINDINGS REGARDING SLEEP DISTURBANCE DUE TO RAILWAY NOISE

Disturbance to sleep as a result of environmental noise is a particularly emotive issue, raising the possibility of effects on health and other effects of which a resident may not be fully aware. For this reason, most researchers have preferred experimental methodologies to study the degree of sleep disturbance caused by noise, rather than social surveys. The sleep disturbance may be assessed by subjectively-reported sleep quality, number of awakenings during the night (either self-reported or as assessed from an electro-encephalograph) or number of changes in sleep state.

The present review of results from this research will include studies of single noise events other than train passbys, such as individual motor vehicle or aircraft passbys. The effects of these various noises on sleep are assumed to be similar, for the same noise level, so that results from a number of studies can be compared. The total number of awakenings due to noise will be taken as the primary indicator of the degree of annoyance caused by the noise.

A number of experimental studies (for example Vallet, 1983; Ohrstrom, 1988) have concluded that the L_{eq} noise level does not provide a good measure of the sleep disturbance produced by noise, and that a better measure would be one which takes account of the level and number of individual noise events, or noise "peaks". For this review, the maximum internal noise level during a noise event will be used as the measure

of noise exposure. The "response" variable will be taken as the number of awakenings per 100 night-time noise events.

The number of awakenings may be registered on an electro-encephalograph (EEG) or reported by subjects the following morning. The number of awakenings for reasons unrelated to noise, as determined from results on nights when subjects experienced very little noise, is subtracted from the total number of awakenings to give the number which are due to noise alone.

For all surveyed studies where the data permitted an approximate calculation of the number of noise-related awakenings per 100 events and the average maximum noise level during those events, the resulting data are shown in Figure 2. Note that the data presented by Griefahn (1990) are in the form of a predictive equation rather than individual points, and this is shown as a line in Figure 2.

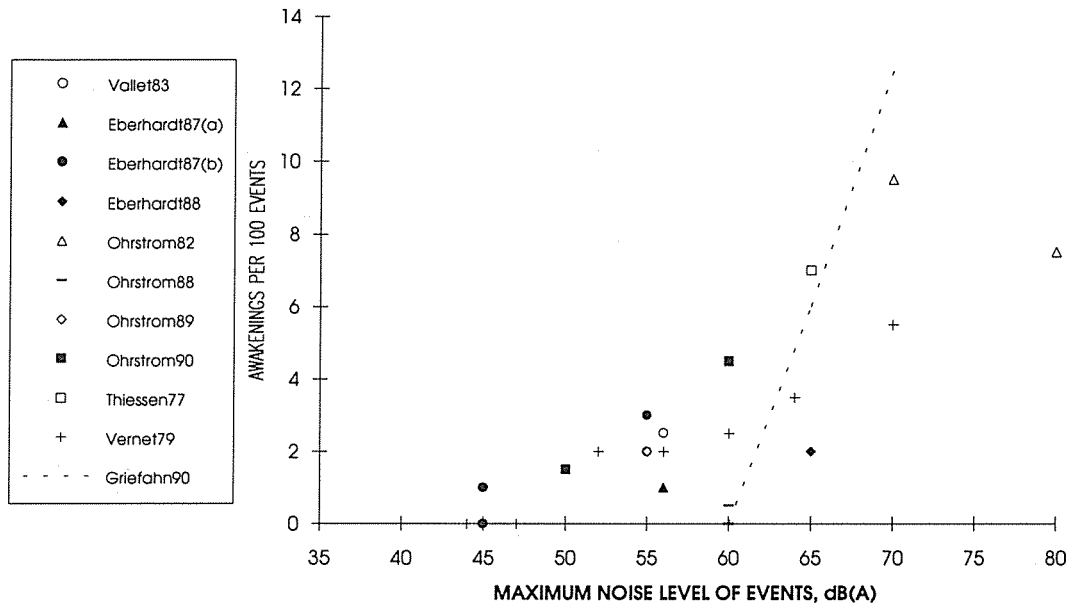

Figure 2 SUMMARY OF DATA ON SLEEP DISTURBANCE

It can be seen that the data in Figure 2 show a definite clustering, which would allow a reasonable estimate of the effect of a given noise condition.

The maximum noise levels in the Figure are internal noise levels within a bedroom. With external windows open, the internal noise level will be approximately 10 dB below the external level. If the noise level from train passbys was 80 dB(A), (the "planning" guideline in NSW and Queensland), and if residents had bedroom windows open, then from Figure 2, between five and ten events per 100 would result in an awakening. Hence, for example, if there were 25 passbys in an eight-hour period between 10 pm and 7 am, residents would be expected to experience an additional one to three awakenings per night due to rail traffic noise, compared with an average of one to two awakenings for other reasons.

REQUIREMENTS FOR AMELIORATIVE MEASURES

To illustrate the application of various criteria in terms of permissible distances between residences and railway, the following parameters will be assumed for a section of track:

- 200 train movements per day;
- average speed 60 kph;
- noise levels as for standard rolling stock used by CityRail, Sydney - half the movements Tangara trains, half non-Tangara.

Table 1 below shows minimum distances from the track required to meet the "planning" and "maximum" criteria for NSW and Queensland under various conditions.

Table 1 MINIMUM DISTANCES FROM TRACK TO MEET CRITERIA

CONDITIONS	Distance in metres to meet 80 dB(A) L_{max}	Distance in metres to meet 55 dB(A) $L_{eq(24hr)}$	Distance in metres to meet 85 dB(A) L_{max}	Distance in metres to meet 60 dB(A) $L_{eq(24hr)}$
Standard track	16	42	7	16
Points	30	88	14	34
Steel girder bridge, no vibration isolation	78	280	35	110

From Table 1 it is clear that the distances required to meet the L_{eq} criteria are considerably higher than those to meet the L_{max} criteria. Only for lines where there were less than approximately 60 movements per day would the L_{max} criteria be more stringent than the L_{eq} criteria.

To met the "planning" criterion of 55 dB(A) $L_{eq(24hr)}$, ameliorative measures would be required wherever residences were situated within 42 m of standard track, or within 88 m of the track if points are present.

COMPARISON WITH OTHER CRITERIA

Figure 3 below compares existing Australian criteria with those used in other countries.

Daytime or 24-hour noise criteria range from 55 to 70 dB(A) L_{eq}. The only criterion which is as low as that set by NSW and Queensland is by the UK. Midlands Joint Action Committee for Clean Air and Noise Control. This is stated as being the level below which there would be no significant disturbance. Many countries, however, place a more stringent limit on the night-time L_{eq} level due to rail traffic noise than the daytime L_{eq} limit. These range from 40 to 63 dB(A) L_{eq}.

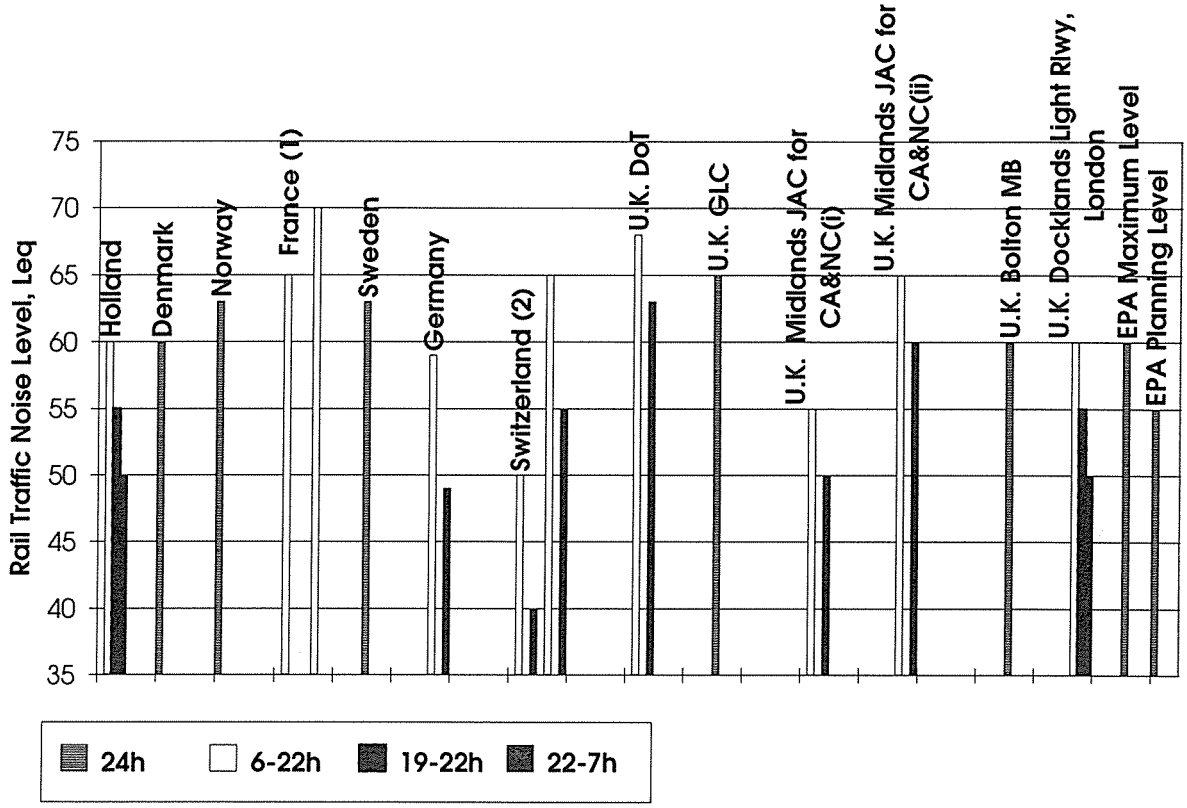

Figure 3 OVERSEAS RAIL TRAFFIC NOISE CRITERIA

In Japan, a criterion for rail traffic noise is set in terms of the maximum passby level, namely that the average of maximum noise levels should not exceed 70 dB(A). This is the only identified country having a criterion for rail traffic noise which is more stringent than that of NSW and Queensland. In the United States, rail traffic noise criteria are concerned with the noise emitted by the train itself, and not with the noise level at residences.

For other transportation-related noise sources, the point at which 10% of residents are highly annoyed has commonly been used as an indication of the maximum tolerable noise level for new developments. For example, for aircraft noise, Australian Standard AS 2021 recommends that within the 20 ANEF zone new residences should incorporate noise reduction measures in their design, and that areas with ANEF higher than 25 are "unacceptable" for new residential development. At 20 ANEF, approximately 10% of residents are seriously affected by aircraft noise and 48% are moderately affected. From the discussion above, this point is approximately equivalent to 60 dB(A) $L_{eq(24hr)}$ for rail traffic noise.

The NSW Roads and Traffic Authority sets noise level objectives for new road projects which in most cases represent noise levels of 60 dB(A) $L_{eq(24hr)}$ and 55 dB(A) $L_{eq(10pm\text{-}6am)}$. For road traffic noise, this corresponds to the point at which approximately 18% of residents would be highly annoyed. Other Australian road traffic authorities use similar criteria.

DISCUSSION AND CONCLUSIONS

On the basis of the above discussion, the current NSW and Queensland "maximum" criterion of 60 dB(A) $L_{eq(24hr)}$ corresponds more closely with criteria used for planning purposes in assessment of other types of noise. This would also be more consistent with rail traffic noise criteria used for planning purposes in other countries, and represents the point at which approximately 10% of long-term residents would be highly annoyed by the noise.

Adoption of this criterion would mean that for a typical suburban track, ameliorative measures would be required if residences were located within approximately 16 m of the track (assuming there are no points or other special noise sources). This is clearly a more achievable goal than a planning criterion of 55 dB(A) $L_{eq(24hr)}$, which for the same conditions would require ameliorative measures wherever residences are within 42 m of the track.

The potential for sleep disturbance due to rail traffic noise is best assessed using the maximum noise level from train passbys and the number of passbys per eight-hour sleeping period. Assuming approximately 25 passbys per sleep period, with a maximum level of 80 dB(A), residents sleeping with windows open facing the line could expect to experience one to three awakenings per night due to the rail noise.

Rather than limiting the maximum noise level of events, an alternative method of protecting against sleep disturbance is to limit the night-time L_{eq} noise level. This is the method which is generally adopted overseas, and has the advantage that the rail operator can "trade off" a higher maximum noise level against lower numbers of night-time operations.

With a criterion of 50 dB(A) $L_{eq(10pm-7am)}$, and 25 suburban train passbys during this period, the maximum noise level of events would be limited to approximately 79 dB(A). Ameliorative measures would be required where residences were located within approximately 19 m of the track. If the number of movements were increased to 50 per night, the maximum level would be limited to 76 dB(A) and ameliorative measures would be required for residences within approximately 30 m of the track. In either case, if bedroom windows in the worst-affected residences were open and facing the track, residents would experience approximately one to three awakenings per night due to the rail noise, compared with an average of one to two awakenings for other reasons.

In summary, the existing NSW and Queensland planning criterion of 55 dB(A) $L_{eq(24hr)}$ would appear to be inconsistent with criteria used in other countries and for other sources, and also difficult to achieve in practice. For protection against sleep disturbance, a criterion in terms of the night-time L_{eq} noise level may be preferable to a maximum-level criterion which does not limit the number of events.

A suggested formulation for a general rail traffic noise criterion is that the $L_{eq(24hr)}$ noise level should not exceed 60 dB(A) at residential premises, and the $L_{eq(10pm-7am)}$ level should not exceed 50 dB(A). This would be consistent with a number of criteria used internationally, and is seen as a realistic and achievable rail traffic noise criterion for planning purposes.

REFERENCES

1) Ahrlin, U and Rylander, R (1979) *Journal of Sound and Vibration (JS&V) 1979 vol 66(3).* Annoyance Caused by Different Environmental Noises

2) Andersen, TV et al (1983) *JS&V 1983 vol 87(2).* Reactions to Railway Noise in Denmark

3) Andersen, TV, et al (1988) *JS&V 1988 vol 120(2).* Reactions to Railway Noise in Denmark - A Correction

4) Eberhardt, JL (1988) *JS&V 1988 vol 127(3).* The Influence of Road Traffic Noise on Sleep

5) Eberhardt, JL and Akselsson, KR (1987).*JS&V 1987 vol 114(3).* The Disturbance by Road Traffic Noise of the Sleep of Young Male Adults as Recorded in the Home

6) Eberhardt, JL et al (1987) *JS&V 1987 vol 116(3).* The Influence of Continuous and Intermittent Traffic Noise on Sleep

7) Fields, JM (1977) *JS&V 1977 vol 51(3).* Railway Noise and Vibration Annoyance in Residential Areas: Current Findings and Suggestions for Future Research

8) Fields, JM (1979) *JS&V 1979 vol 66(3).* Railway Noise and Vibration Annoyance in Residential Areas

9) Fields, JM (1983) *JS&V 1983 vol 87(2).* Rapporteur's Report: Community Response to Railway Noise

10) Fields, JM and Walker, JG (1982) *JS&V 1982 vol 85(2).* The Response to Railway Noise in Residential Areas of Great Britain

11) Howarth, HVC and Griffin, MJ (1988) *JS&V 1988 vol 120(2).* Human Response to Simulated Intermittent Railway-Induced Building Vibration

12) de Jong, RG (1979) *JS&V 1979 vol 66(3).* A Dutch Study on Railroad Traffic Noise

13) de Jong, RG (1983) *JS&V 1983 vol 87(2).* Some Developments in Community Response Research Since the Second International Workshop on Railway and Tracked Transit System Noise in 1978

14) Langdon, FJ and Griffiths, ID (1982) *JS&V 1982 vol 82.* Subjective Effects of Traffic Noise Exposure, II: Comparison of Noise Indices, Response Scales, and the Effects of Change in Noise Levels

15) Ohrstrom, E et al (1980) *JS&V 1980 vol 70(3).* Lab. Annoyance and Different Traffic Noise Sources

16) Ohrstrom, E (1989) *JS&V 1989 vol 133(1).* Sleep Disturbance, Psycho-Social and Medical Symptoms - A Pilot Survey Among Persons Exposed to High Levels of Road Traffic Noise

17)Ohrstrom, E and Bjorkman, M (1988) *JS&V 1988 vol 122(2).* Effects of Noise Disturbed Sleep - A Laboratory Study on Habituation and Subjective Noise Sensitivity

18) Ohrstrom, E and Rylander, R (1982) *JS&V 1982 vol 84(1).* Sleep Disturbance Effects of Traffic Noise - A Laboratory Study on After Effects

19) Ohrstrom, E and Rylander, R (1990) *JS&V 1990 vol 143(1).* Sleep Disturbance by Road Traffic Noise - A Laboratory Study on Number of Noise Events

20) Ohrstrom, E et al (1988) *JS&V 1988 vol 127(3).* Effects of Night Time Road Traffic Noise - An Overview of Laboratory and Field Studies on Noise Dose and Subjective Noise Sensitivity

21) Richards, EJ (1975) *JS&V 1975 vol 43(4).* A Method of Assessing the Noise Nuisance Arising from the Channel Tunnel High Speed Rail System

22) Sorensen, S and Hammar, N (1983) *JS&V 1983 vol 87(2).* Annoyance Reactions due to Railway Noise

23) Thiessen, GJ and Lapointe, AC (1977) *JASA Fall 1977 vol 62(1) (94th meeting 13 Dec 1977, Session C12).* Effect of Truck Noises on Percentage of Deep Sleep

24) Vallet, M et al (1983) *JS&V 1983 vol 90(2).* Long Term Sleep Disturbance Due to Traffic Noise

25) Vernet, M (1979) *JS&V 1979 vol 66(3).* Effect of Train Noise on Sleep for People Living in Houses Bordering the Railway Line

26) Walker, JG (1988) *JS&V 1988 vol 120(2).* Railway Noise Exposure: A Possible Method of Establishing Criteria for acceptability

27) Waters, DM (1979) *JS&V 1979 vol 66.* Overall Railway Noise Impact in the UK

NOISE MANAGEMENT IN THE WORKPLACE

W Williams

National Acoustic Laboratories

Introduction

It is still common for people to talk about Hearing Conservation Programs and noise induced hearing loss (NIHL) in industry and occupational health areas rather than the concepts of noise management and noise injury. The concept of hearing conservation programs compared to noise management programs is one of risk control as compared to hazard minimisation or removal.

Noise Injury

To date the concept of noise injury has been avoided by industry and the phenomenon is discretely referred to as noise induced hearing loss as opposed to the more simple and more committing term, noise injury. The term noise injury has resulted from legal definitions with respect to workers' compensation. It is common practice to date to regard an individuals who have suffered hearing loss as the result of exposure to excessive noise levels with some suspicion. An individual who has undergone a 'noise induced hearing loss' has not undergone the same "rights of passage" as someone with an obvious external physical injury.

A physical injury typically involves the spilling of blood, calling an ambulance and a treatment period all followed by convalescence and rehabilitation. This process then 'legitimises' the passage into the compensation system and all of the benefits that follow. Noise injury is usually gradual in nature and offers no easy path into the rehabilitation area. It is an unseen problem and therefore doesn't need a solution. who goes home from work and says "I almost got industrially deafened today"?

Until the cultural view of a noise injury is accepted it will continue to be very difficult to get a total solution to the noise problem. Because it is an unseen problem with gradual onset and the concept of damage is very much related to statistics and the probability of damage, there is a tendency on the part of all individuals to adopt a 'this won't happen to me or any one I know' attitude.

Existing "Hearing Conservation" Programs

Sad to say a typical "hearing conservation" program will consist of a noise survey of the work area to establish 'noise hazard areas'; the issue of personal hearing protection to exposed workers, perhaps with some education in their use; and periodic audiometric monitoring of workers to see if the hearing conservation program is effective. Sometimes there is an attempt at implementing some form of engineering noise control but often this is seen by management as too expensive or simply not possible.

There are several problems with this approach to the reduction of noise injury in the workplace and indeed in society in general. By the issue of personal hearing protection the worker is still exposed to the noise only from now on, the employer hopes, it will be in a controlled way and thus reduce the worker's daily noise dose resulting from the exposure. Unfortunately recent indications from the United States, where this approach was common, has shown that this method of hearing conservation is not working (Waugh, 1993).

The failure of this approach through the reliance of personal hearing protection come under two main categories:-

1) Insufficient attenuation is provided to the wearer through;

a) failure to supply an individual with protection that fits correctly and is comfortable to wear;
b) failure to correctly use or fit the protection correctly each time it is worn; and
c) the lack of an adequate maintenance program.

and

2) Failure on the part of the individual to wear the protection for the entire duration of the exposure. This can arise from many reasons such as lack of individual awareness, discomfort of the supplied protectors, communication is made difficult due to over protection or a simple choice not to wear protectors for some personal or social reason.

Unfortunately the carelessness of the employee is always the responsibility of the employer. A case reported recently in the magazine Factory Equipment News (1993) that:-

> "The High Court has continually reinforced the view that employers need to realise that some of their workers are hasty, careless, inadvertent, unreasonable and even disobedient" and that "employers have a responsibility to guard against both likely and unlikely accidents".

So what ever happens the employer's workers compensation insurance will be called on to pay the bill.

To keep employees constantly aware of the potential for noise injury it is necessary to initially supply comfortable, appropriate personal hearing protection and an on going education program coupled with a regular maintenance program. Initial enthusiasm must not be allowed to wain.

The use of audiometric monitoring of exposed personnel to see if a hearing conservation program is working is, unfortunately, a case of "closing the stable door after the horse has bolted". The practice with audiometric monitoring is that unless there is a drop of at least 15 dB in response to any frequency compared to a base line audiogram, there is not considered to be any change in the subjects hearing (AS 1269-1989).

Couple this with the natural variability to which all audiometric tests are subject and diagnosis becomes very difficult indeed. In practice the ascertaining of a definite hearing loss from an audiogram tends to be much more complex than just outlined. However, the point to be made is that when a hearing loss is discovered, which may only be after a considerable time period, the damage is irreversible.

Monitoring audiometry should be regarded as a part of the program that is undertaken as an absolute last step or when other requirements (eg legal) dictate that it is required. It should never be regarded as a test to see if the noise reduction program is working. If there are limited available funds in an organisation for a noise management program then the money is better spent on noise monitoring or engineering noise controls. "Workplace health surveillance should never take the place of safe work practices" (Caswell, 1993).

The one plus of monitoring audiometry is that it can identify individuals with a hearing loss and permit them to undergo evaluation and commence appropriate rehabilitation as soon as possible (Hogan, 1993).

Too often management are convinced that there cannot possibly be a solution to the noise problems in their work areas. Any of a number of excuses exist to support their assertion it's too expensive; too hard; an inherently noisy process; if there's no noise there's no work; and on and on. It follows that the site Occupational Health and Safety Officer or representative becomes the proverbial "meat in the sandwich" as they are caught in the dilemma of knowing from the work place and from complaints that there is a site noise problem, and from management that there is reluctant to implement any positive action as management feels that little can be done or is worthwhile doing.

However, the main objection to a hearing protection program is that it personalises the noise problem and turns the view of the program into one of risk control rather than one of hazard prevention.

Noise Management

Noise management encompasses the total concept of not only removing the noise problem but initiating the necessary changes in management philosophy that are required to implement a total noise management program. Inherent in the total program must be the necessary mechanism to include rehabilitation of those who have

suffered noise injury. It must be realised that when an institution accepts that there is a noise injury potential in a workplace the probability exists that some individuals may have already suffered some form of noise injury.

It starts with the planning stages before new plant is purchased or factories and work areas are designed and never truly concludes as it should always include an on going program monitoring component. With existing facilities and plant there must be the concept of a positive planning approach such that even if a solution cannot be implemented tomorrow the commencement of a long term plan can start today.

A noise management program must cover a wide range of areas including:-

- The formation of a "Noise Committee" either as a separate body or as part of the work place Occupational Health and Safety Committee.

- The initialisation of changing management philosophy toward noise and noise injury.

- Site planning. Locating noisy areas or plant physically far away from areas that require quite conditions.

- Buy quiet. Purchase machinery and plant that has noise emissions that are as low as practical. Plant always gets more noisy as it ages and it is much less expensive to purchase plant with noise control attached rather than to try and fit controls retrospectively.

- Work practices. When looking at new plant or processes go to the basic process and see if it can be replaced with a different process or at least one that is less noisy.

- Survey. In an existing area carry out a noise survey and list the priority for remedial or engineering control work to be carried out. This sort of survey can be in the form of a simple walk through audit or could go as far as a comprehensive noise survey by an professional consultant.

- Protection. The supplying of personal hearing protection to individuals in exposed areas. This step is best regarded as an interim measure until the individual can be removed from the risk of exposure to noise.

- Administrative controls. Administrative controls or rotating individuals from noisy environments to quieter ones can be used but should be used very carefully and only after partial daily noise doses have been calculated and checked.

- Noise monitoring and program evaluation. The regular monitoring of noise will permit a useful evaluation of the noise management program for the site and allow remedial action to be proactive in terms of hearing injury rather than retroactive.

- Monitoring audiometry. As mentioned above, if there is a legal requirement, excess money or some other pressure for this service then certainly use monitoring audiometry. However, it should not be used in place of noise monitoring to evaluate a noise management program.

- Legal requirements. Through out this process all of the relevant legal requirements must be met.

To rank these areas in priority is very dependent on the existing or future workplace. Some areas, such as site planning, may have low consideration in the context of 'what to do next' for an existing workplace, however, for the long term it should always be kept in mind. Factories and workplaces change or evolve over time and what seems an unlikely requirement today may be the imperative tomorrow.

As a consequence of multiplicity of requirements of a noise management program and the necessity that the program must be on going, the whole process can be viewed in terms of a change 'cycle'. This can be exemplified by the organisation setting goals that are to be reached in the noise management program, such as overall noise levels in work areas, and slowly working toward those goals as opportunities arise. Such opportunities as buying quieter machinery, changing to less noisy processes and redesigning work areas all have the ultimate goal of reducing workplace noise levels. Thus the cycle can be entered at any point and as long as momentum is maintained long term goals will be reached.

It is important that the 'Noise Committee' be aware of all possibilities and be open to discussion as to what may be the best course of action. As with any business enterprise planning must include long term goals and short term objectives.

Implementation

It is no easy task for an organisation to admit that there are noise problems within it's areas of responsibility. Admitting that there is a noise problem can be equated to accepting that there will already be some individuals in the organisation with a noise injury resulting from excessive exposure. The company will be concerned about a 'round' of compensation claims and individuals may be reluctant to admit to the fact that they have a hearing loss. This is a process that must be worked through on an individual and a company level sometimes with professional assistance.

When setting up a noise committee or task force it is important to ensure that all groups that want or should have an input are involved. Too often it is observed that management will install a sound proof enclosure around a machine on a production line only to find that operators leave access doors open thus negating the purpose of the enclosure. Why are the doors left open? Usually the operators have not had an input to the design of the enclosure, however, they are paid on an incentive basis and are expected to maintain high output levels. As the operators were not consulted when the design of the enclosure was being considered, no thought went into the constant necessity for opening and closing the doors. Consequently the operators' solution is to leave the panels off, or open, in order to maintain the required production output.

All parties need to be involved. For a solution to work effectively all parties need to have commitment to and personal 'ownership' of that solution.

Engineering and noise management

Why should those involved with acoustics or acoustic consulting be interested in noise management?

Quite often it will be the acoustic consultant who will have the opportunity to raise the issue in such a manner that management will be predisposed to hear. The consultant will be seen as an independent expert with no vested interest. It is an excellent opportunity to get a company started on a noise management solution to their noise problems rather than an ad hoc implementation of engineering solutions, hearing protection and monitoring audiometry drawn together under the guise of a Hearing Conservation Program.

More importantly it is the opportunity to bring hope to an otherwise hopeless situation. Where the organisation who previously declared that "this is a noisy business and will always be that way" can be given the tools to see the way out of one of the largest and most rapidly growing health problems (Workcover Authority, 1993).

References

Australian Standard AS 1269 - 1989, Acoustics - Hearing conservation

Caswell, A (1993), First steps towards a surveillance program, in Australian Doctor, 13 August 1993

Factory Equipment News (1993), Employee carelessness can cost employer, March 1993

Hogan, A (1993), An integrated approach to rehabilitation for workers with noise injury in the workplace, paper presented at the National Seminar on Noise Management in the Workplace, Brisbane, April 1993

Waugh, D (1993), Do Hearing Conservation Programs Really Work, paper presented at the National Seminar on Noise Management in the Workplace, Brisbane, April 1993

Workcover Authority (1993), "Industrial Deafness, Workers Compensation Statistics, New South Wales 1991/92, Workcover Authority of NSW

PUBLIC POLICY AND THE PREVENTION OF INDUSTRIAL DEAFNESS AMONGST AUSTRALIAN FARMERS

Ian Eddington
University of Southern Queensland.

David Moore
David Moore and Associates, Brisbane

Patricia Rooney
University of Southern Queensland.

INTRODUCTION

This paper is about the role of noise experts in meeting the prevention challenge occasioned by the presence of noise induced hearing loss amongst Australian farmers. Although, of necessity, the paper contains a description of the nature of farmers and farming as work, its main concern is with the prevention of industrial deafness and the manner in which public policy strategy might call up the expertise of noise professionals for this purpose. It is thus a paper about how expert knowledge may be communicated to those who might best benefit by it, and about strategy to help ensure that such knowledge might become enshrined in habit, safe job procedure, and equipment design.

Noise induced hearing loss is preventable but not curable and recognition of this simple fact is essential if progress is to be made in eradicating what, technically, is a well understood affliction. Data presented here reveal the severity of industrial deafness discovered amongst a sample of Australian farmers and initiate an enquiry into best content and management practice for public policy preventative action. There are three parts to the paper: 1 presentation of industrial deafness data, 2 discussion of the farming work environment as a special case requiring tailor made strategy of its own, and 3 on the basis of 1 and 2 above, derivation of a general guide to best practice in the design of public policy preventative strategy.

INDUSTRIAL DEAFNESS AMONGST AUSTRALIAN FARMERS

Anthony Hogan[1] draws attention to the question of industrial deafness amongst Australian farmers. Plakke and Dare[2] provide evidence of its presence amongst North American farmers. In a forthcoming paper the authors prove the existence of quite severe industrial deafness amongst farmers in Australia. In the paper hearing threshold profiles are constructed for farmers and non farmers across three age categories: 25-34: 35-49; and 50+. By defining the presence of industrial deafness as a 19 dBA average threshold over frequencies of 1,000, 2,000 and 3,000 Hz, it is possible to discern the likelihood of industrial deafness amongst the 35-49 and 50+ age categories. Inspection of the frequency profiles of each of the people in the age/occupation groups specified allows two facts to be

---

1 Hogan, Anthony *Workers with Noise Induced Hearing Loss,* Journal of Occupational Health and Safety- Aust NZ, 1992, 8 (2): pp 129-134.

2 Plakke, Bruce L and Dare, Elizabeth, *Occupational Hearing Loss in Farmers,* Public Health Reports, Vol 107, March-April, 1992, pp 188-192.

stated: (1) for the 35-49 group 20% of non farmers and 60 % of farmers suffer industrial deafness in at least one ear and, (2) for the 50+ group 12 % of non farmers and 87 % of farmers suffer industrial deafness in at least one ear. Differences between farmers and non farmers in these two groups are significant at P = 0.05 for the single tailed t test.

This data and the test confirmations reveal that farmers as a group are more prone to industrial deafness than non farmers. While farmers and non farmers in a sample will be shown to exhibit very similar profiles in their second decades and be free from industrial deafness, differences emerge in the third decade and widen thereafter. The data on which these statements are based were cleaned in the sense that subjects whose hearing acuity was likely to be the result of factors other than age, non-occupational social exposure and occupational exposure were excluded. Exclusions were made on the basis of a detailed questionnaire and interview. Testing procedures and testing equipment met Australian Standards 1269 - 1989 Acoustics, Hearing Conservation and 1259-1990 Acoustical Sound Level Meters respectively and testing was carried out by a trained nurse.

Because of the data cleaning technique, the samples can not be said to be truly random. However we believe they are representative of the groups we wished to compare namely, single job farmers whose hearing profile is, after allowing for presbyacusis and socioacusis, primarily a function of ***their*** occupational exposure: and non farmers, unexposed to excessive noise and whose hearing profile, apart from presbyacusis and socioacusis, is primarily a function of ***their*** occupational exposure. The groups are different and illustrate the need for special preventative programs aimed at farmers.

Some interesting sub groups emerged as a result of data cleaning and amongst them were farmers using firearms and farmers holding more than one job. Firearms use and double jobbing will be shown to occur in the presence of substantial noise induced hearing loss.

The forthcoming paper will clearly demonstrate the presence of a preventable disease. The data will also call into question the effectiveness of present public policy preventative programmes. Are these programmes generally flawed? Do rural workers constitute a difficult and hard to reach audience requiring special attention? Or is it a combination of both these things? These questions will be discussed in the next section.

PUBLIC POLICY: PREVENTATIVE STRATEGY FOR FARMING AS A SPECIAL CASE.

(a) Rural work as a special kind of work.

There are indeed a number of factors which set rural workers apart from other occupational groups.

First the family unit is often the work unit. In the USA it is estimated that up to 25% of the agricultural workforce is under 16 years of age. Young children are invincible and are notorious for not wearing protective equipment such as hats and shoes. Perhaps damage in some begins early if *protective hearing devices are not used or equipment is not correctly maintained.*

Second farming work is said to be lonely work which fosters a stoic independence and resourcefulness which is sometimes *hostile to outside advice and opinion.*

Third, farmers are said to suffer from work overload in intensive seasonal bottle-neck periods. They are jacks of all trades and in this are often seen *to be careless of the precautions that should be taken with the tools they are using.* There is often not enough time in the day to acquire the knowledge.

Fourth the physical environment in which farmers work is naturally harsh and *noise and vibration are present in this environment in unique ways:* squealing hogs, bellowing animals, barking dogs, increasingly loud radio cabin noise, explosions, and machinery and equipment of all kinds. Concerning this latter category: there may well be a psychological element present in that, just as the shopkeeper associates the ring of the cash register with good work and profitability, so to may some farmers use noise as a reinforcing measure of hard work and honest endeavour. Hence the exhortation to "make the tractor work" by continually pouring on the power with monitoring by listening. This was certainly an impression gained by the authors when researching. For example one farmer would not have it that removing the baffles from a chain saw exhaust would (he did not wear muffs) hasten the onset of deafness. Rather his claim was that this act gave the machine more power and allowed him to work more quickly.

Fifth the organisational and structural dimensions of the farm are different. The hours of work are the hours demanded by the market, climatic conditions, and the vagaries of crop cycle. The job tasks to be carried out are the job tasks demanded by a dynamic and ever changing environment. First aid and medical attention is not always on tap and workplace amenities, not always being portable, are often absent. *The*

elements of this organisational vector often reinforce the stoic independence and "stubborn" culture of the "die hard" farmer. The exception often disproves the rule as in the case of the chain saw user mentioned above, whose hearing was unaffected by his habit. Unfortunately those following his example may not always be so lucky.

The brief outline above summarises farmers qua target audience as being independent, somewhat distrustful of authority and officialdom, somewhat careless of self, isolated in terms of work location, organisational structure and availability of face to face and print expertise, and subject to periods of work overload in a naturally harsh and noisy environment. If this description is valid then some credence may be given to the view that, when it comes to health promotion and communication, and therefore to the effectiveness of public policy preventative strategy, farmers are not as easy to reach as other work groups. How then might policy strategy be adjusted to accommodate the difference? An answer will now be offered to this question. It will emerge from an enquiry into current public health policy practice and the problem of how to communicate with the *hard to reach* audience.

(b) public health strategy and communicating with the difficult or hard to reach audience.

Friemuth and Mettger[3] have recently investigated the problem of communicating public policy strategy to the *hard to reach* audience. Inter alia, these authors comment on the problems caused by using pejorative labels like *hard to reach* and suggest that such labels are, in some sense, an **excuse** for policy failure. The policy failed because the audience was *hard to reach*. Policy design is/was not at fault. The audience is/was. Of course neither policy nor audience may be to blame: the failure may be in the nature of a communication block occasioned by the mismatch of policy instrument and audience characteristics.

But there can be no denying that there are particular audiences which are troublesome for policy strategy and health communication. In our view although farmers may be said to be different and challenging for public policy they are not among those audiences perceived to be *very* difficult to reach, eg those of low socio economic status, ethnic minorities etc. Policy strategy appropriately structured, correctly delivered and compatible with its audience characteristics, should, in the case of farmers, be capable of producing positive results in eliminating industrial deafness. What then are the vectors of a successful policy?

---

3 Freimuth, Vicki S and Mettger, Wendy, *Is there a Hard to Reach Audience?,* Public Health Reports, Vol 105 No 3, May-June 1990, pp 232-238.

There are three sides to this question: policy design per se, the audience (and the extent of its *hard to reachness)* and the matching of policy instrument with audience. Childers and Post[4], Mechanic,[5], and Feldman[6], amongst others, have researched characteristics of audiences at the *hard to reach* end of the spectrum. Four characteristics, present in varying degrees, are said to identify such audiences: 1, fatalism, 2 possession of poor information processing skills, 3, limited access to communication channels, and 4, a distrust of officialdom and dominant institutions. In connection with point 3, there is said to be an emphasis placed on ends information (television information emphasising what one wants to achieve, as opposed to print information telling one how to achieve it.

With the exception of point 2, these audience characteristics sit comfortably with the description of farmers given earlier and because of this are appropriate inclusions in a check-list of elements which might serve as a guide to policy design and delivery. But what of the policy instrument side? The literature[7] provides insights. Public policy strategy is typified as one of two kinds of approach. Interventions may be at the level of the individual or at the level of the population.

The individual approach is based on a one to one transaction between expert and patient requiring assessment, diagnosis, treatment, support and follow up. Such schemes, as *preventative* strategy, are said to be costly and of questionable efficiency. They are, by their very nature, difficult to apply in the case of farming, especially because, given the disparate locations, assessment is difficult in the first place. Help is certainly available but it is help at the *cure* end after the farmer personally seeks a medical opinion.

The population approach has been given much attention. Under this approach the employee population is targeted and there is an emphasis on prevention. The emphasis is on building an organisational culture which includes a preventative ethic. Under this approach, interventions are designed to reward employees for positive health behaviour. Interventions

---

4 Childers, T. and Post, J: The Information Poor in America, Scarecrow Press, Metuchen, NJ 1975.
5 Mechanic, D: *Socioeconomic Status and Health: an Examination of Underlying Processes,* in Pathways to Health: the Role of Social Factors, edited by Bunker, J. P., Gomby, D. S., and Kehrer, B. H., Henry J. Kaiser Foundation, Menlo Park, CA, 1989, pp 29-69.
6 Feldman, J. The Dissemination of Health Information, Aldine Publishing, Chicago, Illinois, 1966.
7 Freimuth, Vicki S and Mettger, Wendy op. cit.

themselves may be specific (eg no smoking zones) or general, such as awareness advertising and marketing outlining the bad effects of the unwanted behaviour. It has already been pointed out that farming lacks the organisational structure required for such strategy. Given that often the farmer is at once the employer and the employee, there is a second reason why the population approach is less suitable: it is an added burden to logically target oneself when there is no organisational incentive (as catalyst) for doing so. Yet if preventative action is to work, it will work essentially because individuals do apply the information to themselves and their own situation.

Thus on the policy instrument side there are two intervention models which are not a good fit for the farming environment. On the target side, there is something of a hard to reach audience. Furthermore there is a dislocation between instrument and target in that none of the intervention models (either individual or population) can easily incorporate the target audience characteristics. Indeed policy strategists have little choice but to design a composite strategy which catches farmers (and their partners and children) at the individual level through specific education and training, and which catches them at the *organisational* level through professional societies, legislation, and in the market place. An additional point needs to be made before the question of appropriate policy is discussed. It concerns the communication *channel* between policy maker and target audience.

Friemuth and Mettger[8] report the essence of some 40 studies about the audience as listener and learner in a communication as dialogue model of health promotion. These findings (reproduced in the box below) are relevant for those designing communication channels. The four boxed statements prescribe the channel transaction.

1 People inform themselves primarily at moments of need.

2 People rely first on their own responses. If these are not sufficient they turn first to sources close to them or those contacted habitually.

3 People judge information on how it helped them rather than on its expertise or credibility.

These findings, innocuous in themselves, are particularly troublesome for strategists wishing to enshrine expert knowledge about noise in a public policy communication. First, with industrial deafness, once a need is perceived, it is already too late for cure. Second, the affliction is

8 op. cit.

incremental, and given the isolation of farmers and the loneliness of farm work, may not, in the early stages, be meaningfully discernible through cognitive processes, or through those who are close or by habitual contact. Third, the *help* component of information about industrial deafness can have little impact in motivating acceptance of its message. This is because it is not possible at any one time to sample the *before* and *after* and make a positive choice for one of the two positions as say it would be in choosing between two methods of lifting or the ergonomics inherent in two different tractor cabins.

Figure 1 below highlights all of the difficulties discussed to date in a summarising schema which allows the complexity of the public policy challenge to be more fully appreciated.

Figure 1: Schematic representation of the policy design problem

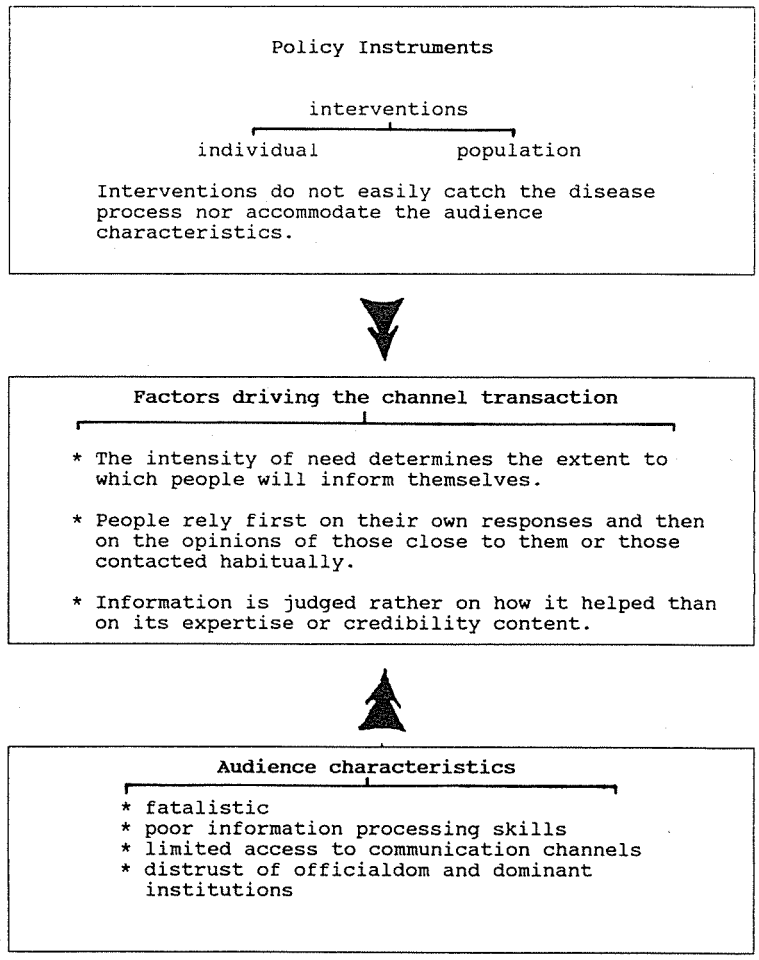

Figure 1 suggests that, by its very nature, industrial deafness is a disease which is (a), not easily covered by individual or population strategy, (the top box) (b) is at odds with the basic tenets upon which the channel transaction is predicated, (the middle box) and (c), afflicts an audience which is characterised by features typical of those who are hard to reach (the bottom box). Given this situation, how should strategy be constructed to ensure that the knowledge of noise experts is effectively utilised in farming activity? It is to this question that the paper now turns.

A GENERAL GUIDE TO DESIGN OF PUBLIC POLICY STRATEGY TO PREVENT INDUSTRIAL DEAFNESS AMONGST FARMERS

The lack of a close knit organisational structure in farming, the arms length stance sometimes taken by farmers towards outside expert knowledge, and the manner in which the disease itself and its progress are not caught by the dynamics said to drive audiences to listen and act all suggest that, where possible, farmers should be presented with a fait accompli. Damage potential should be designed out of the situation before farmers arrive. Thus radios in cabs should not be capable of producing damaging volumes, mufflers should reduce outputs to safe levels and so on. Where design is not possible preventative education programmes should begin with the very young and should be delivered at the *local* level by members of the farming community trained for the purpose. The family unit, as well as individuals, should also be targeted.

This finding, at the end of the day, is not extraordinary and is probably acceptable generally for many workplace diseases. However there is something to be said for the manner in which the knowledge of noise experts might be enshrined in design and safe job practice. Legislative interventions should be such as to harness the forces of the market to this endeavour. This last statement can be further explained using say, chain saws, as an example. Proactive legislation would require noise labelling, including health warnings together with some form of economic incentive (a) to entice farmers to buy equipment emitting lower noise levels and (b) to entice firms and their noise control engineers to design equipment emitting less noise. There could be a legislative requirement, say, that manufacturers of chain saws which emit noise above a certain level must supply ear muffs within the purchase package. Likewise there might be an increased tax concession allowed for the purchase of chain saws which emit lower noise levels. If the consumer sovereignty version of market theory is correct, then market forces, marshalled by legislative strategy like that just outlined, would work to enshrine preventative equipment design in the purchase transaction. Both buyer and

seller would benefit by dealing in safe equipment, society would benefit in the long run by savings won against promotion, testing and the quality of life and the market would naturally select out the expertly designed products.

There will always be those situations which escape design. Quiet explosives have not yet been invented. In such cases education and/or regulation and policing all have their place. The essential feature of these tools is that they should be operated on by locals, for locals, and towards establishing a culture of good habit. They should be preventative in nature, owned by the farmers and/or their organisations, and always aim at fostering self awareness and self respect.

CONCLUSION

Industrial deafness amongst farmers is a disease which can be prevented. The challenge is there for public policy strategy. This paper has offered broad guide-lines for strategy design.

LOW FREQUENCY NOISE DUE TO HVAC SYSTEMS AND ITS ASSESSMENT

By : Dr. Norman Broner
Vipac Engineers & Scientists Ltd

1.0 INTRODUCTION

The issue of sound quality in offices and other occupied spaces has been of continuing interest since the 1950's and with increased emphasis on total sensory comfort, has recently become even more important. A major component of comfort in buildings is the level of backgroud noise. In developing an acceptable noise criterion and an appropriate assessment method, the needs of work efficiency have to be balanced against the cost of noise reduction.

Very little work has been done to directly address the question of how people react to indoor noise in situations where the low frequency background sound level is established by the operating HVAC system, and in particular where such a system causes a dominant low frequency rumble.

Beranek (1957) proposed his Noise Criterion (NC) curves and was followed by Kosten and Van Os (1962), who developed the Noise Rating (NR) curves. These latter curves were orignally proposed for rating exterior noises when heard indoors. The NR curves are similar in shape to the NC curves but are extended to higher levels. Indeed, the NR curves permit higher low frequency noise levels than the NC curves.

It was realised by Beranek et al (1971) that a noise spectrum which closely followed an NC curve did not itself give a pleasant sound but rather had a rumble characteristic and hiss. They therefore modified the NC curves to the Preferred Noise Criterion. These were not widely accepted though.

In 1981, Blazier (1981) was also cosidering the issue of sound quality and identified four dimensions that need to be considered in HVAC system assessment. Considerations of speech communication masking critria and of noise–induced vibration at low frequencies led to the development of the RC room criterion curves which include octave bands down to 16Hz.

Simultaneously, Broner (1980) was conducting research into low frequency noise annoyance and, based on his research and case history experience, developed the Low Frequency Noise Rating curves. These curves significantly reduce the amount of low frequency noise below 100 Hz that is considered acceptable in comparison with the standard NR curves.

More recently, Beranek (1989) proposed the Balanced Noise Criterion (NCB) curves . A major result of this revision was the extension of the curves down to 16 Hz octave band . The author supports the concern expressed by Blazier and Ebbing (1992) about the permissiveness of the NCB contours in the 16 Hz and 31.5 Hz octave bands particularly because of the field experience which suggests greater sensitivity than Beranek allows. This is indeed the reason for the derivation of the LFNR curves by Broner.

In selecting an acceptable acoustic environment for such spaces as recording studios, auditoria and lecture halls, the engineer will often specify that the noise level due to mechanical services must not exceed a given NR or NC level. Using the NR or NC curves to specify maximum background levels for recording spaces can, however, lead to unacceptable results, particularly due to low frequency rumble. In recent years, with an increase in the utilization of available space and the introduction of floor–by–floor air handling systems, it has been found that the extent of low frequency noise problems has increased i.e. the existing criteria have not been found to be adequate. ASHRAE (the American Society of Heating Refrigerating and Air Conditioning Engineers Inc.) has been aware of this problem and has recently sponsored some research into the most appropiate metrics for evaluation of low frequency noise problems and for the setting of adequate low frequency noise criteria.

The current ASHRAE assessment method is based on the RC room criterion curves which include octave–bands down to 16Hz – see Figure 1. In order to directly address the question of how people react to HVAC noise in situations where the dominant energy is below 250Hz, ASHRAE recently sponsored a research project with a view to determining an improved descriptor for low frequency noise evaluation and for setting criteria. Below, we describe some of the initial results obtained during the objective phase of the research.

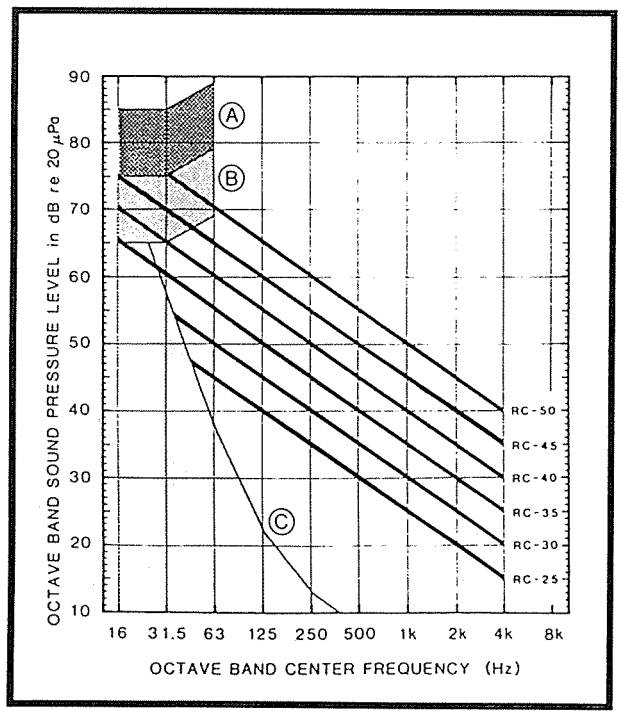

Figure 1 : RC noise criterion curves for specifying design level in terms of balanced spectrum shape (After Blazier 1981)

2.0 LOW FREQUENCY LOUDNESS CURVES

It can be seen from Figure 2 below, that the loudness curves at low frequencies are much closer together than at higher frequencies. Thus, for example, the distance between the 20 and the 80 phon (loudness) curves decreases from 60 dB at 1kHz to approximately 10dB at 8Hz. A small change in sound pressure level at low frequencies would therefore result in a considerable change in loudness (and annoyance) as compared to a similar change in level at high frequencies. This phenomenon is particularly important with respect to the annoyance impact of low frequency "rumbly" HVAC noise where it is possible that the loudness may change from imperceptible to loud at the modulation rate of the noise.

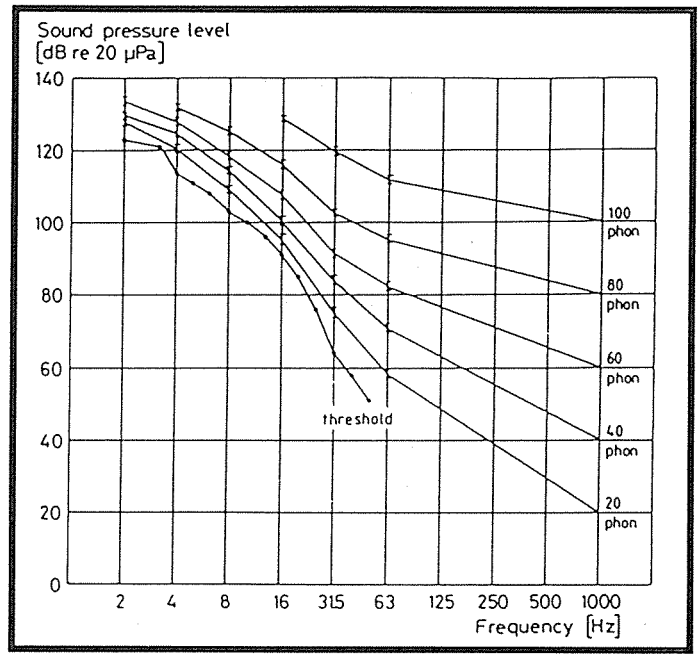

Figure 2 : Curves of equal loudness (After Moller and Andresen 1984)

3.0 DATA COLLECTION

Over 60 sites were visited in some major cities in Northern America to collect and analyse a range of (low frequency) HVAC noise samples. In the main, the samples were collected in offices and meeting rooms of various sizes. Some corridors/lobbies were also included.

At the majority of locations, the site was free of occupants during the measurements and it was therefore not possible to obtain a subjective assessment concerning the annoyance due to the HVAC noise. In general, absence of occupants was the preferred option by owners so as not to disturb on-going activities. In addition, this situation was also preferred for ensuring integrity of the noise sample recording.

It was found to be nearly impossible to obtain a "clean" recording of HVAC noise for even two minutes where sites were occupied. The owners also did not wish tenants to be questioned so as not to raise tenant's sensitivity concerning an existing or potential noise problem.

4.0 DATA ANALYSIS

The raw data collected for each site was in the form of spectra (1200 in total) and in the form of a statistical analysis for the 2–minute sample for each site for one–third octaves from 6.3Hz to 12kHz.

4.1 SUBJECTIVE ASSESSMENT

In order to separate out the possible metrics/assessment methods that would warrant further investigation, it was necessary to determine some form of subjective assessment against which the objective metrics could be correlated. A high correlation with subjective response would then indicate an obvious candidate for the comprehensive subjective study which is to be the subject of further ASHRAE research. It was not possible to conduct sufficiently useful limited subjective testing within the scope of the current research. Therefore, an initial subjective assessment was conducted by the Principal Investigator based on his memory of each of the sites concerned and considering the relativity of each site. The magnitude estimation technique was loosely used and the subjective scale was effectively assigned a range of approximately 0–10 and a score provided for each site. On this basis, a site assigned a subjective assesment value of four is twice as annoying as a site with an assessment of two.

4.2 CHOICE OF A METRIC

The following factors are likely to be important in determining annoyance due to low frequency HVAC noise:

(a) overall level **(b)** spectrum balance **(c)** temporal modulation

Therefore, noise "measures" were initially chosen for invetigation based on these factors. These included overall weighted noise levels and measures of temporal variation such as the L_{10}, the overall level exceeded for 10% of the time. In addition, spectral balance measures were also considered.

5.0 RESULTS

For each site, the L_{10}, L_{50} and L_{90} statistics (the levels exceeded for 10%, 50% and 90% of the time respectively, were plotted for the 2–minute HVAC noise sample as well as the hearing threshold, e.g. see Figure 3. Other noise measures such as various weighted noise levels and spectral balance measures e.g. Linear –A, C–A were also plotted against time so as to determine the degree of and rate of amplitude modulation.

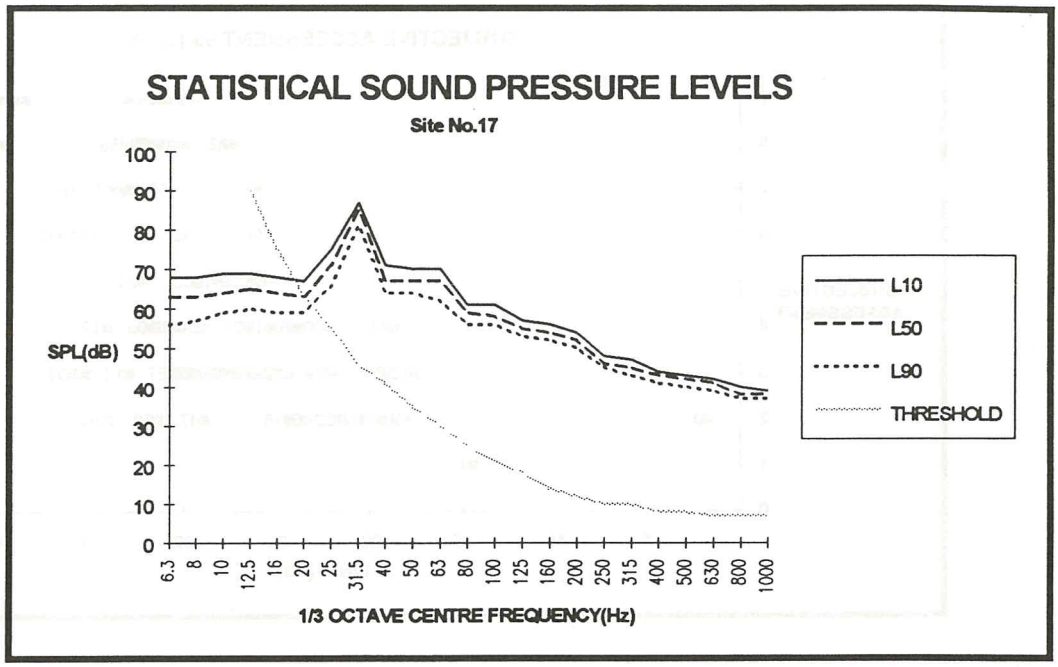

Figure 3 : L_{10}, L_{50} and L_{90} Sound Pressure Levels For Site 17 (based on complete 2–minute sample)

5.1 CORRELATION

Plotting the subjective assessment against "noise measure" should result in a monotonically increasing curve with little standard deviation of data from the mean curve. A typical output is shown in Figure 4 below.

Most successful in rating the sites appeared to be the measures which in some way accounted for spectral imbalance e.g. Linear–A, C – A. These clearly should be investigated further, though due to its simplicity, the (Linear–A) level difference should find more ready application.

5.2 SPECTRUM SHAPE

It is interesting to compare all the spectra for the sites visited and compare the overall slope with the average slope of –5dB/octave found by Blazier (1981) for "neutral" site. Figure 5 shows a plot of the average spectra for the most annoying and least annoying sites. It can be seen that above 63Hz, the average slope for all spectra is similar at –5dB/octave.

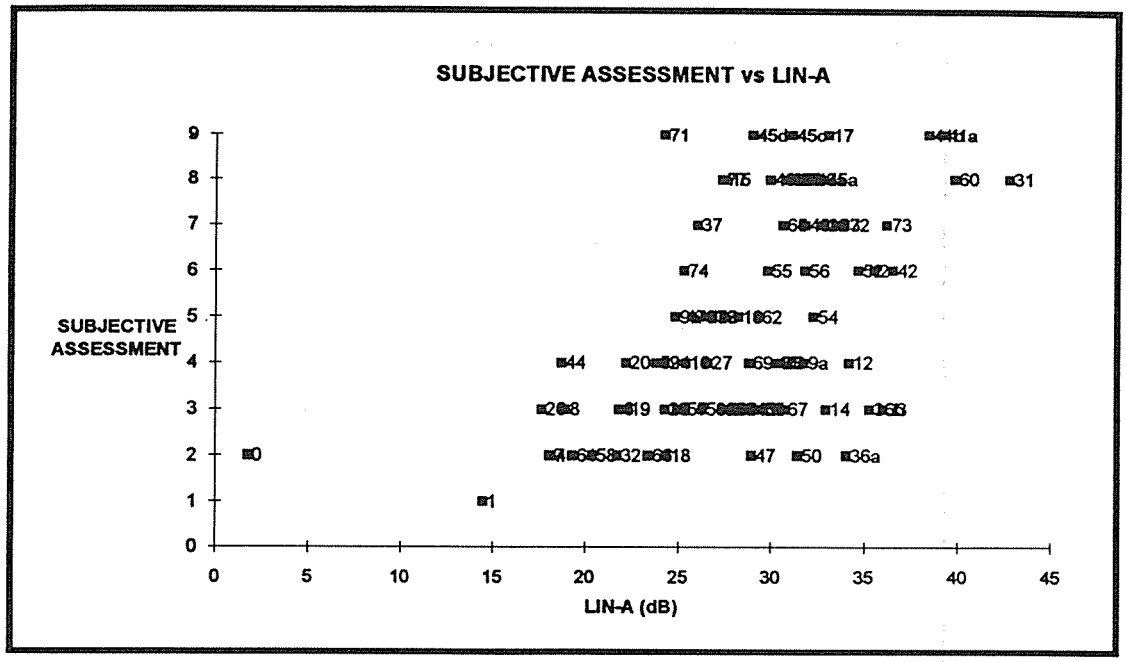

Figure 4 : Correlation between subjective assessment and the (Linear – A) value obtained for each site

Below 63Hz, the neutral sites display a similar negative slope down to 16 Hz and are therefore entirely similar to the sites and average slope determined by Blazier (1981). However, the rumbly sites show a significantly greater negative slope (approximately –24dB/octave, somewhat parallel to the threshold of hearing) below 63Hz and then below 31.5Hz, a positive slope of approximately 5dB/octave. From this we can conclude that is quite clearly energy below 80–100Hz that results in the impression of subjective annoyance. The question that remains to be answered is whether the annoyance is due to to the overall level in itself or some other characteristic of this low frequency energy viz. its temporal characteristic.

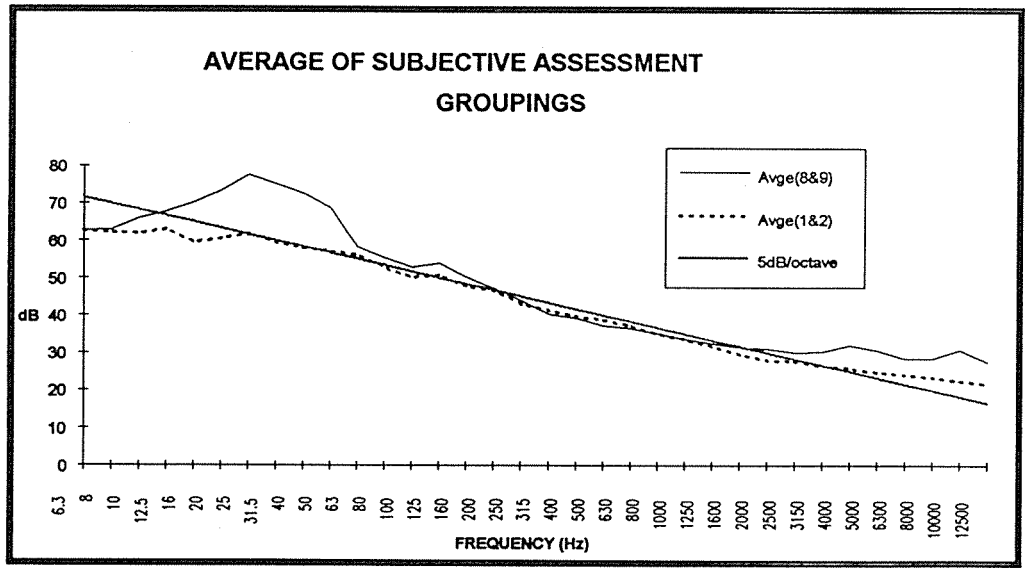

Figure 5 : Comparison of average of L_{10} spectra for most annoying and least annoying sites. Also shown is the line representing the –5dB/octave slope for neutral sites as found by Blazier (1981)

6.0 DISCUSSION

The research to date confirms that the NR/NC curves that are currently being used for specifying maximum background noise levels due to HVAC systems do not adequately account for the low frequency rumble that is present in many installations.

The research indicates that a simple metric such as the (Linear–A) sound pressure level difference could be used to set acceptability criteria and that metrics can be derived based on third–octave band analysis which could also provide diagnostic information

With respect to the simple assessment approach, it currently appears that a (Linear–A) difference of 30 dB or more would result in an environment which is considered "rumbly"and unacceptable. This result is in accordance with the findings of Broner and Leventhall (1983) that for A–weighted SPL's greater than 30 dBA, the overall Linear SPL should be limited to 30 dB greater so as to avoid complaints of low frequency noise annoyance. For A–weighted SPL's less than 30 dBA, they recommended an upper limit of 55 dB overall Linear SPL.

Such criteria will allow the derivation of the maximum acceptable background noise levels due to HVAC system noise and will ensure that occupied spaces are more often acceptable acoustically.

7.0 REFERENCES

Beranek, L. L. 1957. "Revised Criteria for Noise in Buildings" *Noise Control, January* 1957, 19–27.

Beranek, L.L. 1989b. "Application of NCB Noise Criterion Curves" *Noise Control Eng.*, 33(2), 45 – 56.

Beranek, L. L. et al 1971. "Preferred Noise Criterion (PNC) Curves and Their Application to Rooms" *J.Acoust. Soc. America*, 50, 1223–1228.

Blazier, W.E. 1981. "Revised Noise Criteria for Application in the Acoustical Design and Rating of HVAC Systems" *Noise Control Engineering*, Vol.16, No.2, 64–73.

Blazier, W.E. Jr. and Ebbing, C.E. 1992. "Criteria for Low Frequency HVAC System Noise Control in Buildings" *InterNoise 92*, Proc. 761–766.

Broner, N. 1980. "A Criterion for Low Frequency Noise Annoyance" *10th ICA Sydney*, July, Paper C1 – 4.4.

Broner, N. and Leventhall, H.G. 1983. "Low Frequency Noise Annoyance Assessment by Low Frequency Noise Rating (LFNR) Curves" *J.Low Frequency Noise and Vibration 2(1), 20 – 28.*

Kosten, C.W. and Van Os G.J. 1962. "Community Reaction Criteria for External Noises" N.P.L., Symposium No. 12, London, 373–387.

Moller, H. and Andresen J. 1984. "Loudness of Pure Tones at Low and Infrasonic Frequencies" *J.Low Frequency Noise and Vibration*, 3(2), 78 – 87.

PREDICTION OF ROAD BARRIER INSERTION LOSS BY THE BOUNDARY ELEMENT METHOD

Xiaojun Du and Robin J. Alfredson
Department of Mechanical Engineering
Monash University
Clayton, Victoria 3168
Australia

ABSTRACT

This paper presents an acoustic boundary element model for the numerical solution of a two-dimensional sound field above an infinite flat plane and exterior to a barrier of arbitrary shape and surface sound-absorption. Careful treatment of integration involved in setting up the system of equations enables a sufficiently accurate solution to be obtained in an efficient computational scheme. The validity of the model has been confirmed by comparing its predictions with those obtained from analytical or approximately analytical solutions. The model has been used to investigate the effectiveness of barrier height, width and absorbent cover for various geometrical configurations. All of the predictions appear reasonably good and the trends observed are consistent with those indicated by other researchers.

1 Introduction

It is common to use road barriers as a means of reducing exposure to noise from road traffic. Numerous investigations have been carried out for the purpose of predicting the performance of barriers. A variety of theoretical prediction models is now available, in which the effects of both diffraction by a barrier and reflection from the ground are taken into account. Most of these models are based on the geometrical theory of diffraction and determine the sound field at a receiver behind the barrier by the summation of the sounds from four possible ray paths from a source and its image to the receiver and its image. Whereas these theoretical models provide useful predictions for simple barriers, they are incapable of modelling barriers of complicated shape and arbitrarily located absorbent-cover.

In our previous work on this subject, we have used the finite element method to approximate the solution of the Helmholtz equation, which governs the linearized sound field exterior to a road barrier, and hence to predict the performance of the barrier. An extensive comparison between predictions obtained using our finite element model and those obtained from the existing theoretical models has been presented [1]. The comparison shows that, within the frequency range up to 1000 Hz and the source-receiver distance up to 50 m, the finite element method does provide reliable predictions. Beyond the above ranges of frequency and distance, however, it is cumbersome to employ the finite element method for this kind of calculation, owing to the excessive computing time and the large amount of computer storage required. Therefore we have been exploring the use of the boundary element method to solve the sound field exterior to a barrier.

The boundary element method is a very suitable technique for the numerical solution of exterior acoustic problems. It has been applied to predict the performance of barriers by Seznec

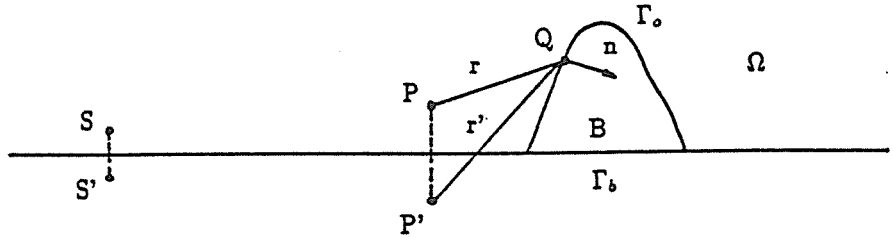

Figure 1: Geometry of the problem to be solved

[2], Hothersall et al. [3,4], and Antes [5]. Like the finite element method, the boundary element method has a distinct advantage over the methods based on the geometrical theory of diffraction in that it can, in principle, accommodate barriers of arbitrary shape and arbitrary treatment of surface sound-absorption. However, the boundary element method is more effective than the finite element method since, with this numerical method, only the boundary of the acoustic domain under consideration needs to be discretized to obtain a numerical solution. This permits a considerable reduction in the resulting linear algebraic equations, together with a reduction in the amount of computing time and computer storage.

2 The Boundary Element Model

The problem to be solved is shown in FIG.1. It is a two-dimensional acoustic scattering problem in which a scattering body (barrier) of arbitrary shape sits on an infinite, flat and locally reacting ground surface. An infinite coherent line source of sound ($e^{+i\omega t}$ time dependence) is located at S above the ground. B denotes the barrier which is assumed to be infinitely long and to have a uniform cross-sectional shape Γ ($\Gamma = \Gamma_o + \Gamma_b$) and uniform acoustical properties along its length. Ω denotes the acoustic domain above the ground and exterior to Γ_o. n is a unit normal on Γ_o directed away from Ω.

The boundary element method for solving steady-state acoustic problems consists in transforming the Helmholtz equation plus appropriate boundary conditions into a boundary integral equation, and then determining the numerical solution of this integral equation. The boundary integral equation for bodies sitting on the ground in a three-dimensional space has been developed by Seybert et al. [6]. It can be written for two-dimensional problems as follows,

$$C(P)\phi(P) = \int_{\Gamma_o} \left(G\frac{\partial\phi(Q)}{\partial n} - \phi(Q)\frac{\partial G}{\partial n} \right) d\Gamma + \phi^I(P) \qquad (1)$$

In Eq.(1), ϕ is the velocity potential satisfying the Helmholtz equation in Ω and the Sommerfeld radiation condition in the far-field. Q is any point on Γ_o, and P may be in Ω, in B, or on Γ_o. $\phi^I(P)$ is the prescribed incident wave potential at P, determined by the source at S and its image at S' in the absence of the barrier. C(P) is a constant determined by the location of the point P. C(P) is 1, 0, and 0.5 for P in Ω, in B and on a smooth boundary Γ_o, respectively. A scheme of calculating C(P) when P is at the corners of Γ_o has been proposed by Seybert et al. [6]. G is the half-space Green function satisfying both the Helmholtz equation and Sommerfeld condition. The two-dimensional form of the half-space Green function is

$$G = \frac{i}{4}H_o^{(1)}(kr) + R_H\frac{i}{4}H_o^{(1)}(kr') \qquad (2)$$

where k is the wave number, r the distance between P and Q, r' the distance between Q and P', H_o^1 the Hankel function of the first kind and zero order, R_H the reflection coefficient of the ground. It is noted that in Eq.(1) only Γ_o, a part of the barrier boundary, is used to define

the path of the integration as Γ_b, the bottom boundary of the barrier, is no longer a part of the boundary of Ω. The contribution from the far-field boundary of Ω has been removed by invoking the Sommerfeld radiation condition and that from the ground has also been removed by using the half-space Green function.

Eq.(1) is the starting point for building our boundary element model. Assume that the barrier surface is locally reacting and the boundary condition on it is of the mixed form

$$ik\beta\,\phi \;=\; \frac{\partial\phi}{\partial n} \tag{3}$$

where β is the normalized specific acoustic admittance ratio. Substitution of Eq.(3) into Eq.(1) gives

$$C(P)\phi(P) \;=\; \int_{\Gamma_o} (ik\beta\,G \;-\; \frac{\partial G}{\partial n})\phi(Q)d\Gamma \;+\phi^I(P) \tag{4}$$

To obtain the numerical solution of Eq.(4), the boundary Γ_o must be discretized into elements. In order to avoid problems with the corners of the domain when determining the constant C(P) and to easily treat the singularities in the case of P close to Q, we use the straight line element, with the node being at the middle of the element , and assume that ϕ is constant within each element. Thus Eq.(4) can be discretized as follows

$$C(P)\phi(P) \;=\; \sum_{j=1}^{N} \phi(Q_j) \int_{\Gamma_j} (ik\beta\,G \;-\; \frac{\partial G}{\partial n})d\Gamma \;+\phi^I(P) \tag{5}$$

where Γ_j is the jth element (j=1,...,N). Notice that, in Eq.(5), $\phi(Q_j)$ is taken out of the integral as the value of $\phi(Q_j)$ is assumed to be constant over Γ_j. C(P) is always 0.5 for P on Γ_o as the boundary is always smooth at the nodes.

The application of Eq.(5) to our problem begins with the placement of P on Γ_o. By placing P at each node from 1 to N, we obtain N linear algebraic equations, which can be expressed in matrix form as

$$[\,A\,]\{\,\phi\,\} \;=\; \{\,\phi_I\,\} \tag{6}$$

In Eq.(6), $[\,A\,]$ is an N×N matrix, containing N×N integrals as in Eq.(5). $\{\,\phi\,\}$ is a vector of unknown values of ϕ and $\{\,\phi_I\,\}$ a vector of the values of ϕ^I. After solving Eq.(6) for $\{\phi\}$, P is placed in Ω and Eq.(5) is used, as a formula, with C(P)=1 to calculate the velocity potential at any desired point P in Ω. Finally, the barrier insertion-loss IL is calculated by

$$IL \;=\; 20\log|\frac{\phi^I(P)}{\phi(P)}| \tag{7}$$

where $\phi^I(P)$ and $\phi(P)$ denote the velocity potential at the point P behind the barrier in the presence of the ground, without and with the barrier present, respectively.

While the above precedure for the application of the boundary element method to our problem is maintained, careful treatment of the integrals in Eq.(5) is needed to obtain the required accuracy of the solutions in an efficient computational scheme. In the case of $Q_j \neq P$, standard Gaussian quadrature is employed to numerically implement the integrals; however, two modifications have been made to avoid excessive computations for numerical integration. As mentioned before, the half-space Green function involves the Hankel function, whose series expansion converges very slowly. One modification lies in the replacement of the infinite series expansion for the Hankel function by the finite polynomial approximations for the Bessel functions [7]. (Notice that $H_n^1(x) = J_n(x) + iY_n(x)$.) The other modification is to tailor the

number of the quadrature points according to the distance between P and Q_j. The larger the distance, the fewer points needed. These two modifications are similar to those proposed by Yoon et al. [8].

In the case of $P = Q_j$, where two points are on the same element, the presence of the singularity due to the first term of the half-space Green function requires a more accurate integration. Instead of still using the standard Gaussian quadrature and choosing more quadrature points as Yoon et al. did, we use a logrithmic Gaussian quadrature for the numerical integration of the first term in the half-space Green function as it has a logrithmic singularity. Our calculations have shown that in this way the inaccuracies involved are efficiently minimized.

It is well-known that the boundary element method for external problems fails to provide a unique solution at certain frequencies corresponding to the eigenvalues of the enclosed internal region. This difficulty is overcome by using the CHIEF method proposed by Schenck [9]. The resulting overdetermined system of equations is solved by a least squares procedure in which the orthogonal decomposition of the $M \times N$ matrix ($M > N$) is implemented by applying a sequence of the Householder transformations.

3 Numerical Results

The validity of our boundary element model has been confirmed by comparison of its predictions with those obtained from some existing analytical or approximate analytical models. Two test cases are presented below. FIG.2 (a) shows a comparison for a grass-covered barrier of semi-circular section sitting on a flat rigid ground. The configuration of the source, barrier and receiver is indicated in the figure. Notice that it is one of the few cases in which the exact analytical solution for two-dimensional diffraction problems is available [10]. The barrier insertion-loss spectra presented are determined at each one-third octave centre frequency in the frequency range of 100 to 2000 Hz. Excellent agreement between the two predictions is observed, with the difference being always less than 0.5 dB within the frequency range considered.

FIG.2 (b) shows the case for a thin rigid barrier on a flat rigid ground and for the geometrical configuration indicated. The insertion-loss spectrum obtained using an approximate analytical solution is given by Isei et al. [11]. Whereas the model of Isei et al. assumes a point source of sound, our boundary element model assumes a coherent line source. However, the two predictions agree well and undergo similar marked variations due to interference effects. This confirms the conclusion given by Hothersall et al. [3], who stated that predictions provided by the two-dimensional boundary element model can be related to those for a point source.

Our model has been applied to predict the performance of barriers for various geometrical configurations. In our computation, no account is taken of the influence of wind, temperature gradients and atmospheric absorption. This is one of the limitations of the boundary element method. To obtain a meaningful comparison of the performance of different barriers, however, the hypothesis of a neutral quiescent atmosphere is highly desirable. In this way, the effects of the barrier noise reduction can be separated from those of outdoor parameters.

The ground surface is assumed to be perfectly reflecting. Such a ground can be regarded as an asphalt surface for practical purpose. When the source or receiver is located above the ground, the predicted insertion-loss spectrum presents marked variations, as shown in FIG.2 (b), due to interference effects. In practice, it is obvious that the interference pattern is not particularly interesting since traffic noise is broadband. In order to remove interference effects while keeping the ground present, both the source and receiver are set on the ground surface in our computations. Under this consideration, the configuration of source, barrier and receiver is

indicated by two parameters, i.e., the source-barrier distance (the horizontal distance between the source and the centre line of the barrier.) and the barrier-receiver distance. Since the performance of barriers is, in general, dependent on both distances, different combinations of them have been considered in our computations.

The acoustic admittances of the absorbent surfaces are calculated using the Bies and Hansen model [12]. The flow resistivity is assumed to be 20 cgs Rayls.

It was found that 10-12 elements/wavelengh gave a sufficiently accurate solution. Computing time is of the order of less than 10 minutes on an Apollo 10000 computer for a boundary (Γ_o) of length 8 m and a frequency range up to 1000 Hz.

Effect of Barrier Height In FIG.3 are shown the effect of barrier height for a thin rigid barrier on a flat rigid ground. In every geometrical configuration considered, the performance of the barrier is improved by the increasing barrier height, but the rate of improvement decreases with the increase in height. The improvement in insertion-loss produced by increasing the height from 2 to 3 m is around 4 dB, while that obtained by increasing the height from 4 to 5 m is only around 2 dB. The former is approximately double the latter. Furthermore, in every case, the insertion-loss increases with frequency at the rate of about 3 dB/octave. These trends have been predicted by Hothersall et al.[3]. We note that these trends are independent of the configuration of the source, barrier and receiver within the distances considered.

FIG.3 (b) shows insertion-loss spectra for the geometry in which the source-barrier distance is 10 m and the barreir-receiver distance is 30m. On the other hand, FIG.3 (d) shows the case in which the source-barreir distace is 30 m and the barrier-receiver distance is 10 m. these two sets of spectra are approximately the same, which is what we anticipated because of the reciprocity principle. This indicates that our model does in fact respect this principle.

Effect of Barrier Width FIG.4 shows the effect on performance of barrier width for a rigid barrier of rectangular cross-section on a flat rigid ground. Any great improvement can be obtained only for sufficiently wide barriers. The improvement obtained by increasing the width is greatly dependent on the geometrical configuration. When the source and receiver are far from the barrier, the improvement is negligible. In addition, unlike the trend observed in the effect of barrier height, the insertion-loss increases with frequency at different rates for different barrier widths. In each geometry considered, the larger the width, the more quickly the insertion-loss increases with frequency. This trend is more accentuated for small source-barrier and barrier-receiver distances. The similarity between two sets of spectra, as shown in FIG.4 (b) and (d), due to the reciprocity principle is also observed.

Effect of Surface Absorbent Cover From spectra presented in FIG.5, it is obvious that, in the case of a vertical thin barrier on a flat rigid ground, the effect of covering the barrier surfaces with absorbent material is not significant. However, when both the source and receiver are close to the barrier, covering the surfaces with absorbent material does offer an improvement in insertion-loss of a few decibels. In traffic noise control practice, it is believed that improvements in insertion-loss of even a few decibels could well be worthwhile. Moreover, it is more efficient to place the absorbent cover on the surface associated with the smaller of the source-barrier and barrier-receiver distances. When the two distances are the same, the improvement in insertion-loss obtained by covering both side surfaces will double that obtained by covering only one side surface, as shown in FIG.5 (a). This confirms the conclusion given by L'Esperance et al. [13].

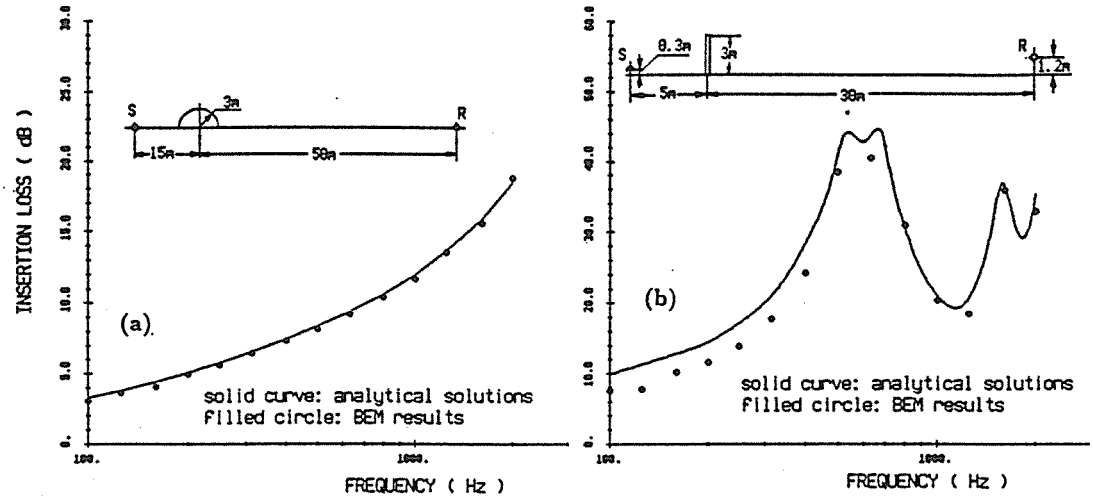

Figure 2: Comparison of BEM results with analytical solutions

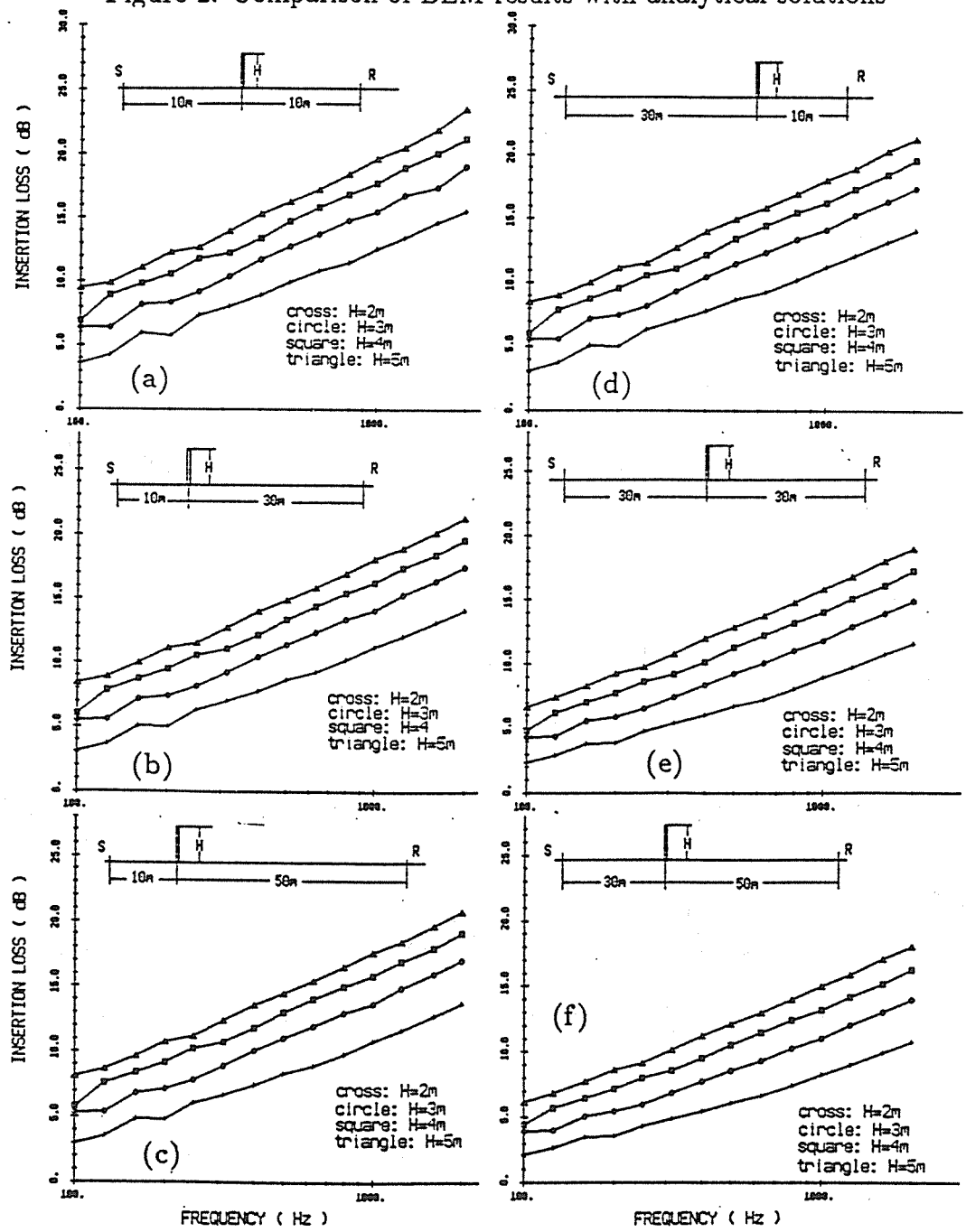

Figure 3: Effect of Barrier Height On Barrier Performance

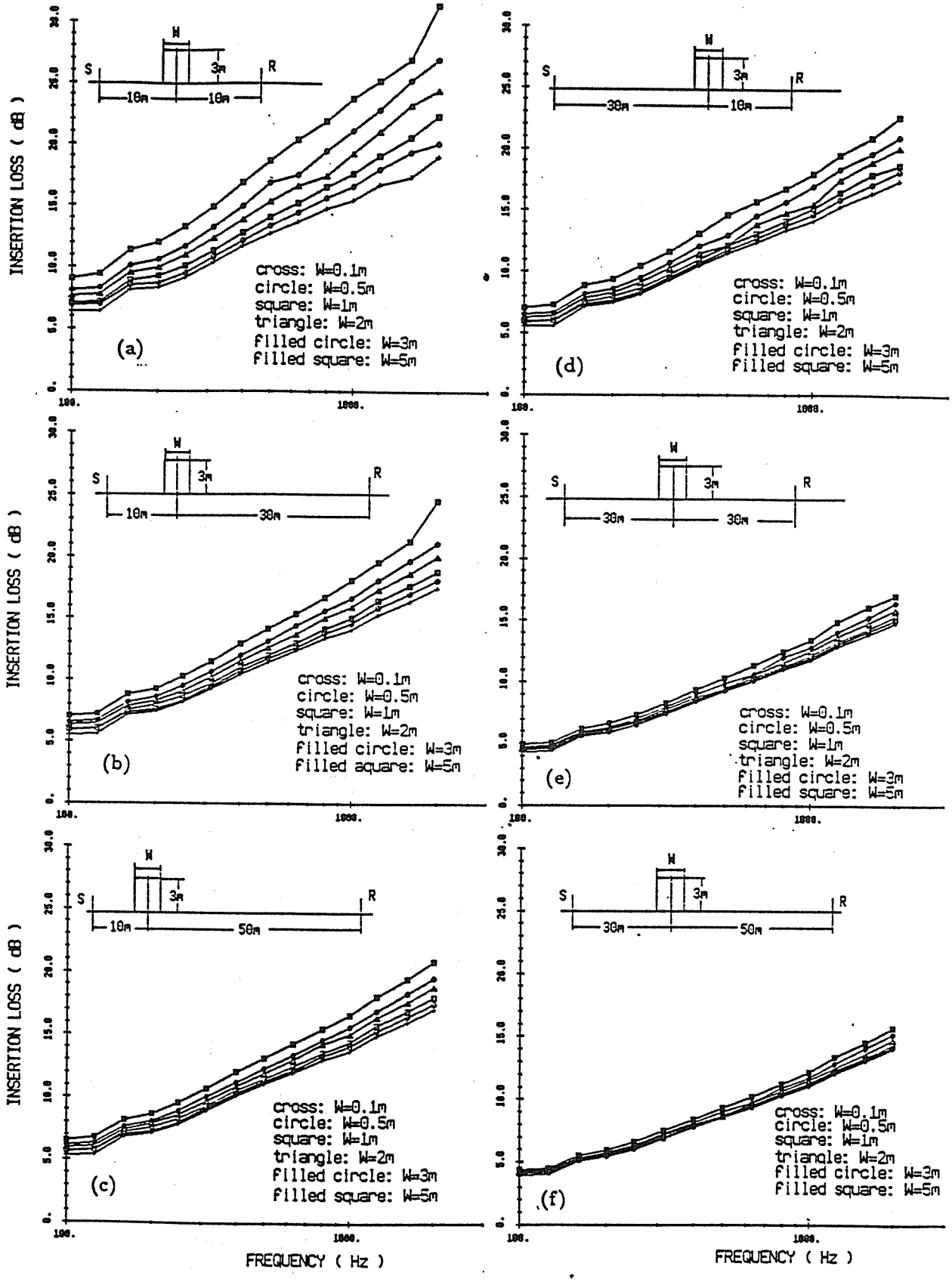

Figure 4: Effect of Barrier Width On Barrier Performance

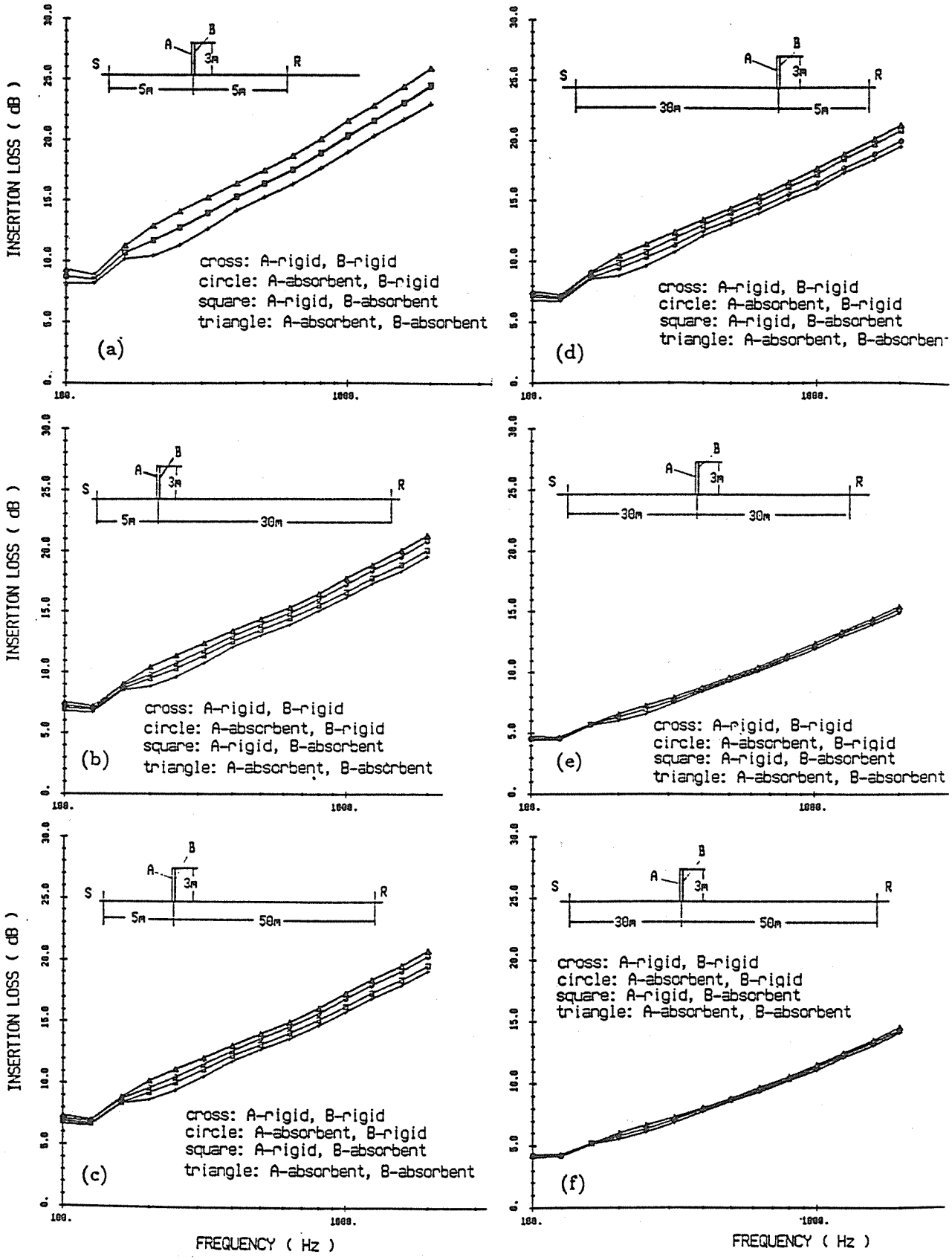

Figure 5: Effect of Absorbent Cover On Barrier Performance

4 Conclusion

The boundary element model has been developed for the numerical solution of the sound field around a barrier. Its predictions have been successfully compared with those of some existing theoretical solutions. The model has been applied to predict the performance of barriers for various geometrical configurations but only for a rigid ground. The predictions are reasonably good and the overall trends observed comfirm those indicated by other researchers. This in turn contributes to confirmation of the validity of the model. The case in which a barrier sits on a ground with a finite impedance is being considered for inclusion in our model.

5 Acknowledgement

This research was jointly sponsored by VicRoads and the Australian Road Research Board. Their generous sponsorship is gratefully acknowledged.

6 References

1. R.J.Alfredson & X.Du, *A comparison of the finite element method with other methods for predicting sound reduction around barriers*, **Proceedings of Inter-noise and Vibrasion Control Conference**, St.Petersburg, Russia, Vol.1, 1993, p181-186.

2. R.Seznec, *Diffraction of sound around barriers: use of the boundary elements technique*, **J.Sound.Vib.**, 73(2), 1980, p195-209.

3. D.C. Hothersall, S.N. Chandler-Wilde & M.N. Hajmirzae, *Efficiency of single noise barriers*, **J.Sound.Vib.**, 146(2), 1991, p303-322.

4. D.C. Hothersall, D.H. Crombie & S.N. Chandler-Wilde, *The performance of T-profile and associated noise barriers*, **Applied Acoustics**, 32(4), 1991, p269-287.

5. H.Antes,*Applications in environmental noise*, *Boundary Element Methods in Acoustics*, R.D.Ciskowski & C.A.Brebbia, ed. **Computational Mechanics Publications**,1992.

6. A.F. Seybert & T.W. Wu, *Modified Helmholtz Integral Equation for Bodies Sitting on an Infinite Plane*, **J.Acoust.Soc.Am.** 85(1), 1989, p19-23.

7. M.Abramowitz & I.A.Stegan, *Handbook of Mathematical Functions*, **Dover Publications Inc.**, 1970, p335-370.

8. W.S. Yoon, J.M. Park & W. Eversman, *Two-dimensional radiation and scattering at short wave length*, **J. Vib. Acoust.** 112, 1990, p384-391.

9. H.A.Schenck, *Improved integral formulation for acoustic radiation problems*,**J.Acoust. Soc.Am.**, 44, 1968, p41-58.

10. J.E.Cole III, *Diffraction of sound by a refracting cylindrical barrier*, **J.Acoust.Soc.Am.**, 81(2), 1987, p222-225.

11. T. Isei, T.F.W. Embleton & J.E. Piercy, *Noise reduction by barriers on finite impedance ground*, **J.Acoust.Soc.Am.**, 67(1), 1980, p46-58.

12. D.A.Bies & C.H.Hansen, *Engineering Noise Control*, **UNWIN HYMAN**, 1988, p361-374.

13. A. L'Esperance, J. Nicolas & G.A. Daigle, *Insertion loss of absorbent barriers on ground*, **J.Acoust.Soc.Am.**, 86(3), 1989, p1060-1064.

NUMERICAL ACOUSTICS - WHAT ARE ITS APPLICATIONS?

Joseph C.S. Lai
Acoustics & Vibration Centre
University College, The University of New South Wales
Australian Defence Force Academy
Canberra, ACT 2600.

ABSTRACT

Since the 1970s, advances in computer technology and numerical techniques have seen an almost exponential increase in the use of computational methods in engineering applications such as computational fluid dynamics. It is, however, only until recently that commercial finite element/boundary element software have been made available and numerical techniques have been used more widely for solving acoustics problems. In this paper, the principles of these numerical methods are briefly described and their potentials are illustrated by some examples. The advantages, accuracies and limitations of these methods are discussed.

1.0 INTRODUCTION

In acoustics, the propagation of sound is governed by the wave equation. Although the Helmholtz equation was first given by Euler in 1759 and then by Helmholtz in 1860, it was difficult to obtain analytical solutions with complex geometries and/or complex boundary conditions. With the advent of powerful desktop computers/workstations, numerical techniques based on geometrical acoustics (primarily ray tracing for high frequencies) have been applied to problems in room acoustics and environmental acoustics. While commercial finite element software has been available for over two decades for engineering applications such as stress analysis, it is only until recently that commercial software utilising advanced numerical techniques such as finite element and boundary element methods (primarily more suitable for low frequencies) have been made available. It has often been claimed that the most effective noise control method is the control of the source through engineering means but this is often very difficult to achieve unless prior considerations have been given to the design of a product. With the use of computational methods for acoustics, it is now possible to incorporate 'numerical' acoustic analysis in the design process so that the effects of noise radiation can be analysed even before prototypes are built and innovative engineering techniques in reducing noise radiation may be examined.

In this paper, the advantages and disadvantages of finite element and boundary element methods, their accuracies and limitations will be discussed. Their potentials in solving a range of acoustics problems will be illustrated with examples on acoustic cavity analysis and external radiation problems.

2.0 GOVERNING EQUATION AND BOUNDARY CONDITIONS

The propagation of sound waves in a medium is governed by the familiar wave equation:

$$\nabla^2 p - \frac{1}{c^2}\frac{\partial^2 p}{\partial t^2} = 0 \qquad (2.1)$$

where c is the speed of propagation of sound waves; p is pressure, t is time; and ∇ is the Laplace operator.

By assuming a steady state harmonic motion of the form $p(x,y,z) = \hat{p}(x,y,z)e^{i\omega t}$, (i is the imaginary number), equation (2.1) can be reduced to the Helmholtz equation (2.2)

$$\nabla^2 p + k^2 p = 0 \qquad (2.2)$$

where k is wavenumber = ω/c and ω is the circular frequency in radians/sec.

The Helmholtz equation can be solved by imposing appropriate boundary conditions on some boundary surfaces which involve prescribing usually (a) the surface pressure (p_s); (b) the normal surface velocity(v_n); or (c) the normal surface admittance(A) or impedance as follows:

$$\begin{aligned} p &= p_s && \text{on surface } S_1 \\ \frac{\partial p}{\partial n} &= -i\rho\omega v_n && \text{on surface } S_2 \\ \frac{\partial p}{\partial n} &= -i\rho\omega A p && \text{on surface } S_3 \end{aligned} \qquad (2.3)$$

where n is the coordinate normal to the surface.

Furthermore, for external radiation problems, the acoustic field vanishes at points farther than $c(t-t_o)$ because a wave disturbance initiated at time (t_o) would not have reached that distance in the time (t)of interest. This condition is known as the Sommerfeld radiation condition (see ref.[6]) and may be expressed in spherical coordinates as

$$\lim_{r\to\infty} r^{\alpha}\left[\frac{\partial p}{\partial r} + ikp\right] \to 0 \qquad (2.4)$$

where r is the distance from the surface of source excitation and α is 1/2 for 2-D problems and 1 for 3-D problems.

The boundary-valued problem as described by equations (2.2)-(2.4) is difficult to solve analytically except for very simple geometries and boundary conditions. Approximate analytical solutions can be obtained for high and low frequencies using perturbation methods (see ref. [3]). Consequently, numerical methods have to be sought for general problems.

3.0 NUMERICAL METHODS

Numerical methods available for solution of equation (2.2) are finite difference, finite element and boundary element methods. While finite difference techniques have been used for some acoustic problems (see ref. [4]), they are basically only suited for simple and bounded geometries and require large number of calculation points compared with finite element methods. Hence only finite element and boundary element methods will be considered here.

3.1 Finite Element Method

Finite element methods have been applied to interior problems which involve applying the weighted residual formulation to incorporate the field and boundary residuals into a set of weighted equations (see [3], [4]). The whole solution domain has to be discretised as shown in Figure 1(a). The system of discretised equations can be written as a matrix equation of the form (3.1):

$$\{[K] - i\rho\omega[C] - \omega^2[M]\}\{p\} = -i\rho\omega\{F\} \qquad (3.1)$$

where [C] is an acoustic damping matrix;
{F} is an acoustic forces vector;
[K] is an acoustic stiffness matrix;
[M] is an acoustic mass matrix; and
{p} is the unknown acoustic pressure vector.

Eigenfrequencies and eigenmodes can be obtained from equation (3.1) by setting {F}={0} and the response at a given frequency can be expressed as a linear combination

of the eigenmodes. While the finite element method has been well established and equation (3.1) can be solved efficiently due to the banded nature of the matrices, it is not suitable for solving exterior radiation problems which would require an 'infinite' expansion of the finite element mesh. Nevertheless, 'infinite' elements and 'wave envelope' elements are being developed to solve exterior radiation problems.

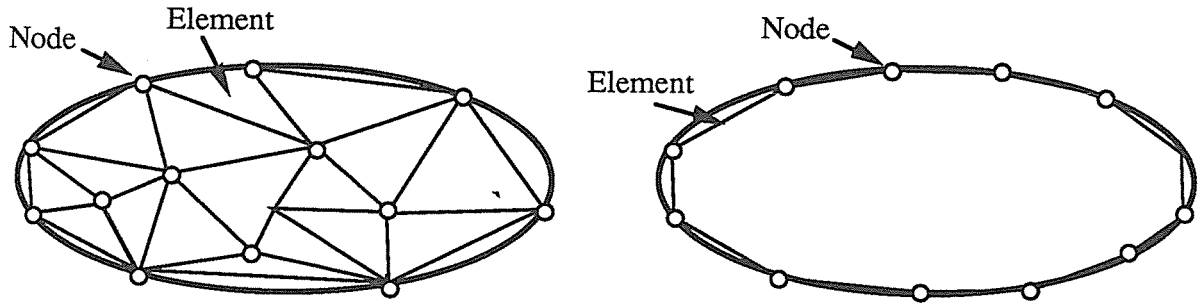

(a) Finite element (b) Boundary element

Figure 1 Discretisation of solution domain.

3.2 Boundary Element Methods

A good description of various boundary element methods is given in [1]. Only the direct boundary integral formulation based on Kirchoff-Helmholtz theorem ([6]) is given here. The pressure at a field point X in the interior (V_i) or the exterior (V_e) volume can be expressed in terms of the pressure p(Y) and the normal velocity v_n at a boundary point Y on the related closed boundary surface S as given in equation (3.2).

$$c(X)p(X) = \int_S \left\{ p(Y)\frac{\partial G(X,Y)}{\partial n_Y} + i\rho\omega v_n(Y)G(X,Y) \right\} dS(Y) \qquad (3.2)$$

where n_Y is the normal at the boundary point Y directed into the fluid domain;
G(X,Y) is a Green's function satisfying the Helmholtz equation; and
c is a coefficient dependent on the location of the field point X and on whether the problem is an interior or exterior problem.

Unlike the finite element method, only the boundary surface of a boundary element model has to be discretised as shown in Figure 1(b). The resulting discrete set of equations relate nodal pressures {p} to nodal velocities {v} by:

$$[A]\{p\} = [B]\{v\} \qquad (3.3)$$

While boundary element methods are most suited for solving interior or exterior radiation problems, the matrices [A] and [B] are fully populated and sometimes nonsymmetric. Furthermore, for exterior problems, the solution may not be unique at frequencies that correspond to the interior cavity resonant frequencies but this can be overcome by using an overdetermination procedure (see ref. [2]).

4.0 NUMERICAL EXAMPLES

All the calculations reported here were made on a SUN SPARC workstation using a finite element/boundary element package SYSNOISE version 4.4a. The pre- and post-processor used is ANSYS version 4.4. For the highest frequency of interest, a minimum of at least 6 elements per wavelength was used.

4.1 Car compartment problems

Figures 2(a) and (b) display respectively a finite element model and a boundary element model for a car compartment. In the finite element model, 258 elements and 287 nodes

were used, giving an upper frequency limit of about 440 Hz. In the boundary element model, 111 elements and 111 nodes were used, giving an upper frequency limit of about 400 Hz. The first 5 acoustic modes calculated with the finite element model occur at frequencies 75, 124, 132, 177 and 232 Hz and the acoustic modes corresponding to 75 Hz and 123 Hz are shown in Figures 3(a) and (b) respectively. The response near the driver's ear due to vibration excitation of the panel near the driver's feet has been calculated with the boundary element method and is shown in Figure 4 for both rigid and absorptive interior roofs. The reduction of sound pressure level due to the addition of absorptive linings is clearly seen from Figure 4(a). The advantage of being able to examine the influence of material properties on the sound pressure level cannot be underestimated.

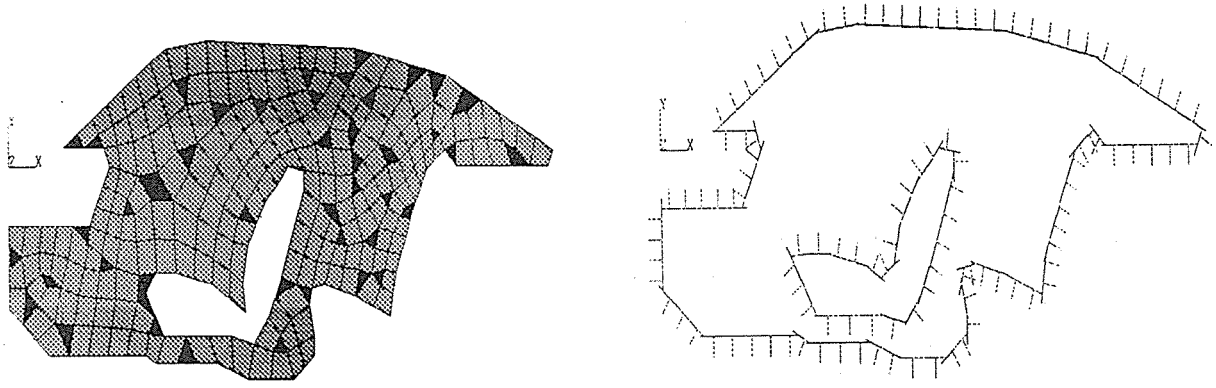

(a) Finite element model . (b) Boundary element model.

Figure 2 Discretisation of a car compartment.

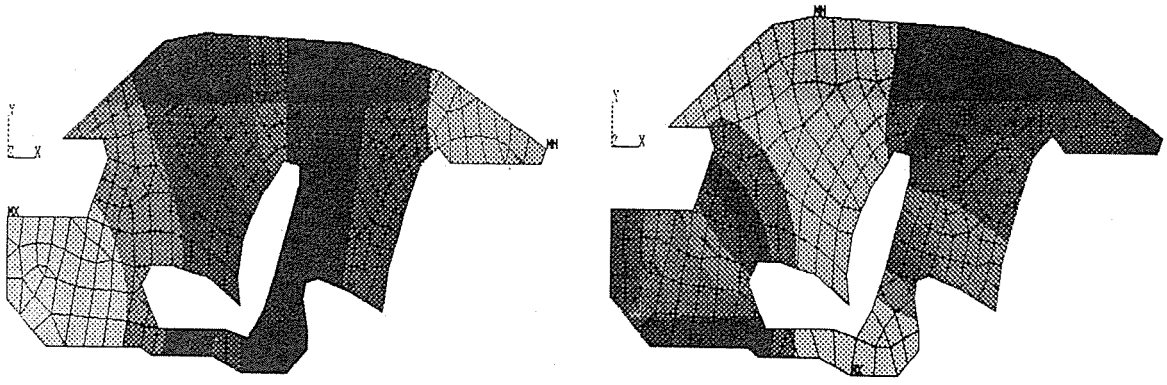

(a) at 75 Hz. (b) at 123 Hz.

Figure 3 Car compartment acoustic modes.

4.2 Radiating sphere

In this example, the radiation efficiency of a spherical shell with radius a of 1 m and thickness t of 200 mm was calculated for three different types of excitation, namely (a) uniform radial velocity pulsation; (b) velocity pulsation on one meridian plane; and (c) force excitation on two meridian planes, as shown in Figures 5(a)-(c) respectively. Boundary element method has been used for the calculations and the problem has been assumed to be axisymmetric with 46 elements and 47 nodes, giving an upper frequency limit of about 900 Hz. It has been shown analytically (see ref. [6]) that the radiation efficiency (α) of a pulsating sphere is given by

$$\alpha = \frac{(ka)^2}{1 + (ka)^2} \qquad (4.1)$$

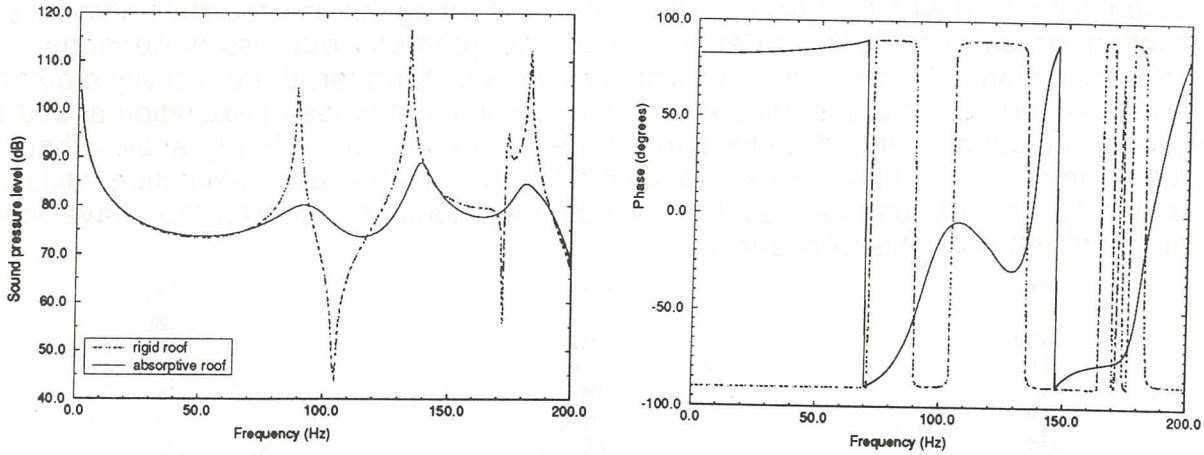

(a) Sound pressure level (b) Phase

Figure 4 Response near driver's ear for rigid and absorptive boundaries.

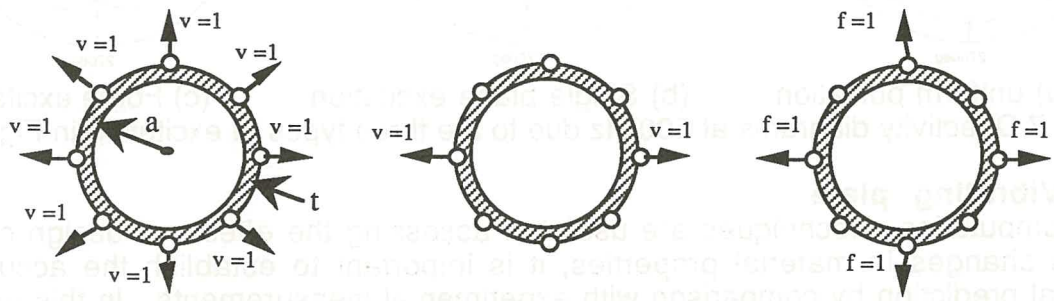

(a) uniform pulsation (b) Single plane excitation (c) Force excitation

Figure 5 A spherical shell subject to three different types of excitation.

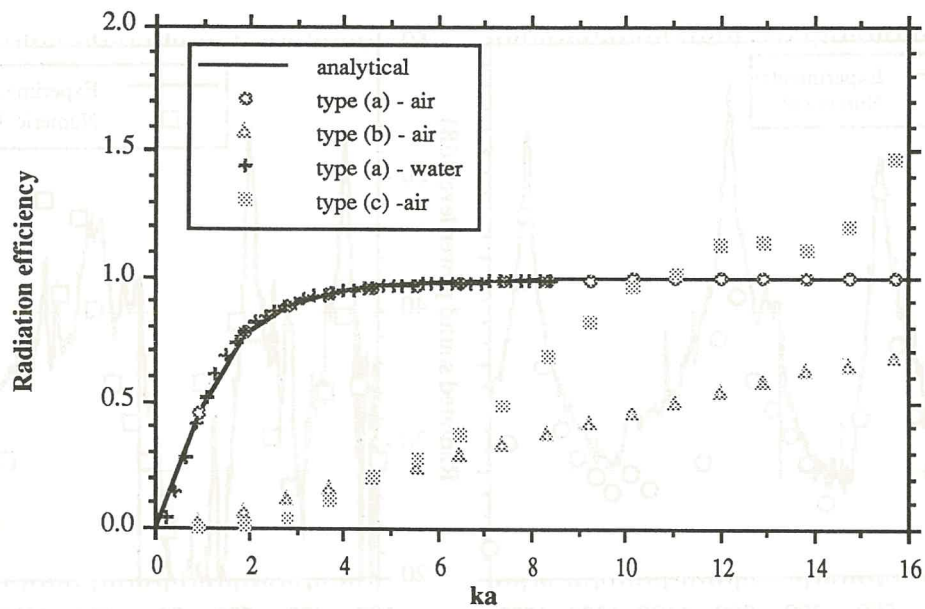

Figure 6 Radiation efficiency of a spherical shell.

The variation of the radiation efficiency with ka for the three types of excitation is shown in Figure 6 for air as the medium and for water with type (a) excitation. It can be seen that the numerical results for type (a) excitation with air or water as the medium agree very well with the analytical solution given in equation (4.1). There are, however,

significant differences between the radiation efficiency results for types (b) and (c) excitation compared with type (a) excitation, thus indicating that the radiation efficiency of a radiating structure not only is dependent on the geometry but also is dependent on how the excitation is introduced. To illustrate this point further, the directivity diagrams at 10 m from the centre of the sphere for the three different types of excitation at 500 Hz have been calculated and displayed in Figure 6. Figure 6(a) clearly shows that the source is omnidirectional as to be expected from an uniform radial excitation while the other two types of excitation result in directional radiation patterns that have lower radiation efficiency at this frequency.

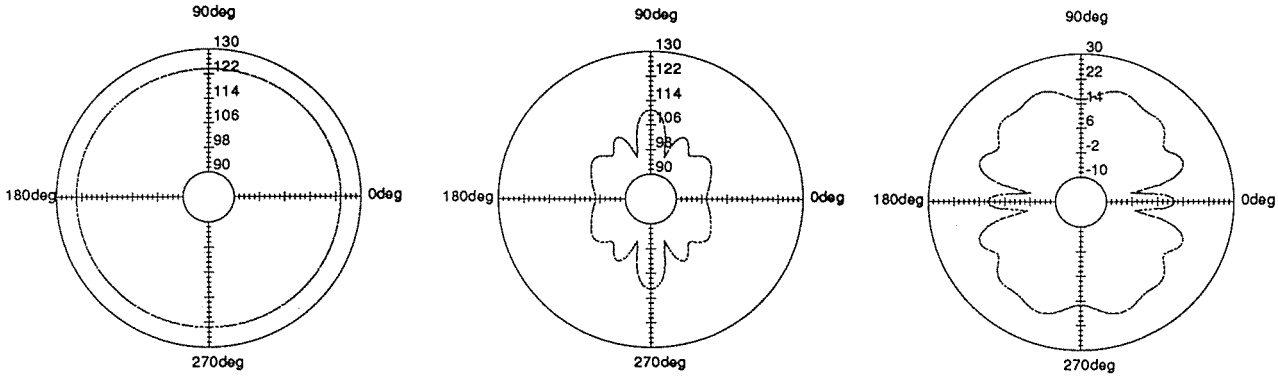

(a) uniform pulsation (b) Single plane excitation (c) Force excitation

Figure 7 Directivity diagrams at 500 Hz due to the three types of excitation in Figure 5.

4.3 Vibrating plate

While computational techniques are useful in assessing the effects of design changes such as changes in material properties, it is important to establish the accuracy of numerical prediction by comparison with experimental measurements. In this example, a circular steel plate with radius 200 mm, thickness 1.2 mm and mass of 1.16 kg was driven at its centre by an electromagnetic shaker with a broad band signal in the frequency range 0 - 1600 Hz.

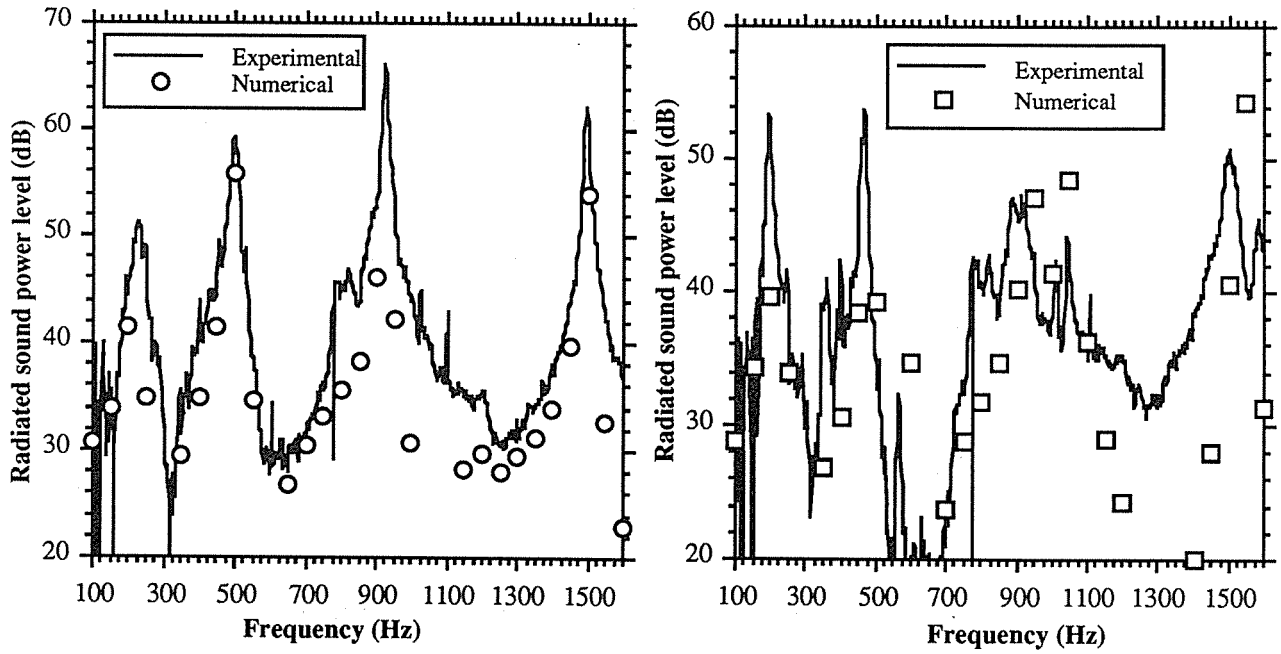

(a) Original circular plate (b) Modified circular plate

Figure 8 Comparisons between numerical and experimental results for the radiated sound power level.

The radiated sound power level was measured by the sound intensity technique and predicted using the boundary element method with 1220 quadrilateral plate bending elements (typical dimension 14 mm). Details of the measurement technique and numerical calculations are given in ref. [5]. The agreement between the numerical and experimental results is generally quite good, being within about 5 dB except in the frequency range 900 - 1000 Hz. It should be noted that no structural damping has been included in the calculations.

The circular plate was subsequently modified by the addition of two masses, one of 0.1 kg at the centre and one of 0.05 kg at a point 50 mm from the centre: this configuration is referred to as the 'modified plate'. Both the experimental measurements and numerical predictions were repeated for the modified plate. The discrepancies between the experimental and numerical results are greater for the modified plate than for the original plate, as shown in Figure 8(b). This is understandable because unless the original plate has been modelled accurately, any modification made to the plate is going to amplify the discrepancies. It must be pointed out that the modified plate has been modelled as an inhomogeneous plate with three regions of different material density; however, due to the coarseness of the elements used, the two additional masses are distributed over larger areas in the numerical model than in the experimental set-up.

4.4 Barriers

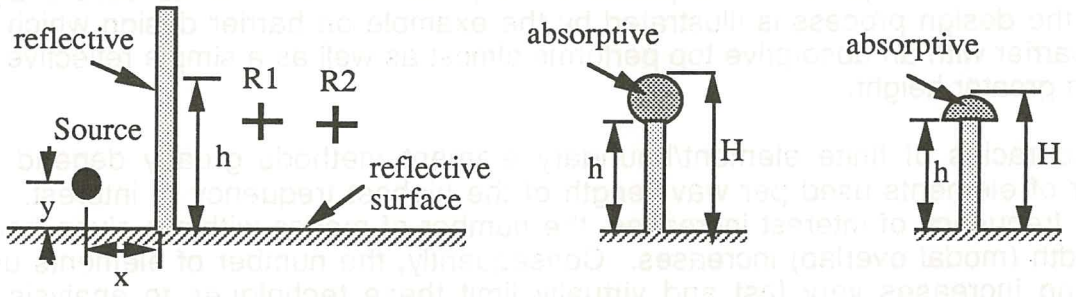

(a) simple barrier (b) spherical top (c) hemispherical top

Figure 9 Schematic of barrier models.

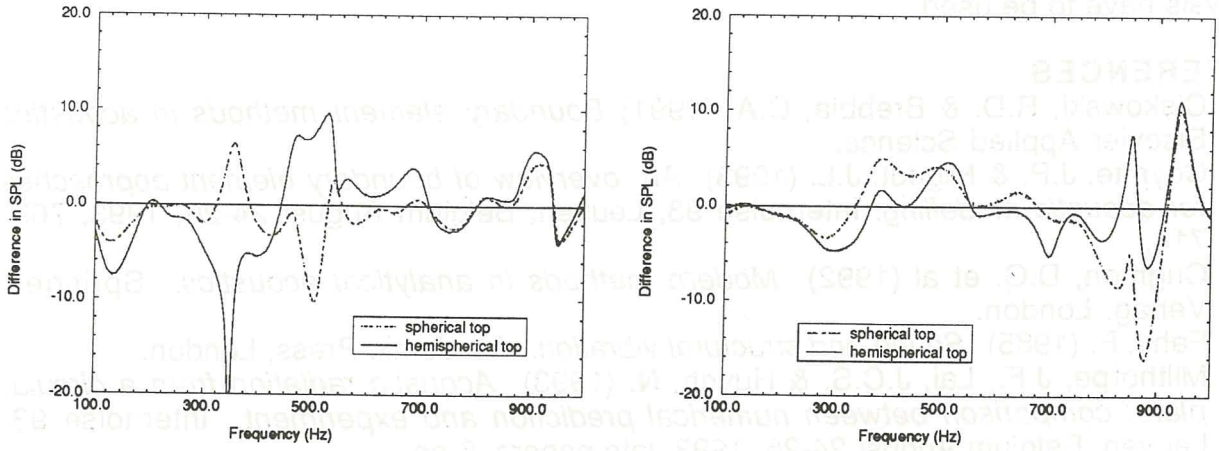

(a) at R1 (b) at R2

Figure 10 Difference in sound pressure levels at receiver points for barriers with spherical top and hemispherical top compared with the simple barrier.

In this example, boundary element methods have been used to assess the insertion loss of barriers of three different designs. As shown in Figure 9(a), a simple reflective barrier of height h (2 m) is used as a base reference for the other two barriers, namely one with a spherical absorptive top with a height H (1.5 m) and another with a hemispherical absorptive top with a height H of about 1.25 m, as shown in Figures 9(b)-(c) respectively.

A spherical source at a height y of 0.5 m and a distance x of 1.5 m from the barrier was used. The ground surface has been assumed to be reflective. Two receiver points R1 and R2 at the same height of 1 m above the ground and 1 m and 3 m respectively from the barrier were used. The differences in sound pressure levels at R1 and R2 between barrier (b) and barrier (a) and between barrier (c) and barrier (a) are displayed in Figures 10(a)-(b). While the performance of the barriers depend on the frequencies, it can be seen that for the frequency range of 100-1000 Hz, the overall performance of both barriers (b) and (c) is almost comparable to that of the simple barrier with a greater height.

5.0 CONCLUSIONS

Commercially available finite element/boundary element packages have been used to solve acoustic cavity and external radiation problems. The car compartment example has illustrated how resonant frequencies and the response due to vibration excitation can be calculated. The ability of numerical acoustic analysis to study the effect of changes in material properties on the sound pressure level has been highlighted. The agreement between numerical results and the analytical solution of a pulsating sphere is excellent and the influence of the type of excitation on the radiation efficiency and directivity has been clearly illustrated by the numerical solution. Comparisons of experimentally measured sound power level radiated from a circular plate with numerical predictions indicate that provided a structure is modelled properly, reasonable agreement can be expected. The potential and power of numerical acoustic analysis as part of the design process is illustrated by the example on barrier design which shows that a barrier with an absorptive top performs almost as well as a simple reflective barrier of much greater height.

The accuracies of finite element/boundary element methods greatly depend on the number of elements used per wavelength of the highest frequency of interest. As the highest frequency of interest increases, the number of modes within a given frequency bandwidth (modal overlap) increases. Consequently, the number of elements used for modelling increases very fast and virtually limit these techniques to analysis at low frequencies. For analysis at high frequencies where the modal overlap is high, techniques based on geometrical acoustics (such as ray tracing) or statistical energy analysis have to be used.

REFERENCES

1. Ciskowski, R.D. & Brebbia, C.A. (1991) *Boundary element methods in acoustics* Elsevier Applied Science.
2. Coyette, J.P. & Migeot, J.L. (1993) *An overview of boundary element approaches for acoustic modelling.* Internoise 93, Leuven, Belgium August 24-26, 1993, 709-714.
3. Crighton, D.G. et al (1992) *Modern methods in analytical acoustics.* Springer-Verlag, London.
4. Fahy, F. (1985) *Sound and structural vibration.* Academic Press, London.
5. Milthorpe, J.F., Lai, J.C.S. & Huynh, N. (1993) *Acoustic radiation from a circular plate: comparison between numerical prediction and experiment.* Internoise 93, Leuven, Belgium August 24-26, 1993, late papers, 6 pp.
6. Pierce, A. D. (1981) *Acoustics : an introduction to the physical principles and applications.* McGraw-Hill, New York.